Evaluating Salmonid and Stream Ecosystems Response to Conservation Measures and Environmental Stressors in the Columbia River Basin: Annual Report 2023

publication date: March 1, 2024

Authors: Casey Justice, Matthew Kaylor, Anna Ringelman, Ben Staton and Marshall Wolf

Technical Report 24-04

Columbia River Inter-Tribal Fish Commission

700 NE Multnomah St, Ste 1200, Portland OR 97232 · (503)238-0667 · www.critfc.org

Evaluating salmonid and stream ecosystem response to conservation measures and environmental stressors in the Columbia River basin

BPA Project # 2009-004-00

Report covers work performed under BPA contract # 92202

Report covers work performed from:

January 2023– December 2023

Authors: Casey Justice, Matthew Kaylor, Anna Ringelman, Ben Staton and Marshall Wolf

Columbia River Inter-Tribal Fish Commission, Portland, OR 97232

March 2024

This report was funded by the Bonneville Power Administration (BPA), U.S. Department of Energy, as part of BPA's program to protect, mitigate, and enhance fish and wildlife affected by the development and operation of hydroelectric facilities on the Columbia River and its tributaries. The views in this report are the author's and do not necessarily represent the views of BPA.

Table of Contents

List of Common Abbreviations

Abbreviation	Description
AqI	Aquatic Inventories Project
BPA	Bonneville Power Administration
BSR	Biologically Significant Reach
CC or CAT	Catherine Creek
CHaMP	Columbia Habitat Monitoring Program
CRB	Columbia River basin
CRITFC	Columbia River Inter-Tribal Fish Commission
CTUIR	Confederated Tribes of the Umatilla Indian Reservation
CTWSRO	Confederated Tribes of the Warm Springs Reservation of Oregon
DEQ	Oregon Department of Environmental Quality
EPA	Environmental Protection Agency
FL	Fork Length
GR	Grande Ronde River
GRMW	Grande Ronde Model Watershed
(SS)LCM	(State-Space) Life Cycle Model
LOS	Lostine River
MFJD	Middle Fork John Day River
MIN	Minam River
NOAA	National Oceanic and Atmospheric Administration
NPCC	Northwest Power and Conservation Council
ODFW	Oregon Department of Fish and Wildlife
OSU	Oregon State University
OWRD	Oregon Water Resources Department
PNAMP	Pacific Northwest Aquatic Monitoring Program
RM&E	Research, Monitoring, and Evaluation
UAS	Unmanned Aircraft System
UGR	upper Grande Ronde River
USBR	U.S. Bureau of Reclamation
USFS	U.S. Forest Service
USGS	U.S. Geological Survey
USWCD	Union Soil and Water Conservation District

Executive Summary

Background and Objectives

The Columbia River Inter-Tribal Fish Commission is conducting a research, monitoring, and evaluation study designed to determine the effectiveness of aggregate restoration actions in improving freshwater habitat conditions and viability of ESA-listed spring Chinook Salmon (*Oncorhynchus tshawytscha*) populations. A critical uncertainty for fisheries managers in the Columbia River basin is whether freshwater habitat restoration actions will improve basin-wide habitat quantity/quality and thereby salmon productivity to a level sufficient to offset human-caused survival impairments elsewhere in the life cycle. Geographically, this project is focused on the Grande Ronde River basin (tributary of the Snake River in the Columbia River basin), but with applications and testing of research, monitoring, and evaluation approaches also occurring in other Columbia River tributaries.

We have hierarchically structured our work into four primary goals and associated objectives in our current and proposed work plan (Figure 1):

Goal 1: Assess status and trends of key fish habitat limiting factors in the Grande Ronde basin.

- Objective A: Describe habitat conditions of the Grande Ronde basin as compared to historical and/or reference target values.
- Objective B: Evaluate annual and decadal trends of key limiting factors in the Grande Ronde basin.

Goal 2: Evaluate effectiveness of aggregate restoration actions in the Grande Ronde basin.

- Objective C: Evaluate if the pace of restoration can counteract habitat and temperature degradation.

Goal 3: Relate biological responses to habitat change.

- Objective D: Relate life stage-specific fish response to habitat change in the Grande Ronde basin and nearby basins.
- Objective E: Relate population-level fish response to habitat change in the Grande Ronde basin and potentially other basins.

Goal 4: Apply lessons learned from RM&E to Grande Ronde basin salmon recovery efforts and other emerging concerns or locations.

- Objective F: Address needs of CRITFC tribal and other partners evaluating emerging concerns in the Grande Ronde basin and other geographic locations.

A complete list of goals, objectives, and tasks (i.e., sub-objectives) for this project over a seven year time frame (2021-2027) are laid out in Figure 1 (a and b) with timelines in the corresponding Gantt chart (Table 1). These goals and objectives were originally developed as part of our 2021 project proposal to ISRP (CRITFC 2021) which received favorable reviews (ISRP 2022). Progress made in 2022 and 2023 towards these objectives is presented in this report.

Progress and Key Findings

Goal 1: Assess status and trends of key fish habitat limiting factors in the Grande Ronde basin

Objective A: Describe habitat conditions of the Grande Ronde basin as compared to historical and/or reference target values

Objective A-1: Finalize tributary habitat protocol

- This sub-objective was completed and presented in the 2021 annual report (White et al. 2022).

Objective A-2: Collect habitat data using the Tributary Habitat Assessment Protocol (TribAP) in Atlas Tier I-II priority areas within the current Chinook extent in the Grande Ronde basin.

- In 2022, we worked collaboratively with the GRMW (funded partly by USFS) and a subcontractor (Foresight Drone Services) to survey a total of 67.9 km (mainstem length) and 172 acres of stream habitat in the upper Grande Ronde River basin using the Tributary Habitat Assessment Protocol. Surveys were intended to cover the current extent of Chinook Salmon spawning and rearing habitat within the Grande Ronde Atlas Tier 2 priority areas and small portions of Tier 1 areas that were not surveyed in 2021.
- Due to the large extent of area surveyed, challenges with drone image quality in some areas, inconsistent numbering of channel units and issues arising from use of different coordinate systems during postprocessing of drone imagery, the QAQC process has taken much longer than expected. We intend to complete data processing and metric calculation by the end of the second quarter of 2024.

Objective A-3: Set target values for restoration

- This sub-objective was completed and described in the 2022 Annual Report.

Objective A-4: Habitat status assessment (LiDAR)

- We are in the process of using topobathymetic LiDAR data acquired in 2020 to describe spatially continuous instream fish habitat metrics and floodplain conditions and to compare how habitats have changed since our previous LiDAR acquisition in 2009.
- Some progress was made in 2022 through a subcontract with NV-5 Geospatial using the geomorphic unit tool (GUT) to classify geomorphic units and large wood from LiDAR data, but additional work is needed to refine these methods and apply them to the entire LiDAR survey area.
- We expect to complete this task in 2024.

Objective A-5: Meadow Creek aquatic habitat and biota data synthesis

- We analyzed CHaMP data collected between 2011-2017 from the Meadow Creek watershed within a Before-After-Control-Impact framework to determine if large wood additions and riparian plantings influenced fish habitat and *O. mykiss* abundance estimates.
- We are in the process of analyzing historic juvenile outmigration trap data from the Meadow Creek watershed collected by the USFS from 1987-2000.

Goal 2: Evaluate effectiveness of aggregate restoration actions in the Grande Ronde basin

Objective C: Evaluate if the pace of restoration can counteract habitat and temperature degradation

Objective C-1: Develop list of restoration scenarios

- CRITFC staff hosted a collaborative workshop in November of 2021 with Grande Ronde basin partners to develop a draft suite of riverscape restoration and management scenarios intended to be used as inputs to the Grande Ronde spring Chinook life cycle model described in Objective D.
- Further development of these restoration scenarios was put on hold in 2023 to prioritize finalizing and publishing the life cycle model. We plan to resume development of restoration/management scenarios with the goal of finalizing and running them through the life cycle model during 2024 and 2025.

Objective C-2: Quantify change in habitat limiting factors relative to restoration actions

- To address a critical gap in our ability to translate restoration actions into habitat change across large geographic extents (e.g., biologically significant reaches [BSRs], Chinook population areas), we plan to quantify observed changes in habitat limiting factors before and after restoration at selected sites within the study area.
- While no progress was made on this objective in 2023 due in part to insufficient information of restoration project locations, we plan to complete this objective in late 2024 or early 2025.

Objective C-3: Extrapolate impacts of restoration scenarios across historical Chinook extent in upper GR basin

- Using observed changes in habitat characteristics at selected restoration sites from Objective C-2, we plan to extrapolate the expected uplift to habitat conditions throughout the stream network in the study area. This objective is planned to be completed in 2025.

Goal 3: Relate biological responses to habitat change

Objective D: Relate life stage-specific response to habitat change in the Grande Ronde and nearby basins

Objective D-1: Collect data on fish and macroinvertebrate distribution

- We conducted snorkel count surveys in 58 monitoring sites subsampled from habitat segments surveyed using the Tributary Habitat Assessment Protocol (TribAP) during summer of 2022.
- We conducted paired snorkel count and mark-recapture surveys at 25 sites across the Grande Ronde basin and tributaries of the Middle Fork John Day during the summer and early fall of 2023, for a total of 57 individual channel units sampled.
- We conducted basin-wide snorkel surveys across the Middle Fork John Day with our partners to evaluate juvenile Chinook Salmon distribution in 2023 and assess how distribution patterns and use of restoration areas change under different climate and hydrologic conditions. We surveyed 39 mainstem reaches (11.2 km) and 88 tributary reaches (8.6 km) across 18 tributaries.
- We conducted a PIT tag study in Lookingglass Creek to assess growth and recapture rates in juvenile Steelhead/Rainbow Trout in preparation for the insulin-like growth factor-1 (IGF1) field pilot planned for summer 2024. We are ultimately interested in determining the potential application of IGF1 as a method of assessing juvenile salmonid growth in habitats where traditional mark-recapture methods are not very effective (e.g., complex floodplains, large rivers, estuaries).
- We conducted a hatchery pilot study at the OHRC assessing mortality across a range of sizes of juvenile Steelhead/Rainbow Trout to determine a minimum size threshold for non-lethal blood sampling in juvenile salmonids. These efforts are ongoing as part of our IGF1 growth study, with a follow-up study currently being conducted in Hagerman, ID.
- Snorkel surveys conducted in Tier 2 areas of the upper Grande Ronde basin during 2022 will be described in the 2024 annual report.

Objective D-2: Index of Chinook Salmon rearing capacity

- This work was completed and described in the 2021 annual report.

Objective D-3: Finalize pre-spawn mortality analysis

- This work was completed and described in the 2021 annual report.

Objective D-4: Complete study of juvenile fish emergence timing and floodplain inundation

- We are working with partners to address challenges with modeling floodplain inundation dynamics in river systems spanning the transition from snow- to rain-dominated hydrology. This has slowed progress in 2023, but we are finalizing an approach to accurately and effectively address this complexity. We expect to complete floodplain inundation modeling for the three planned subbasins – the Middle fork John Day, Upper Grande Ronde, and Catherine Creek – in 2024 and relate inundation dynamics to the already completed emergence timing predictions.

Objective D-5: Complete study of juvenile Chinook dispersal and floodplain use

- We continued analysis of juvenile dispersal patterns from spawning locations to summer rearing habitats in the Middle Fork John Day River using genetic-based parentage assignments.
- These additional analyses demonstrated 1) the importance of temperature as a driver of dispersal, with juveniles originating in warmer mainstem sections generally dispersing to cooler

sections of the mainstem or tributaries, and 2) the influence of emergence timing on competitive advantages of dispersal direction.

- A draft manuscript has been included in Appendix D.

Objective E: Relate population-level fish response to habitat change in the Grande Ronde basin and potentially other basins

Objective E-1: Grande Ronde Phase 1 – Development of spring Chinook statistical estimation Life Cycle Model

- We have finalized development of the statistical life cycle model for Grande Ronde spring Chinook salmon and have made significant progress on a manuscript documenting it. The draft manuscript text/figures are included in Appendix E, and complete mathematical details are in Appendix F.

Objective E-2: LCM Phase II – Management scenarios

- Restoration scenarios to impose on the statistical estimation life cycle model output are in development but have not been finalized. Several planning meetings have occurred, including a well-attended workshop devoted to brainstorming with partners in the basin and a loose plan has been developed.
- We plan to assess combinations of restoration and other management actions (e.g., changes to supplementation) of various intensities. More details will be forthcoming in the 2024 annual report.

Objective E-3: LCM Phase III – Simulation of outcomes

- With the finalization of the LCM Phase I estimation model, we have now started constructing a simulation model that accepts output from the estimation model to simulate the populations into the future. We plan to make significant progress and have results available for the 2024 report.

Goal 4: Apply lessons learned from RM&E to Grande Ronde salmon recovery efforts and other emerging concerns or locations

Objective F: Address needs of CRITFC tribal and other partners evaluating emerging concerns in the Grande Ronde and other geographic locations

Objective F-1: Continue developing/applying Adaptive Management framework with GRMW and Grande Ronde basin partners

- In 2022 and 2023, we participated in the Grande Ronde State of the Science meeting hosted by GRMW to discuss restoration progress, RM&E findings, and emerging uncertainties/questions pertinent to management efforts in the basin.
- Coordination with other entities involved in fish habitat restoration and associated data collection in the Grande Ronde, Upper Columbia, Mid-Columbia, and Snake River watersheds is a critical component of this project. Numerous examples of our collaborative efforts in 2023 are described within including: 1) participation in Atlas review and updates, 2) collaboration

with USFS, CTUIR, and ODFW on Meadow Creek restoration and RM&E which includes hiring a Forest Service-funded post-doc position (Marshall Wolf) supervised by CRITFC to focus on this work, 3) coordination with OSU, CTUIR, NOAA, and ODFW on juvenile salmon dispersal study in the Grande Ronde Basin, 4) collaborating with CTWSOR and ODFW to evaluate juvenile salmonid dispersal, floodplain habitat use, and distribution across the Middle Fork John Day River, and 5) collaborating closely with NOAA and ODFW on development of a spring Chinook statistical estimation life cycle model for the Grande Ronde basin.

- We identified protocol updates and additional research needs related to some of our RM&E methods and designs based on lessons learned from previous work in the Grande Ronde basin including 1) collection of additional paired mark-recapture and snorkel survey work in 2023 to better estimate snorkel detection efficiency in deep or complex habitat types, 2) collection of pilot data on freshwater mussel distribution in the Minam River using a Xerces Society draft survey protocol, which we provided feedback on, and 3) conducted pilot hatchery studies at the Oregon Hatchery Research Center and Hagerman Fish Culture Experiment Station to evaluate the use of IGF1 as an index of growth and determine a minimum size threshold for non-lethal sampling that will be applied to a field study in 2024.

Objective F-2: Represent tribal concerns in Columbia River basin tributary habitat RM&E policy discussions

- We participated in regular meetings with the Columbia Basin Collaborative's (CBC) Estuary, Tributary & Mainstem Habitat workgroup to develop regional recommendations to the Integration/Recommendations Group (IRG) regarding best management practices for habitat and salmon recovery in the Columbia River basin. A website providing public access to the recommendations generated from the CBC process is available here: https://columbiabasin.idaho.gov/recommendation-tracker/
- Our group has been actively participating in both internal and regional meetings focused on better aligning CRITFC's work with the goals of the newly-developed Columbia Basin Restoration Initiative (CBRI).

Dissemination of Project Findings

- Staff from CRITFC's River Ecology group delivered 9 scientific presentations during 2023 describing project findings.
- We produced 4 peer-reviewed publications and 1 technical report during 2023.

Introduction

The Columbia River Inter-Tribal Fish Commission (CRITFC) is conducting a research, monitoring, and evaluation (RM&E) study designed to determine the effectiveness of aggregate restoration actions in improving freshwater habitat conditions and viability of spring Chinook Salmon (*Oncorhynchus tshawytscha*) populations. A critical uncertainty for fisheries managers in the Columbia River basin (CRB) is whether freshwater habitat restoration actions will improve basin-wide habitat quantity/quality and thereby salmon productivity to a level sufficient to offset human-caused survival impairments elsewhere in the life cycle. Geographically, this project is focused on the upper Grande Ronde River, Catherine Creek, and Minam River watersheds (tributaries of the Snake River in the Columbia River basin), but with recent applications and testing of approaches in other Columbia River tributaries.

Many studies in recent years have examined the current condition of fish habitat in Columbia River subbasins and how these habitat conditions influence salmon survival and productivity. Some of the most common impediments to the survival of salmon include high water temperatures, increased concentrations of fine sediment in spawning gravel, loss of riparian vegetation, channelization and diminished channel and floodplain complexity and hydrologic connectivity, loss of large wood in the channel, loss of large pools for adult fish holding and juvenile rearing, and depletion of summertime streamflow. More recent studies have additionally identified food webs (e.g., nutrient limitation, primary productivity, prey availability, or predation) as limiting factors for salmonids. Climate change presents an additional threat, as it can lead to changes in the quantity, timing, and type (i.e., snow vs rain) of precipitation as well as increased summer air and water temperatures.

Habitat restoration in the upper Grande Ronde River and Catherine Creek basins is being conducted by agencies including the USDA Forest Service, Confederated Tribes of the Umatilla Indian Reservation (CTUIR), Oregon Department of Fish and Wildlife (ODFW), Union Soil and Water Conservation District (USWCD), Grande Ronde Model Watershed (GRMW), Trout Unlimited and U.S. Bureau of Reclamation (USBR). However, it remains unclear how these collective restoration actions affect salmon habitat quantity and quality in the freshwater tributary life stages, let alone how they impact salmon populations in the context of the complete life cycle. Fish-habitat relationships are inherently complex as they are influenced by interactions among intrinsic watershed factors (e.g., geology, valley form, natural streamflow regime), biological factors (e.g., predation, prey availability, competition) and anthropogenic factors (e.g., land use, climate change, restoration). These in turn affect ecological conditions and ultimately drive changes in fish abundance and productivity. This project incorporates several of these interacting factors in a holistic analytical framework.

This project serves the needs of the CRITFC 1855 Treaty Tribes in their obligations related to the 2008 Columbia Basin Fish Accords to ensure implemented habitat projects are "linked to biological benefits based on limiting factors for ESA-listed fish" (Accords 2008, p. 10). Among other general provisions for non-hatchery projects, the Accords states the Tribes shall "provide estimated habitat quality improvement and survival benefits from the project (or suite of projects) to a population or populations of listed salmon and steelhead based on key limiting factors" (p. 14). This project provides the knowledge basis to ensure benefits to populations from habitat projects can be estimated with reasonable precision and accuracy. Our project additionally serves the mission laid out in Wy-Kan-Ush-Mi Wa-Kish-Wit (Spirit of the Salmon

Plan) developed by CRITFC and the Tribes, which takes a holistic approach to salmon and aquatic ecosystem recovery over multi-generational time scales.

Our project directly supports the goals of the Habitat sub-strategy of the Council's 2014 Columbia River Basin Fish and Wildlife Program, namely in terms of developing "assessments of current physical and biological conditions and also identify factors that limit the productivity and capacity of focal species in priority reaches." This includes evaluating how climate change may affect fish population responses to habitat restoration emphasized in the Program's 2020 Addendum. More specific to the study area, the Grande Ronde Subbasin Plan describes the need for RM&E efforts to address both project-level ("bottom-up") habitat assessments but also large-scale landscape and ecosystem-level ("top-down") monitoring; the latter is a gap our project strives to fill.

Beyond monitoring and evaluation of limiting factors, our project has a strong research emphasis consistent with the Council's 2017 Research Plan by evaluating whether "improvements in tributary habitat conditions not only boost survival and productivity of fish in the tributaries but also contribute to survival benefits at the population scale" (p. 6). In our project this is primarily addressed using life cycle models, but we also conduct research on several critical uncertainties (e.g., climate change, food webs, juvenile salmonid ecology) so their influence on the expected benefits to fish populations from habitat projects can be understood and shared with the broader scientific community. These combined efforts are intended to provide guidance on whether and how restoration implementers and basin managers can meet important biological targets, such as the minimum abundance and productivity thresholds for natural origin spawners expressed in NOAA's Recovery Plans for Grande Ronde/Imnaha River populations of Snake River Spring Chinook Salmon.

Overall goals of the project include the following:

Goal 1: Assess status and trends of key fish habitat limiting factors in the Grande Ronde basin—Objectives towards this goal involve describing habitat conditions as compared to historical and/or target values (Objective A) and evaluating annual and decadal trends of key limiting factors (Objective B).

Goal 2: Evaluate effectiveness of aggregate restoration actions in the Grande Ronde basin—Objectives towards this goal involve evaluating if the pace of restoration (current or projected) can counteract habitat and temperature degradation (Objective C).

Goal 3: Relate biological responses to habitat change—Objectives towards this goal involve collecting biological data and developing life stage-specific (Objective D) and population-level (Objective E) models relating habitat change to fish response in the Grande Ronde and other basins.

Goal 4: Apply lessons learned from our research, monitoring, and evaluation (RM&E) to Grande Ronde salmon recovery efforts and other emerging concerns or locations—Objectives towards this goal involve remaining engaged in the Grande Ronde Atlas adaptive management framework (Objective F-1), representing tribal concerns in development of a regional tributary habitat evaluation framework (Objective F-2), and developing a new work plan adapting our program to other emerging concerns, locations, or focal species (Objectives F-3, F-4, F-5). It was the intention in the original 2009 proposal that lessons learned in the Grande Ronde subbasin would be applied to other geographic areas in the Columbia River basin.

Detailed goals, objectives, and tasks for this project over a seven year time frame (2001-2007) are presented in Figure 1 (a and b) with timelines in the corresponding Gantt chart (Table 1).

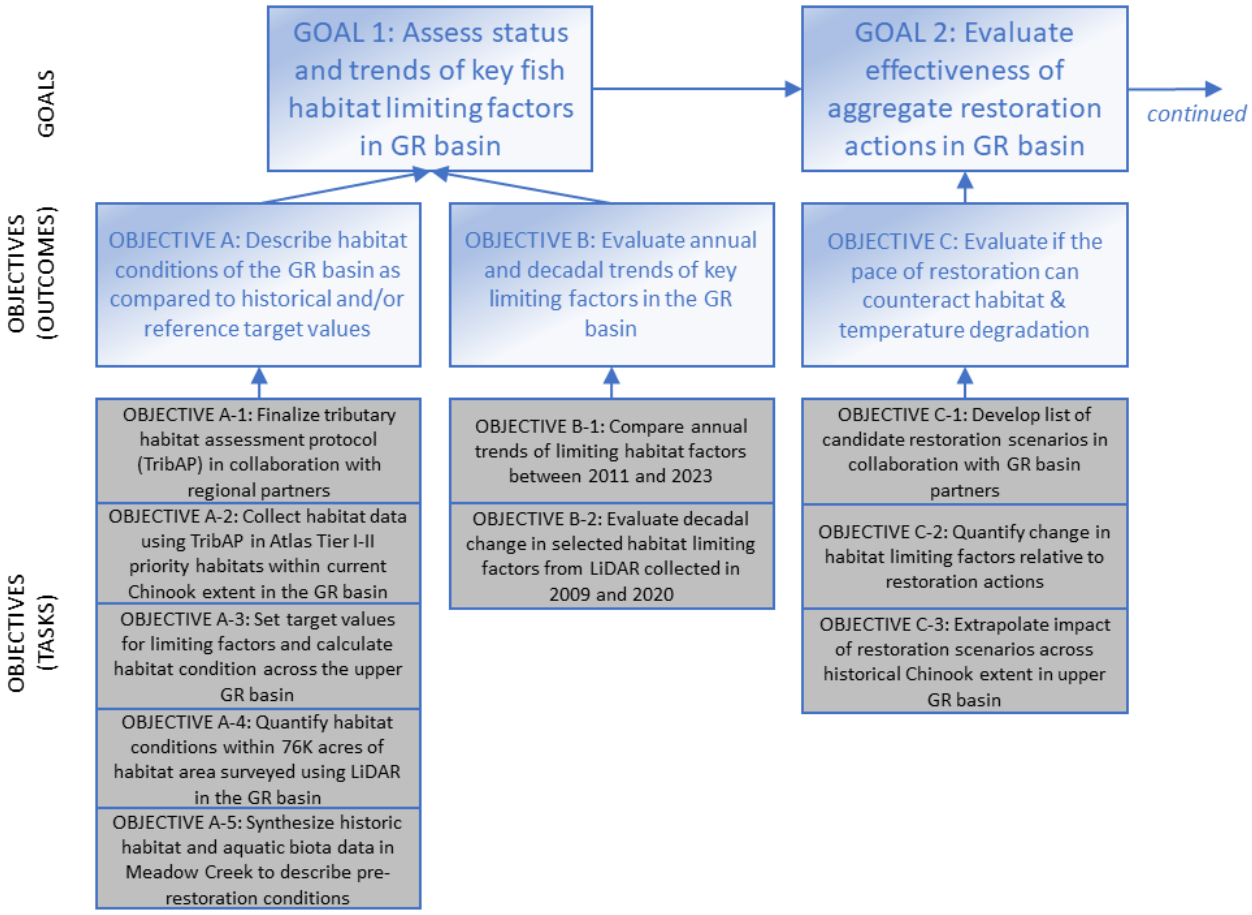

Figure 1a. Project goals, objectives, and tasks for goals 1 and 2.

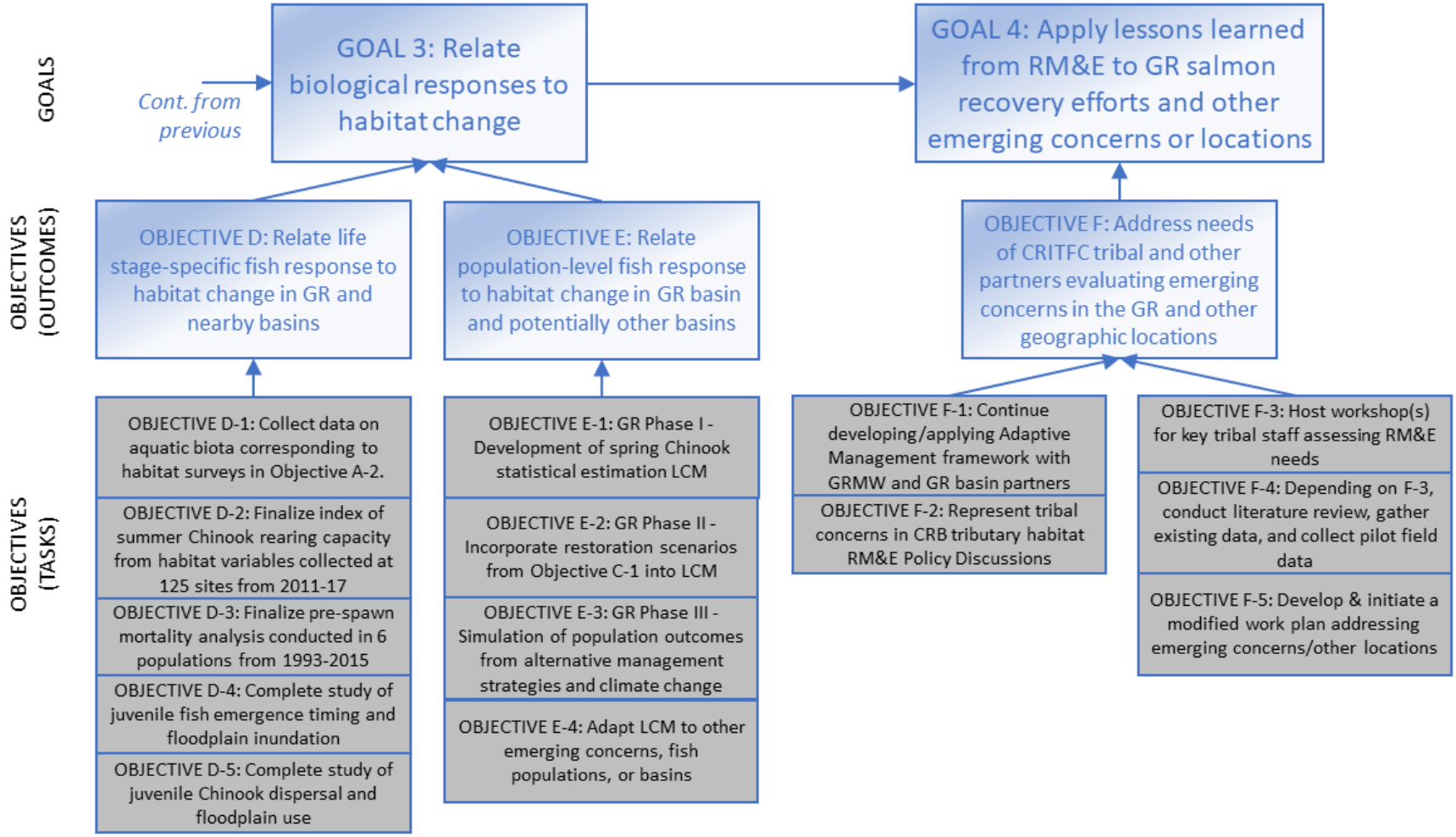

Figure 1b. Project goals, objectives, and task for goals 3 and 4.

Table 1. Gantt chart showing projected timelines of project goals and objectives. Years represent contract years (e.g., 2023 = April 1, 2023 – March 31, 2024).

Goal	Objective (Task)	Short description	2021	2022	2023	2024	2025	2026	2027
1	A-1	Finalize tributary habitat protocol							
	A-2	Apply habitat protocol in GR basin							
	A-3	Target habitat values analysis							
	A-4	Habitat status assessment (LiDAR)							
	A-5	Meadow Creek data synthesis							
	B-1	Annual habitat trends analysis (ground)							
	B-2	Decadal habitat trends analysis (LiDAR)							
2	C-1	Develop candidate restoration scenarios							
	C-2	Quantify restoration impact on habitat							
	C-3	Spatial extrapolation of restoration							
3	D-1	Collect fish and macroinvertebrate data							
	D-2	Index of Chinook rearing capacity							
	D-3	Finalize pre-spawn mortality analysis							
	D-4	Emergence phenology of rearing Chinook							
	D-5	Juvenile Chinook dispersal study (MFJD)							
	E-1	LCM Phase I: Statistical estimation							
	E-2	LCM Phase II: Management scenarios							
	E-3	LCM Phase III: Simulation of outcomes							
	E-4	Adapt LCM for other factors/populations							
4	F-1	Adaptive management with GRMW							
	F-2	Trib Habitat RM&E Framework for CRB							
	F-3	Needs assessment with CRITFC tribes							
	F-4	Draft workplan and pilot fieldwork							
	F-5	Final work plan and implementation							

Study Area

This project is occurring primarily in the Grande Ronde River and its tributaries, which originates in the Blue Mountains of NE Oregon and flows 334 km to its confluence with Snake River (Figure 2). Focal study watersheds include the upper Grande Ronde River (UGR) upstream of the town of La Grande, Catherine Creek (CAT), and to a lesser extent the Minam River (MIN). Spring Chinook Salmon populations in these basins were listed as threatened under the Endangered Species Act in 1992. Population declines over the past century were due in part to overharvest, hydropower impacts, and degraded habitat conditions resulting from intensive anthropogenic disturbances including timber harvest, cattle grazing, levee and road construction, stream diversions for irrigation, and removal of beaver populations (*Castor canadensis*). Specifically, stream temperature, streamflow, habitat diversity, large wood structures, and quantity of key habitats such as large pools, have been identified as key limiting factors for recovery of salmonid populations in these basins. The Minam River is a designated wilderness area and represents a minimally impacted reference stream. We additionally conduct limited research in nearby basins with similar biophysical conditions and land use history, such as Lookingglass Creek (Grande Ronde basin) and the Middle Fork John Day River.

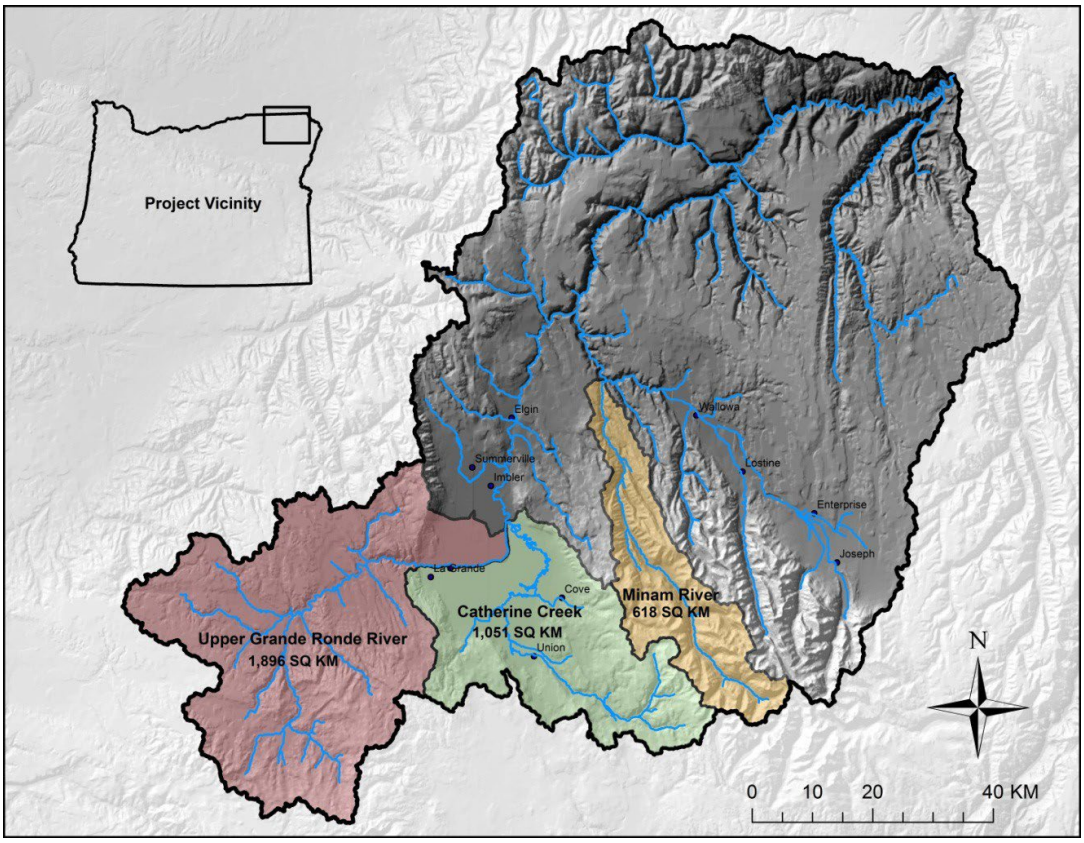

Figure 2. Study area in the Grande Ronde River basin, NE Oregon. Focal watersheds include the upper Grande Ronde River, Catherine Creek, and Minam River. The upper Grande Ronde and Catherine Creek are basins with significantly impacted habitat, currently undergoing restoration in various locations. The Minam River basin is the local reference area that has far less anthropogenic impact.

Progress on project goals

Goal 1: Assess status and trends of key fish habitat limiting factors in the Grande Ronde basin

Objective A: Describe habitat conditions of the Grande Ronde basin as compared to historical and/or reference target values

Objective A-1: Finalize tributary habitat protocol

This sub-objective was completed and presented in the 2021 annual report.

Objective A-2: Collect habitat data using the Tributary Habitat Assessment Protocol (TribAP) in Atlas Tier I-II priority areas within the current Chinook extent in the Grande Ronde basin.

Habitat Surveys

Background

CRITFC began monitoring fish habitat conditions in the upper Grande Ronde River, Catherine Creek, and Minam River in 2009. After initially drafting our own agency stream monitoring protocol, CRITFC supported the development and implementation of the Columbia Habitat Monitoring Program (CHaMP 2016). Data collected from these programs (2011-2017) provided the basis for describing status and trends of limiting habitat factors for Chinook Salmon in the study basins. In 2017, Bonneville Power Administration (BPA) commissioned a review of the Columbia Habitat Monitoring Program (CHaMP) which highlighted potential problems or shortcomings concerning repeatability, efficiency, and validity of some monitoring methods, and with extrapolation of metrics to unsampled portions of the basin. In response to these concerns and feedback from the Independent Science Review Panel (ISRP), our project reassessed the components that would ensure the success and longevity of a new monitoring approach and allow for the continuation of status and trends analysis. We identified four major considerations when reconceptualizing a new monitoring strategy: 1) the methods used should be based on regionally accepted practices, which are both repeatable and could reliably be used for comparison to previously-derived metrics from other protocols, 2) it should incorporate measures of long-term impacts of land use and climate change, 3) it increases efficiency of previous fish habitat survey methodologies by reducing the intensity of ground-based measurements and integrating data collected by unmanned aircraft systems (UAS), and 4) it promotes partnership and garners regional support as a means for funding and continued long-term monitoring.

Using these considerations as a guide, we developed the Tributary Habitat Assessment Protocol (Justice et al. 2020). This protocol includes a pared-down list of metrics identified as having minimal observer bias, clear linkage to common ecological concerns in Columbia basin tributaries (i.e., water temperature, channel and floodplain complexity, pool habitats, fine sediment, etc.), and consistency (i.e., cross-walkability) with previously-collected habitat monitoring data. This protocol was tested during the 2018 field season and implemented during summer of 2021 and 2022. The methods outlined in this protocol are based on widely accepted and previously implemented monitoring methods used throughout the Pacific Northwest (i.e.,

CHaMP, ODFW Aquatic Inventories Project [AqI]). Acknowledging previous criticisms, the monitoring approach outlined within the CRITFC Tributary Habitat Assessment Protocol aims to cover more ground with less effort and cost, while obtaining high resolution aerial imagery using UAS that will provide a rich, georeferenced dataset with numerous current and future analytical opportunities. Our application of this monitoring protocol corresponds to biologically significant reaches (BSRs) in the project areas, with a specific focus on areas designated as high or medium priority for habitat restoration (i.e., Tier 1 and 2 BSRs; Atlas partners 2015). However, the protocol is flexible enough to be tailored to specific limiting factors or needs of a particular basin such as prioritization of stream segments with active or planned restoration.

The Tributary Habitat Assessment Protocol was designed to provide a comprehensive and continuous riverscape perspective of the status and trends in fish habitat by merging datasets from multiple spatial scales (channel unit ~ 1-100m, reach ~ 100-1000 m, segment ~ 1000-10,000m, watershed) and components of the riverscape (hydrology, geomorphology, biology). The major components of this protocol are split into ground- and aerial-based methods. The ground-based methods are a fusion of two widely used and accepted protocols within the CRB including AqI (Moore et al 2019) and CHaMP (CHaMP 2016), while the aerial-based portion of the protocol utilizes drones. Drones have become ubiquitous in monitoring throughout a range of disciplines within the CRB. Drones are used in this protocol to collect imagery of the stream channel and floodplain and to develop georeferenced orthomosaics, digital surface models, and digital terrain models. To increase efficiency and repeatability, we reduced the frequency and total number of measurements collected within habitat units (i.e., channel units) by ground crews compared with previous CHaMP surveys. We attempted to reduce the reliance on qualitative or visually estimated metrics to the degree possible with the intention of producing metrics that are robust enough to provide meaningful evaluations of habitat change over time.

Methods

Prior to conducting field surveys, the stream network was classified into segments to set the spatial boundaries for measurements of fish habitat and biota and to help organize the survey workflow into units of manageable size. We delineated stream segments using the National Hydrography Dataset High Resolution flowlines (NHDPlus HR, 1:24K scale; USGS 2016) as a starting point. Similar to the U.S. Forest Service (USFS) Region 6 Level I Stream Inventory Handbook (USDA 2018), segment boundaries were based on the presence of large tributary junctions (Strahler order ≥ 4) or significant changes in valley confinement and gradient. Stream reaches falling between these break points were lumped together into a 'segment' and assigned a unique identification number. With a few exceptions, we used a minimum segment length of 1 km, consistent with the spacing of Generalized Random Tessellation Stratified (GRTS) master sample points used by CHaMP and other programs to characterize broad-scale status and trends in fish habitat conditions. Segments were grouped by 12-digit hydrologic unit code (HUC) watershed boundaries, consistent with the National Watershed Boundary Dataset (WBD; USGS et al. 2015) to facilitate data tracking and management.

In 2022, we worked collaboratively with the GRMW (funded partly by USFS) and a subcontractor (Foresight Drone Services) to survey a total of 67.9 km (mainstem length) and 172 acres of stream habitat in the upper Grande Ronde River basin using the Tributary Habitat Assessment Protocol. Surveys were intended to cover the current extent of Chinook Salmon spawning and rearing habitat within the Grande Ronde Atlas Tier 2 priority areas and small portions of Tier 1 areas that were not surveyed in 2021 (Figure 3; Atlas 2015).

Within each segment, we collected aerial imagery (standard red/green/blue [RGB] and multispectral) using a variety of unmanned aircraft systems. Surveys conducted by CRITFC utilized a DJI Matrice 600 Pro drone outfitted with a dual payload including a Zenmuse X5 RGB camera (16 MP resolution) and Micasense Rededge MX multispectral sensor (1.2 MP) flown at an altitude of 90 m (295 ft) above ground level. We used DJI Map Pilot Pro on an Apple iPad mini for flight planning and control. Front and side image overlap was set to 80% and flight speed was generally below 8 m/s. Aerial targets consisting of bright spray paint or painted bucket lids were surveyed with an EOS Arrow 100 GNSS receiver (sub-meter accuracy) and used for georeferencing the aerial imagery. A detailed summary of the UAS imagery acquisition conducted by Foresight Drone Services is provided in Appendix B.

Ground-based measurements such as channel unit number, type (pool, fast turbulent, fast non-turbulent, etc.), large wood count, water depth, etc. were recorded using ArcGIS Survey123 on iPad mini or Samsung Galaxy tablets. To tie ground-based measurements to aerial imagery, we surveyed the boundaries of channel units and the edge of water using an EOS Arrow 100 GNSS receiver (Figure 4). The Arrow 100 typically achieved submeter accuracy except in rare cases with deep canyon walls (e.g., Dark Canyon Creek). Data collection with the Arrow 100 receiver was managed using ArcGIS Field Maps on an iPad mini or Samsung Galaxy tablet. Detailed survey methods are available on monitoringresources.org at http://www.monitoringresources.org/Document/Protocol/Details/3554.

Status and Next Steps

Results from 2022 habitat surveys will be provided in the 2024 annual report. For each survey segment, we plan to calculate a suite of metrics describing key characteristics of habitat quantity and quality/diversity for both mainstem and floodplain/side channel habitats (Table 2). However, due to the large extent of area surveyed, challenges with drone image quality in some areas, inconsistent numbering of channel units and issues arising from use of different coordinate systems during postprocessing of drone imagery, the QAQC process has taken much longer than expected. We intend to complete data processing and metric calculation by the end of the second quarter of 2024.

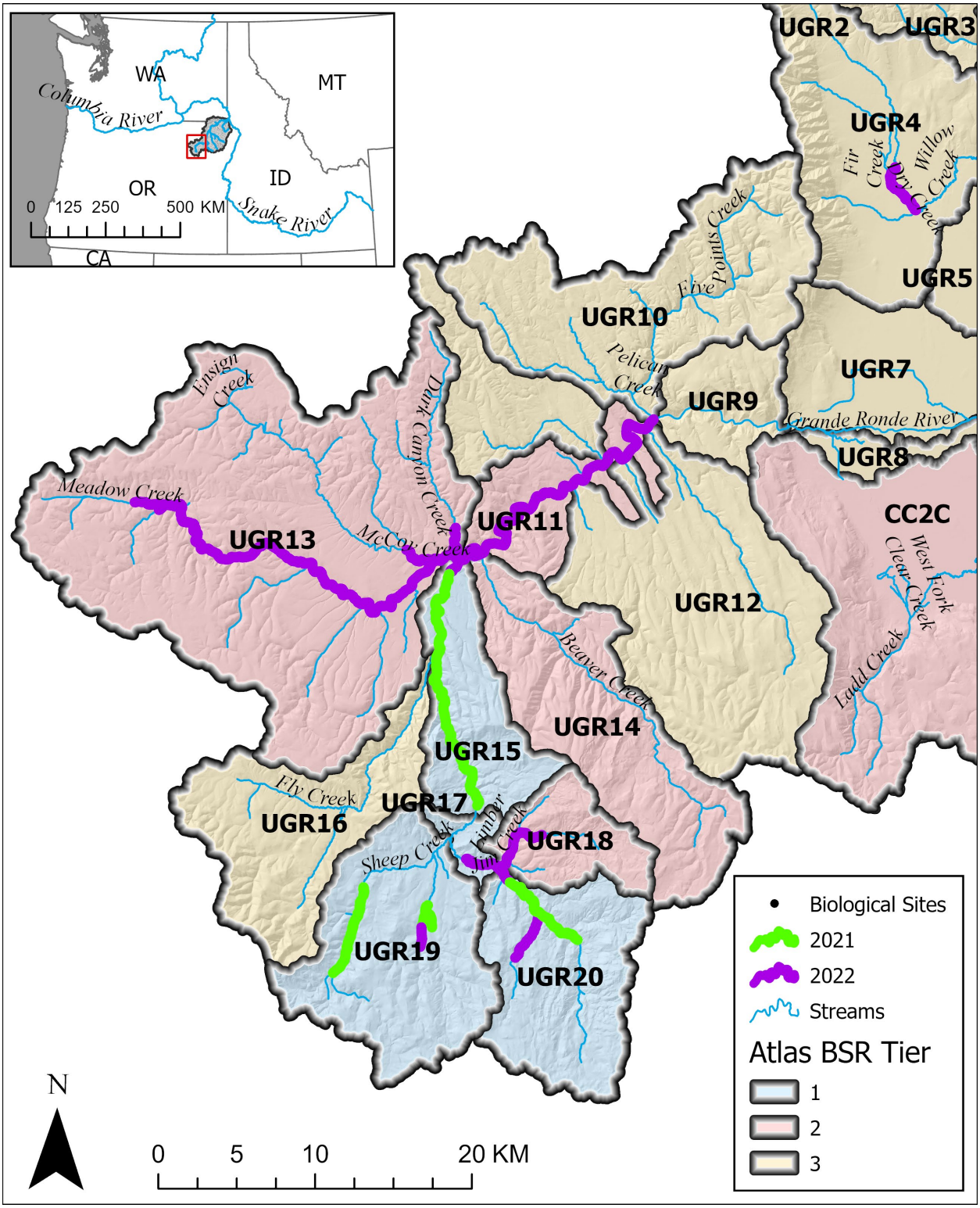

Figure 3. Survey area in the upper Grande Ronde River basin in NE Oregon

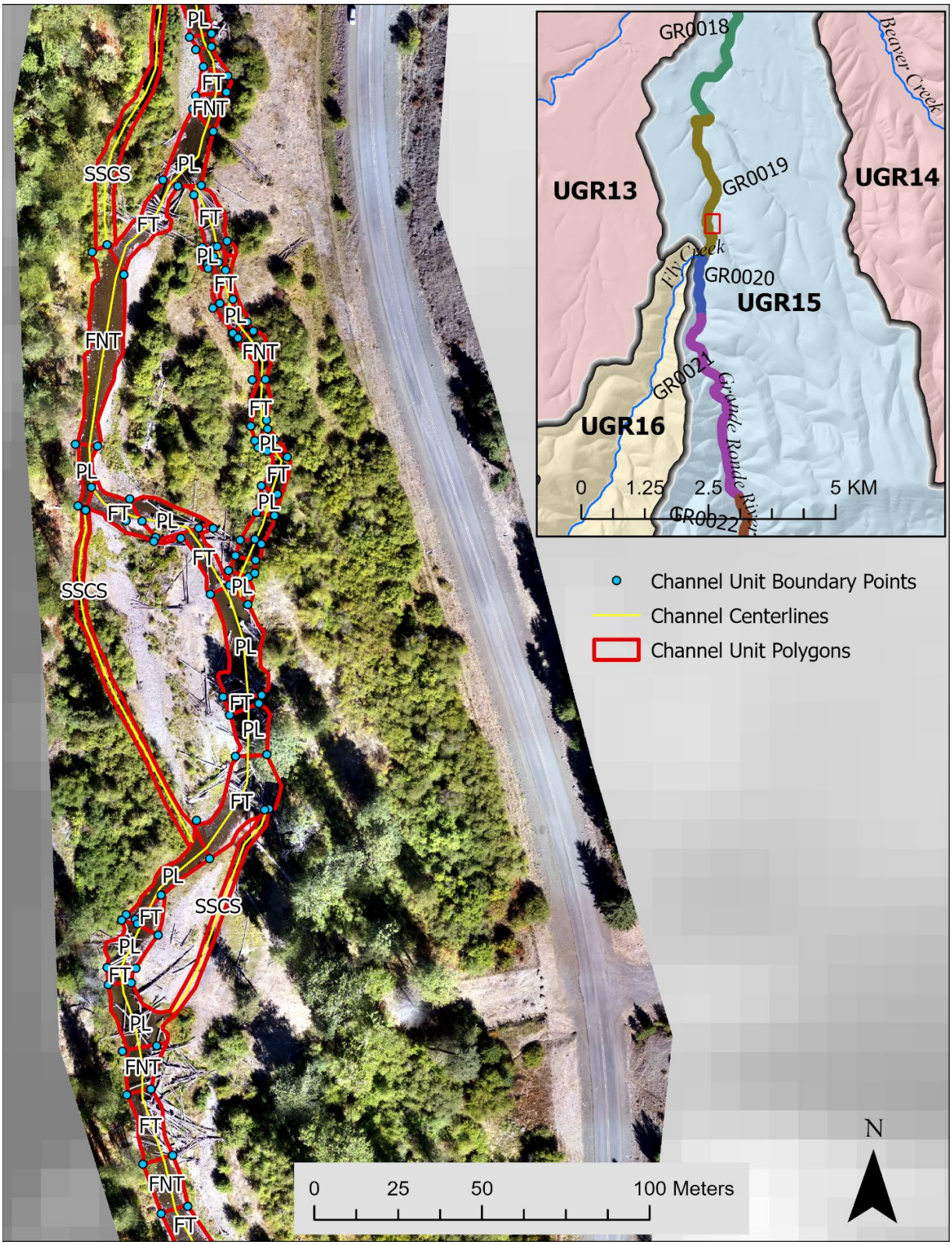

Figure 4. Example of spatial data collected within each survey segment including the unmanned aircraft system (UAS) orthomosaic, channel unit boundary points and polygons and channel centerlines.

Table 2. Description of stream habitat metrics derived from the Tributary Habitat Assessment Protocol.

Primary metric type	Secondary metric type	Metric	Description	Data source
Habitat quality/ diversity	Floodplain/ side channels	River complexity index (*RCI*)	River complexity index (RCI) = S*(1+J) where S = stream sinuosity, J = # of side channel junctions (Brown 2002)	Field/LiDAR/ UAS
	Floodplain/ side channels	Side channel ratio (*SCRatio*)	Length of side channels divided by length of main channel during base flow (Beechie et al. 2017)	Field/LiDAR/ UAS
	Riparian condition	Riparian tree cover (*RipTreeCov*)	Average percent tree canopy cover in the riparian zone (50 m stream buffer)	UAS/LiDAR
	Riparian condition	Riparian tree height (*RipTreeHt*)	Average tree height (m) in the riparian zone (50 m stream buffer)	UAS/LiDAR
	Riparian condition	*Riparian vegetation departure index (*RVD*)	Average percentage departure of current vegetation from simulated historical vegetation reference conditions in the riparian zone (Macfarlane et al. 2017)	Satellite/ Modeled
	Riparian condition	Normalized difference vegetation index (*NDVI*)	Average NDVI index in the riparian zone (50 m stream buffer) calculated as the ratio between visible and near-infrared reflectance of vegetation cover (Bhandari et al. 2012). NDVI is used as an index of vegetation greenness or health.	UAS/ Satellite
	River channel (cover)	Large wood area percentage (*LWAreaPct*)	Percentage of stream surface area covered by large wood during base flow.	UAS/LiDAR
	River channel (cover)	Large wood frequency bankfull (*LWFreqBF*)	Number of large wood pieces (> 3m length and 0.15 m diameter) within the bankfull channel per 100 m stream length (Moore et al. 2019)	Field
	River channel (cover)	Large wood frequency wetted (*LWFreqWet*)	Number of large wood pieces (> 3m length and 0.15 m diameter) within the wetted channel during base flow per 100 m stream length	Field
	River channel (cover)	Overhanging vegetation cover (*OverVegCov*)	Percentage of stream surface area covered by vegetation during base flow	UAS/LiDAR
	River channel (cover)	Undercut bank percentage (*UcutBankPct*)	Percentage of the total bank length that is undercut	Field/UAS

Primary metric type	Secondary metric type	Metric	Description	Data source
	River channel (pools)	Residual pool depth (*PoolResidDpth*)	Mean residual pool depth (max depth – pool tail depth in meters; Mossop and Bradford 2006)	Field/LiDAR
	River channel (pools)	Large pool frequency (*PoolFreqLg*)	Number of large pools (> 20 m² area and > 0.80 m max depth) per km stream length (McIntosh et al. 2000)	Field/UAS/ LiDAR
	River channel (pools)	Medium pool frequency (*PoolFreqMd*)	Number of medium- or larger-sized pools (> 20 m² area and > 0.50 m max depth) per km stream length	Field/UAS/ LiDAR
	River channel (substrate)	Median sediment particle size (*D50*)	Median sediment particle size on the streambed surface in riffles (Wolman 1954)	Field
	Water quality	*Coldwater refuge density (*ColdRefDen)*	Number of cold-water refuges per km stream length (Dugdale et al. 2015)	FLIR
	Water quality	Maximum weekly maximum temperature (*MWMT*)	Maximum 7-day running average of daily maximum temperature (EPA 2003)	Field/Modeled
	Water quality	*Observed/Expected benthic macroinvertebrates (*O/E*)	Ratio of observed to expected (O/E) benthic macroinvertebrate taxa as predicted by the River Invertebrate Prediction and Classification System (RIVPACS, Hawkins et al. 2000)	Field
Habitat quantity	Floodplain/ side channels	Off-channel habitat base flow (*OCHabBase*)	Surface area (m²) of connected off-channel habitat (alcoves, backwaters, and side channels) during base flow	LiDAR/UAS
	Floodplain/ side channels	Side channel length (*SCLength*)	Length (m) of side channels during base flow	Field/UAS
	River channel (fast water)	Fast water area (*FastArea*)	Surface area (m²) of fast water habitat (e.g., fast turbulent, fast non-turbulent, fast small side channels) during base flow	Field/UAS
	River channel (total length)	Main channel length (*MCLength*)	Length (m) of main channel habitat during base flow	Field/UAS
	River channel (pools)	Slow water area (*SlowArea*)	Surface area (m²) of slow water habitat (e.g., pools, off-channel units, slow small side channels) during base flow	Field/UAS

References

Atlas partners. 2015. Atlas implementation guidelines - Catherine Creek and upper Grande Ronde River. Page 17. https://www.grmw.org/static/documents/atlas/Atlas%20Implementation%20Guidelines%20(6-8-15).pdf

Beechie, T. J., O. Stefankiv, B. Timpane-Padgham, J. E. Hall, G. R. Pess, M. Rowse, M. Liermann, K. Fresh, and M. J. Ford. 2017. Monitoring Salmon Habitat Status and Trends in Puget Sound: Development of Sample Designs, Monitoring Metrics, and Sampling Protocols for Large River, Floodplain, Delta, and Nearshore Environments. U.S. Department of Commerce, NOAA Technical Memorandum NMFSNWFSC-137. https://doi.org/10.7289/V5/TM-NWFSC-137.

Bhandari, A. K., A. Kumar, and G. K. Singh. 2012. Feature Extraction using Normalized Difference Vegetation Index (NDVI): A Case Study of Jabalpur City. Procedia Technology 6:612–621.

Brown, A. G. 2002. Learning from the past: palaeohydrology and palaeoecology. Freshwater Biology 47(4):817–829.

CHaMP (Columbia Habitat Monitoring Program). 2016. Scientific protocol for salmonid habitat surveys within the Columbia Habitat Monitoring Program.

Dugdale, S. J., N. E. Bergeron, and A. St-Hilaire. 2015. Spatial distribution of thermal refuges analysed in relation to riverscape hydromorphology using airborne thermal infrared imagery. Remote Sensing of Environment 160:43–55.

EPA (U.S. Environmental Protection Agency). 2003. EPA region 10 guidance for Pacific Northwest state and tribal temperature water quality standards. Page 49. U.S. Environmental Protection Agency, EPA 910-B-03-002, Region 10 Office of Water, Seattle, Washington.

Hawkins, C. P., R. H. Norris, J. N. Hogue, and J. W. Feminella. 2000. Development and evaluation of predictive models for measuring the biological integrity of streams. Ecological Applications 10(5):1456–1477.

Justice, C., L. Burns, S. White. 2020. Tributary Habitat Assessment Protocol v2.0. Monitoring Resources.org. http://www.monitoringresources.org/Document/Protocol/Details/3554

Macfarlane, W. W., J. T. Gilbert, M. L. Jensen, J. D. Gilbert, N. Hough-Snee, P. A. McHugh, J. M. Wheaton, and S. N. Bennett. 2017. Riparian vegetation as an indicator of riparian condition: Detecting departures from historic condition across the North American West. Journal of Environmental Management 202:447–460.

McIntosh, B. A., J. R. Sedell, R. F. Thurow, S. E. Clarke, and G. L. Chandler. 2000. Historical changes in pool habitats in the Columbia River basin. Ecological Applications 10(5):1478.

Moore, K., K. Jones, J. Dambacher, C. Stein, and et al. 2019. Aquatic Inventories Project: methods for stream habitat and snorkel surveys. Page 89. Oregon Department of Fish and Wildlife, Version 29.1, Corvallis, OR.

Mossop, B., and M. J. Bradford. 2006. Using thalweg profiling to assess and monitor juvenile salmon (*Oncorhynchus* spp.) habitat in small streams. Canadian Journal of Fisheries and Aquatic Sciences 63(7):1515–1525.

U.S. Department of Agriculture (USDA). 2018. Stream inventory handbook Level I and II. Page 142. U.S. Department of Agriculture, Forest Service, Pacific Northwest Region, Region 6, Version 2.18.

U.S. Geological Survey (USGS), U.S. Department of Agriculture – Natural Resource Conservation Service (NRCS), U.S. Environmental Protection Agency (EPA), et al. 2015. National Watershed Boundary Dataset (WBD). Downloaded as part of the NHDPlus HR dataset from https://www.usgs.gov/core-science-systems/ngp/national-hydrography/access-national-hydrography-products on 6/16/2020.

U.S. Geological Survey (USGS). 2016. BETA - USGS National Hydrography Dataset Plus High Resolution (NHDPlus HR) Best Resolution for HU4-0101 (Subregion) Publication Date 20160512 HU-4 Subregion FileGDB 10.1. Downloaded from https://www.usgs.gov/core-science-systems/ngp/national-hydrography/access-national-hydrography-products on 6/16/2020.

Wolman, M. G. 1954. A method of sampling coarse river-bed material. Transaction of the American Geophysical Union 35:951–956.

Water Temperature

Background

CRITFC has maintained an extensive network of year-round water temperature loggers in the Grande Ronde basin since 2009 with the goal of tracking long-term trends in water temperature related to land use, restoration, and climate change. These data have also been used to develop fish-habitat relationships and parameterize water temperature models such as Heat Source. Temperature data has also been shared widely with basin partners and others to aid in assessment of site-specific restoration effectiveness or development of large-scale temperature models (e.g., NorWeST, DEQ TMDL).

Methods

CRITFC actively maintains 83 year-round water temperature sites in the upper Grande Ronde, Catherine Creek, and Minam River watersheds, but has monitored up to 192 sites in past years (Figure 5). Additionally, we maintain a database of external agency temperature loggers for data collected between 1988 and 2017 totaling 452 unique sites. External agencies included the Bureau of Land Management (BLM), CTUIR, Oregon Department of Environmental Quality (DEQ), GRMW, Nez Perce Tribe, ODFW, Oregon Water Resources Department (OWRD), Union Soil and Water Conservation District (USWCD), USFS, and U.S. Geological Survey (USGS). In 2023, we installed 22 new loggers in the Meadow Creek watershed during July to ensure adequate coverage for effectiveness monitoring of planned watershed-scale restoration work beginning in 2027. We visited all active sites during fall (late September to early October) to download data, check the status of logger batteries, and assess deployment conditions.

Raw hourly temperature measurements were checked for errors using a combination of automated and manual/visual inspection QAQC routines. Any hourly measurements that exceeded 30 °C, were less than -1 °C, had an absolute hourly change > 3 °C, or had an absolute field audit temperature difference > 0.5 °C were flagged as potential errors and were subsequently verified manually by CRITFC staff. For each temperature monitoring site, we generated a suite of daily, weekly, and annual water temperature metrics using SQL scripts within CRITFC's centralized database management system (CDMS) that describe key components of stream thermal regimes (e.g., magnitude, variability, frequency, duration, and timing) using guidance from Heck et al. (2018) (Table 3). To avoid errors associated with missing data, metrics were only

computed for sites that had valid measurements for at least 90% of the total possible records for a given time period as per Isaak et al. (2017).

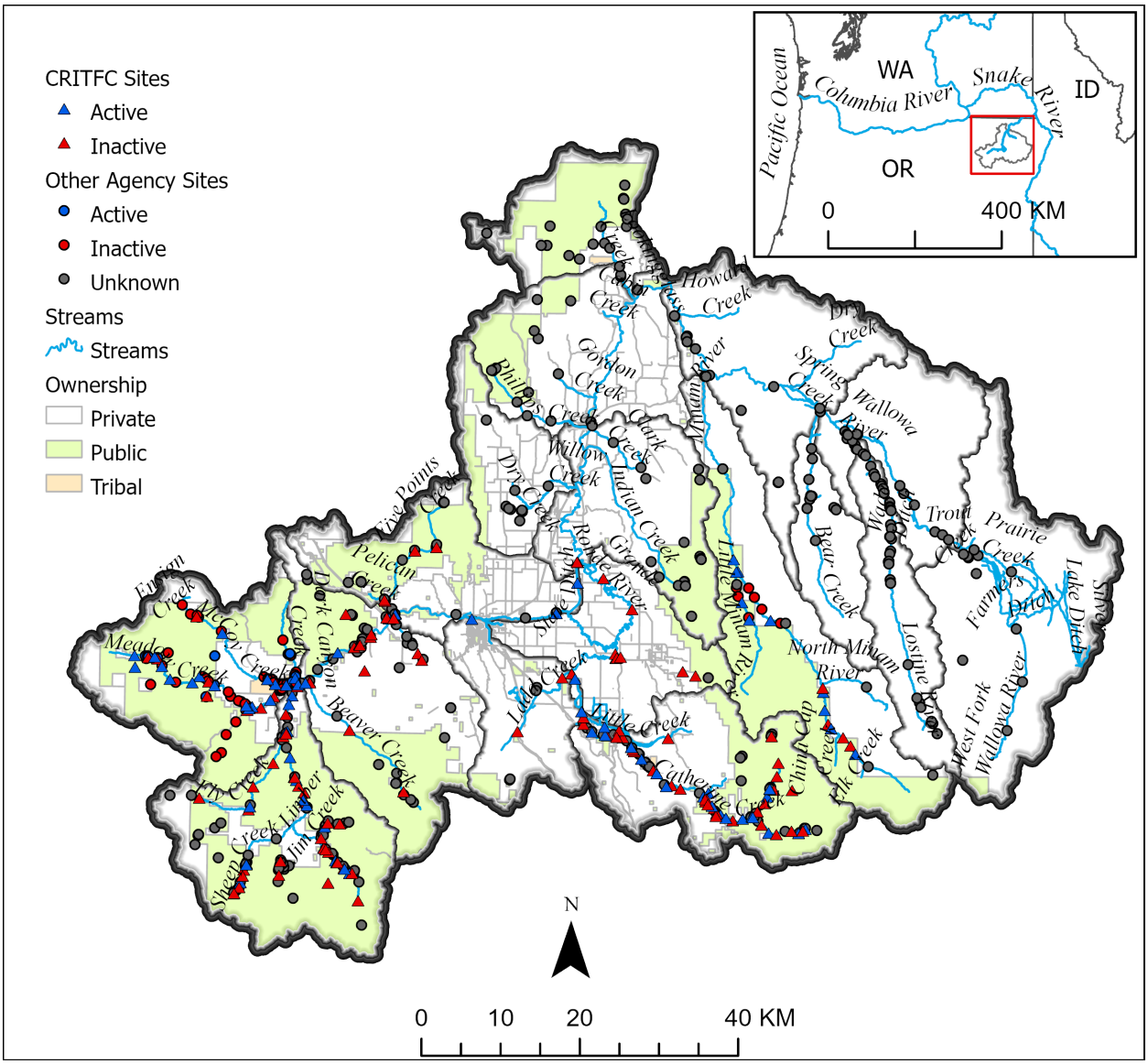

Figure 5. Water temperature monitoring sites in the Grande Ronde River basin from 1988 to 2023.

Table 3. Annual water temperature metrics calculated in the CRITFC water temperature database. Metrics based on Heck et al. (2018) with some additions.

Category	Metric	Definition
Magnitude (°C)	*Maximum*	Warmest temperature of the year
	MWMT	Maximum Weekly Maximum Temperature (i.e., highest 7-day average of daily maximum temperatures in summer [Jul. 1 - Aug. 31])
	MWAT	Maximum Weekly Average Temperature (i.e., highest 7-day average of daily mean temperatures in summer [Jul. 1 - Aug. 31])
	DegreeDays	Sum of daily mean temperatures > 0 °C in a year
	JuneAvg	Average of daily mean temperatures in June
	JulyAvg	Average of daily mean temperatures in July
	AugAvg	Average of daily mean temperatures in August
	SeptAvg	Average of daily mean temperatures in September
Variability (°C)	*MeanRange*	Difference between the highest and lowest daily mean temperature in a year
	MaxRange	Difference between the highest and lowest daily maximum temperature in a year
	MeanVariance	A statistical measure of deviations from the mean among daily mean temperatures in a year
	MaxVariance	A statistical measure of deviations from the mean among daily maximum temperatures in a year
Frequency (n)	*Days16*	Number of days in a year where the daily maximum temperature exceeded 16 °C
	Days18	Number of days in a year where the daily maximum temperature exceeded 18 °C
	Days20	Number of days in a year where the daily maximum temperature exceeded 20 °C
Duration (n)	*CD16*	Consecutive number of days in a year where daily maximum temperature exceeded 16 °C
	CD18	Consecutive number of days in a year where daily maximum temperature exceeded 18 °C
	CD20	Consecutive number of days in a year where daily maximum temperature exceeded 20 °C
Timing	*CTD50_Day*	Day of year of attaining 50% of the cumulative degree days in a given year
	CTD75_Day	Day of year of attaining 75% of the cumulative degree days in a given year

Results

Maximum weekly maximum temperatures (*MWMT*) followed a typical warming trend in the downstream direction among the four rivers we examined (Figure 6). The Lostine River was coolest overall (range = 13.6 – 21.7 °C, mean = 18.3 °C, years 1995-2022), followed by the Minam River (range = 13.1 – 26.8 °C,

mean = 20.1 °C, years 1995-2023), Catherine Creek (range = 17.2 – 27.7 °C, mean = 21.9 °C, years 1991-2023) and finally the upper Grande Ronde River (range = 12.4 – 30.4 °C, mean = 23.8 °C, 1991-2023). Peak temperatures in the upper Grande Ronde River exhibited rapid warming from the headwaters (~ rkm 290) downstream about 30 km to the outlet of Vey Meadows (~ rkm 264) below which temperatures were near or exceeded the upper incipient lethal limit for Chinook Salmon of 25 °C (McCullough et al. 2001). Many of the tributaries entering the upper Grande Ronde River and Catherine Creek provided substantially cooler temperatures than the adjoining mainstem such as Little Catherine Creek, Rock Creek, Jordan Creek, Beaver Creek, Fly Creek, and Clear Creek, though *MWMT* tended to be more variable among years in many of these tributaries.

Maximum weekly temperatures averaged over the most recent 10 years (2013-2022) were generally coolest in higher elevation sites near the headwaters and within Wallowa River basin drainages compared with sites in the upper Grande Ronde basin (Figure 7). Of the 241 sites across the upper Grande Ronde and Wallowa River basins with valid MWMT measurements, 181 (75%) exceeded the EPA temperature standard of 18 °C for non-core juvenile salmonid rearing habitat (EPA 2003) and 70 (29%) exceed the upper incipient lethal limit for Chinook Salmon of 25 °C.

Variance of daily maximum temperatures within a year was notably higher in the upper Grande Ronde River and its lower-elevation tributaries (Rock, Meadow, Fly and Beaver Creeks) compared with the other rivers of interest, particularly downstream of Vey Meadows (~ rkm 264; Figure 8). In contrast, daily max temperatures were relatively stable in the Lostine River and middle to upper portions of the Minam River, and moderately variable in Catherine Creek. Similar to *MWMT*, temperature variance generally increased in a downstream direction, although there was some deviation from this trend, especially in the Lostine River where temperature variance was generally low throughout and in portions of the upper Grande Ronde River (e.g., middle upper Grande Ronde canyon from Vey Meadows down to Fly Creek [rkm 264 – 252]).

The frequency of days in which water temperatures exceeded 18 °C followed similar patterns as *MWMT* (e.g., high in upper Grande Ronde (range = 0 – 114 days; mean = 60.9 days), moderate in Catherine Creek (range = 0 – 107 days, mean = 51.1 days) and low in Lostine (range = 0 – 62 days, mean = 20.6 days) and Minam (range = 0 – 87 days, mean = 30.8 days; Figure 9). As with the other temperature metrics, the number of days exceeding 18 °C increased in a downstream direction and was 0 or near 0 in the upper portions of Lostine and Minam Rivers.

The duration of high temperature exposure, expressed as the consecutive number of days exceeding 18 °C, also increased in magnitude and variability from upstream to downstream and was highest in the upper Grande Ronde River (Figure 10). The median number of consecutive days over 18 °C in the upper Grande Ronde exceeded 50 at most locations downstream of Vey Meadows (rkm 264), which highlights the extreme challenges that cold-water fishes face with the current thermal regime in this system.

In contrast with the other temperature metrics we examined, the day of year that the cumulative degree days achieved the 50th percentile (*CTD50_Day;* a measure of timing of thermal accumulation) did not exhibit a consistent longitudinal trend across rivers (Figure 11). The *CTD50_Day* in the upper Grande Ronde and Lostine rivers appeared to occur earlier in a downstream direction, consistent with earlier snowmelt in lower elevation portions of the watersheds. However, *CTD50_Day* in Catherine Creek and Minam River varied somewhat across sites with no apparent longitudinal trend along the river corridor. Water temperatures warmed earlier on average in the upper Grande Ronde River (*CTD50_Day* range = 193 – 221 [July 12 – Aug 9], mean = 206 [July 25]), compared with Catherine Creek (range = 192 – 248 [July 11 – September

5], mean = 208 [July 27]), Minam River (range = 202 – 220 [July 21 – August 8], mean = 211 [July 30], and Lostine River (range = 200 – 224 [July 19 – August 12], mean = 212 [July 31], though the differences were minor. A map of *CTD50_Day* across the whole watershed (Figure 12) revealed substantially earlier warming in lower elevation tributaries like Meadow Creek and Rock Creek consistent with more rapid snow melt and earlier declines in the hydrograph.

Temporal patterns in peak summer temperatures across selected sites in the upper Grande Ronde River mainstem since 1992 exhibited similar interannual variations across sites but no overall trends (positive or negative) were apparent (Figure 13). *MWMT* reached a high point around 2005-2007, declined to a low point around 2010-2011 and then steadily increased to another high point around 2015. Temperatures have remained near that high level since 2015. It is likely that changes in water temperature in the Grande Ronde basin over last the 30 years will differ substantially by river and the history of land use and degradation/restoration in a given area. Additionally, some aspects of a river's thermal regime (i.e., magnitude, variation, timing, frequency, and duration) may vary substantially over time, while others may not. We intend to do a more in-depth exploration of these temporal trends in the 2024 annual report.

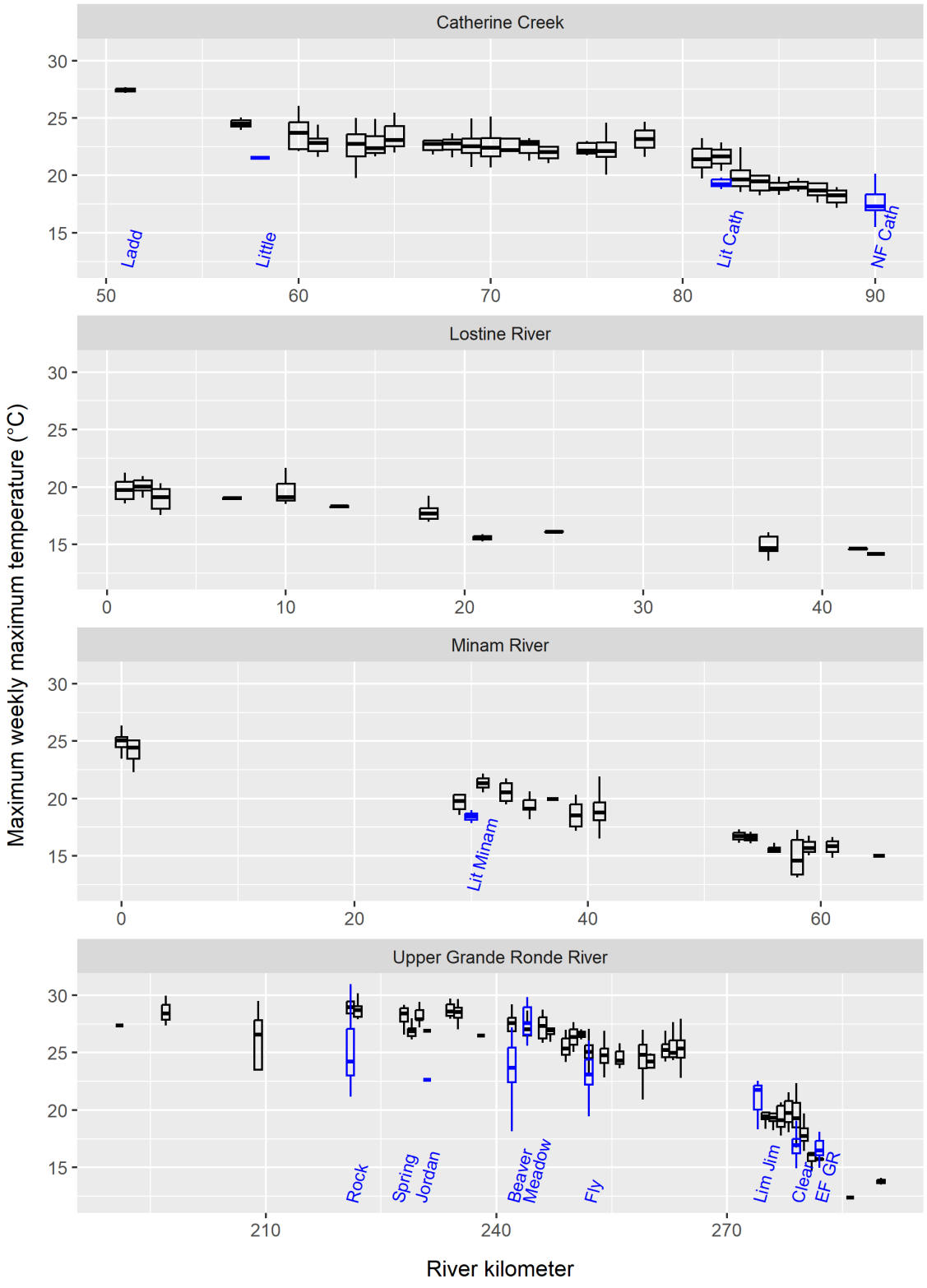

Figure 6. Maximum weekly maximum water temperature (°C) in Catherine Creek (1992-2023), Lostine River (1999-2021), Minam River (1997-2023), upper Grande Ronde River (upstream of Catherine Creek; 1992-2023) and mouths of associated tributaries (shown in blue).

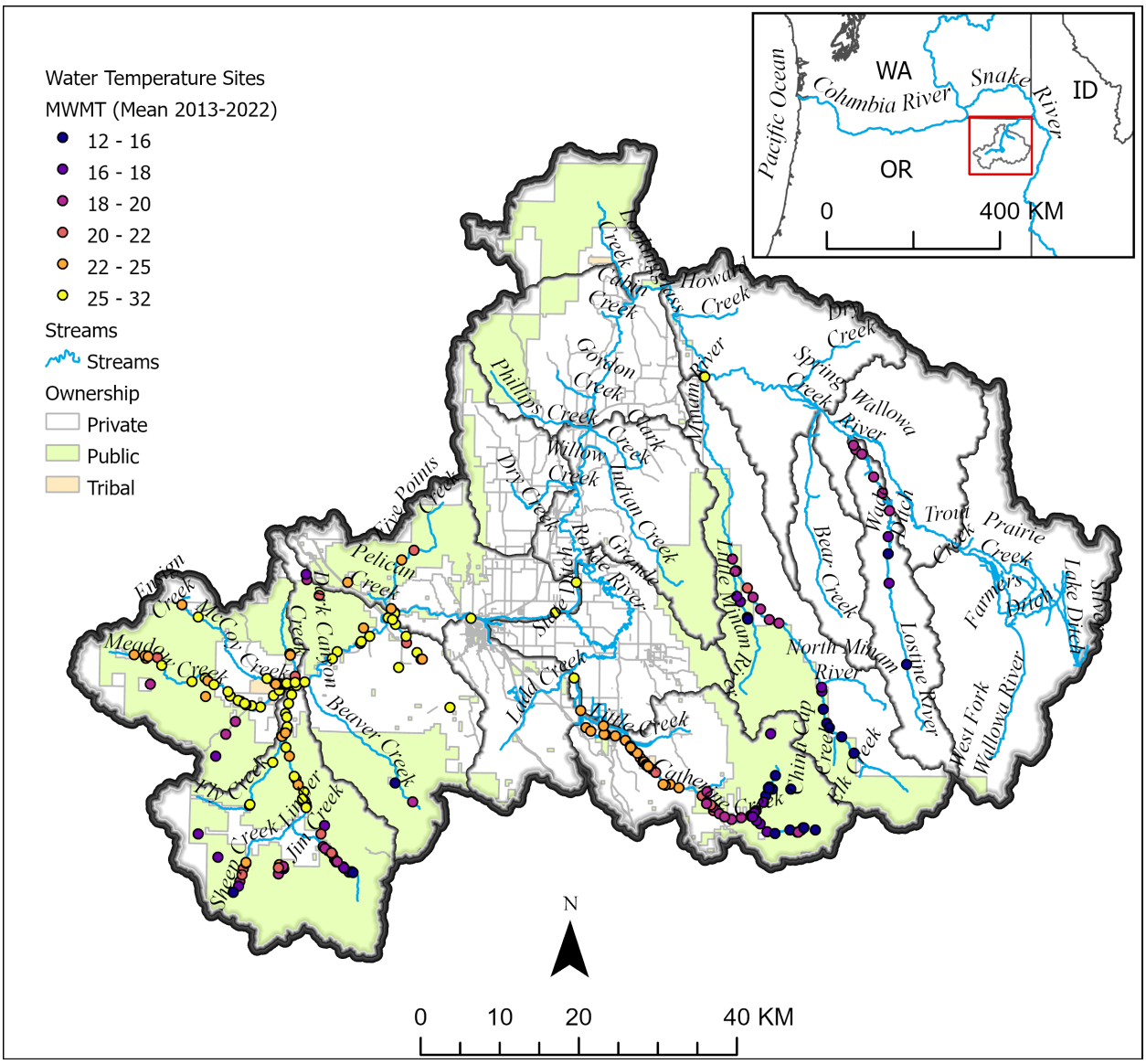

Figure 7. Ten-year average (2013-2022) of maximum weekly maximum water temperatures (°C) at 241 sites in the upper Grande Ronde River and Wallowa River basins.

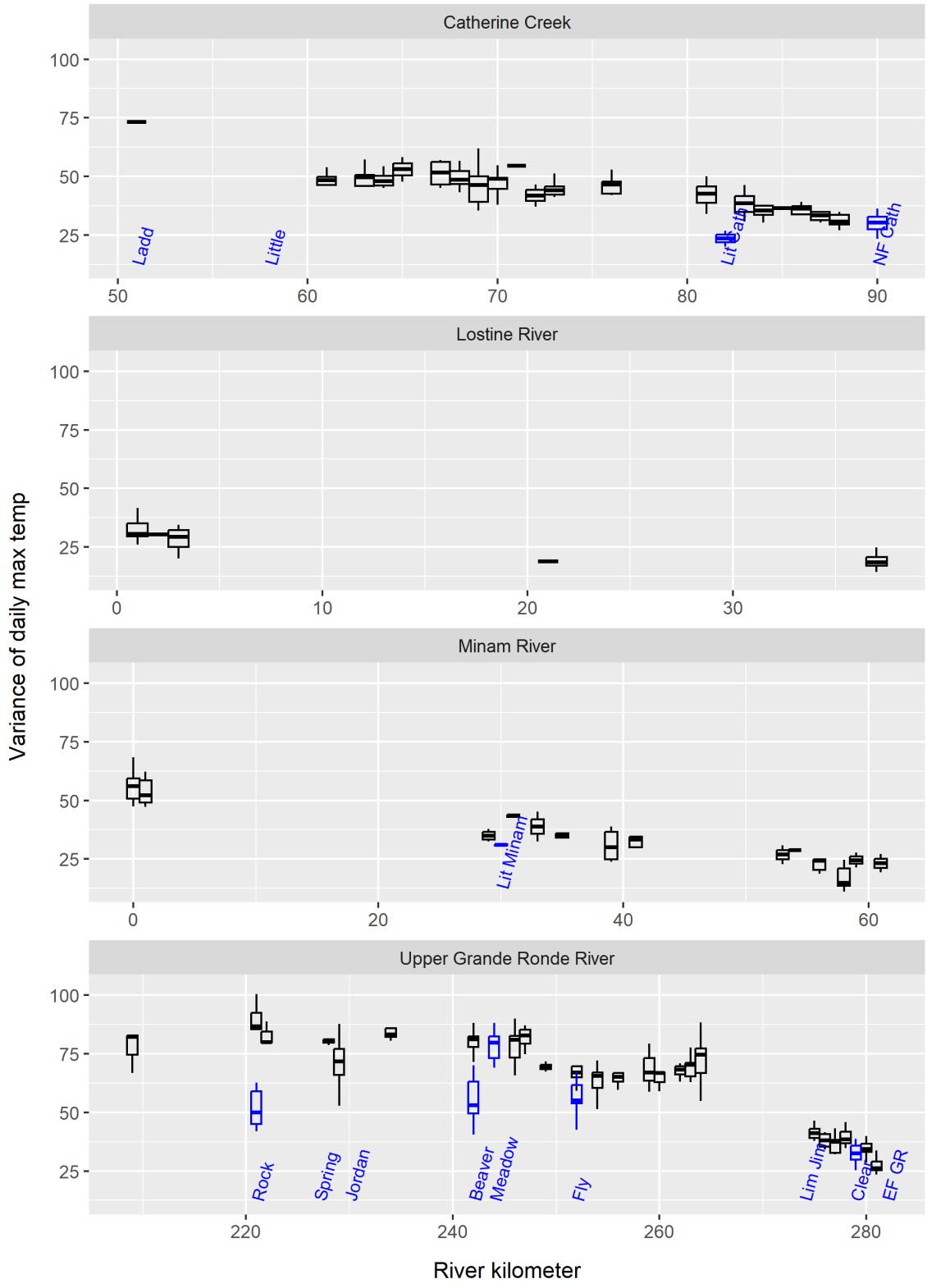

Figure 8. Variance of daily maximum water temperatures in Catherine Creek (1999-2022), Lostine River (2001-2021), Minam River (2003-2022), upper Grande Ronde River (upstream of Catherine Creek; 1999-2022) and mouths of associated tributaries (shown in blue).

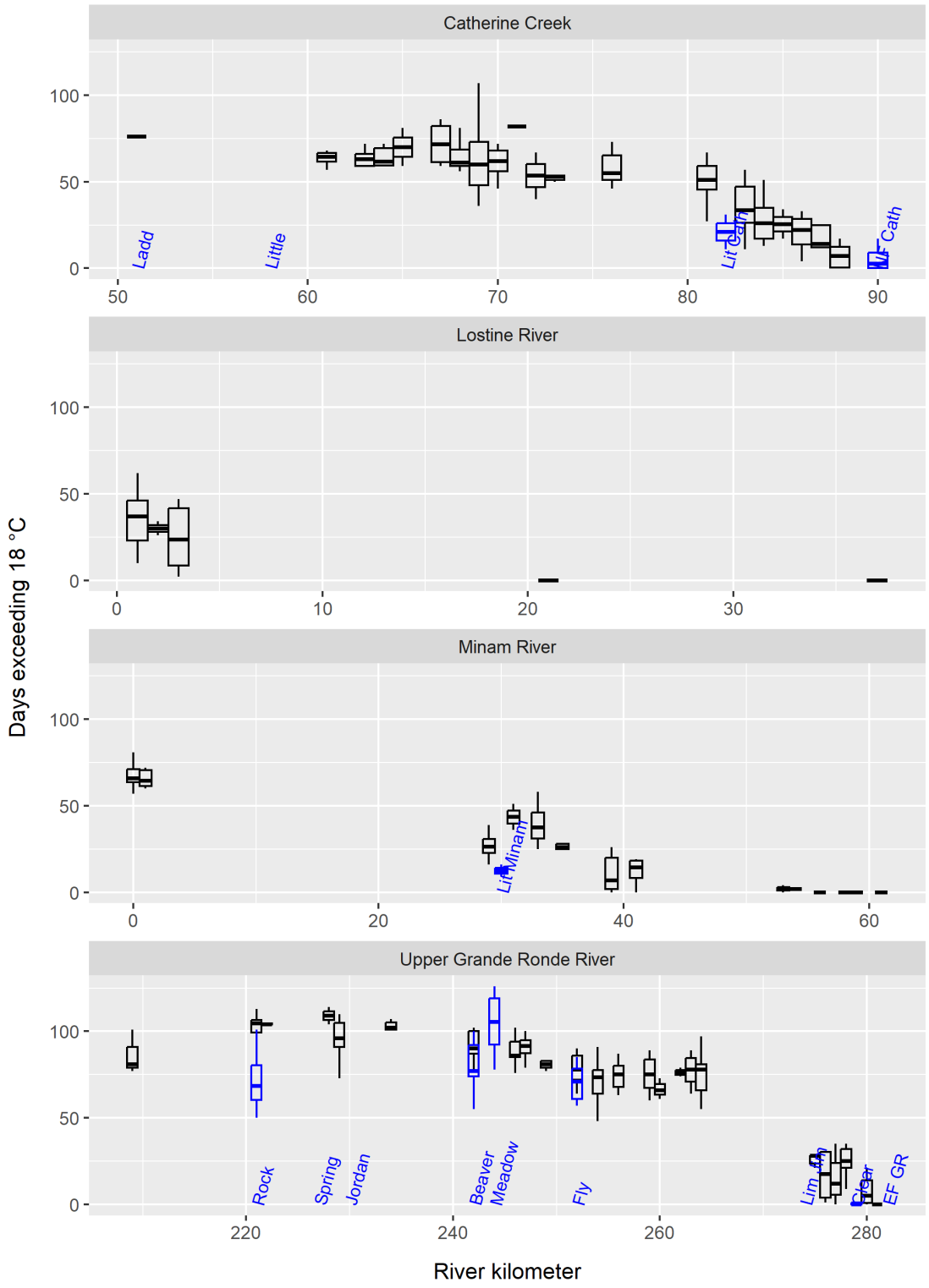

Figure 9. Number of days exceeding 18 °C in Catherine Creek (1999-2022), Lostine River (2001-2021), Minam River (2003-2022), upper Grande Ronde River (upstream of Catherine Creek; 1999-2022) and mouths of associated tributaries (shown in blue).

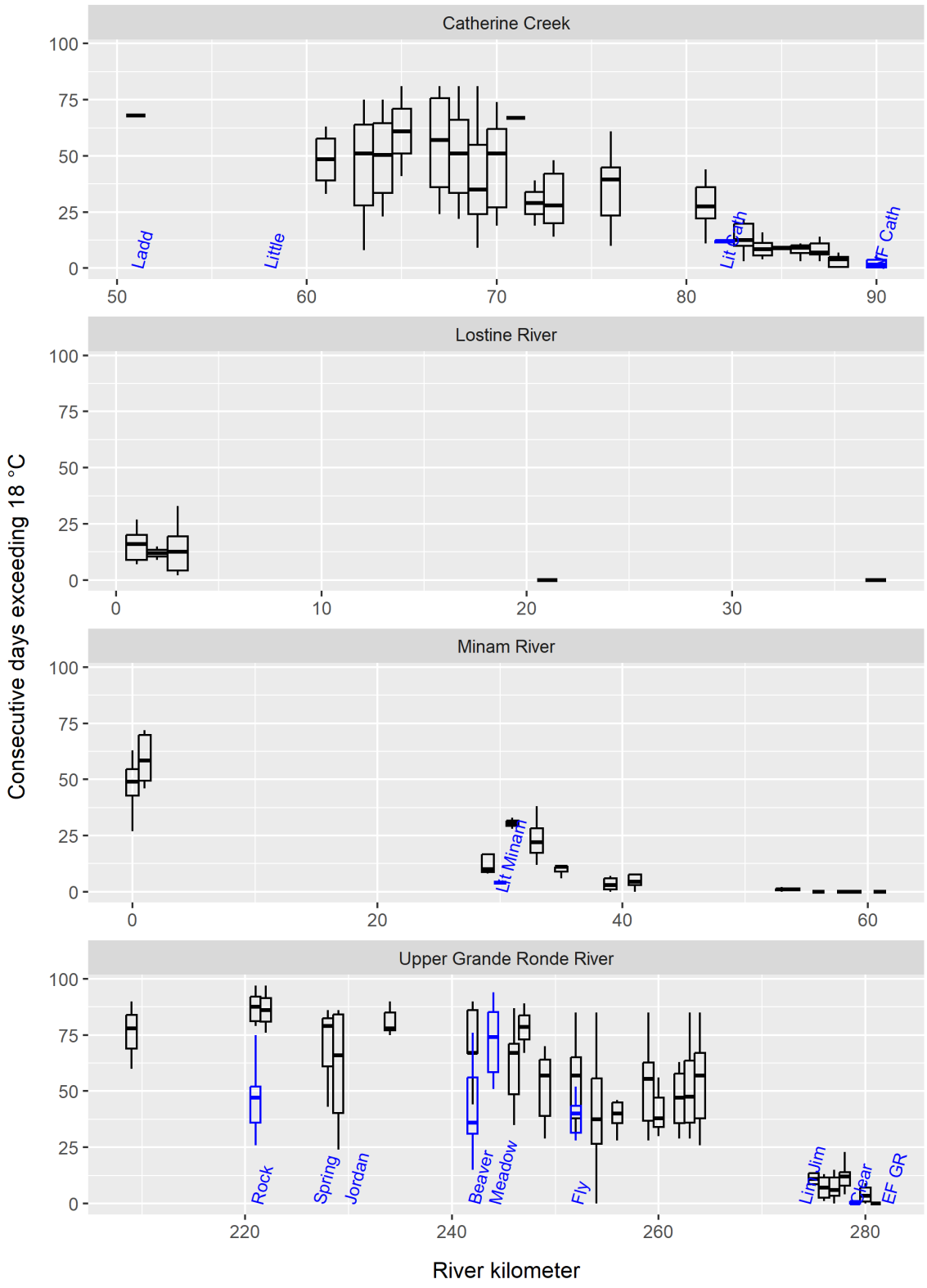

Figure 10. Number of consecutive days exceeding 18 °C in Catherine Creek (1999-2022), Lostine River (2001-2021), Minam River (2003-2022), upper Grande Ronde River (upstream of Catherine Creek; 1999-2022) and mouths of associated tributaries (shown in blue).

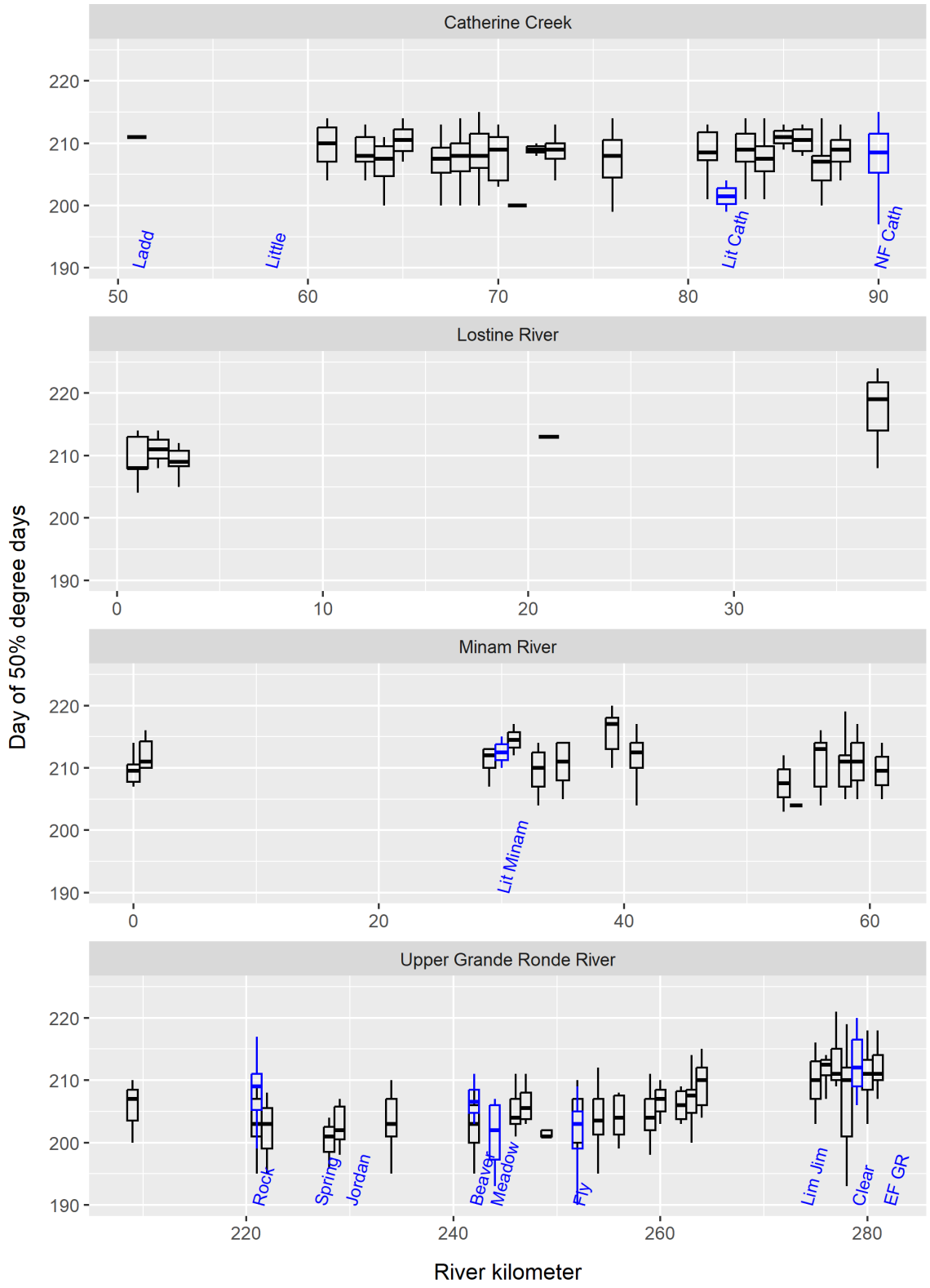

Figure 11. Day of the year that 50% of the cumulative degree days was attained in Catherine Creek (1999-2022), Lostine River (2001-2021), Minam River (2003-2022), upper Grande Ronde River (upstream of Catherine Creek; 1999-2022) and mouths of associated tributaries (shown in blue).

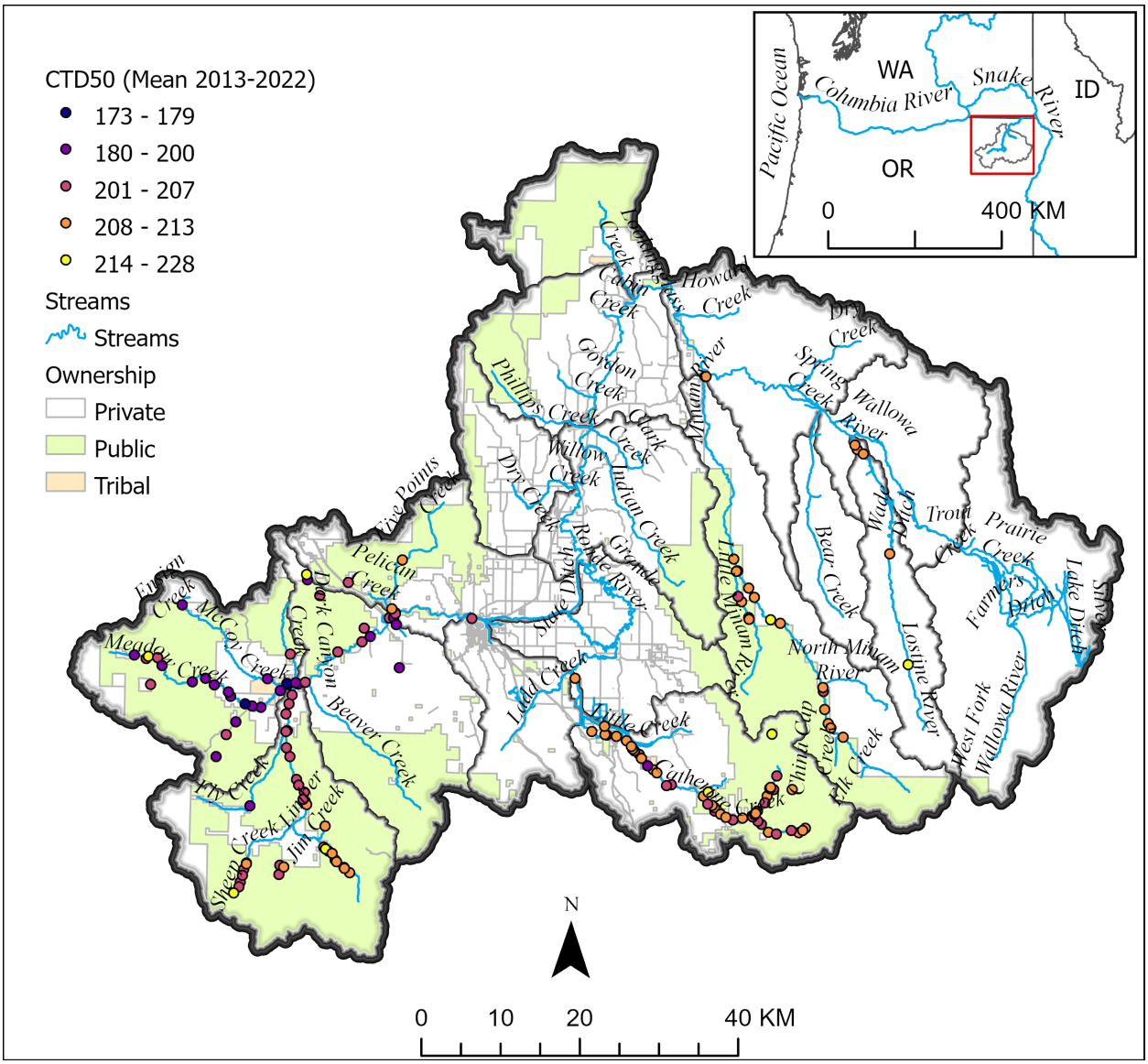

Figure 12. Ten-year mean (2013-2022) of the day of the year that 50% of the cumulative degree days was attained (CTD50) at 152 sites within the upper Grande Ronde River and Wallowa River basins.

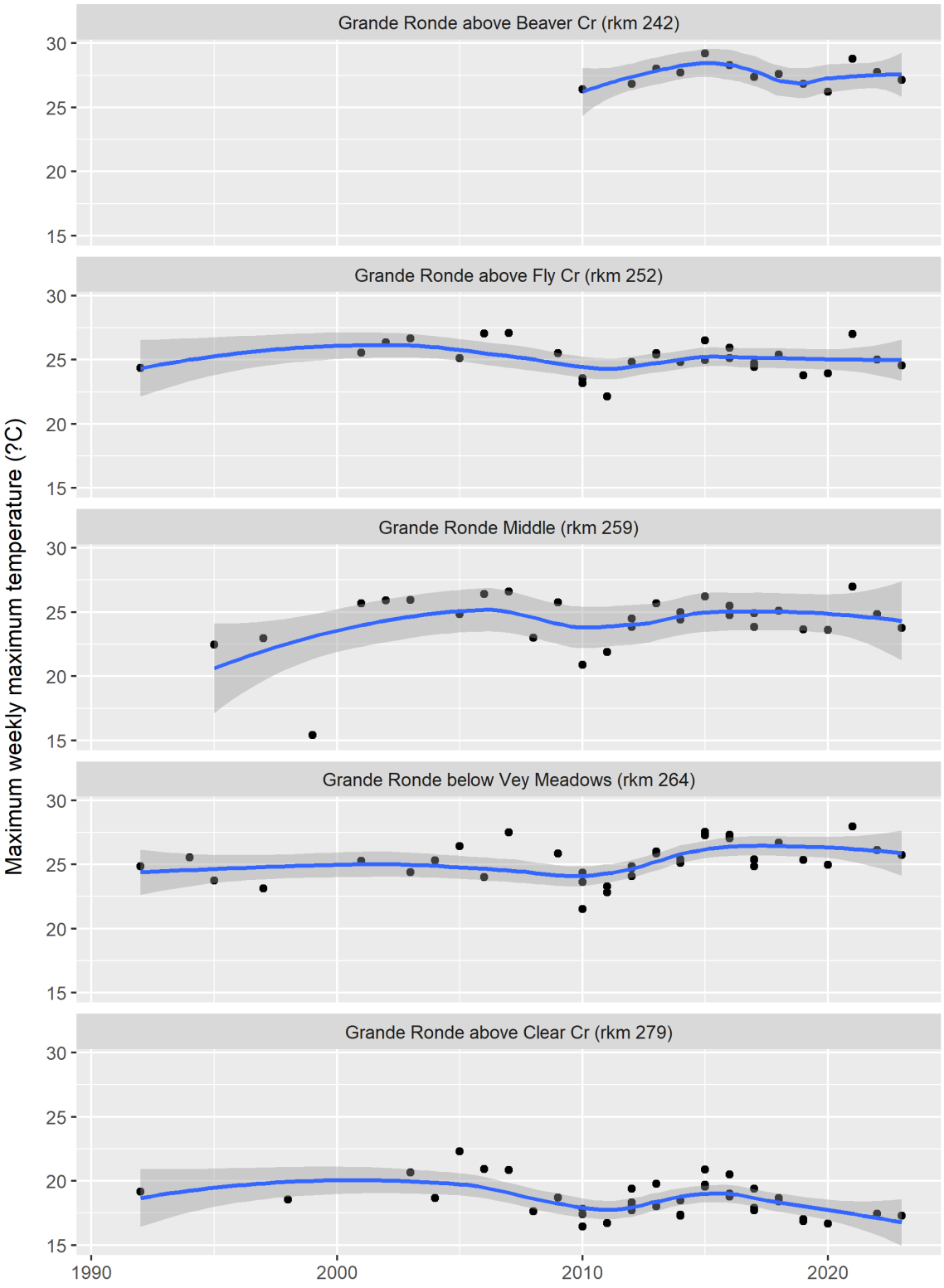

Figure 13. Temporal trends in maximum weekly maximum water temperature (°C) at selected locations along the upper Grande Ronde River. Blue lines represent locally estimated scatterplot smoothing (LOESS) lines and gray ribbons represent 95% confidence intervals. Temperature data for these plots was collected by the USFS and CRITFC.

References

Heck, M. P., L. D. Schultz, D. Hockman-Wert, E. C. Dinger, and J. B. Dunham. 2018. Monitoring stream temperatures—A guide for non-specialists. Page 76 U.S. Geological Survey Techniques and Methods, book 3, chapter A25.

EPA (U.S. Environmental Protection Agency). 2003. EPA region 10 guidance for Pacific Northwest state and tribal temperature water quality standards. Page 49. U.S. Environmental Protection Agency, EPA 910-B-03-002, Region 10 Office of Water, Seattle, Washington.

Isaak, D. J., S. J. Wenger, E. E. Peterson, J. M. Ver Hoef, D. E. Nagel, C. H. Luce, S. W. Hostetler, J. B. Dunham, B. B. Roper, S. P. Wollrab, G. L. Chandler, D. L. Horan, and S. Parkes-Payne. 2017. The NorWeST Summer Stream Temperature Model and Scenarios for the Western U.S.: A Crowd-Sourced Database and New Geospatial Tools Foster a User Community and Predict Broad Climate Warming of Rivers and Streams: Stream climates in the Western U.S. Water Resources Research 53(11):9181–9205.

McCullough, D., S. Spalding, D. Sturdevant, and M. Hicks. 2001. Issue paper 5: summary of technical literature examining the physiological effects of temperature on salmonids. Page 113. U.S. Environmental Protection Agency, EPA-910-D-01-005.

Objective A-3: Set target values for limiting factors and calculate habitat condition across the upper Grande Ronde basin

This sub-objective was completed for large wood and pool targets and was described in the 2022 Annual Report. Restoration targets for other limiting factors such as water temperature and off-channel habitats will require a different analytical approach and will likely rely on existing models and published literature (e.g., Heat Source-Justice et al. 2017, floodplain reconnection-Bond et al. 2019).

References

Bond, M. H., T. G. Nodine, T. J. Beechie, and R. W. Zabel. 2019. Estimating the benefits of widespread floodplain reconnection for Columbia River Chinook salmon. Canadian Journal of Fisheries and Aquatic Sciences 76(7):1212–1226.

Justice, C., S. M. White, D. A. McCullough, D. S. Graves, and M. R. Blanchard. 2017. Can stream and riparian restoration offset climate change impacts to salmon populations? Journal of Environmental Management 188:212–227.

Objective A-4: Habitat status assessment (LiDAR)

In summer 2020, CRITFC, in collaboration with GRMW and BPA, acquired topobathymetric ("green") LiDAR across 76,188 acres of the Grande Ronde River and Wallowa River watersheds, including tributaries currently or historically occupied by Chinook Salmon and steelhead. Data were collected by the contractor Quantum Spatial, Inc. (QSI, now NV5 Geospatial) and detailed results of imagery acquisition, QA/QC, image processing, and a list of post-processed deliverables are available in a report (NV5 Geospatial 2021) and presented in our 2020 annual report. We are in the process of developing procedures

and a workflow to describe spatially continuous instream fish habitat metrics and floodplain conditions, including developing and refining methods to classify large wood from LiDAR points and classify geomorphic channel units. In 2022, NV5 Geospatial presented a preliminary analysis focused on classifying large wood from the topobathymetric LiDAR point cloud data. Preliminary results from this work looked promising, but funding was lacking to support additional refinements of the method. We intend to follow up with NV5 in 2024 to determine whether they've made any progress on these analysis tools and how much it would cost to re-process the 2020 LiDAR dataset to include large wood classification. We began a change detection analysis in early 2024 comparing LiDAR data from 2009 and 2020 to assess how riparian vegetation and channel complexity has changed over time and in response to restoration actions. We hope to complete this analysis and report on the results in the 2024 annual report.

In September of 2021, we worked with NV5 Geospatial to delineate and classify geomorphic channel units within 13 previously surveyed sites in the upper Grande Ronde River using topobathymetric LiDAR data collected in 2020. This analysis utilized the Geomorphic Unit Tool (GUT) which was originally adapted from the geomorphic classification system described in Wheaton et al. (2015) and is publicly available from their website at https://gut.riverscapes.net/. Our intention was to test this methodology on a small subset of sites, assist NV5 with development of automated protocols for many of the steps in GUT, and then apply it to the whole watershed if results proved useful. Overall findings from this work indicated that the GUT tool did a good job of identifying pool habitats but tended to overrepresent glide habitats and underrepresent riffle habitats compared with ground-based habitat surveys using methods such as CHaMP. The tool also tended to split micro-habitats into separate units, whereas most ground-based protocols would have lumped more of these micro-habitats into a contiguous unit. NV-5 determined that additional work would be needed to develop scalable automation procedures for delineation of primary and secondary channel thalweg lines, which are required inputs to the GUT tool. While this work looks promising, we did not have an immediate use in mind for a full watershed-scale GUT analysis and have therefore not pursued future refinements of these methods with NV5 or other contractors. However, if additional topobathymetric surveys are completed in the future, it would be useful to use GUT to assess change in channel unit composition and diversity over time and in response to restoration. A report documenting this work (NV5 Geospatial 2022) is provided in Appendix C.

References

NV5 Geospatial. 2021. Grande Ronde basin, Oregon, Topobathymetric Lidar Technical Data Report. Page 36. NV5 Geospatial, powered by Quantum Spatial, Corvallis, OR.

NV5 Geospatial. 2022. Grande Ronde Geomorphic Unit Tool Analysis. Page 13. NV5 Geospatial, powered by Quantum Spatial, Corvallis, OR.

Wheaton, J. M., K. A. Fryirs, G. Brierley, S. G. Bangen, N. Bouwes, and G. O'Brien. 2015. Geomorphic mapping and taxonomy of fluvial landforms. Geomorphology 248:273–295.

Objective A-5: Meadow Creek aquatic habitat and biota data synthesis

This objective is funded by the U.S. Forest Service's (USFS) Pacific Northwest Research Station and provides in-kind support to this contract. Meadow Creek is a tributary of the upper Grande Ronde River with much of Meadow Creek's watershed managed by the USFS. Additionally, Starkey Experimental

Forest covers about 7.5 miles of the mainstem of Meadow Creek within the upper watershed. Meadow Creek is slated for a watershed-scale restoration project focusing on restoring ecosystem processes and improving habitat for native biota. In riparian terms, the planned restoration actions largely focus on floodplain reset or Stage-0 approaches. Extensive RM&E effort is planned by a collaborative group involving CRITFC, USFS, CTUIR, and ODFW to evaluate the response of aquatic biota relative to project objectives. An abundance of historical data exists for Meadow Creek with respect to prior restoration actions and their impacts to aquatic habitat and biota. However, much of that data remains unanalyzed and could provide valuable information to guide the forthcoming restoration and RM&E designs.

For this contract year, we focused on two main data sources. The first was historical outmigrant trap data and the second was habitat and snorkel data collected from 2011-2017 using the Columbia Habitat Monitoring Program (CHaMP) protocol. Our progress towards analyzing these data is summarized below.

Historical juvenile outmigrant trap data was collected in the Meadow Creek watershed across various locations by the USFS from 1987-2000. Preliminary QAQC checks have been made for the dataset in preparation for estimating trap efficiencies and abundances of out-migrating *O. mykiss* parr and smolt life stages. Work on historical outmigrant estimates will continue into 2024.

The CHaMP analysis is summarized below in manuscript form.

Starkey Experimental Forest Large Woody Debris Restoration and its Impacts to Aquatic Habitats and instream Biota

Background

Native migratory salmonids of the upper Grande Ronde River face a multitude of challenges ranging from extensive habitat degradation, high migration mortality through the dam-influenced reaches on the Columbia and Snake Rivers, and habitat constriction due to climate change (Mcintosh et al. 2000; White et al. 2017; Justice et al. 2017; ODFW 2020). Population-level declines in salmon and steelhead across the Columbia and Snake Rivers is well documented (Gresh et al. 2000). Snake River spring/summer run Chinook (*Oncorhynchus tshawytscha*) were listed in 1992 as an Endangered Species Act threatened species and Snake River summer Steelhead (*Oncorhynchus mykiss*) were listed as threatened in 1997 (NOAA Fisheries 2017).

The Grande Ronde River is a major tributary to the Snake River and supports threatened Chinook and Steelhead. Several studies have documented declining salmonid habitat conditions within the upper Grande Ronde River (UGR) basin, with the number of medium and large pools declining significantly over the last 80 years (Miller 1997; Mcintosh et al. 2000). Historical evidence also suggests widespread loss of riparian vegetation due to grazing management, timber harvest, splash damming, and ice floes (Filip et al. 1989; Miller 1997; Gildemeister 1998). Restoration of tributary habitat within the UGR started in earnest in the late 1980's with the implementation of passive restoration efforts through grazing management and active restoration in the form of instream log structures.

Meadow Creek is a major tributary of the UGR, experiencing a similar suite of stressors to salmonid populations as the broader UGR (Miller 1997; Gildemeister 1998). At present, only Steelhead spawn annually within the Meadow Creek watershed. Most of Meadow Creek's upper watershed lies within USFS land, with several miles of the mainstem running through Starkey Experimental Forest (SEF). As such, Meadow Creek was subject to several restoration efforts led by the USFS that focused on adding large

woody debris (LWD) to the structurally starved channel. In 1990, approximately 2.5 miles of mainstem Meadow Creek received LWD additions. During this time, ice gates were installed in SEF to limit the downstream movement of ice floes along with protecting riparian plants and LWD additions from ice scours (Boehne 1996; Miller 1997). Further restoration efforts occurred on Meadow Creek in the mid 2010's, with 7.5 miles of mainstem Meadow Creek through SEF receiving another substantial LWD treatment in 2012 and 2013. At the same time, extensive planting of a variety of riparian species occurred throughout the treatment reach along with the modification of grazing management to enhance the establishment and growth of riparian plants (Averett et al. 2017, 2019).

Here, we examine the impacts of the most recent restoration efforts within SEF to the Meadow Creek mainstem with particular attention to fish habitat and the juvenile *O. mykiss* population using a before-after-control-impact (BACI) study design.

Methods

We assessed the impacts of LWD restoration conducted on Meadow Creek within SEF using a BACI study design. Specifically, we used ANOVA and generalized linear model (GLM) frameworks to examine the effects of restoration to fish habitat metrics and juvenile *O. mykiss* counts. Sites were organized into a post-hoc BACI experimental design, whereby sites within the SEF were treated as impact sites receiving restoration treatment in the summers of 2012 and 2013 (Figure 14). We identified an approximately equal number of sites outside of the SEF that did not receive LWD additions to serve as control sites. Restoration was completed in Fall of 2013, therefore surveys conducted in 2014 and after were considered part of the after period. Our BACI experimental design allowed us to test for differences between the treatment and control sites whilst filtering out the environmental variation occurring during the sampling period (Smith 2012).

We used habitat and fish abundance data collected from 2011-2017 for this analysis. The habitat data were collected using the CHaMP protocol (CHaMP 2016). The fish data were collected via snorkel surveys after the habitat assessments were completed. Snorkel count data were further refined into abundance estimates through a Bayesian model relating habitat characteristics of individual channel units to snorkel survey detection estimates. This model corrected for imperfect detection during snorkeling by using covariates and abundance estimates derived from mark-recapture to adjust snorkel counts to represent true abundance estimates (Staton et al. 2022).

The first step of our analysis was to test for changes in habitat variables after LWD restoration using two-way ANOVAs. Habitat variables were checked for normality, with most variables receiving log transformations to improve normality. Zero-inflated variables were given $\log(x + 1)$ transformations to accommodate zeros. Our model-adjusted snorkel abundance estimates were further standardized by wetted habitat area to account for differences among sites and years(i.e., number/m^2). Areal density estimates were then divided by the total number of steelhead redds observed in the prior spawning season within the index spawning ground reaches of Meadow Creek surveyed by Oregon Dept. of Fish and Wildlife (ODFW). This resulted in areal densities adjusted for relative reproductive effort by the Steelhead population over the prior spawning season. Finally, these data were $\log(x + 1)$ transformed to improve normality and accommodate zeros. Two-way ANOVAs testing for differences between the before-after periods, control-impact sites, and the interaction between period and site types were then run on the transformed habitat and fish abundance data at an $\alpha = 0.05$ level.

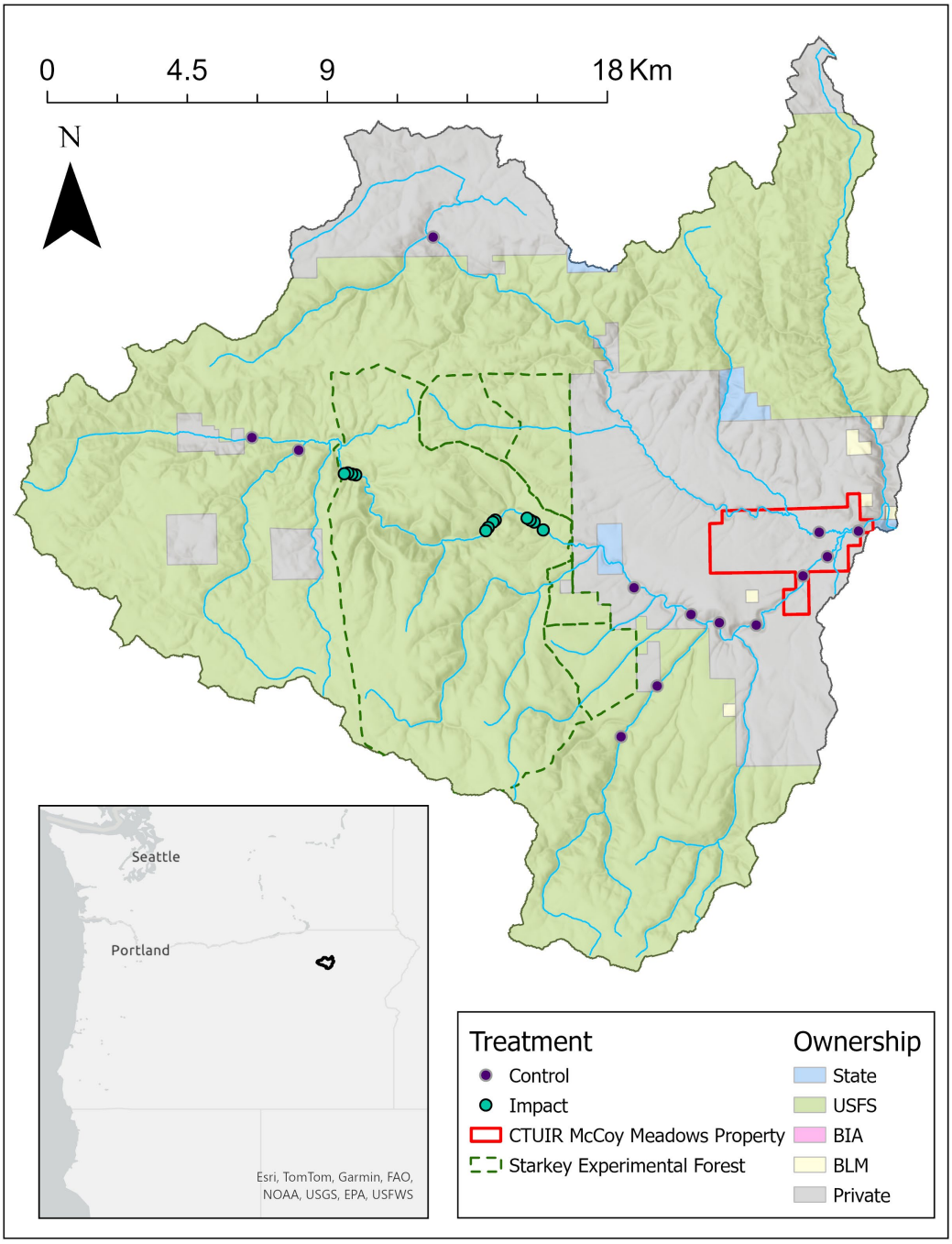

Figure 14: A map of our study sites, control sites in purple and impact sites in turquoise. The black outline denotes the Meadow Creek watershed.

The second step of our analysis was to model the relative importance of the CHaMP-derived habitat variables to *O. mykiss* juvenile abundance at our sites. Using GLMs allowed us to build models combining habitat variables, population effects (e.g., redd counts), or environmental conditions (e.g., annual

streamflow) to predict *O. mykiss* abundance within a site. Further, GLMs allowed us to model these effects within the context of a BACI experimental design by including terms for the before-after periods and control-impact sites. We chose a negative-binomial GLM structure because preliminary analysis using a Poisson model structure indicated overdispersion within the snorkel abundance data.

To select habitat covariates for inclusion in our GLMs, we first checked the correlation coefficients between our habitat covariates and the model-adjusted snorkel abundance estimates (Staton et al. 2022). Variables with high correlation coefficients to the snorkel data were selected for potential model inclusion, with care taken to exclude multiple correlated variables describing similar habitat features (e.g., LWD volume within the wetted channel and LWD volume within the bankfull channel). We then conducted an iterative model building exercise starting with a base model of EstimatedFish ~ Period x Treatment + TotalRedds, whereby we added additional covariates to the model in the order of their correlation coefficient to EstimatedFish. During each iteration, we determined if the additional covariates were significant within the model structure and used Akaike information criterion (AIC) to determine if the new model performed better than the old model. Finally, we examined the marginal effects of each habitat variable from the top model to evaluate their influence on fish density. Marginal effects represent the change in Y (e.g., *O. mykiss* juvenile abundance) associated with a single unit change in an explanatory variable X when all other explanatory variables are held at a fixed value. This approach allowed us to evaluate the relative effects of each of our explanatory variables, along with predicting the number of *O. mykiss* juveniles found across an "average" site within the before-after-control-impact site continuum.

Results

We analyzed a total of 73 site visits across 25 unique site locations. There were 16 before-control, 12 before-impact, 21 after-control, and 23 after-impact visits (Table 4). Streamflows were highest in Spring of 2011 and 2014, as measured by the Oregon Water Resources Department gauges on Meadow Creek within the SEF and at the Meadow Creek mouth with the Grande Ronde River (Figure 15). The ODFW spawning ground index surveys indicated that 2015 was by far the year with the highest reproductive effort for the Steelhead population with 85 redds observed (Figure 16). This was more than 4 times larger than any other year we analyzed. Juvenile *O. mykiss* numbers peaked in 2014, with an average of 8.5 fish/m^2, which was more than double the next most abundant year of 3.3 fish/m^2 in 2013.

Many of the analyzed habitat variables experienced no detectable changes during our study period, as shown by a lack of significant differences between treatment type (control-impact) and treatment type's interaction with period (before-after). We found significant differences between only treatment type in 12 of the 37 variables (32%) examined, indicating there were structural differences between our treatment and control sites. One of the 37 habitat variables examined, substrate D16, had significant differences between treatment type and the interaction between treatment and period, indicating a change in D16 around the time of LWD restoration. We found that two of 37 habitat variables (5%) examined, residual pool depth and fast turbulent unit percentage, had significant differences between period only, indicating a change around the time of LWD restoration that could not be attributed to the restoration itself through our BACI analysis. Interestingly, none of the LWD-related habitat metrics contained significant differences that could be attributed to LWD restoration.

We found that D16 of the channel substrate changed significantly in control sites around the time of the LWD restoration. Substrate D16 had significant differences between site types ($p = .01$) and the interaction between period and site types ($p = .03$). Substrates in control sites were finer after the LWD restoration

(8.69mm ± 1.67; mean ± standard error), compared to the before period (13.6mm ± 2.32). Within the impact sites, we found little change in D16 values from the before period (14.6mm ± 3.38) to the after period (15.3mm ± 1.19).

Our two-way ANOVA for juvenile *O. mykiss* area-based abundances adjusted for relative reproductive effort (fish/m^2/redd) indicated significant differences between control-impact site types ($p = .03$) but not period or the interaction between period and site types (Figure 17). Juvenile *O. mykiss* adjusted abundance (fish/m^2/redd) in the control reaches was similar in the before (0.0183 ± 0.006) and after periods (0.0154 ± 0.005). Meanwhile, juvenile adjusted abundance in the treatment reaches increased from the before period (0.0223 ± 0.006) to the after period (0.0345 ± 0.007; Figure 17).

Table 4. Number of sites included in the BACI analysis

Period	Treatment	n Site Visits	n Unique Sites
Before (2011-2013)	Control	16	13
Before (2011-2013)	Impact	12	12
After (2014-2017)	Control	21	11
After (2014-2017)	Impact	23	12

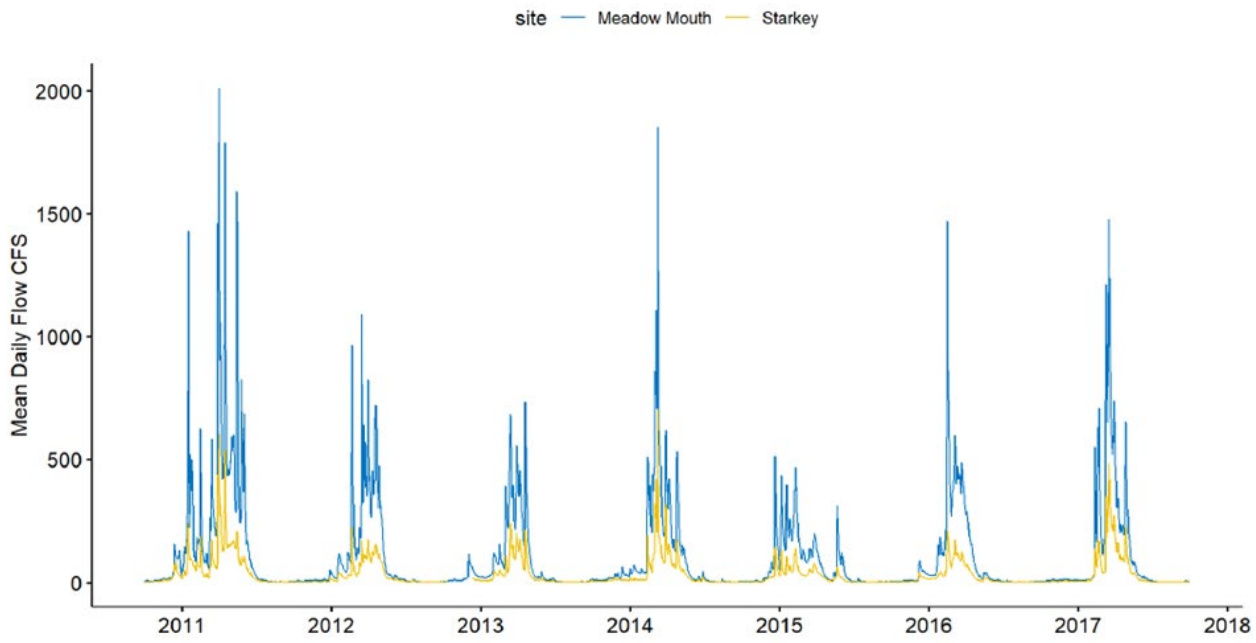

Figure 15: Streamflow data from the two OWRD gauges within Meadow Creek. Blue line is at the Meadow Creek mouth with the Grande Ronde River, yellow line is within the Starkey Experimental Forest.

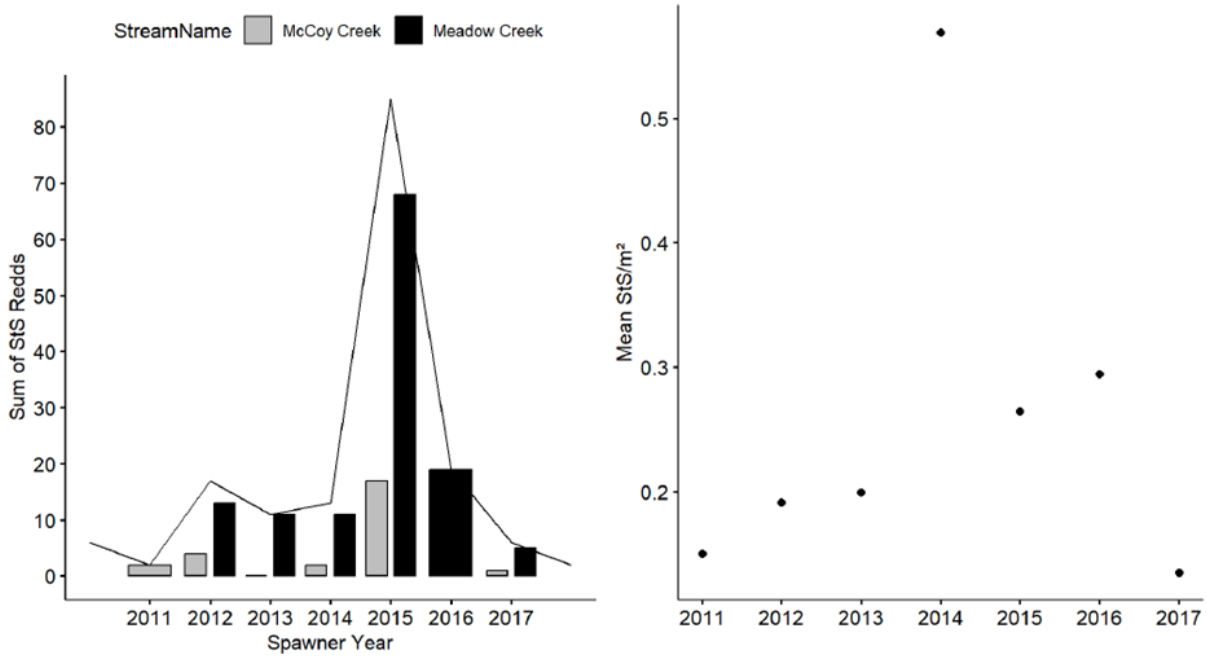

Figure 16: Left is Steelhead redd counts from the Meadow Creek watershed with the black line representing the sum of Meadow and McCoy Creek reaches. McCoy Creek is Meadow's largest tributary. Right is mean juvenile O. mykiss counts / m2 of habitat available within the site.

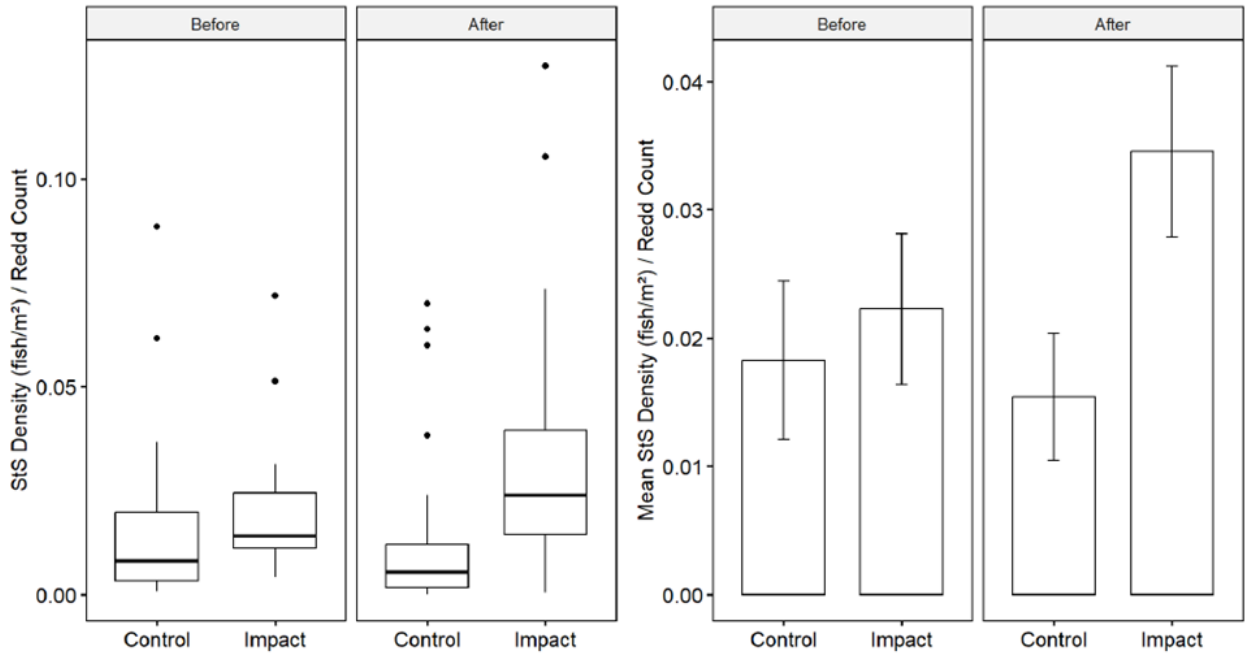

Figure 17: Juvenile O. mykiss abundances adjusted for site wetted area and the annual total number of Steelhead redds within Meadow Creek. Left is a traditional box and whiskers plot, right is mean adjusted abundance ± 1 standard error.

Our top-performing negative binomial GLM for estimating juvenile *O. mykiss* abundances included terms for the intercept, Period, Treatment (site type), Total Redds, Mean Annual Flow, Maximum Weekly Maximum Water Temperature(MWMT), Large Pool Frequency, and the interaction between Period and Treatment. All model terms were significant at the $\alpha = 0.05$ level except for the interaction between Period and Treatment. The null deviance was 110.58 on 70 degrees of freedom while the residual deviance was 79.46 on 63 degrees of freedom.

We then estimated the marginal effects of each covariate within the model whilst holding all other variables at their mean values. A 1 cubic meter per second increase in mean annual flow was associated with 1.07 times as many *O. mykiss* per site (Figure 18A). Surprisingly, increasing the large pool frequency per km by 1 reduces the number of fish at the site by 0.95 times (Figure 18B). A 1 degree C increase in MWMT reduces the number of *O. mykiss* at a site by 0.56 times (Figure 18C). Increasing the redd count from the prior year by 1 increases the number of fish at the site by 1.02 times (Figure 18D).Within our BACI framework, there were 0.81 times fewer fish per site in the after period than the before period. Impact sites contained 1.84 times more fish than the control sites did (Figure 19).

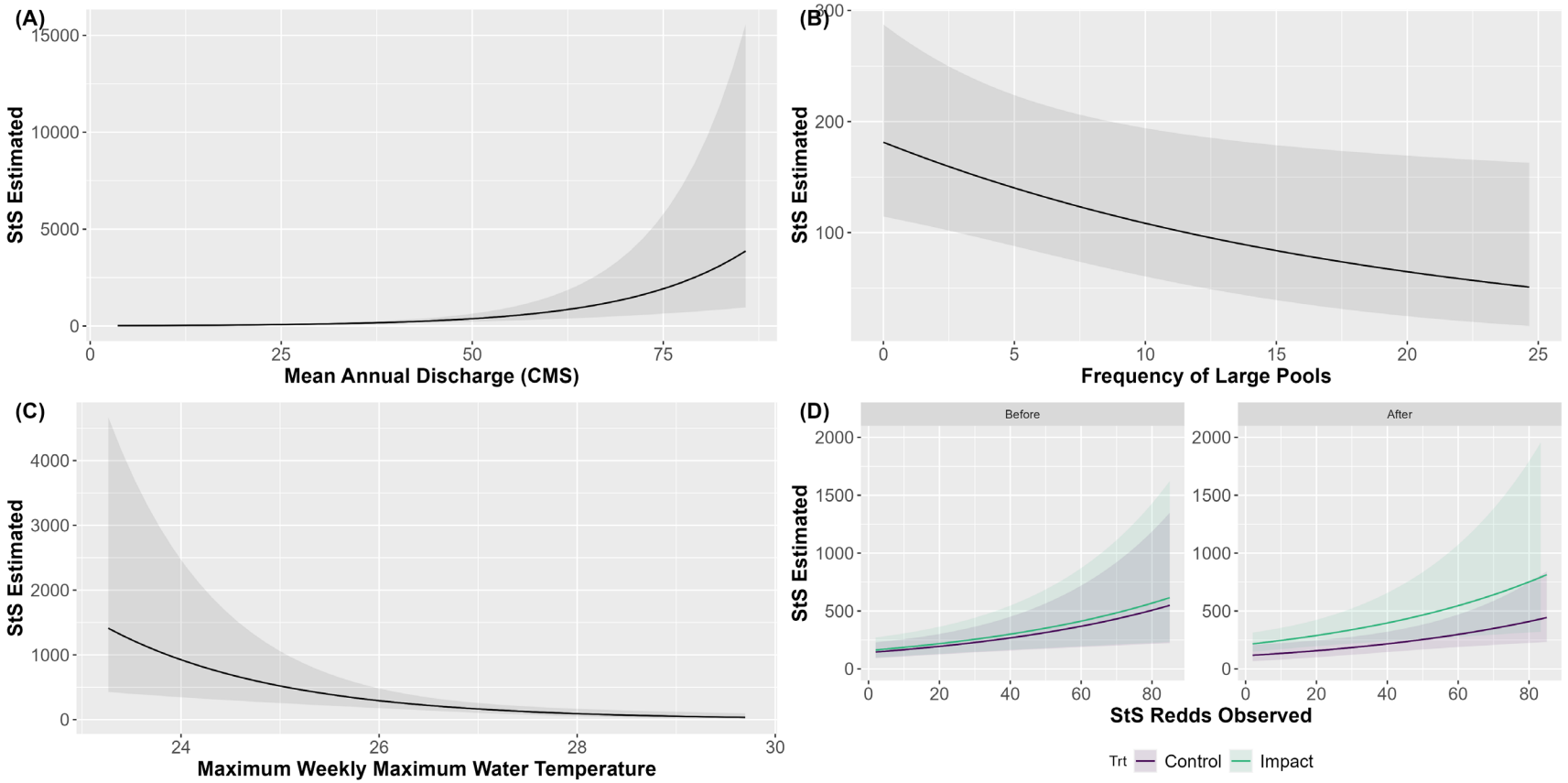

Figure 18: Marginal effects plots showing the relationship of a single variable to the number of juvenile *O. mykiss* at a site if all other variables in the model are held at their mean values. Solid line shows the modeled relationships with shading indicating the 95% confidence interval. (A) mean annual discharge in CMS, (B) frequency of large pools per KM, (C) maximum weekly maximum water temperature in degrees C, (D) total number of redds observed within the ODFW index spawning reaches for before-after periods at control-impact site.

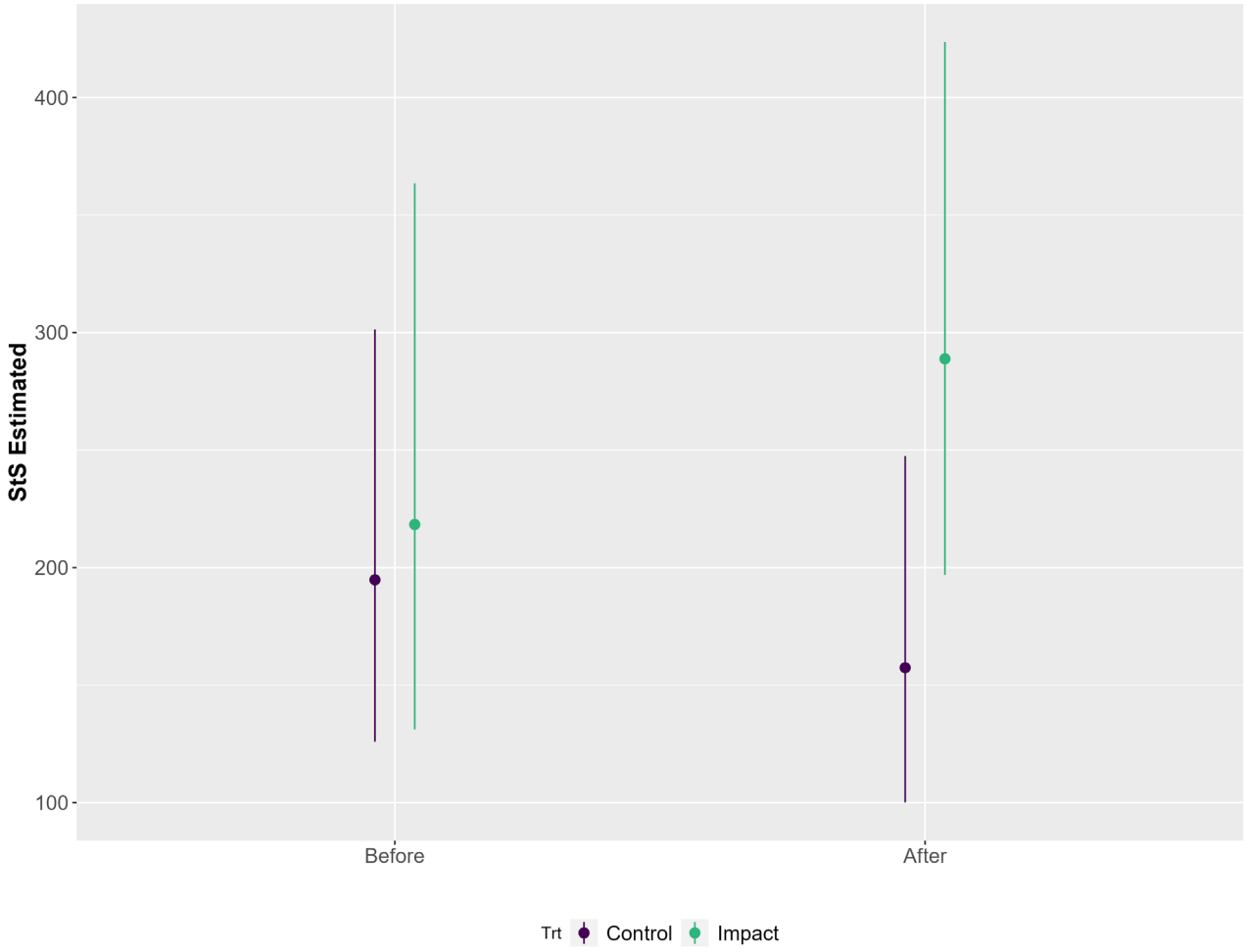

Figure 19: The predicted number of juvenile O. mykiss at an "average" site where all other model variables are held at their mean values. This is the marginal effects of the BACI experimental design within the GLM.

Discussion & next steps

Our results highlight that LWD additions through the mid 2010's did not result in wholesale detectable changes to habitat metrics within the SEF. Our BACI analysis indicated substrate D16 within the treatment reaches remained similar and coarser post-restoration than control sites, potentially enhancing spawning habitat relative to other sites within the watershed. Juvenile *O. mykiss* abundances increased within the SEF treatment sites; however, the differences could not be attributed to the LWD restoration through our two-way ANOVAs. Surprisingly, LWD-based habitat metrics were unaffected by LWD restoration, potentially attributed to low wood loading in treatment reaches relative to natural variation among sites or high variation between survey crews and years with respect to LWD counts.

The GLMs allowed us to better evaluate which habitat variables were influencing juvenile *O. mykiss* abundances at sites within the Meadow Creek watershed. Of our four period-treatment combinations, impact sites in the after period had the highest average number of *O. mykiss* juveniles per site, while impact

sites in the before period had the lowest average number of juveniles per site. Mean annual flow and MWMT showed strong connections to juvenile estimates. However, both are difficult to manipulate at timescales relevant to threated species conservation within this relatively unregulated watershed.

Surprisingly, large pool frequency had a negative relationship with fish counts. This is potentially an artifact of most large pools occurring in sites near the bottom of the Meadow Creek watershed where piscivores such as Northen pikeminnow (*Ptychocheilus oregonensis*) and competitors such as sunfish (*Lepomis spp.*) are more common and water temperatures are higher. Furthermore, the Stanton *et al.* 2022 model contained few observations in pools deeper than 0.5m, which may have biased the abundance estimates in sites containing higher frequencies of large pools. As discussed else were in this report, work is ongoing to collect additional data in deep pool and wood rich habitats to better parameterize the model for those habitat conditions.

Future work will focus on refining our modeling approaches for this dataset. Additional explanatory variables such as the number of summer adult Steelhead crossing Lower Granite Dam or remotely sensed floodplain primary productivity within the sites could be used to better fit models to *O. mykiss* juvenile abundance.

References

Averett, J. P., B. A. Endress, M. M. Rowland, B. J. Naylor, and M. J. Wisdom. 2017. Wild ungulate herbivory suppresses deciduous woody plant establishment following salmonid stream restoration. Forest Ecology and Management 391:135–144.

Averett, J. P., M. J. Wisdom, and B. A. Endress. 2019. Livestock Riparian Guidelines May Not Promote Woody Species Recovery Where Wild Ungulate Populations Are High. Rangeland Ecology & Management 72(1):145–149.

Boehne, P. 1996. Outmigration of Wild Summer Steelhead (Oncorhynchus mykiss) Juveniles in Meadow Creek, Oregon an Upriver Tributary of the Columbia Basin. Humboldt State University.

CHaMP (Columbia Habitat Monitoring Program. 2016. Scientific Protocol for Salmonid Habitat Surveys Within the Columbia Habitat Monitoring Program : 2016 Version.

Filip, G. M., L. D. Bryant, and C. A. Parks. 1989. Mass Movement of River Ice Causes Severe Tree Wounds Along the Grande Ronde River in Northeastern Oregon. Northwest Science 63(5):211–213.

Gildemeister, J. 1998. Watershed history Middle & upper Grande Ronde River Subbasins. Oregon Department of Environmental Quality.

Gresh, T., J. Lichatowich, and P. Schoonmaker. 2000. An Estimation of Historic and Current Levels of Salmon Production in the Northeast Pacific Ecosystem: Evidence of a Nutrient Deficit in the Freshwater Systems of the Pacific Northwest. Fisheries 25(1):15–21.

Justice, C., S. M. White, D. A. McCullough, D. S. Graves, and M. R. Blanchard. 2017. Can stream and riparian restoration offset climate change impacts to salmon populations? Journal of Environmental Management 188:212–227.

Mcintosh, B. A., J. R. Sedell, R. F. Thurow, S. E. Clarke, and G. L. Chandler. 2000. Historical changes in pool habitats in the Columbia River Basin. Ecological Applications 10(5).

Miller, A. C. 1997. Response of juvenile steelhead trout to an instream habitat rehabilitation project in Meadow Creek, Oregon. Oregon State University.

NOAA Fisheries. 2017. ESA Recovery Plan for Snake River Spring/Summer Chinook Salmon (Oncorhynchus tshawytscha) & Snake River Basin Steelhead (Oncorhynchus mykiss).

ODFW. 2020. Investigations into the Life History of Naturally Produced Spring Chinook Salmon and Summer Steelhead in the Grande Ronde River Subbasin - Annual Report 2020. Oregon Dept. of Fish and Wildlife, BPA Project # 1992-026-04.

Smith, E. P. 2012. BACI Design. Page *in* A. H. El-Shaarawi and W. W. Piegorsch, editors. Encyclopedia of Environmetrics, 1st edition. Wiley.

Staton, B. A., C. Justice, S. White, E. R. Sedell, L. A. Burns, and M. J. Kaylor. 2022. Accounting for uncertainty when estimating drivers of imperfect detection: An integrated approach illustrated with snorkel surveys for riverine fishes. Fisheries Research 249:106209.

White, S. M., C. Justice, D. A. Kelsey, D. A. McCullough, and T. Smith. 2017. Legacies of stream channel modification revealed using General Land Office surveys with implications for water temperature and aquatic life. Elementa: Science of the Anthropocene 5:3.

Goal 2: Evaluate effectiveness of aggregate restoration actions in the Grande Ronde basin

Objective C: Evaluate if the pace of restoration can counteract habitat and temperature degradation

Objective C-1: Develop list of restoration scenarios

CRITFC staff hosted a collaborative workshop in November of 2021 with Grande Ronde basin partners to develop a suite of riverscape restoration and management scenarios intended to be used as inputs to the Grande Ronde spring Chinook life cycle model described in Objective D. The group developed a draft set of broad management scenarios addressing instream and floodplain restoration, riparian vegetation restoration, food webs, and other in-basin factors (i.e., landowner access, lower valley mortality, hatchery supplementation). Workshop participants discussed a more detailed list of actions that could be implemented to address each of these broad management categories. At this stage, we have been prioritizing finalizing and publishing the life cycle model and have paused further development of restoration scenarios. Once the initial observation model phase of the life cycle model is complete, we will seek additional feedback from basin partners and refine restoration/management scenarios that will be feasible to test with the model. Our goal is to work with partners to finalize the list of management scenarios in the 2024 contract year and begin applying them to the LCM in 2024 and 2025.

Objective C-2: Quantify change in habitat limiting factors relative to restoration actions

To address a critical gap in our ability to translate restoration actions into habitat change across large geographic extents (e.g., biologically significant reaches [BSRs], Chinook population areas), we plan to quantify the observed change in habitat conditions before and after restoration at restoration sites within

the study area. This analysis will focus on changes in key habitat limiting factors (e.g., water temperature, pool frequency, large wood frequency, and floodplain/side channel habitat) in response to restoration actions across a range of restoration categories (e.g., barrier removal, large wood placement, riparian planting, floodplain enhancement; Roni et al. 2021). This assessment has been delayed by the lack of available spatial layers and associated project implementation data (e.g., what, when and where). Despite earlier efforts to compile a geodatabase describing the location of all restoration projects in the basin and quantify what was done at each location (Benge 2015), the project locations were represented as points instead of polygons or lines, making it very challenging to accurately identify what portions of the stream network had been treated. Expert opinion or literature-based estimates of habitat change may be used for some restoration categories if local empirical data is insufficient. We plan to continue working on this objective during 2024 and 2025.

References

Benge, G. 2015. Mapping tributary habitat restoration projects in the Upper Grande Ronde River to support landscape analysis. Page 52. Oregon State University, Corvallis, OR.

Roni, P., M. Krall, K. Ross, and D. Arterburn. 2021. Action Effectiveness Monitoring 2020 Annual Report. Page 121. Cramer Fish Sciences, Annual Report Project Number 2016-001-00, Issaquah, WA.

Objective C-3: Extrapolate impacts of restoration scenarios across historical Chinook extent in upper GR basin

Using observed changes in habitat characteristics at selected restoration sites from Objective C-2, we plan to extrapolate the expected uplift to habitat conditions throughout the stream network in the study area. The resulting product will be a spatially explicit map of habitat uplift that can be used independently in restoration planning, and also incorporated via simulated restoration scenarios in the life cycle model (Objective E-2, E-3). This objective is planned to be completed in 2025.

Goal 3: Relate biological responses to habitat change

Objective D: Relate life stage-specific response to habitat change in the Grande Ronde and nearby basins

Objective D-1: Collect data on fish and macroinvertebrate distribution

Juvenile salmonid abundance and distribution

Background

Snorkel density surveys were conducted across a subset of habitat monitoring survey segments to assess fish response to habitat quality, and to evaluate the effectiveness of aggregate restoration activities in improving freshwater habitat conditions and viability of ESA-listed fish species at the population scale. Snorkel surveys conducted during the summer of 2022 contribute to large-scale monitoring efforts across the upper Grande Ronde basin, with the intent of assessing status and trends in fish habitat conditions, particularly for Chinook Salmon *(Oncorhynchus tshawytscha*).

Methods

During the summer of 2022, snorkel surveys were conducted between August 11th and August 17th to assess the abundance and distribution of juvenile salmonids in summer rearing habitat in the upper Grande Ronde, Meadow Creek, Waucup Creek, McCoy Creek and Limber Jim Creek (Figure 20). Snorkel surveys were conducted at 58 monitoring reaches in the upper Grande Ronde River, with reach lengths of approximately twenty times the bankfull channel width. Surveys were conducted following a protocol developed by CRITFC, drawing heavily from the methods of Thurow (1994) and integrated with the Pacific Northwest Aquatic Monitoring Program (PNAMP) methods. Details about the snorkel survey methodology can be found in White et al. (2012).

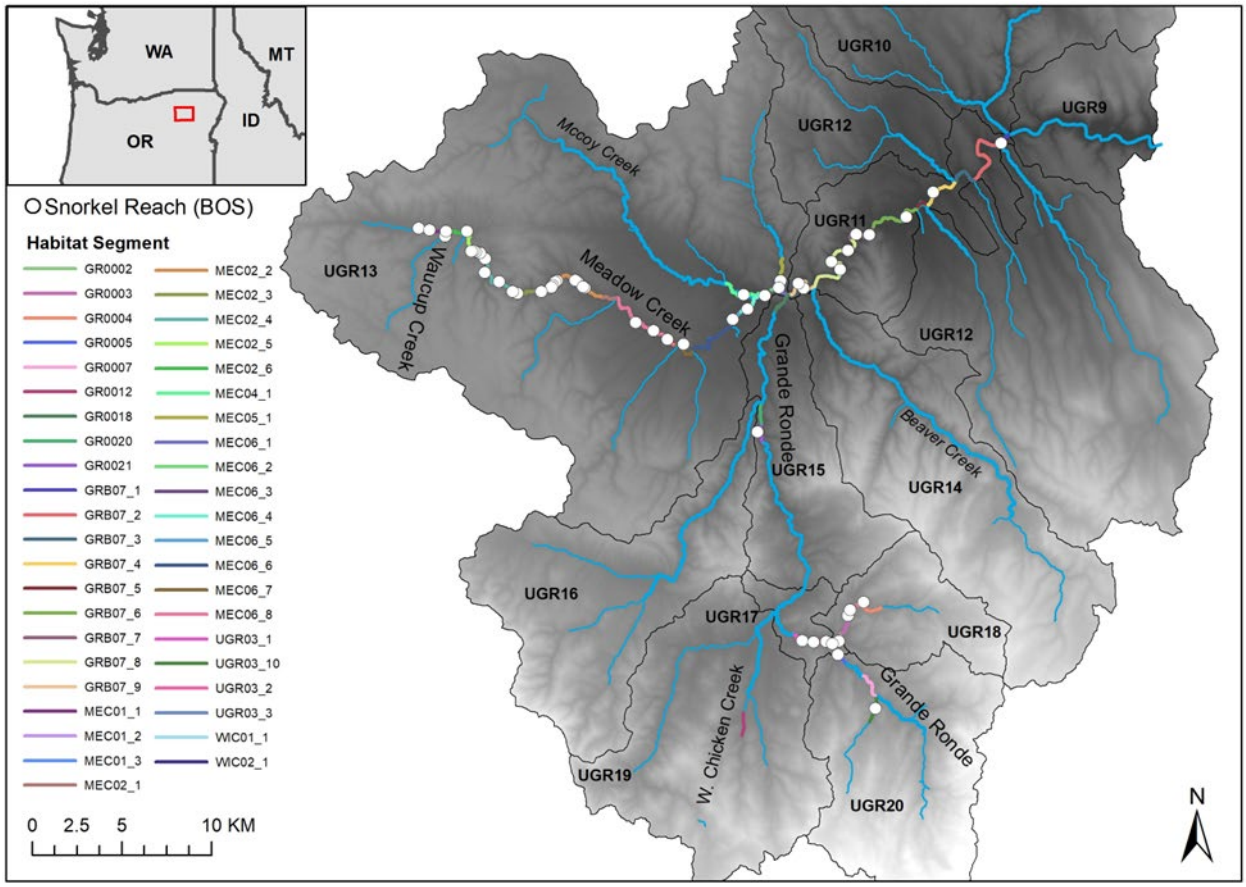

Figure 20. Snorkel reaches (bottom of site) and habitat segment locations for 2022 fish density and distribution sampling.

Results

Estimates of juvenile Chinook and Steelhead/Rainbow Trout (hereafter referred to as *O. mykiss*) densities are still in progress, pending the finalization of habitat metrics derived from ground-based data collected by field crews and spatial imagery collected via drone.

Next Steps

Post-processing of the resulting data from snorkel surveys, corresponding ground-based habitat data, and unmanned aircraft systems (UAS) will be completed and metrics relating to habitat characteristics influencing snorkel detection efficiency will be calculated. The derived habitat metrics required for estimating juvenile salmonid densities (at the channel unit scale) include the density of large wood pieces within the wetted channel and average depth.

These habitat metrics, paired with juvenile snorkel count data for Chinook Salmon and *O. mykiss*, will be used to estimate the probability of detection at the channel unit scale with channel units categorized as either slow (pools) or fast (fast turbulent and fast non-turbulent) using a Bayesian detection probability model that accounts for uncertainty in both snorkel count and mark-recapture estimates, as well as mechanistic links between local conditions and detectability for each species (Staton et al. 2022). Snorkel counts will then be expanded using the predicted detection probability to estimate true abundance.

The CRITFC snorkel survey protocol samples only 25% of riffle or fast turbulent channel units within a sample reach, requiring that estimates of channel unit abundance be further expanded to account for unsampled channel units as well as for any channel units that were subsampled (i.e., only 80% of the channel unit area snorkeled) as the protocol allows for the subsampling of channel units that are excessively long in length and impractical to sample in their entirety (White et al. 2012). After performing this further expansion to account for unsurveyed channel units, estimates will be converted to linear (no.·$100m^{-1)}$ and areal density (no.·$100m^{-2}$) to standardize for differences in stream size across sites. Density and abundance estimates will be provided in the 2024 annual report.

References

Staton, B. A., Justice, C., White, S., Sedell, E. R., Burns, L. A., & Kaylor, M. J. 2022. Accounting for uncertainty when estimating drivers of imperfect detection: An integrated approach illustrated with snorkel surveys for riverine fishes. Fisheries Research, 249, Article 106209. https://doi.org/10.1016/j.fishres.2021.106209.

Thurow, R.F. 1994. Underwater Methods for Study of Salmonids in the Intermountain West. General Technical Report. Ogden, UT: US Department of Agriculture, Forest Service, Intermountain Research Station.

White, S., Justice, C., and McCullough, D. 2012. Protocol for snorkel surveys of fish densities. Columbia River Inter-Tribal Fish Commission. https://www.monitoringmethods.org/Protocol/Details/499.

Lookingglass Creek Steelhead/Rainbow Trout Growth Study

A mark-recapture study was conducted in 2023 in Lookingglass Creek, a tributary of the Grande Ronde River, to assess summer *O. mykiss* growth rates prior to restoration activities planned for 2025 and to provide preliminary growth and size structure data for the insulin-like growth factor-1 (IGF1) field pilot study planned for summer 2024. We are ultimately interested in determining the potential application of IGF1 as a method of assessing juvenile salmonid growth in habitats where traditional mark-recapture methods are not very effective (e.g., complex floodplains, large rivers, estuaries). There was concern regarding the density of juvenile *O. mykiss* in Lookingglass Creek due to low returns of summer Steelhead in recent years (Crump 2022), which brought into question whether recapture rates of PIT tagged fish would

be high enough to support the planned field pilot study pairing PIT tag-derived growth data with IGF1 concentration as an index of recent growth. Over the last several years, CTUIR has collected pre-restoration data for juvenile spring Chinook (growth, diet, and isotopes) in the downstream treatment and upstream control reach; however, juvenile *O. mykiss* data has previously only been collected at the screw trap located upstream of Lookingglass Fish Hatchery. Providing additional pre-restoration data in the control and treatment reaches allows for evaluation of juvenile *O. mykiss* response to restoration efforts that complement ongoing efforts to evaluate spring-run Chinook response.

Methods

Sample reaches were longitudinally distributed within the pre-restoration control and treatment extents, with the downstream-most reach extending 100 m above and below the mid-point of the already established CTUIR treatment and control Chinook tagging reaches. The two additional 200 m reaches in each section were spaced at roughly even intervals to maximize spatial coverage within the control and treatment sections, while maintaining a 400 m buffer between reaches within the treatment and control sections (Figure 21). Initial tagging was conducted the week of August 7th, 2023, in collaboration with CTUIR biologists and fishery technicians. Fish were captured using a combination of backpack electrofishing and seining, most successfully with two backpack electrofisher units used to shock downstream into a seine net while dip netters opportunistically captured fish. Each reach was sampled with one upstream pass followed by a downstream pass to increase the number of *O. mykiss* captured. Captured fish were anesthetized using MS-222, weighed, measured (fork length) and implanted with a 9 mm PIT tag for all individuals between 70 and 240 mm in length. Reaches were sampled for recaptures the week of September 18th, 2023, using the same sample methods.

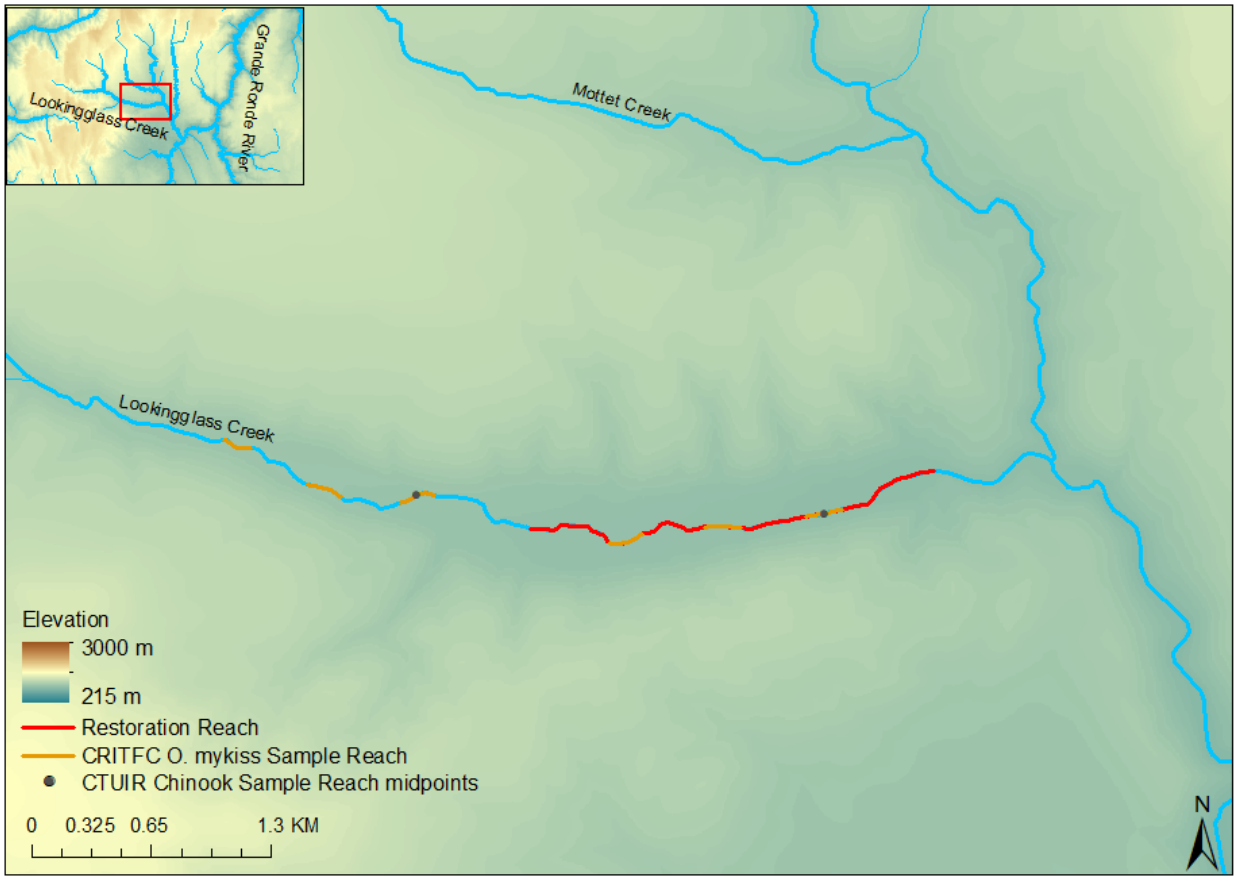

Figure 21. Location of Lookingglass Creek O. mykiss growth study sample reaches for 2023 as well as the planned restoration extent and midpoint locations for CTUIR control and treatment Spring Chinook monitoring reaches.

Growth was characterized as mass standardized growth rate (MSGR; Ostrovsky 1995) to standardize for fish size, as growth potential is linked with body size. MSGR scales growth to the specific growth rate of a 1 g fish:

$$\text{MSGR (\%/day)} = \frac{W_2^b - W_1^b}{b\ x\ t} \times 100$$

where W_1 and W_2 are the mean fish weight during the first and second sampling events, t is the number of days between sample events, and b is a general allometric mass exponent for salmonid fishes as an allometric mass exponent has not been developed for *O. mykiss (*Iwama and Tautz 1981**)**.

Results

Recapture rates ranged from 0.19 to 0.48 among the six reaches, with the lowest recapture rate observed in the downstream-most treatment reach, which was characterized by a simplified channel with limited pool habitat and large wood. The minimum target number of *O. mykiss* tagged per 200 m reach per sample event for the IGF1 field pilot was 85 individuals, while the number of individuals tagged ranged from 61 to 128 during the initial tagging effort in August 2023 (Table 5). Despite the relatively low density observed in some reaches, the high recapture rates suggest that even in reaches where the number of tagged individuals

does not meet the minimum target of 85, a lower number of tagged fish may still be sufficient to pair PIT tag growth data with IGF1 concentrations to validate the use of IGF1 as an index of recent growth.

Growth rates (MSGR) were comparable across treatment and control reaches, with no significant difference observed between reaches observed between reaches ($F_{5,157} = 1.326$, $p = 0.26$) (Figure 22). Mean MSGR for sample reaches ranged from 0.92 %/day in the upper control reach to 1.34 %/day in the middle treatment reach (overall mean = 1.21± 0.16 %/day; mean ± standard deviation). *O. mykiss* captured ranged in length from 48 mm to 240 mm (fork length), representing age 0 fish (< 79 mm), age 1 fish (80-129 mm), age 2 fish (130-199 mm), and age 3 fish (> 200 mm) (Figure 23; Crump 2022). While a minimum size threshold for non-lethal blood sampling in juvenile salmonids is still being refined through a hatchery study at the Hagerman Fish Culture Experiment Station, recent study results from IGF1 sampling in Cle Elum Hatchery showed low mortality (25 out of 400 total fish sampled) in juvenile Spring Chinook ranging in size from 110 to 145 mm. Although juvenile Chinook are typically more robust than juvenile *O. mykiss* of equal length, the observed size structure of the *O. mykiss* population in Lookingglass Creek appears to be suitable for the IGF1 field pilot study objectives of sampling all age 1 fish that meet the minimum body size threshold and all age 2 fish (Figure 23).

Next Steps

The reaches established in this preliminary growth study will be used for the IGF1 field pilot study in the summer and fall of 2024, with an initial tagging event followed by two recapture and blood draw events spaced four weeks apart to standardize growth stanzas. This field pilot will be informed by ongoing hatchery studies to ensure that best practices are used for non-lethal IGF1 sampling.

Table 5. Summary of O. mykiss mark-recapture activities in Lookingglass Creek in summer 2023 by reach. N_{tm} is the number of total marked fish and N_{tr} is the number of total recaptured fish.

	August			September	
Reach	**Marked (N_{tm})**	**Recaptured (N_{tr})**	**Recapture Rate (N_{tr}/N_{tm})**	**Marked**	**Total Marked**
Control Lower	61	23	0.38	89	173
Control Mid	79	19	0.24	46	144
Control Upper	94	28	0.30	43	165
Treatment Lower	68	13	0.19	74	155
Treatment Mid	75	36	0.48	65	176
Treatment Upper	128	48	0.38	58	234

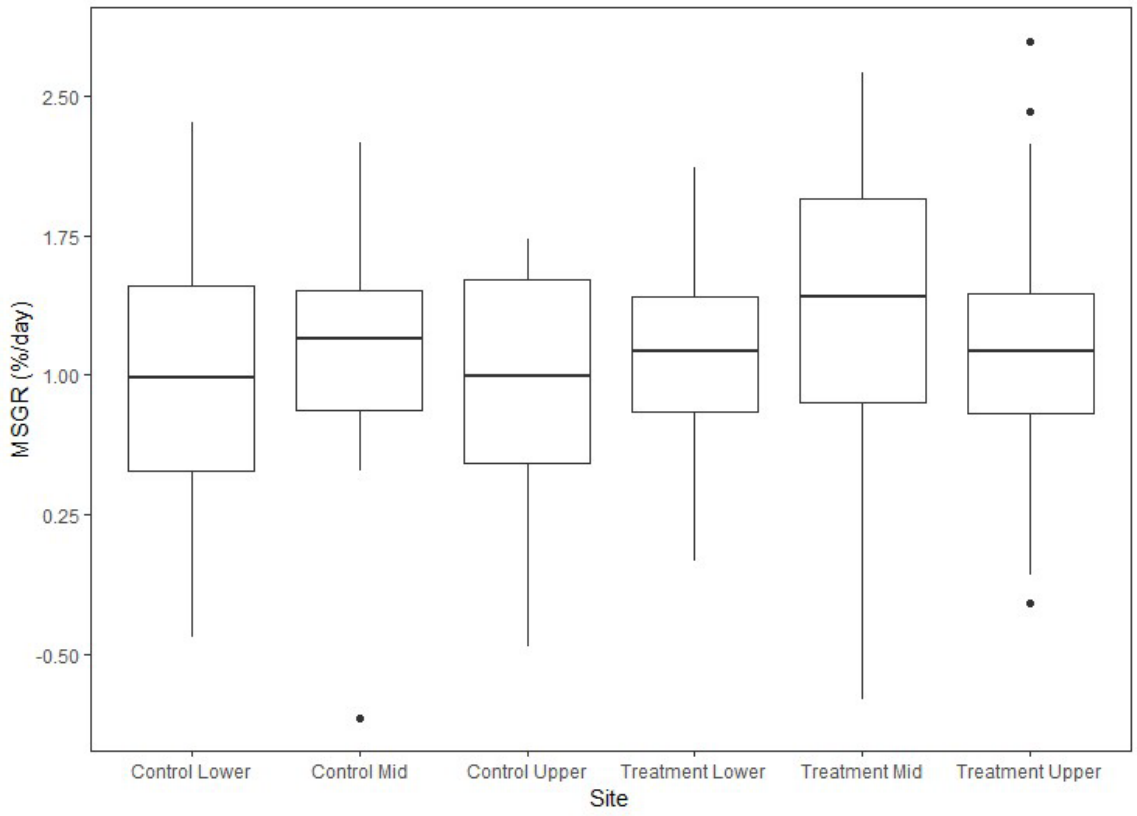

Figure 22. Mean MSGR for each reach sampled in Lookingglass Creek in 2023.

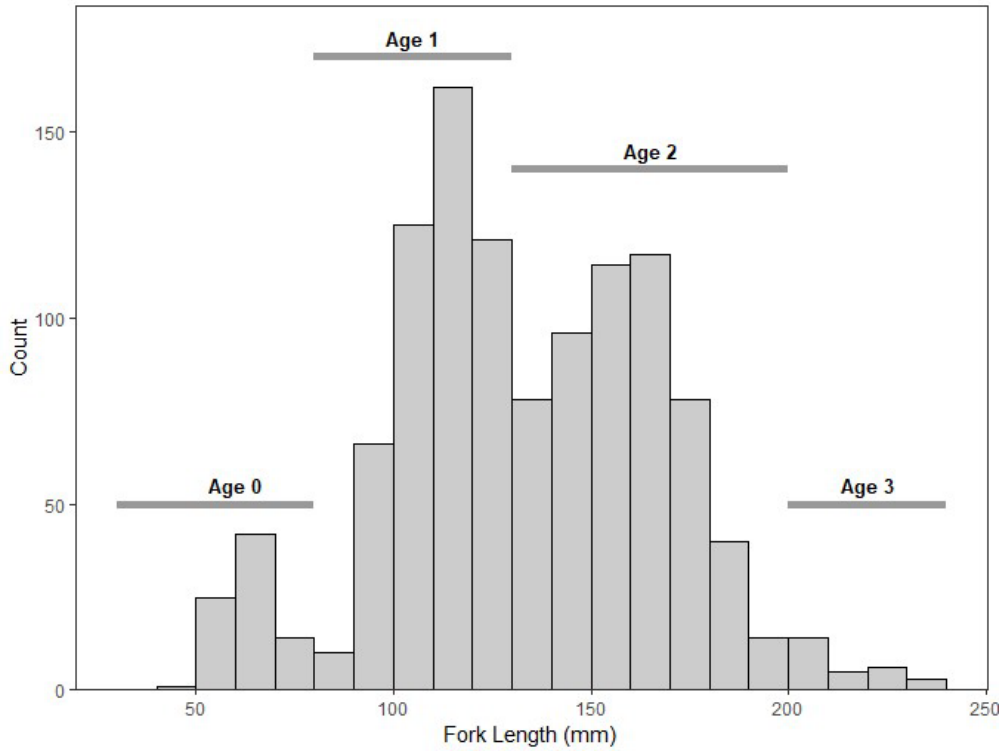

Figure 23. Length frequency of sampled O. mykiss in Lookingglass Creek by age class. Age 0 fish are classified as those < 79 mm, age 1 fish as 80-129 mm, age 2 as130-199, and age 3 as those over 200 mm (Crump 2022).

References

Crump, C., Naylor, L., Van Sickle, A., Kennedy, J., Mathias, Z. and Shippentower, G. Monitoring and evaluation of supplemented Spring Chinook Salmon and life histories of wild Summer Steelhead in the Grande Ronde Basin 2022 Annual Progress Report [Report]: Annual Report. Portland Oregon: Bonneville Power Administration, 2022.

Iwama, G. K. and Tautz, A. F. 1981. A simple growth model for salmonids in hatcheries. Canadian Journal of Fisheries and Aquatic Sciences 38: 649–656.

Ostrovsky, I. 1995. The parabolic pattern of animal growth: determination of equation parameters and their temperature dependencies. Freshwater Biology, 33, 357-371. https://doi.org/10.1111/j.1365-2427.1995.tb00398.x.

Insulin-like growth factor-1(IGF1) Study

Background

A study was conducted at the Oregon Hatchery Research Center to evaluate and develop the use of the plasma hormone insulin-like growth factor-1 (IGF1) as an indicator of recent growth status in field studies on juvenile salmonids. Prior to employing blood sampling in field studies on ESA-listed juvenile salmonids, it is necessary to determine the minimum size of fish that can be sampled to provide enough plasma to run the IGF1 assay without causing mortality or sublethal negative effects on the fish.

Results

The effects of drawing a 100 µl blood sample on mortality, growth, and hematocrit were compared across a range of sizes expected to be encountered in field studies (90-170 mm) over the following 4 weeks. Unfortunately, an unacceptable level of mortality (20-40%) was observed across all size classes. Puzzlingly, however, mortality did not begin until about 10 days post-sampling and did not decrease as expected with fish size. In fact, the largest size class (160-170 mm) experienced the highest mortality rate. These levels of mortality have not typically been seen after drawing a similar volume of blood from juvenile salmonids over 120 mm.

Next Steps

The unexpectedly high levels of mortality led the research team to speculate that an interaction between water quality and the needle puncture wound from blood sampling may have led to secondary infections that produced the high mortality results. Blood sampling had little effect on hematocrit or post-sampling growth, suggesting that the fish were able to replace lost red blood cells over the 4-week period. Ongoing work will use the plasma samples collected to validate modifications of the IGF1 assay and binding protein extraction procedure to use smaller plasma volumes. Additionally, we're replicating this laboratory study in a different location with better water quality (Hagerman Fish Culture Experiment Station in Hagerman, Idaho) to confirm that sampling-related mortality is low prior to implementation in the field.

Snorkel Calibration Data Collection – 2023 Sampling Efforts

Background

The snorkel detection model developed by CRITFC (Staton et al. 2022) has been increasingly used by our group and Grande Ronde partners to estimate abundance from snorkel counts in restoration sites. However, concerns were raised regarding the suitability of the existing model to estimate snorkel detection probability in very deep (>0.5 m average depth) or complex habitat (>0.2 pieces of large wood per m^2) as these values fall outside of covariate ranges in the initial dataset used to develop the model. As restoration efforts aim to increase pool frequency and habitat complexity through large wood additions, this shortcoming decreases the applicability of the current model in evaluating juvenile salmonid abundances in non-simplified habitats. Additionally, while the model is used to estimate abundance of both Steelhead/Rainbow Trout and Chinook Salmon, the original snorkel detection dataset was heavily weighted towards Steelhead/Rainbow Trout habitat, resulting in a smaller sample size for Chinook and increased uncertainty around abundance estimates for Chinook. CRITFC and ODFW collected additional paired snorkel count and mark-recapture data during the 2023 field season, with a combined objective of sampling a) sites characterized by deeper and more complex habitat (relative to simplified/unrestored habitat) and b) sites within the known rearing area for Chinook Salmon.

Methods

Paired snorkel count and mark-recapture surveys were conducted during the 2023 field season at sites in the Grande Ronde River basin as well as tributaries of the Middle Fork John Day River (Figure 24). A minimum of two paired fast water and slow water channel units were sampled at each site, with channel unit classification based on differences in bedform shape, depth, velocity, stream gradient and substrate characteristics following the CRITFC Tributary Habitat Assessment Protocol (version 2) (Justice 2020). Following the delineation of channel units at each site, snorkel count surveys were conducted following a protocol developed by CRITFC, which is based on the methods of Thurow (1994) and integrated with the Pacific Northwest Aquatic Monitoring Program (PNAMP) methods (White et al. 2012).

After the completion of snorkel surveys, block nets were installed at the upstream and downstream ends of the channel units to block fish movement and create a closed population. Fish were then captured using a combination of backpack electrofishing and snorkel seining in both events (mark and recapture) to maximize the number of juvenile *O. mykiss* and Chinook Salmon captured and marked via a fin clip in the first event. An exception to the capture method of conducting an electrofishing pass to target *O. mykiss* and a snorkel seining pass to target juvenile Chinook was the Hall Ranch sample site in Catherine Creek, where the proximity to adult Chinook Salmon prohibited the using of electrofishing. Capture methods were kept consistent between mark and recapture events at each channel unit.

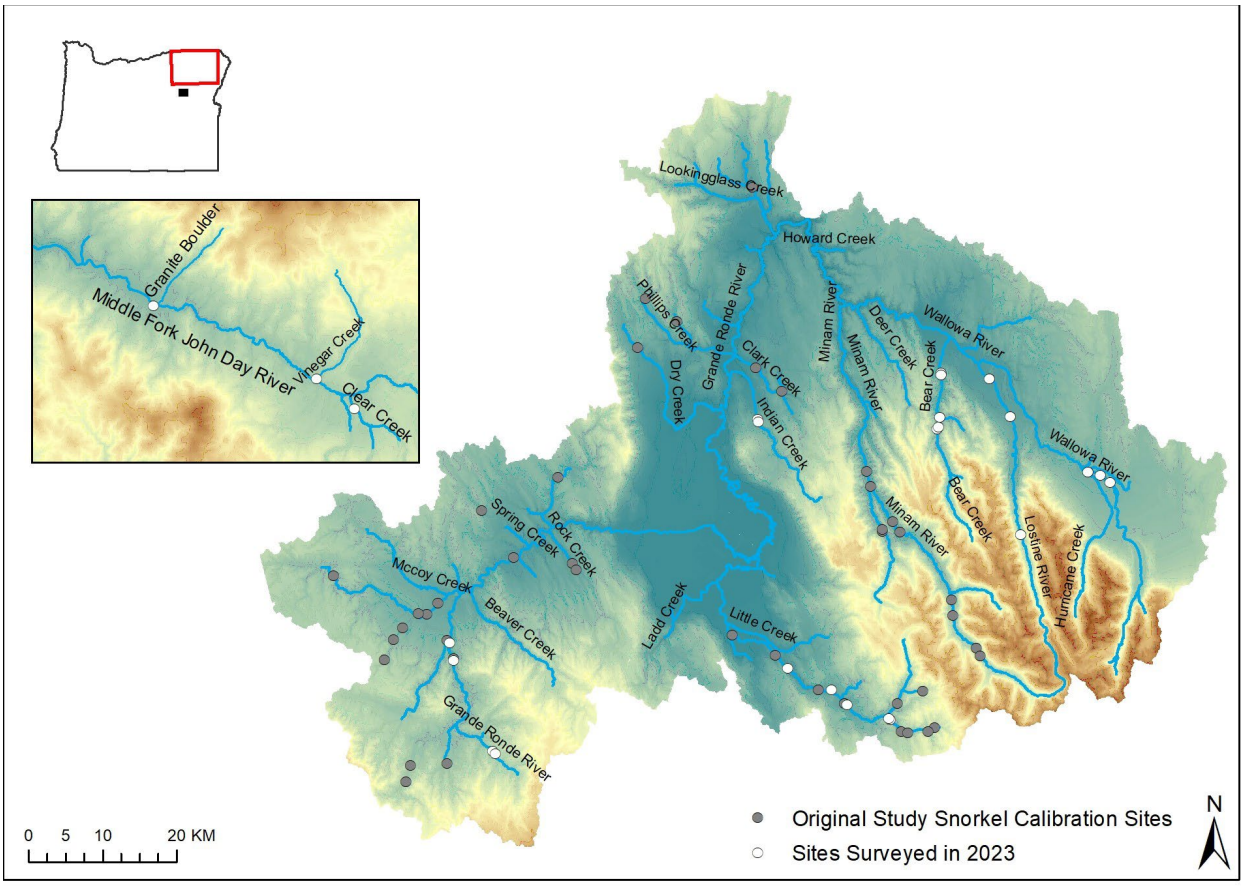

Figure 24. Map of 2023 snorkel calibration sample sites, denoted by white circles, and original snorkel calibration sites sampled in 2012 and 2015.

Results

A total of 25 sites were sampled, for a total of 57 individual channel units comprised of six fast non-turbulent units, 24 fast turbulent units, and 27 pools (Table 6). The distribution of mean channel unit depths in the 2023 dataset, characterized as the average of depth measurements collected at transects at 25%, 50% and 75% the length of each channel unit, included deeper habitats than those in the original dataset (Figure 25). Mean pool (PL) depth sampled in 2023 was 0.53 m (N=27, SD=0.18), with mean depths ranging from 0.22 to 0.96. Mean fast non-turbulent (FNT) channel unit depth was 0.27 m (N=6, SD=0.06), with depths ranging from 0.17 m to 0.34 m. The mean depth for fast (FT) channel units was 0.25 (N=24, SD= 0.08), with depths ranging from 0.12 m to 0.45 m.

Table 6. Summary of 2023 snorkel calibration efforts.

Stream	N Site	FNT	FT	PL	Total Units
Bear Creek	5	1	4	5	10
Catherine Creek	3	0	3	3	6
Clear Creek	1	1	1	1	3
Granite Boulder	1	1	1	1	3
Hurricane Creek	1	1	1	2	3
Indian Creek	2	0	2	2	4
Lostine River	3	0	3	3	6
SF Catherine Creek	2	0	2	2	4
Grande Ronde River	4	1	4	5	10
Vinegar Creek	1	1	1	1	3
Wallowa River	2	0	2	2	4
Total	25	6	24	27	57

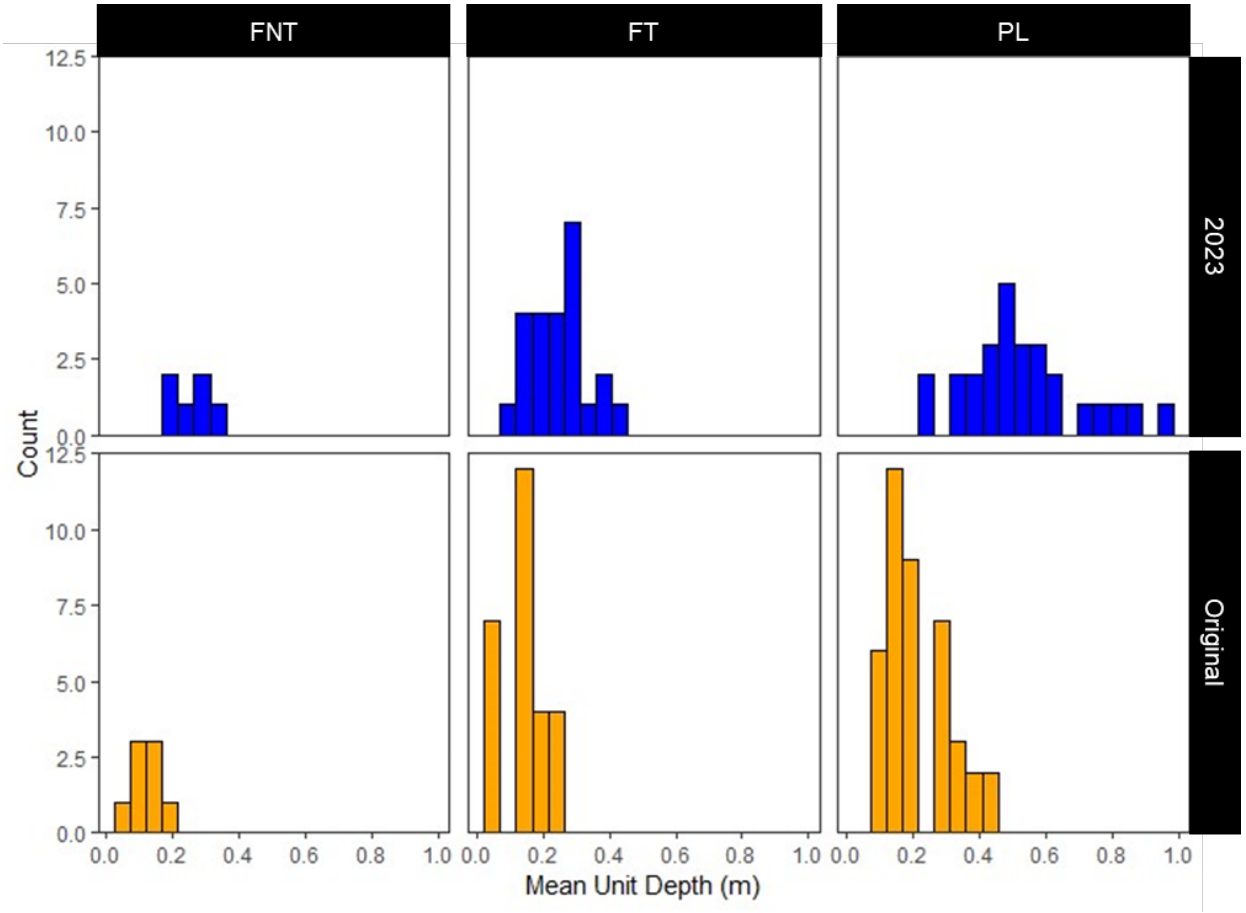

Figure 25. Distribution of mean channel unit depth (m) included in the original dataset (orange bars) and the dataset collected by CRITFC and ODFW in 2023 (blue bars) grouped by fast non-turbulent (FNT), fast turbulent (FT), and pool (PL) units.

Next Steps

The analysis from the expanded snorkel calibration study will be included in the 2024 Annual Report.

References

Justice, C., L. Burns, S. White. 2020. Tributary Habitat Assessment Protocol v2.0. Monitoring Resources.org. http://www.monitoringresources.org/Document/Protocol/Details/3554

Staton, B. A., Justice, C., White, S., Sedell, E. R., Burns, L. A., & Kaylor, M. J. 2022. Accounting for uncertainty when estimating drivers of imperfect detection: An integrated approach illustrated with snorkel surveys for riverine fishes. Fisheries Research, 249, Article 106209. https://doi.org/10.1016/j.fishres.2021.106209.

Juvenile distribution in the Middle Fork John Day River

Background

The extent and quality of juvenile salmonid rearing habitat is an important limiting factor controlling population carrying capacity and productivity through density-dependent processes (Quinn 2007). As reproductive output increases (e.g., number of spawners) the corresponding production of offspring does not increase linearly; instead, the amount of additional offspring production for each unit increase in reproductive output deceases sequentially as juveniles experience greater competition for prey resources and high-quality habitats. Salmon populations across the Columbia River Basin are highly suppressed relative to historic returns, yet density-dependent effects on population dynamics remain persistent (Walters et al. 2013). This may be attributed, in part, to changes in the extent and quality of rearing habitats. For example, if reproductive output were to remain constant but the spatial extent (or quality) of rearing habitat was contracted, density-dependent effects would increase as juveniles experience greater competition for limited resources. Consequently, a main goal of habitat restoration efforts is to increase the amount and quality of rearing habitats to decrease density-dependence.

Density-dependence is not only a function of the number of individuals within a given spatial scale (e.g., total number of juveniles within the entire rearing extent of a given year), but also how juveniles are distributed at finer spatial scales (e.g., spread out uniformly versus clusters of high densities). The extent of thermally suitable summer rearing habitat within watersheds is projected to contract through time as climate change intensifies (Isaak et al. 2015). In thermally heterogeneous watersheds, this contraction may transition from continuous summer rearing extents to a patchwork of thermally suitable rearing habitats nested within warmer habitats (O'Sullivan et al. 2021). These "core" rearing areas are critical in supporting salmonids in warmer years and will be increasingly important with climate change. Evaluating juvenile salmonid distributions in response to inter-annual variation in environmental conditions is an effective tool to identify "core" rearing areas (Flitcroft et al. 2014), providing important information to prioritize the locations of restoration efforts to maintain or enhance summer rearing habitats.

Project overview

The goal of this study is to evaluate how inter-annual variability in environmental conditions and the spatial extents of adult spawning mediate the expansion or contraction of juvenile salmon rearing habitat. This is a highly collaborative project between CRITFC, the Confederated Tribes of the Warm Springs Reservation

of Oregon (CTWSOR), the Oregon Department of Fish and Wildlife (ODFW), and additional partners associated with the Middle Fork John Day Intensively Monitored Watershed.

We first evaluated juvenile Chinook Salmon distribution across the Middle Fork John Day River (MFJDR) in the summer of 2021 – a year with abnormally low discharge and record-breaking temperatures in June and July. Watershed-scale abundance estimates combined with data on dispersal patterns revealed that 1) parr tributary use was high (~23% of all MFJDR parr), 2) parr within the mainstem were concentrated in sections with cooler July average maximum daily temperature, and 3) parr originating in warmer mainstem sections generally moved to cooler mainstem sections (such as within the Oxbow Conservation Area) or to tributaries (see results in Appendix D). Prior parr distribution surveys across the MFJDR in 2014, 2015, and 2016 (Handley et al. 2016) revealed that parr were present across a longer mainstem extent, including as far as 25 kilometers downstream (~ rkm 70) from our sampling extent in 2021. These efforts suggest that the distribution of parr in 2021 may have been an anomaly reflecting the abnormally high temperatures and low flows observed in June and July of 2021. Further, they similarly found that temperature was associated with parr presence within 1 km reaches across the MFJD. Other studies within the MFJDR have found similar associations between temperature and juvenile salmonid distribution (Torgersen et al. 1999, 2006). Cumulatively, these findings suggest that parr distribution across the MFJD at broad spatial scales largely depends on temperature and that inter-annual variation in thermal and flow conditions likely results in expansion (cool, higher flow years) and contraction (warm, lower flow years) of the parr distribution.

We aim to build a long-term dataset of adult spawning and juvenile rearing distributions in Middle Fork John Day River (MFJDR) that will span a range of contrasting environmental conditions and adult run sizes. To date, we have evaluated the rearing extent of Chinook Salmon parr in the MFJDR in 2021 and 2023 relative to spawning distributions in 2020 and 2022. A full description of 2021 efforts including the sampling design, survey methodology, and statistical approach used to extrapolate counts to abundance estimates is provided in Appendix D. Below, we describe the sampling design and methodology for 2023 surveys, which we intend to use consistently in future parr distribution surveys, including summer 2024.

Methods

Spawning ground surveys – led by ODFW and conducted by numerous partnering agencies and volunteers – are conducted annually throughout the spawning extent of the MFJDR (see Bare et al. 2021 for a full description of MFJDR spawning ground survey methodology). Briefly, the MFJDR spawning extent is surveyed weekly throughout peak spawning activity in mid-September, typically resulting in three complete surveys each year. However, in 2020, high smoke levels from wildfires precluded the first planned spawning ground survey, resulting in only two complete surveys (9/16 and 9/23). In 2022, three full surveys were conducted (9/14, 9/19, and 9/26) as well as an additional supplementary survey (10/12) upstream of rkm 110 that could not be sampled on 9/26. The spawning extent of the MFJDR is divided into reaches that are typically surveyed by two individuals walking on opposite stream banks during each spawning ground survey. When new redds are identified, surveyors mark redds with labeled flagging on adjacent vegetation to prevent recounting in subsequent surveys. During the final survey, a GPS point is taken for each redd.

Our 2021 sampling design was intended to characterize parr abundance across the rearing extent of that summer, in which conditions were abnormally warm and the rearing extent was contracted. We modified the sampling design in 2023 to encompass the entirety of the potential rearing extent and be repeatable among years regardless of environmental conditions and anticipated parr distribution. This involved expanding the spatial extent of mainstem survey reaches (2021 rkm range: 83.8 – 117.5; 2023 rkm range:

54.7 - 122.3) and surveyed tributaries (2021 rkm range: 79.8 – 112.8; 2023 rkm range: 58.3 – 112.8), which was informed by previous efforts characterizing Chinook Salmon parr distribution in the MFJDR (Handley et al. 2011; Handley and Ruzycki 2015).

Recognizing that crew availability and effort will vary among future years, we categorized potential mainstem sites and tributaries into priority tiers. With this approach, we plan to survey all Tier 1 reaches each year surveys are conducted, whereas Tier 2 reaches are considered supplementary and surveyed when possible. We used a Columbia Basin-wide set of points generated through a Generalized Random Tessellation Stratified (GRTS) survey design to select mainstem sites from the confluence with Slide Creek (rkm 54) to the headwaters in Phipps Meadows (rkm 121). There were 64 GRTS points along the mainstem of this extent. We determined that it was logistically feasible to survey approximately 30 mainstem reaches each year, and we selected a subset of 30 Tier 1 sites and 10 additional Tier 2 mainstem sites (Table 7). These sites were selected to maximize spatial coverage across the rearing extent. In 2023, we leveraged planned sampling by the Confederated Tribes of the Warm Springs Reservation of Oregon (CTWSOR), in which more intensive snorkel surveys were conducted from Caribou Creek (rkm 105) to Vinegar Creek (rkm 110) and in Phipps Meadows at the headwaters. These 11 CTWSOR reaches overlapped and replaced four Tier 1 and three Tier 2 reaches. We scaled mainstem survey reaches with river width (approximately 15x bankfull width), increasing linearly from 200 m at the farthest upstream site (rkm 120.8) to 400 m at the farthest downstream site (rkm 55).

In 2021, we surveyed nine tributaries via a combination of snorkeling (the 4 largest tributaries) and electrofishing. We surveyed 1-3 discrete reaches for electro-fished tributaries, whereas we snorkeled continuously from tributary mouths upstream until no Chinook parr were observed in three consecutive pools for snorkeled tributaries. Previous parr distribution surveys in MFJDR tributaries (Handley et al. 2011, 2012) demonstrated Chinook parr presence in additional tributaries, although the relative abundance of parr in these tributaries was not presented. For 2023 surveys and future years, we selected 20 tributaries, of which 11 were classified as Tier 1 (Table 8). To standardize methodology and accommodate the increased effort to survey more tributaries, we established discrete reaches at predetermined intervals that would all be surveyed via snorkeling. Chinook parr densities typically decrease with distance upstream from tributary mouths, and consequently, we applied shorter intervals between reaches closer to tributary mouths and increasing intervals farther upstream. For most tributaries, we established reaches every 250 m from the confluence to 1000 m upstream (i.e., reaches at 0, 250, 500, 750, 1000), then every 500 m upstream of 1000 m. Parr have been observed more than 5 km upstream in Camp Creek and Big Creek, and we therefore increased the interval to 500 m for the first 2 km and then 1000 m upstream of 2 km. Some reaches within private lands were removed due to lack of access, including two reaches in Big Creek (at 2000 m and 3000 m) and two reaches in Camp Creek (at 1500 m and 2000 m). Planned reach lengths were 50 m for smaller tributaries (n = 13) and 100 m for larger tributaries (n = 7). We surveyed reaches from downstream to upstream until zero parr were observed in a reach, which we considered the upstream extent of Chinook parr.

Snorkel surveys in summer 2023 were conducted within a 10-day window from 7/17-7/26. Snorkel surveys were conducted at the habitat unit-level, in which snorkelers recorded counts of Chinook Salmon parr (2021, 2023) and juvenile *O. mykiss* (2023) observed. Mainstem reaches were surveyed from the site GPS location upstream until the cumulative survey length exceeded the predetermined site-specific reach length. We visually delineated habitat units as pools, fast-non-turbulent (FNT; i.e., runs, glides), and fast-turbulent (FT; i.e., riffles). We sampled all pools and FNTs in both 2021 and 2023. In 2021, we sampled alternating

FTs in mainstem sites and every fourth FT in tributaries, whereas in 2023 we sampled a minimum of 25% of FTs by length for both mainstem and tributary reaches.

To adjust for imperfect detection in snorkel surveys, we measured unit-specific habitat attributes that can affect detection and applied the model developed by Staton et al. (2022) to predict detection probability of each surveyed unit. These attributes included unit type, average depth, density of large wood pieces, and an observer-determined visibility index. For each unit, we used the mean detection estimate and 80% confidence interval to expand the partial snorkel counts to mean abundance estimates and 80% CIs. We imputed abundance for skipped units (i.e., FTs) using mean density from sampled units of that site and unit type. We then summed abundance estimates across all units within a reach and divided by the cumulative length of units to obtain density estimates (parr m^{-1}) and associated confidence intervals at the reach scale.

Results

Below, we provide an overview of 2023 sampling efforts and a descriptive comparison of preliminary estimates relative to 2021. Note that in summer 2023, we collected paired snorkel count and mark-recapture data (see Appendix D of this report) to update parameter estimates in the Staton et al. (2022) snorkel detection model. We plan to rerun 2021 and 2023 count data through the updated model, which may alter abundance estimates considerably – these expanded counts should be considered preliminary.

The spawning extents of 2020 and 2022 were relatively similar but with several exceptions (Figure 26): 1) there were more redds in 2022 (n = 237) than 2020 (n = 162); 2) there were no redds upstream of rkm 114 in 2020, whereas 10 redds were observed between rkm 114 and rkm 121 in 2022; 3) the proportion of redds between rkms 80-90 was greater in 2020, whereas the proportion of redds between rkms 90-100 was considerably higher in 2022.

In 2021, we conducted snorkel surveys across 7.5 km of the mainstem and 6.1 kilometers of four tributaries, and we conducted electrofishing surveys across 2.6 km of five smaller tributaries. In 2023, we snorkeled all mainstem and tributary reaches. We surveyed 39 mainstem reaches totaling 11.2 km, which included 26 Tier 1 reaches, 11 reaches surveyed by CTWSOR that replaced four Tier 1 and two Tier 2 reaches, and two Tier 2 reaches (Table 7). We surveyed 8.6 km of 18 tributaries (Table 8), including 10 of the 11 Tier 1 tributaries (Summit Creek was dry and not snorkeled) and seven of the nine Tier 2 tributaries (Beaver Creek and Deep Creek not sampled), and one unplanned tributary at the farthest downstream extent that was surveyed due to the presence of greater streamflow than expected (Indian Creek; rkm 58).

Chinook Salmon parr were distributed across a wide spatial extent in the summer of 2023 (Figure 27). Parr were present in 36 of the 39 mainstem reaches, with parr being absent from only the farthest downstream (rkms 55 & 60) and upstream (rkm 122) reaches. This suggests that the spatial extent of our sampling design was appropriate to capture the mainstem parr rearing extent in 2023 and in future survey years. The highest estimated densities were within the Oxbow Conservation Area (rkms 92-98) and in the recently restored section from Vincent Creek to Davis Creek (rkms 109-112).

Parr were observed in all surveyed tributaries except Lick Creek, which is a small tributary of Camp Creek located four km upstream of the mainstem confluence. Parr were observed over 1 km upstream in eight tributaries (Table 8), including 3.0 km in Davis Creek, 3.5 km in Vinegar Creek, and 6.5 km in Camp Creek. Switching our tributary sampling design to reaches spaced at predetermined intervals was an effective approach for evaluating the upstream extent of parr in each tributary. We were able to identify the approximate upstream extent of parr in most tributaries (Figure 28). In 10 tributaries, we progressively

sampled reaches until zero parr were observed within a reach, and in three other tributaries (Vinegar Creek, Clear Creek, and Davis Creek) we identified barriers (Figure 29) within or above the farthest surveyed reach. We briefly snorkeled several units above these barriers to confirm the absence of parr but did not conduct full surveys.

Parr were distributed across a wider spatial extent of the mainstem in 2023 compared to 2021. We recognize that this may be partially attributed to differences in sampling design and extent, but several lines of evidence suggest that the parr rearing distribution was highly contracted in 2021 relative to 2023. First, temperature was negatively correlated with mainstem parr density in 2021, and temperatures for the majority of the mainstem downstream of Big Boulder Creek (rkm 88) exceed the threshold we identified (July mean maximum temperature = 25 °C) above which parr were not present (see Appendix D). Second, in 2021 we found that parr originating from warmer sections of the mainstem moved to cooler sections of the mainstem or adjacent tributaries, suggesting parr originating from or that moved to warmer, lower portions of the mainstem likely moved to tributaries, upstream mainstem habitats, or did not survive. Lastly, while scouting for sites to capture parr, we snorkeled several locations downstream of the farthest downstream mainstem reach indicated on the map (Figure 27, top left panel) and did not observe any parr; however, these data were not included. Additional years of data, especially those with lower flows and higher temperatures, are needed to rigorously draw conclusions about how variability in environmental conditions shape the contraction or expansion of parr distributions.

Next steps

Our goal is to evaluate the extent of inter-annual variability in juvenile Chinook and *O. mykiss* summer rearing distributions, and especially, what environmental (e.g., temperature, discharge) and biological (adult spawning distributions) factors shape this variation. This hinges on characterizing juvenile salmonid distributions in multiple years, including years of contrasting conditions (e.g., lower streamflow and higher temperatures vs higher streamflow and cooler temperatures). Consequently, we do not have a full dataset and have not conducted statistical analyses. Once additional years of data are collected – including planned surveys in summer 2024 – we will evaluate relationships between maximum temperature, parr abundance, and parr presence. These relationships will provide insight into the realized extent of suitable summer rearing habitat under varying conditions.

References

Flitcroft, R., K. Burnett, J. Snyder, G. Reeves, and L. Ganio. 2014. Riverscape Patterns among Years of Juvenile Coho Salmon in Midcoastal Oregon: Implications for Conservation. Transactions of the American Fisheries Society 143(1):26–38.

Handley, K. A., C. James, J. R. Ruzycki, and R. W. Carmichael. 2011. Fish population monitoring in the Middle Fork John Day River intensively monitored watershed - Annual Technical Report 2011. Oregon Department of Fish and Wildlife, Technical Report, La Grande, OR.

Handley, K. A., C. James, J. R. Ruzycki, and R. W. Carmichael. 2012. Fish population monitoring in the Middle Fork John Day River intensively monitored watershed - Annual Technical Report 2012. Oregon Department of Fish and Wildlife, Technical Report, La Grande, OR.

Handley, K. A., and J. R. Ruzycki. 2015. Fish Population Monitoring in the Middle Fork John Day River Intensively Monitored Watershed. Page 51. Oregon Department of Fish and Wildlife, Technical Report 212-920–10249, La Grande, OR.

Isaak, D. J., M. K. Young, D. E. Nagel, D. L. Horan, and M. C. Groce. 2015. The cold-water climate shield: Delineating refugia for preserving salmonid fishes through the 21st century. Global Change Biology. 21: 2540-2553. 21:2540–2553.

O'Sullivan, A. M., E. Corey, R. A. Cunjak, T. Linnansaari, and R. A. Curry. 2021. Salmonid thermal habitat contraction in a hydrogeologically complex setting. Ecosphere 12(10):e03797.

Quinn, T. P. 2007. The Behavior and Ecology of Pacific Salmon and Trout. University of British Columbia Press.

Staton, B. A., C. Justice, S. White, E. R. Sedell, L. A. Burns, and M. J. Kaylor. 2022. Accounting for uncertainty when estimating drivers of imperfect detection: An integrated approach illustrated with snorkel surveys for riverine fishes. Fisheries Research 249:106209.

Torgersen, C. E., C. V. Baxter, H. W. Li, and B. A. McIntosh. 2006. Landscape influences on longitudinal patterns of river fishes: Spatially continuous analysis of fish-habitat relationships. American Fisheries Society Symposium 48:473–492.

Torgersen, C. E., D. M. Price, H. W. Li, and B. A. McIntosh. 1999. Multiscale thermal refugia and stream habitat associations of Chinook Salmon in northeastern Oregon. Ecological Applications 9(1):301–319.

Walters, A. W., T. Copeland, and D. A. Venditti. 2013. The density dilemma: limitations on juvenile production in threatened salmon populations. Ecology of Freshwater Fish 22(4):508–519.

Tables and Figures

Table 7. Characteristics of MFJDR mainstem reaches in our sampling design and 2023 survey information. We plan to sample Tier 1 reaches in each survey year, whereas Tier 2 reaches are considered supplementary and will be surveyed in future years if time allows.

Reach ID	Priority	Rkm	Planned length (m)	utm_x	utm_y	Sampled in 2023	Sampled length (m)	Comments
MFJD_55	Tier 1	54.7	400	346501	4962367	yes	380	
MFJD_60	Tier 1	60.6	400	349836	4960344	yes	280	
MFJD_67	Tier 1	66.6	400	352550	4958102	yes	335	
MFJD_69	Tier 1	69.4	400	353370	4956231	yes	339	
MFJD_72	Tier 1	72.0	400	354847	4954793	yes	428	
MFJD_75	Tier 1	74.6	400	355966	4952363	yes	264	
MFJD_78	Tier 1	78.5	400	356910	4950641	yes	234	
MFJD_83	Tier 1	82.7	400	358546	4949868	yes	449	
MFJD_84	Tier 1	83.8	350	360451	4948705	yes	433	
MFJD_85	Tier 1	85.3	350	361830	4948427	yes	431	
MFJD_86	Tier 2	86.5	350	362889	4948233	no	NA	
MFJD_88	Tier 1	87.9	350	363788	4947278	yes	318	
MFJD_89	Tier 1	88.9	350	364571	4947340	yes	290	
MFJD_90	Tier 1	90.4	350	365538	4946669	yes	268	
MFJD_91	Tier 2	91.5	350	366294	4946458	no	NA	
MFJD_92	Tier 1	92.4	350	366793	4945955	yes	427	
MFJD_93	Tier 1	93.5	300	367399	4945507	yes	360	

Reach ID	Priority	Rkm	Planned length (m)	utm_x	utm_y	Sampled in 2023	Sampled length (m)	Comments
MFJD_95	Tier 1	94.6	300	368010	4944951	yes	288	
MFJD_97	Tier 1	97.0	300	369552	4944471	yes	334	
MFJD_98	Tier 2	98.3	300	370477	4944655	no	NA	
MFJD_99	Tier 1	99.1	300	370910	4944186	yes	314	
MFJD_100	Tier 2	99.8	300	371321	4943739	no	NA	
MFJD_101	Tier 2	100.9	300	372234	4943433	no	NA	
MFJD_102	Tier 1	101.6	300	372628	4943071	yes	398	
MFJD_103	Tier 1	102.6	300	373487	4943133	yes	290	
MFJD_104	Tier 1	104.5	250	374650	4942107	yes	235	
MFJD_106	Tier 2	105.9	250	375603	4941863	replaced	211-216	Replaced by V2C_1 & 3
MFJD_107	Tier 1	106.6	250	376059	4941651	replaced	212	Replaced by V2C_5
MFJD_108	Tier 1	107.7	250	376578	4941020	replaced	220-225	Replaced by V2C_7 & 9
MFJD_109	Tier 2	108.8	250	377305	4940479	replaced	342	Replaced by V2V_1
MFJD_110	Tier 1	109.7	250	377916	4939944	replaced	224-298	Replaced by V2V_3 & 5
MFJD_111	Tier 1	111.1	250	378950	4939325	yes	265	
MFJD_112	Tier 1	112.2	250	379834	4938956	yes	224	
MFJD_113	Tier 1	113.1	200	380635	4938874	yes	191	
MFJD_114	Tier 1	114.1	200	381394	4939152	yes	203	
MFJD_116	Tier 1	115.6	200	382119	4940038	yes	174	
MFJD_117	Tier 2	117.4	200	383378	4939359	no	NA	
MFJD_118	Tier 2	118.1	200	383934	4939453	yes	158.6	
MFJD_119	Tier 1	119.3	200	384599	4938940	yes	188.7	
MFJD_121	Tier 1	120.8	200	385235	4937926	replaced	202-271	Replaced by Phipps_1, 3, & 5

Table 8. Characteristics of MFJDR tributaries in our sampling design and 2023 survey information. Planned length indicates the predetermined target length for individual reaches; Sampled length indicates the summed length of all sampled reaches; Max reach indicates the farthest upstream reach that was surveyed; Max parr obs. indicates the farthest upstream reach that parr were observed.

Tributary	Priority	Rkm	Planned length (m)	Sampled in 2023	# reaches sampled	Sampled length (m)	Max reach (m)	Max parr obs. (m)	Comments
Indian	NA	58.3	100	yes	2	200	250	250	Added
Big	Tier 1	64.1	100	yes	5	600	3500	1500	
Bear	Tier 2	74.7	50	yes	3	308	750	500	
Camp	Tier 1	79.7	100	yes	8	936	6500	6500	
Lick	Tier 2	79.7	50	yes	1	107	0	NA	No parr
Big Bldr.	Tier 1	88.1	100	yes	7	766	2000	2000	
Beaver	Tier 2	92.8	50	no	NA	NA	NA	NA	Not sampled
Ruby	Tier 2	94.2	50	yes	4	395	750	500	
Granite Bldr.	Tier 1	95.1	100	yes	5	558	1000	750	
Butte	Tier 1	96.4	50	yes	5	364	1500	750	
Little Butte	Tier 2	101.1	50	yes	3	315	750	500	
Little Bldr.	Tier 2	103.1	50	yes	4	457	750	750	
Deerhorn	Tier 2	104.0	50	yes	3	302	500	250	

Tributary	Priority	Rkm	Planned length (m)	Sampled in 2023	# reaches sampled	Sampled length (m)	Max reach (m)	Max parr obs. (m)	Comments
Caribou	Tier 2	105.4	50	yes	3	313	500	250	
Dead Cow	Tier 1	108.3	50	yes	4	201	1000	1000	
Vinegar	Tier 1	110.0	100	yes	10	1075	3500	3500	
Davis	Tier 1	110.7	100	yes	9	523	3000	3000	
Bridge	Tier 1	112.0	50	yes	4	231	1500	1500	
Clear	Tier 1	112.8	100	yes	8	951	2500	2500	
Summit	Tier 2	123.5	50	no	NA	NA	NA	NA	Stream was dry

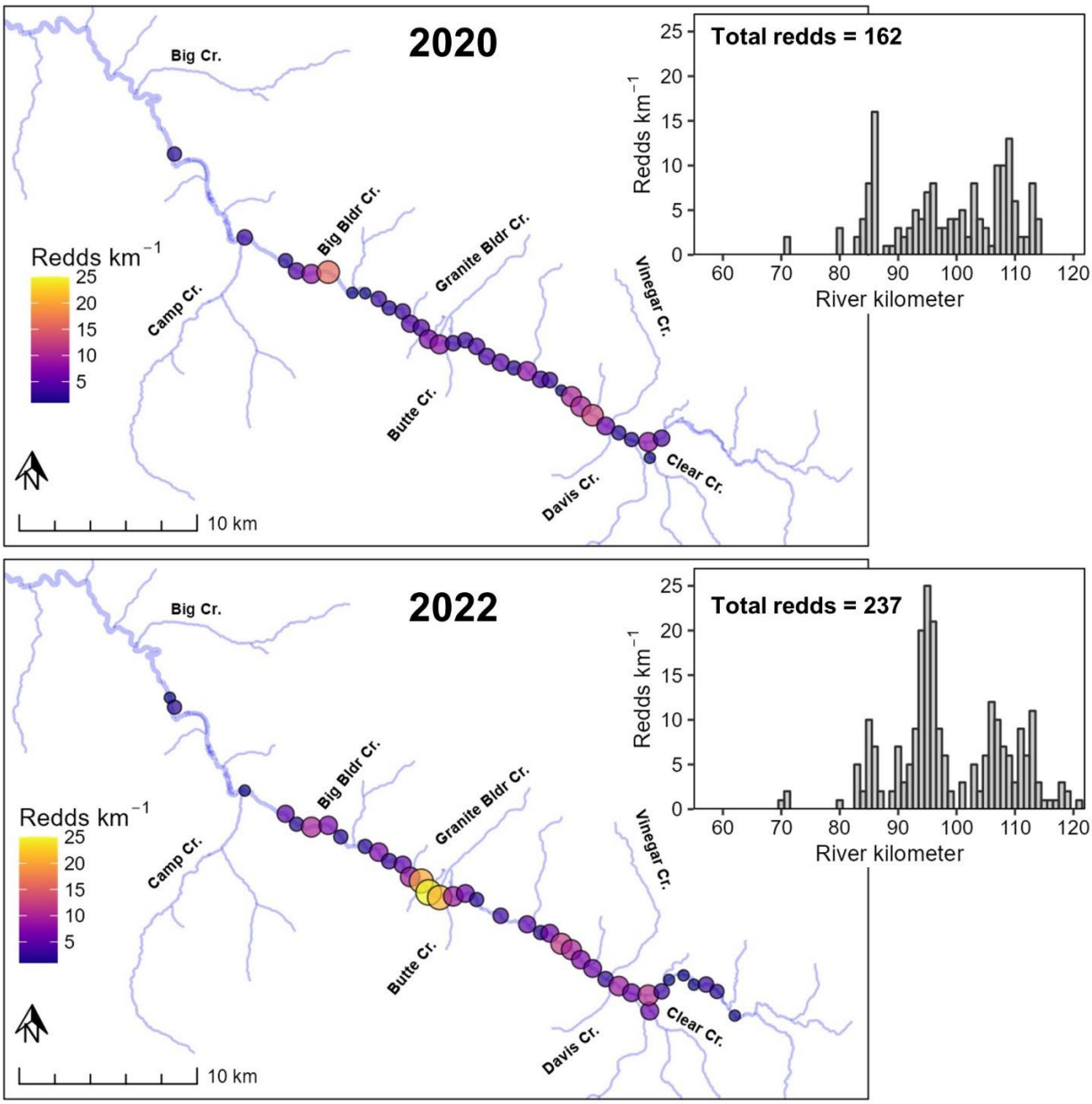

Figure 26: Map of redd density (redds km^{-1}) across the Middle Fork John Day River in 2020 and 2022 and the distribution of redds by river kilometer in each year (insets).

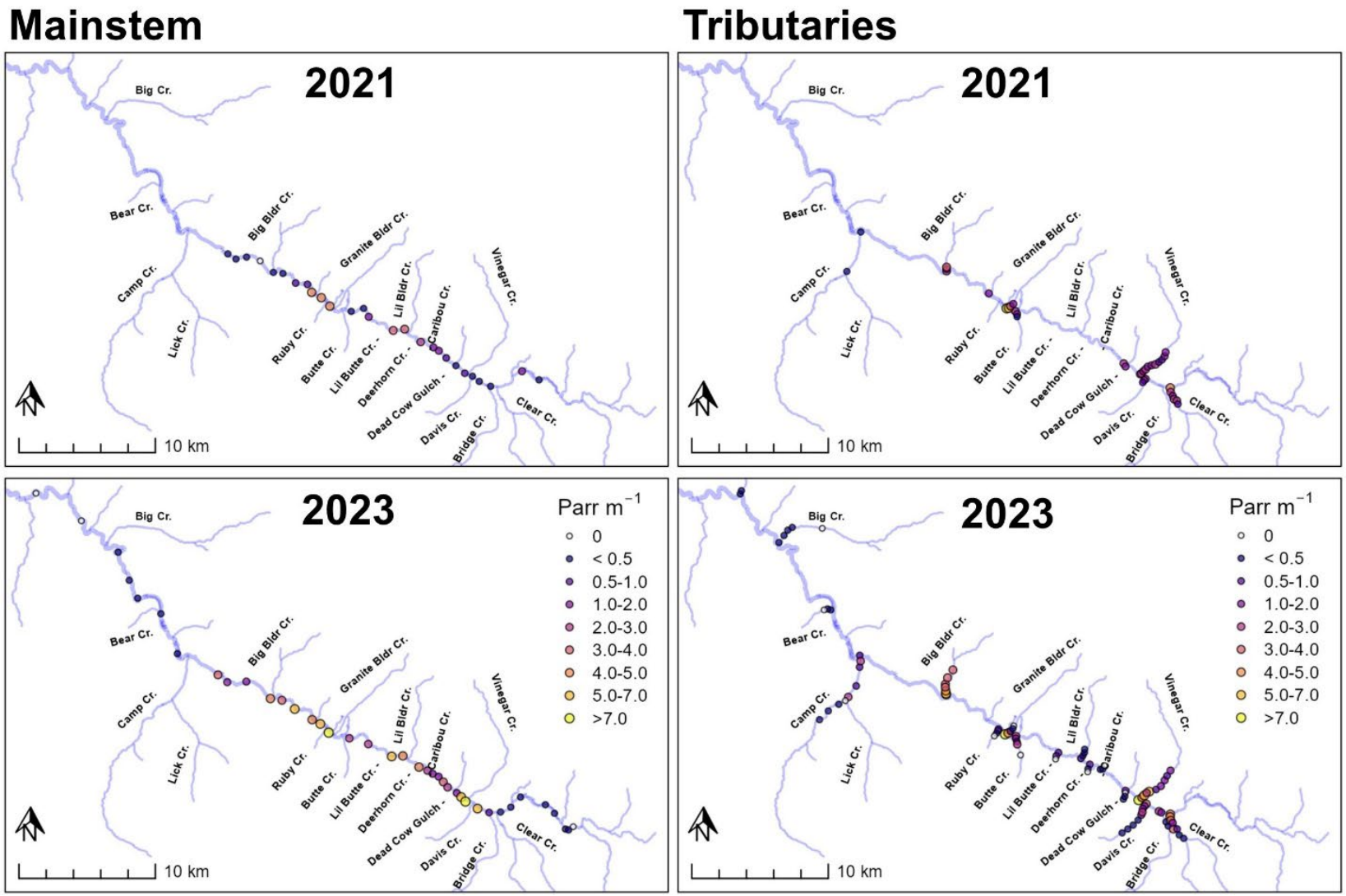

Figure 27: Parr densities at surveyed mainstem (left panels) and tributary (right panels) reaches across the Middle Fork John Day River in the summers of 2021 (top panels) and 2023 (bottom panels).

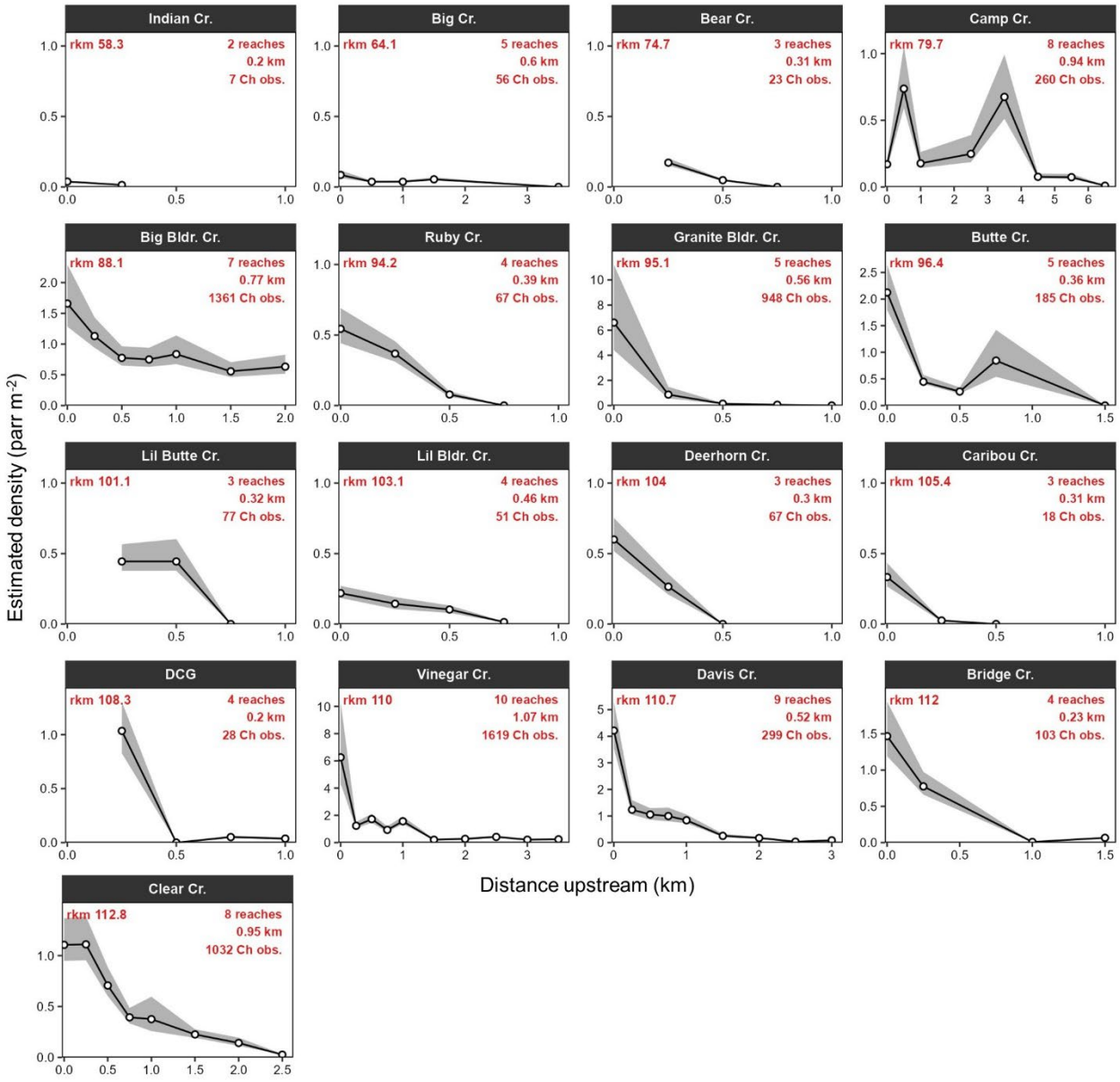

Figure 28: Chinook Salmon parr density estimates (parr m^2) within surveyed reaches of 17 tributaries (Lick Creek not shown as 0 parr were observed in the first reach). Grey shading indicates the 80% confidence interval.

Figure 29: Examples of structures identified as barriers to parr upstream passage in mid-summer.

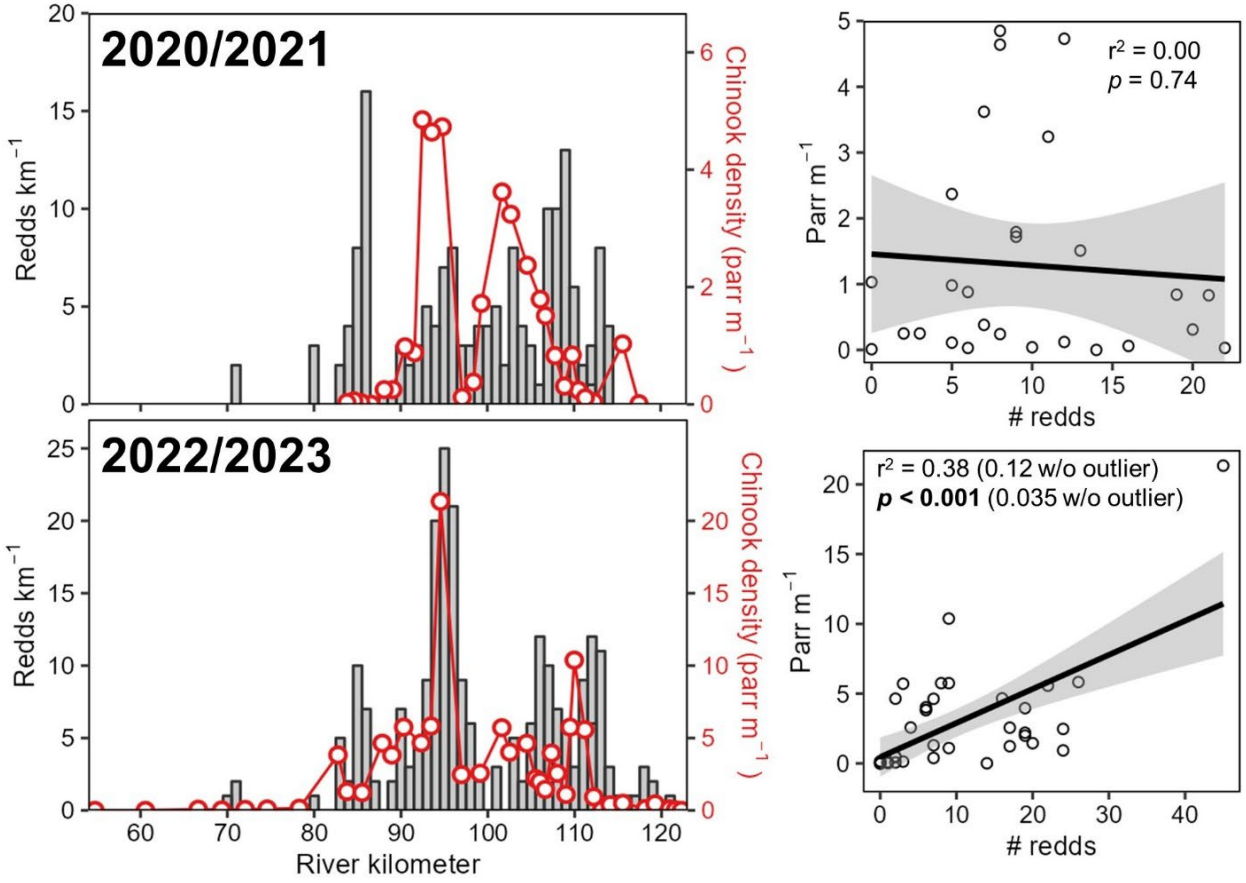

Figure 30: The distribution of 2020 and 2022 redds (grey bars) relative to the distribution of their offspring (parr; red points and lines) the following summer in 2021 and 2023. The right panels show the linear relationship between the number of redds (within 1 km upstream and downstream of parr survey reaches) and estimated parr abundance. The bottom right panel shows model fit with and without the outlier in the upper right corner.

Benthic macroinvertebrates

Background

Aquatic macroinvertebrate communities are important ecological components of river ecosystems; however, these communities have experienced significant declines in species richness, biomass, and distribution as the result of anthropogenic stressors including climate change (Domisch et al. 2011). Assessments of benthic macroinvertebrate diversity and density provide information about water quality and overall river health as well as the integrity of aquatic food webs, which may present a bottleneck for salmonid populations in the Columbia River basin (Independent Scientific Advisory Board 2011; Naiman et al. 2012). Both river basin management and restoration methods typically focus on physical habitat conditions, which may neglect to address the influence of management and restoration actions on aquatic food webs and the corresponding impact to salmonid populations (Bellmore et al. 2017; Sullivan and White 2017).

Since 2010, CRITFC has monitored fish habitat conditions in the Grande Ronde basin, including benthic macroinvertebrate sampling to assess salmonid prey resources as well as overall habitat condition to

evaluate the effectiveness of aggregate restoration activities. Benthic macroinvertebrate (BMI) samples collected during the 2022 field season contribute to long-term BMI monitoring efforts in the Grande Ronde basin conducted by CRITFC as well as partnering tribal, state, and federal agencies. The widespread spatiotemporal scope of this dataset provides the opportunity to evaluate trends in BMI density and diversity in relation to restoration effectiveness and climate change-related variables like streamflow and stream temperature as well as the continued development of BMI metrics as indicators of food availability for salmonids (White et al. 2019).

Methods

Aquatic macroinvertebrate sampling was conducted in 2022 by crews from CRITFC and the Grande Ronde Model Watershed (GRMW) at 22 sites in the upper Grande Ronde River, Meadow Creek, McCoy Creek, Waucup Creek and Limber Jim Creek using a spatially balanced random survey design (Stevens and Olsen 2004; Figure 31). Prior to sampling, each reach was divided into 11 equidistant transects across the river channel. Beginning at the farthest downstream transect, the first sample location was randomly selected as the right, center or left of the transect (25%, 50% and 75% of the wetted width, respectively). Samples were collected using a D-framed kick net with 500 µm mesh, in which substrate within the quadrat (0.3 x 0.3 m) was thoroughly brushed prior to vigorously kicking the substrate to a depth of 10 cm for 30 seconds. In instances where transects fell within slow water habitats such as pools and glides, kick nets were dragged repeatedly through the kicked area to ensure that all organisms were collected. The process was completed at each transect, resulting in a composite sample which was then transferred into one or more sample jars and preserved in 95% ethanol.

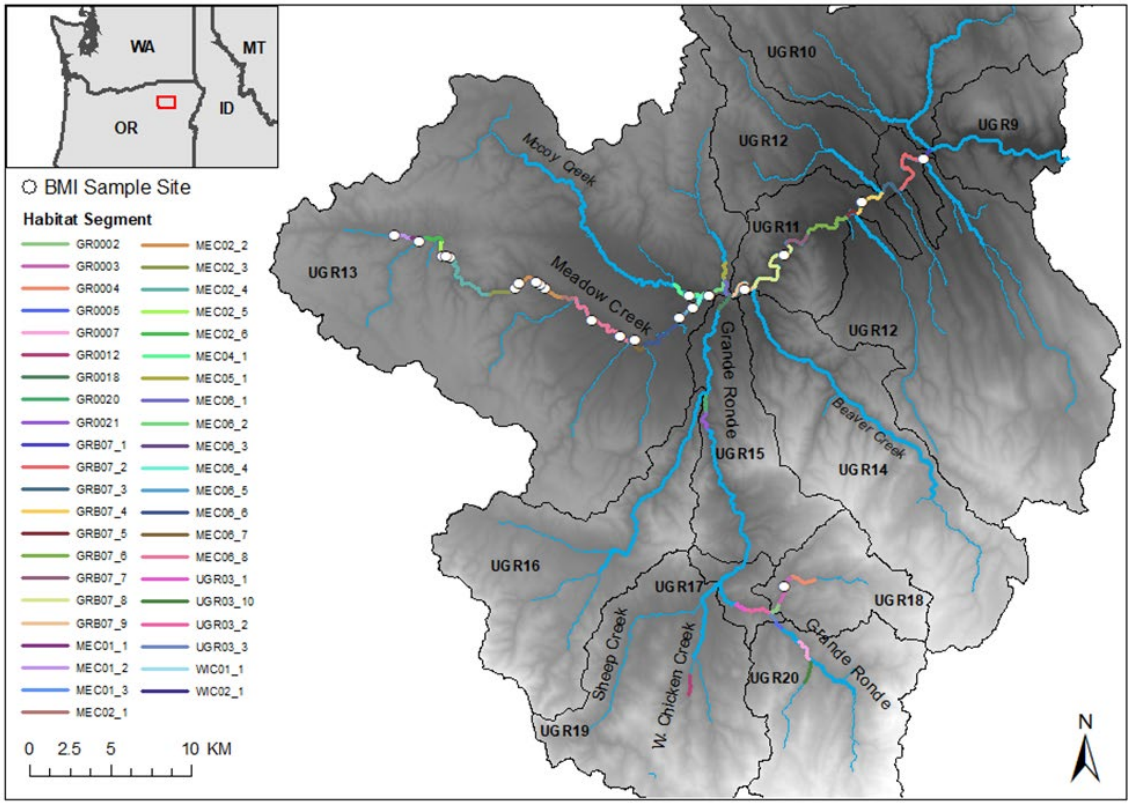

Figure 31. Map of biological sample reaches subsampled for benthic macroinvertebrates in the summer of 2022 *in the upper Grande Ronde (4 sites), Meadow Creek (15 sites), Waucup Creek (1 site) and Limber Jim Creek (1 site).*

Following the completion of benthic macroinvertebrate sampling, samples were delivered to a professional taxonomic lab (Rhithron Associates, Missoula, MT) for subsampling and taxonomic analysis. In addition to standard indices typically derived from benthic macroinvertebrate (BMI) data such as indices of biotic integrity (IBIs), BMI samples were also used to calculate novel metrics including descriptive indices of ecological networks (Cohen et al. 2003) and food availability for salmonids based on life history characteristics, propensity to enter the water column, palatability to salmonids, and other characteristics (Rader 1997). Full details of metric development are found in Sullivan and White (2017).

Results

Benthic macroinvertebrate density (individuals/m^2) varied considerably across reaches sampled during the 2022 field season, with the highest densities observed in Meadow Creek; however, the lowest densities (249 individuals/m^2 and 663 individuals/m^2) were also observed in Meadow Creek, with no clear longitudinal patterns, indicating that the reaches with exceptionally high (relative) density are likely reflective of sampling variability or localized habitat conditions (temperature, flow) rather than an indicator of overall water quality and river health in Meadow Creek (Table 9). Densities in reaches sampled in 2022 ranged from 249 to 3,699 (mean = 2,851.45 individuals/m^2), with similar variability in biomass, which ranged from 0.30 to 167.36 g/m^2.

*Table 9. Benthic macroinvertebrate indi*ces derived from summer 2022 sampling in the upper Grande Ronde River (UGR), Meadow Creek (MC), Waucup Creek (WC), McCoy Creek (MCC) and Limber Jim Creek (LJC).

Stream	Reach	Density (ind. m^2)	Biomass (g m^2)	O/E (obs./exp.)	E. OR. IBI Score	Temp. Sens. Taxa (#)	Rader ASC_{Rel}
UGR	CBW05583-109658	2691	1.71	0.43	30	0	4086
UGR	dsgn4-000245	3699	23.67	0.43	30	0	3255.76
UGR	dsgn4-000205	2235	2.30	0.35	30	0	4066.41
UGR	CBW05583-374874	1049	1.31	0.28	22	0	3547.94
LJC	CBW05583-108010	1541	0.85	0.71	38	17	3496.76
MCC	CBW05583-015162	1725	2.52	0.35	26	3	3524.95
MC	dsgn4-000213	249	0.30	0.21	26	0	3583.46
MC	CBW05583-252730	2588	2.80	0.43	32	0	3809.07
MC	CBW05583-514874	7941	167.36	0.43	28	0	3761.92
MC	CBW05583-498490	1670	0.79	0.35	24	0	3502.53
MC	ORW03446-139144	3082	82.70	0.50	34	0	3911.42
MC	CBW05583-020282	1109	0.62	0.43	32	0	3991.11
MC	CBW05583-275866	663	0.31	0.35	36	2	3549.26
MC	Stky-P2Cntrl	8029	6.96	0.43	32	0	3870.38
MC	Stky-P2-Ex1	3948	1.47	0.43	36	0	4027.88
MC	Stky-P3-Ex2	2578	4.47	0.35	28	0	3937.95
MC	Stky-P5-Ex2	5020	36.81	0.43	30	0	3942.49
MC	dsgn4-000093	2637	8.83	0.28	26	0	3670.50
MC	ORW03446-101560	2007	0.98	0.35	30	0	3618.64
MC	ORW03446-125832	1971	2.03	0.28	22	0	3859.21
MC	Stky-P2-Ex3	3159	1.75	0.43	34	0	4154.08
WC	CBW05583-480666	3141	29.43	0.35	30	2	3787.10

At the biologically significant reach (BSR) scale, UGR11, which encompasses the upper Grand Ronde River from Hilgard Junction State Park to the confluence with Meadow Creek, had a mean density of 2,418 individuals/m^2 and a mean biomass of 7.25 g/m^2 (Table 10). UGR13, encompassing the Meadow Creek subbasin, had a mean density of 3,030 individuals/m^2 and the highest biomass among the three BSRs (20.60 g/m^2). UGR18, which encompasses Limber Jim Creek, had the lowest density (1,541 individuals/m^2) and correspondingly the lowest biomass (0.85 g/m^2), but was only represented by a single site.

Table 10. Benthic macroinvertebrate summary statistics averaged by biologically significant reach (BSR).

BSR	Reaches Sampled	Mean Density (ind. m^2)	SD	Mean Biomass (g m^2)	SD	Mean O/E	SD	IBI Score	SD
UGR11	4	2418.50	1098.96	7.25	10.96	0.37	0.07	28.00	4.00
UGR13	17	3030.41	1964.37	20.60	43.32	0.36	0.08	29.76	4.12
UGR18	1	1541.00	NA	0.85	NA	0.71	NA	38.00	NA

The macroinvertebrate Observed/Expected Taxa Loss model (O/E) quantifies the ratio of taxa loss or gain by comparing a list of "Expected" taxa based on reference locations with the BMI sample collected at a monitoring location (the "Observed") (Hubler 2008). Sites with scores of less than one had fewer taxa at a site than were predicted by the model, while sites with scores greater than one are either equivalent to reference locations or may even surpass reference locations as the result of management or restoration actions (i.e., carcass supplementation, etc.). All reaches sampled in 2022 had O/E scores lower than one, ranging from 0.21 to 0.71 (Table 9). At the BSR scale, UGR11 had a mean O/E score of 0.37, while UGR13 had a mean O/E score of 0.38, indicating similar levels of benthic macroinvertebrate assemblage loss between the upper Grande Ronde below the confluence with Meadow Creek and the Meadow Creek watershed (Table 10). UGR1 (Limber Jim Creek) had a mean O/E score of 0.71, which also suggests degraded stream conditions relative to reference areas, but to a lesser extent than warmer areas of the basin.

Aquatic species composition (ASC_{Rel}), a score which incorporates the expected or actual abundance of taxa for each site, is weighted to account for the potential contribution of each taxon to the salmonid prey base determined by life history and ecological traits related to drift propensity (Sullivan and White 2017; Rader 1997). As a BMI metric, ASC_{Rel} indicates the proportional abundance of taxa in a sample likely to be contributing to the concentration of macroinvertebrate drift, making it a pertinent metric for assessing habitat suitability for drift foraging fish such as juvenile salmonids (Hayes et al. 2007).

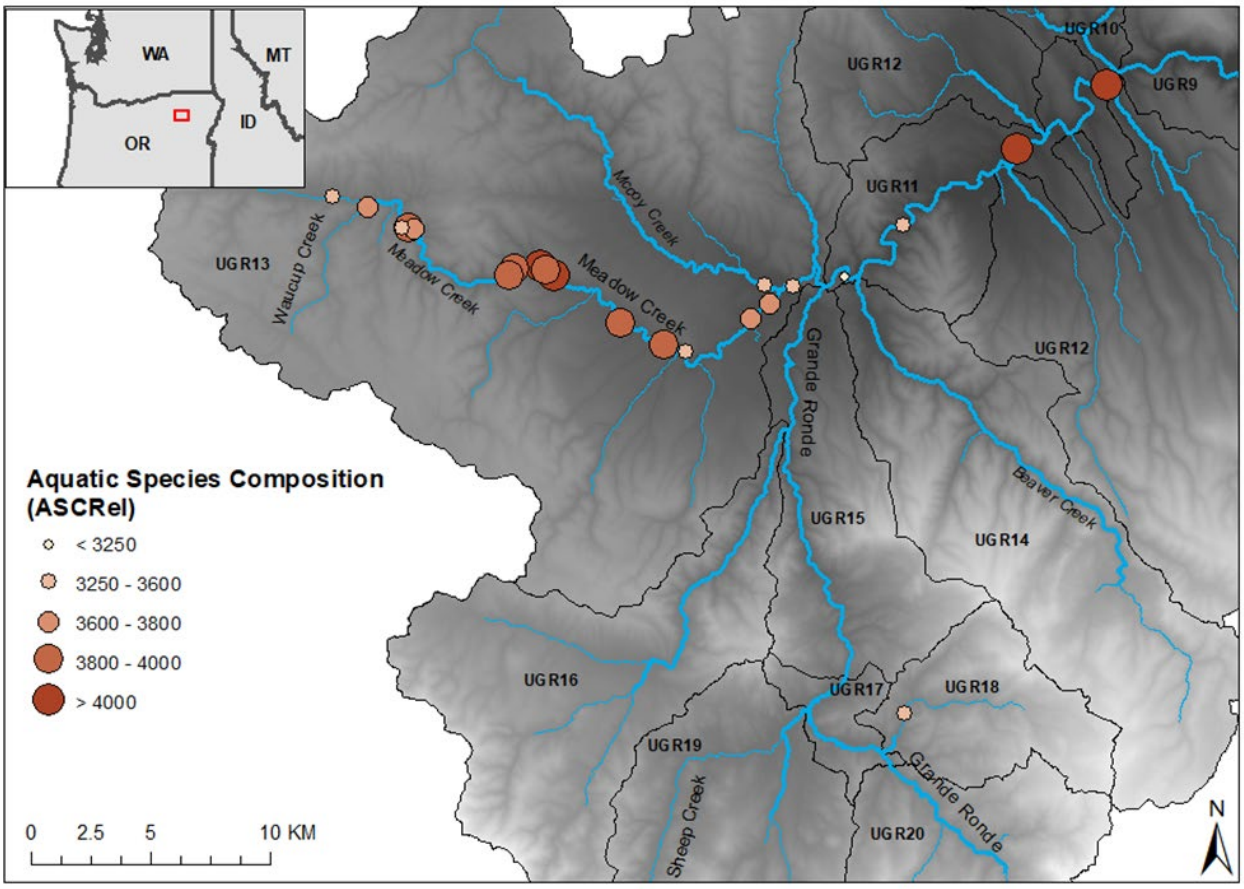

Figure 32. Distribution of drift propensity metric (ASC_{Rel}) values in the upper Grande Ronde River, Meadow Creek, Waucup Creek and Limber Jim Creek. Increasing symbol size and shade indicate increasing ASC_{Rel} scores.

Higher scores observed in the downstream reaches of the Grande Ronde River than those observed farther upstream and highly variable scores observed in the Meadow Creek watershed from the confluence with the Grande Ronde River to the headwaters upstream of the confluence with Waucup Creek (Figure 32). The two highest scores observed in the Grande Ronde were from sites in Hilgard Junction State Park and Longley Meadows at the downstream edge of the 2022 sample extent. Extensive restoration aimed at fish habitat enhancement was implemented in Longley Meadows in 2020 and 2021, and the high ASC_{Rel} observed at this site may be an indicator of restoration effects as compared to the two upstream sample locations, which had substantially lower scores (including the lowest overall score) and have received no restoration efforts. Limber Jim Creek, another post-restoration reach that was sampled in 2022, had a relatively low score compared to the rest of the sample sites (Figure 32).

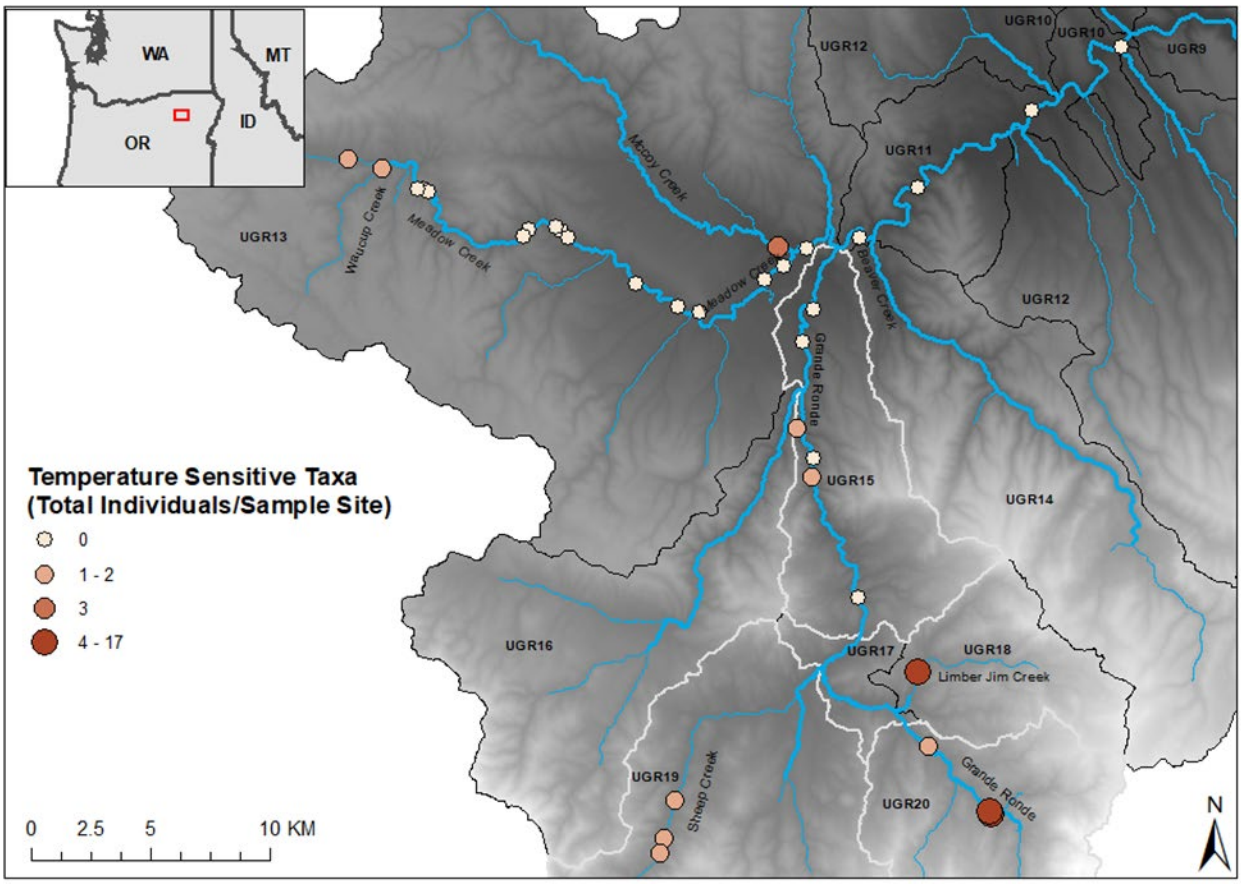

Figure 33. Distribution of temperature sensitive taxa (individuals/sample) observed at BMI sites in 2022 in the upper Grande Ronde River, Meadow Creek, Waucup Creek and Limber Jim Creek (UGR18). BSRs outlined in light gray indicate sites sampled in 2021 in the upper Grande Ronde River and Sheep Creek. Increasing symbol size and shade indicate increasing ASC_{Rel} scores.

The number of temperature-sensitive indicator taxa observed in sample reaches in 2022 ranged from 0 to 17, with all samples in which no temperature-sensitive taxa were observed occurring in UGR15, the farthest downstream BSR, while the highest numbers of temperature-sensitive indicator taxa were observed in UGR18. The mean number of sensitive taxa in UGR11 was 0, the mean in UGR13 was 0.41 and the mean in UGR18 was 17 (Table 10). Samples collected in 2021 and 2022 indicate higher numbers of temperature-sensitive indicator taxa with increasing distance upstream in the basin, with the majority of samples detecting no temperature-sensitive taxa (Figure 33). These observed patterns correspond with water temperature data collected throughout the basin.

The Eastern Oregon Benthic Index of Biological Integrity (IBI) score provides an index value which describes the condition of stream macroinvertebrate communities and is calculated based on a multi-metric approach utilizing a suite of metrics (taxa richness, percent pollution-tolerant taxa, percent sensitive taxa, etc.) to describe various aspects of assemblage composition (Hubler 2008). IBI scores range from 10-50, with 10 indicating very poor biotic integrity and 50 indicating conditions equivalent to what would be found in a reference stream. IBI scores in reaches sampled during summer 2022 ranged from 22 to 38, with the highest score observed in Limber Jim Creek (UGR18) and the lowest observed in the Grande Ronde River (UGR11) (Table 9). The mean IBI score for UGR11 was 28, indicating poor to fair conditions with depressed taxa richness and dominance of tolerant taxa. The mean IBI score for UGR13 was 30, indicating

lower taxa richness, lower relative abundance of predators, and a greater proportion of tolerant taxa relative to predicted reference streams. The mean score for UGR18 was 38 (only one sample collected), the only BSR sampled that indicated fair to good conditions (Table 10).

Next Steps

Further analysis is needed relating food availability metrics and other BMI derived metrics to fish abundance, diet, growth, and productivity as well as an evaluation of spatiotemporal trends in the diversity and abundance of macroinvertebrates using spatial stream-network (SSN) models. Additionally, we are working with Rhithron Associates, LLC to compile all macroinvertebrate data (benthic, drift and diet) collected by CRITFC, CTUIR, and ODFW between 2010 and 2022 and recompute metrics using a consistent set of code and associated models. This effort was deemed necessary because previously collected data was not organized into a single usable database, metrics were inconsistent across years, computational methods have changed over time, and metadata describing the various metrics was lacking. The new and comprehensive database will facilitate long-term comparative analyses of macroinvertebrate communities.

References

Bellmore, J. Ryan, Joseph R. Benjamin, Michael Newsom, Jennifer A. Bountry, and Daniel Dombroski. 2017. Incorporating Food Web Dynamics into Ecological Restoration: A Modeling Approach for River Ecosystems. Ecological Applications 27 (3): 814–32. https://doi.org/10.1002/eap.1486.

Cohen, J. E., T. Jonsson, and S. R. Carpenter. 2003. Ecological community description using the food web, species abundance, and body size. Proceedings of the National Academy of Sciences 100(4):1781–1786.

Domisch, Sami, Sonja C. Jähnig, and Peter Haase. 2011. Climate-Change Winners and Losers: Stream Macroinvertebrates of a Submontane Region in Central Europe. Freshwater Biology 56 (10): 2009–20. https://doi.org/10.1111/j.1365-2427.2011.02631.x.

Independent Scientific Advisory Board. 2011. Columbia River Food Webs: Developing a broader scientific foundation for fish and wildlife restoration. Portland, Oregon.

Hayes, John W., Nicholas F. Hughes, and Lon H. Kelly. 2007. Process-Based Modelling of Invertebrate Drift Transport, Net Energy Intake and Reach Carrying Capacity for Drift79 Feeding Salmonids. Ecological Modelling 207 (2–4): 171–88. https://doi.org/16/j.ecolmodel.2007.04.032

Hubler, S. 2008. PREDATOR: Development and use of RIVPACS-type macroinvertebrate models to assess the biotic condition of wadeable Oregon streams. Unpublished report prepared by the Oregon Department of Environmental Quality, Watershed Assessment Section.

Naiman, R.J., J.R. Alldredge, D.A.Beauchamp, P.A. Bisson, J. Congleton, C.J. Henny, N. Huntly, R. Lamberson, C. Levings, E.N. Merrill, W.G. Pearcy, B.E. Rieman, G.T. Ruggerone, D. Scarnecchia, P.E. Smouse, and C.C. Wood. 2012. Developing a broader scientific foundation for river restoration: Columbia River food webs. Proceedings of the National Academy of Sciences of the United States of America 109(52): 21201–21207. doi:10.1073/pnas.1213408109. PMID:23197837.

Rader RB. 1997. A functional classification of the drift: traits that influence invertebrate availability to salmonids. Can. J. Fish. Aquat. Sci. 54:1211–1234.

Stevens, D.L., and A.R. Olsen. 2004. Spatially Balanced Sampling of Natural Resources. Journal of the American Statistical Association 99 (465): 262–78.

Sullivan S.P. and White S.M. 2017. Methods supporting the development of food web metrics from benthic macroinvertebrate data. CRITFC Technical Report No. 17-05. Prepared for the Bureau of Indian Affairs Rights Implementation Climate Change Contract AO9AV00480 by Rhithron Associates, Inc., Missoula, MT, and Columbia River Inter-Tribal Fish Commission, Portland, OR.

White, S., C. Justice, L. Burns, B. Staton, D. Graves, and M. Kaylor. 2020. Assessing the status and trends of spring Chinook habitat in the upper Grande Ronde River and Catherine Creek: annual report 2019. Columbia River Inter-Tribal Fish Commission Technical Report 20-04. Portland, OR. 249p.

Objective D-2: Index of Chinook Salmon rearing capacity

This work was completed and described in the 2021 annual report (White et al. 2022).

References

White, S., C. Justice, B. Staton, L. Burns, and M. Kaylor. 2022. Evaluating salmonid and stream ecosystem response to conservations measures and environmental stressors in the Columbia River basin. Page 74. Columbia River Inter-Tribal Fish Commission, BPA Project # 2009-004-00, Portland, OR.

Objective D-3: Finalize pre-spawn mortality analysis

This work was completed and described in the 2021 annual report.

See references from Objective D-2.

Objective D-4: Complete study of juvenile fish emergence timing and floodplain inundation

Little progress has been made since the 2022 annual report as we and our collaborators on this project experienced time constraints associated with prioritizing other work elements. We expect to make substantial progress in 2024. The goal of this project is to evaluate juvenile salmon floodplain use potential by linking floodplain inundation dynamics (e.g., timing, duration, magnitude) to emergence timing in three NE Oregon subbasins: The Middle Fork John Day River (MFJD), Catherine Creek (CC), and the Upper Grande Ronde River (UGR). We have completed floodplain inundation modeling for MFJDR and we dedicated considerable effort in 2023 to modeling CC and UGR floodplain inundation. However, we encountered challenges with the complex and variable hydrology of these subbasins, particularly the transition from snow-dominated headwaters to rain-dominated lower areas of each subbasin. This presented a problem because streamflow data from fixed-location stream gauges are used to predict temporally continuous estimates of floodplain inundation for each 200 m reach, but the timing of streamflow at gauges differs from the timing expected at individual reaches along the 50 km extent of mainstem. We explored several options to account for streamflow timing along this snowmelt- to rain-dominated gradient and determined that the most appropriate approach is to use National Water Model predictions to apply

weighting factors to each reach that reflects the proportional influence of upstream snow-dominated vs. downstream rain-dominated gauges on reach-scale flow predictions. Once we complete floodplain modeling for CC and UGR, we will integrate already completed emergence timing estimates from each basin to assess the temporal overlap of floodplain accessibility and emergence timing.

Objective D-5: Complete study of juvenile Chinook dispersal and floodplain use

A draft manuscript associated with this study is attached to this report (Appendix D). We included an abstract overviewing the study and findings below.

Abstract

For many aquatic taxa, juvenile dispersal from spawning locations to rearing habitats is a critical process influencing individual fitness and population dynamics. However, our understanding of dispersal patterns in naturally spawning populations remains largely unknown due to the logistical challenges of tracking movement at early life stages using traditional marking and tagging approaches. We evaluated dispersal patterns of a spring-run Chinook Salmon population in a NE Oregon riverscape using genetic parentage-based tagging to trace juveniles captured from summer rearing habitats to maternal parents sampled from spawning locations the prior year. We also estimated parr abundance across the watershed to adjust dispersal estimates for sampling bias, and to evaluate dispersal as the link between the distributions of spawners and their offspring. Overall dispersal of the 1,326 parr (*n* sampled = 3,388) paired to female adults (*n* = 64) was downstream-biased (median = -0.77 km; 68% dispersed downstream). Dispersal distances were high relative to those found in other studies, with 25% of parr dispersing more than 0.9 km upstream and 25% dispersing more than 3.7 km downstream (range = -28.6 -10.6 km). Dispersal patterns followed longitudinal trends with parr originating higher in the watershed showing downstream dispersal bias, higher variability in dispersal, and farther dispersal distances whereas juveniles originating downstream showed upstream bias, lower variability, and shorter distances. Nested within these trends, parr originating in the warmest sections of the mainstem typically dispersed to cooler portions of the mainstem or tributaries, suggesting that thermal conditions were a primary driver of observed dispersal. Lastly, dispersal distance was associated with larger length-at-capture for parr that dispersed downstream but not upstream, which may reflect the unique pattern of earlier emergence upstream, providing competitive advantages for downstream dispersers over later emerging conspecifics. Overall, these findings suggest that heterogeneity in biophysical conditions within and among watersheds may translate to variable patterns of dispersal. These findings additionally provide guidance for prioritizing restoration efforts to address limiting factors and maximize habitat use through better alignment with juvenile salmon ecology.

Objective E: Relate population-level fish response to habitat change in the Grande Ronde basin and potentially other basins

Objective E-1: Grande Ronde Phase 1 – Development of spring Chinook statistical estimation Life Cycle Model

We have finalized development of the statistical life cycle model for Grande Ronde spring Chinook Salmon and have made significant progress on a manuscript documenting it. The abstract of the current draft is

included below. The draft manuscript text/figures are included in Appendix E, and complete mathematical details are in Appendix F (which will accompany the manuscript upon submission as a supplement).

ABSTRACT: Pacific salmon populations face different mortality sources throughout life, requiring monitoring and modeling at various life stages to understand the relative influence of regulating processes. For example, density-dependence may be more important for freshwater juveniles, whereas environmentally forced ocean conditions may drive later-life outcomes independent of density – quantification of these kinds of phenomena requires spatiotemporal analyses with sufficient resolution. State-space models are a flexible and robust approach to analyzing time series population data. We constructed a state-space model for Grande Ronde Basin (NE Oregon, USA) spring Chinook Salmon that tracks the abundance of ~30 cohorts from 4 spawning populations as they transition through life, modeling variability in freshwater juvenile growth/survival using density-dependent relationships and stochastic process noise that acknowledges synchronous dynamics. Model substructures include rearing origin type, juvenile life history type, and adult age-of-return to account for heterogeneity at these scales. The model fits to empirical information collected by many monitoring projects and includes an index of habitat quality to scale density-dependent processes. Posterior predictive examinations revealed the model could reproduce data patterns and that noise terms largely conformed to model assumptions. We found evidence of early-life density-dependent survival and growth, with subsequent over-wintering and out-migration survival mediated by early-life growth rates. Parr rearing capacity and growth rates showed positive, though uncertain, relationships with weighted usable habitat availability. We found covariances to be overwhelmingly positive, indicating synchrony among populations within the basin. Simple post-hoc analyses illustrated that juvenile life history is important for increasing smolt production and inter-annual stability, and that increasing habitat availability would weaken density-dependence. Posteriors from this model reflect our current understanding of regulating processes throughout life for these populations that can be used to parameterize prospective simulations of alternative management actions on future population status.

Objective E-2: LCM Phase II – management scenarios

Restoration scenarios to impose on the statistical estimation life cycle model output are in development but have not been finalized. Several planning meetings have occurred, including a well-attended workshop devoted to brainstorming with partners in the basin and a loose plan has been developed. Briefly, we plan to assess combinations of restoration and other management actions (e.g., changes to supplementation) of various intensities. In-basin management scenarios will be crossed with additional scenarios that involve out-of-basin factors, such as changes to the hydrosystem or ocean mortality. More details will be forthcoming in the 2024 annual report.

Objective E-3: LCM Phase III – simulation of outcomes

With the finalization of the LCM Phase I estimation model, we have now started constructing a simulation model that accepts output from the estimation model to simulate the populations into the future. We plan to make significant progress and have results available for the 2024 report.

Goal 4: Apply lessons learned from RM&E to Grande Ronde salmon recovery efforts and other emerging concerns or locations

Objective F: Address needs of CRITFC tribal and other partners evaluating emerging concerns in the Grande Ronde and other geographic locations

Objective F-1: Continue developing/applying Adaptive Management framework with GRMW and Grande Ronde basin partners

Adaptive Management Plan

We continue to work closely with colleagues at the Grande Ronde Model Watershed (GRMW) and other partners on formalizing and documenting an Adaptive Management Plan for the Grande Ronde basin. An initial version of the Adaptive Management Plan was presented in White et al. (2021) – a collaborative publication assessing progress to date in habitat and salmon restoration in the Grande Ronde basin – and we have continued refining this plan through 2023 (Figure 34). In 2023, we participated in the Grande Ronde State of the Science meeting hosted by GRMW, which provides a forum to present and discuss restoration progress, RM&E findings, and emerging uncertainties/questions pertinent to management efforts in the basin. Some important highlights from the workshop included 1) a recent study evaluating thermal heterogeneity in response to restoration which demonstrated that post-restoration stratification in deep pools may provide thermal refuge habitat , 2) an evaluation of reference valley bottoms in the Grande Ronde basin was presented (Cramer Fish Sciences), which emphasized the variability in stream channel morphology present in reference areas and may help to refine targets for restoration in unconstrained valley settings, 3) several additional PIT tag arrays will be deployed in Grande Ronde tributaries in 2024, positioned at key locations where information on reach- or site-specific mortality is needed, and 4) restoration projects have increased in intensity and capacity at the site scale, but cumulative restoration impacts are probably not enough to see measurable changes in population-scale carrying capacity.

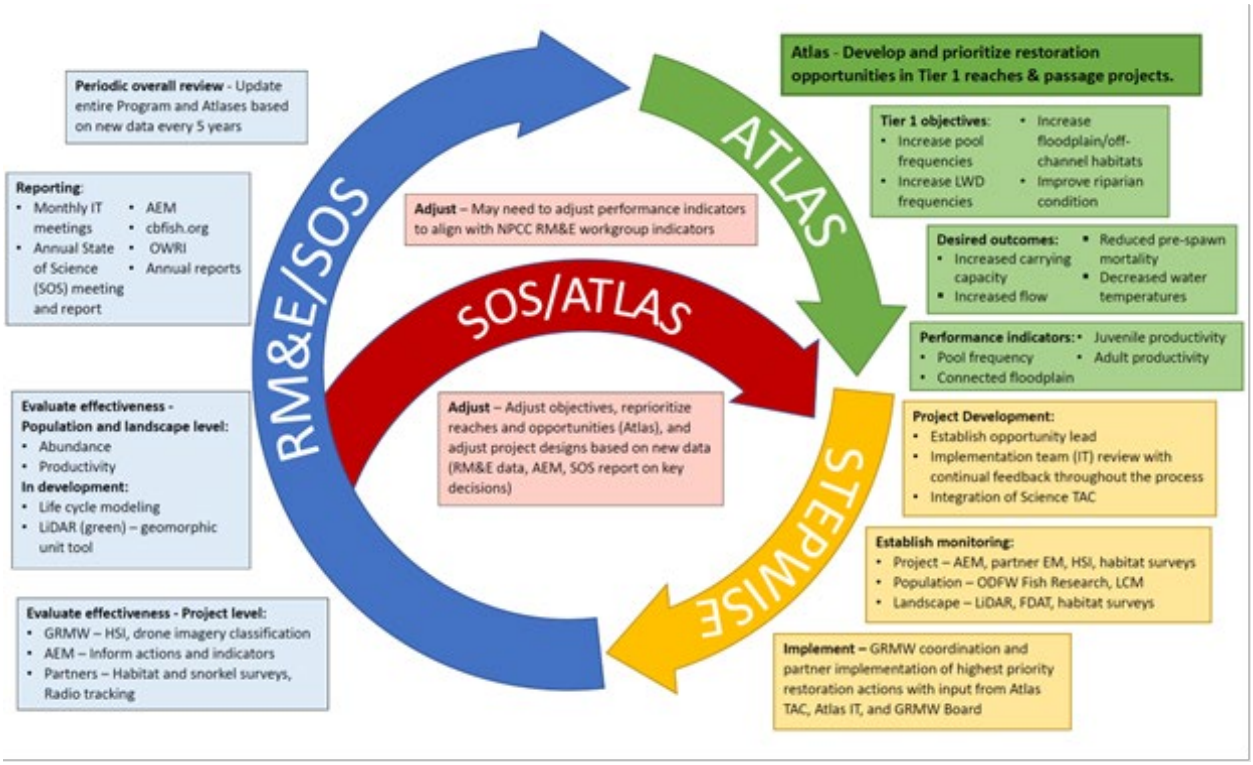

Figure 34. The adaptive management framework established by GRMW and Grande Ronde basin partners.

Watershed Coordination

Coordination with other entities involved in fish habitat restoration and associated research, monitoring and evaluation across the Columbia River basin is a critical component of this project. Close coordination and communication are essential to ensure that data being collected across various watersheds are similar enough that they can be used to draw inferences about the broader Columbia River basin (e.g., Is the habitat adequate for salmonid survival to specific life-cycle stages?; Are key limiting factors for habitat quality improving with time and as an aggregate or site-specific expression of restoration actions taken?). Coordination among agencies also helps to reduce duplication of effort and allows pooling of resources and knowledge to answer broader and more impactful research questions. A list of key partner projects that are closely related to this project are listed in Table 11.

CRITFC is a partner in the Grande Ronde Atlas process and provides basin-scale analysis of restoration effects, which feed into restoration management decisions (e.g., Figure 35). While we have not been directly involved in the Wallowa Atlas process to date, we have provided monitoring data (e.g., LiDAR, water temperature, snorkel and habitat surveys) to basin partners that are used in the Wallowa Atlas process.

In 2022, the USDA Forest Service spearheaded a multi-agency project to implement and monitor a whole-watershed, process-based restoration effort in Meadow Creek, a tributary to the upper Grande Ronde River. As a key partner in this collaborative restoration project, we continue to participate in regular meetings with staff from the USFS, CTUIR, ODFW and other basin partners to collectively determine RM&E approaches to assess key metrics relevant to restoration objectives that are appropriate for a project of this scale. We have also continued to contribute to the formal development of a comprehensive restoration plan including

assembling available data and content describing the current status of physical characteristics, biota and land use history across the watershed. In 2023, we entered a formalized cooperative agreement with the USFS PNW Research station to collaborate on research and monitoring of restoration projects in the Grande Ronde basin and hired a USFS-funded post-doc position (Marshall Wolf) supervised by CRITFC to focus on this work.

We worked closely with partners from OSU, CTUIR, NOAA and ODFW to develop and plan a master's student (OSU) project evaluating juvenile Chinook Salmon dispersal in Catherine Creek, including how restoration, location within the watershed and adult origin may influence juvenile salmon dispersal patterns, distribution, and habitat use. We assisted in sampling tissue from adult salmon for genetic analysis in September 2023. These adult samples provide the parentage baseline for offspring sampling in summer 2024 that we will be contributing towards.

We have continued working with partners in the John Day River basin (CTWSOR, ODFW) including contributing to RM&E efforts associated with the Middle Fork John Day Intensively Monitored Watershed working group. We are working closely with ODFW and CTWSOR to evaluate Chinook Salmon fry dispersal and floodplain habitat use using genetic parentage-based tagging (PBT). We developed a study design with CTWSOR and ODFW to expand the use of PBT to evaluate female reproductive success (out-migrating smolts/female) as a function of spawning location. Tissue was collected from adult salmon from spawning locations in September 2023, and we plan to collect out-migrating parr and smolts in fall 2024 and spring 2025. Results from this study will provide data to evaluate spatial patterns of female reproductive success to identify habitat characteristics and areas within the watershed where female reproductive output are higher or lower, providing critical information to guide conservation and restoration efforts. Over multiple years, these data may provide an approach to evaluate how inter-annual variation in biophysical conditions may alter longitudinal patterns of reproductive success, and potential changes in reproductive success pre- and post-restoration.

The development of the state-space life cycle model for Grande Ronde spring Chinook Salmon has been a highly collaborative process between CRITFC, NOAA, and ODFW. Staff from each organization have contributed to the development following their individual strengths. NOAA staff developed an early version of the state-space model and have been instrumental in providing advice and feedback on changes to the model structure. ODFW staff, being most intimately familiar with the biological monitoring programs in the basin, have been primarily in charge of decisions around how to treat the various data sources and for compiling and maintaining the data sets into a format usable by the state-space model. CRITFC staff have led the model development and have compiled estimates of weighted usable rearing habitat that will serve a key role in all phases of this work. All parties have been consulted prior to making major developmental changes to the model and will be invited to serve as co-authors on manuscripts that are produced as result of this collaboration (such as Appendix E).

Table 11: List of key partners and projects related to the proposed work in the Grande Ronde (GR) basin and beyond.

Organization	Related project(s)	Relationship to proposed project
Bonneville Power Administration	Project Action Effectiveness Monitoring (AEM) Programmatic (BPA 2016-001-00)	Findings from the BPA AEM project will be useful in developing and evaluating CRITFC's models of aggregate restoration impacts on limiting factors
Bureau of Indian Affairs	Climate Change Threats to Salmonid Food Webs (BIA A19AV00480); Resilient Aquatic Food Webs for Tribal Communities (BIA A19AP00024)	Provided funding for development and analysis of benthic macroinvertebrate metrics related to salmonid food webs; funded expansion of benthic macroinvertebrate sampling to tribal partners in the Columbia basin
Confederated Tribes of the Umatilla Indian Reservation	Grand Ronde Watershed Restoration (BPA 1996-083-00); Grande Ronde Supplementation M&E (BPA 2007-083-00); Biomonitoring of Fish Habitat Enhancement (BPA 2009-014-00)	GR Atlas Partner; implements habitat projects that CRITFC's surveys of habitat and biological monitoring characterize; has adopted CRITFC M&E methodologies (e.g., snorkel surveys, benthic macroinvertebrate collections); leads weir sampling of adult Chinook which produces data used in our life cycle model; Chinook Salmon supplementation program will be assessed using a life cycle model
Confederated Tribes of the Warm Springs Reservation of Oregon	John Day Habitat Enhancement Implementation Strategy (BPA 2007-397-00)	Key partner with CRITFC and ODFW in evaluating juvenile salmonid dispersal, habitat use, and distribution within the Middle Fork John Day River. Implements habitat restoration projects in the John Day basin and collects RM&E data used by CRITFC.
Grande Ronde Model Watershed Foundation	Grande Ronde Model Watershed (BPA 1992-026-01)	Leads coordination of adaptive management framework (Atlas) in GR basin; uses CRITFC's limiting factors assessments to guide restoration prioritization; documents restoration activities in basin that CRITFC will use for modeling restoration impacts on limiting factors; co-funded collection of topobathymetric LiDAR in 2020
National Oceanic and Atmospheric Administration	Various	Key partner with CRITFC and ODFW in developing the life cycle model; co-funding CRITFC's research on emergence phenology, floodplain use, and early life history of Chinook Salmon; co-funded a public outreach film with GRMW, CRITFC, and USFS on restoration in the GR basin
Nez Perce Tribe	Protect & Restore NE OR & SE WA Watershed Habitat (BPA 2007-393-00)	GR Atlas associate; utilized GIS products developed by CRITFC for restoration planning in the Wallowa basin; CRITFC collected topobathymetric LiDAR in Wallowa basin in 2020 that will be used for limiting factors assessment; provided water temperature data used in recent analysis of Chinook pre-spawn survival
Oregon Department of Fish and Wildlife	Grande Ronde Fish Habitat Improvement (BPA 1984-025-00); Grande Ronde Salmonid Life Cycle Monitoring (BPA 1992-026-04); John Day Basin Escapement and Productivity of Spring Chinook and	GR Atlas partner; implements habitat projects that CRITFC's surveys of habitat and biological monitoring characterize; has adopted CRITFC M&E methodologies (e.g., snorkel surveys, benthic macroinvertebrate collections); collects population level fish data (e.g., spawner abundance) used in life cycle model; key partner

Organization	Related project(s)	Relationship to proposed project
	Steelhead (BPA project 1998-016-00)	with CRITFC and NOAA in developing the Grande Ronde life cycle model. Key partner with CRITFC and CTWSOR on several projects evaluating juvenile salmonid dispersal, habitat use, and distribution within the Middle Fork John Day River.
Oregon State University	Long-term ecological effects of passive restoration in the Middle Fork John Day (OWEB 218-6041); CTUIR John Day Watershed Restoration (BPA 2007-397-00); ODFW John Day Habitat Enhancement (BPA 1984-021-00); Co-sponsored a post-doc (Matt Kaylor) to conduct research on juvenile salmon ecology; Juvenile Chinook dispersal patterns in Catherine Creek led by M.S. student Kayla Kelly and advisor Dr. Seth White.	OSU & UO Initiated study of long-term effects of cattle grazing management on river channel, riparian, and floodplain conditions in Middle Fork John Day; CRITFC contributed benthic macroinvertebrate sampling and analysis; Research led by post-doc Matt Kaylor directly addressed key objectives of this project relating to juvenile salmon ecology and prioritization of river restoration and management actions; CRITFC is collaborating closely with Kayla Kelly and Seth White on data collection and analysis related to juvenile Chinook dispersal in Catherine Creek.
University of Oregon	Long-term ecological effects of passive restoration in the Middle Fork John Day (OWEB 218-6041); CTUIR John Day Watershed Restoration (BPA 2007-397-00); ODFW John Day Habitat Enhancement (BPA 1984-021-00)	OSU & UO Initiated study of long-term effects of cattle grazing management on river channel, riparian, and floodplain conditions in Middle Fork John Day; CRITFC contributed benthic macroinvertebrate sampling and analysis
Trout Unlimited	Various	Implements stream and floodplain restoration projects in the Grande Ronde basin (e.g., Sheep Creek, Indian Creek, Wallowa River) that CRITFC's surveys of habitat and biological monitoring characterize
U.S. Bureau of Reclamation	Various	Implements and conducts RM&E on various restoration projects in GR basin, implements habitat projects that CRITFC's surveys of habitat and biological monitoring characterize
U.S. Forest Service	Various	GR Atlas partner; conducts M&E (Level II surveys) and implements habitat projects that CRITFC's surveys of habitat and biological monitoring opportunistically characterize
Union Soil and Water Conservation District	Various	GR Atlas partner; implements habitat projects that CRITFC's surveys of habitat and biological monitoring opportunistically characterize

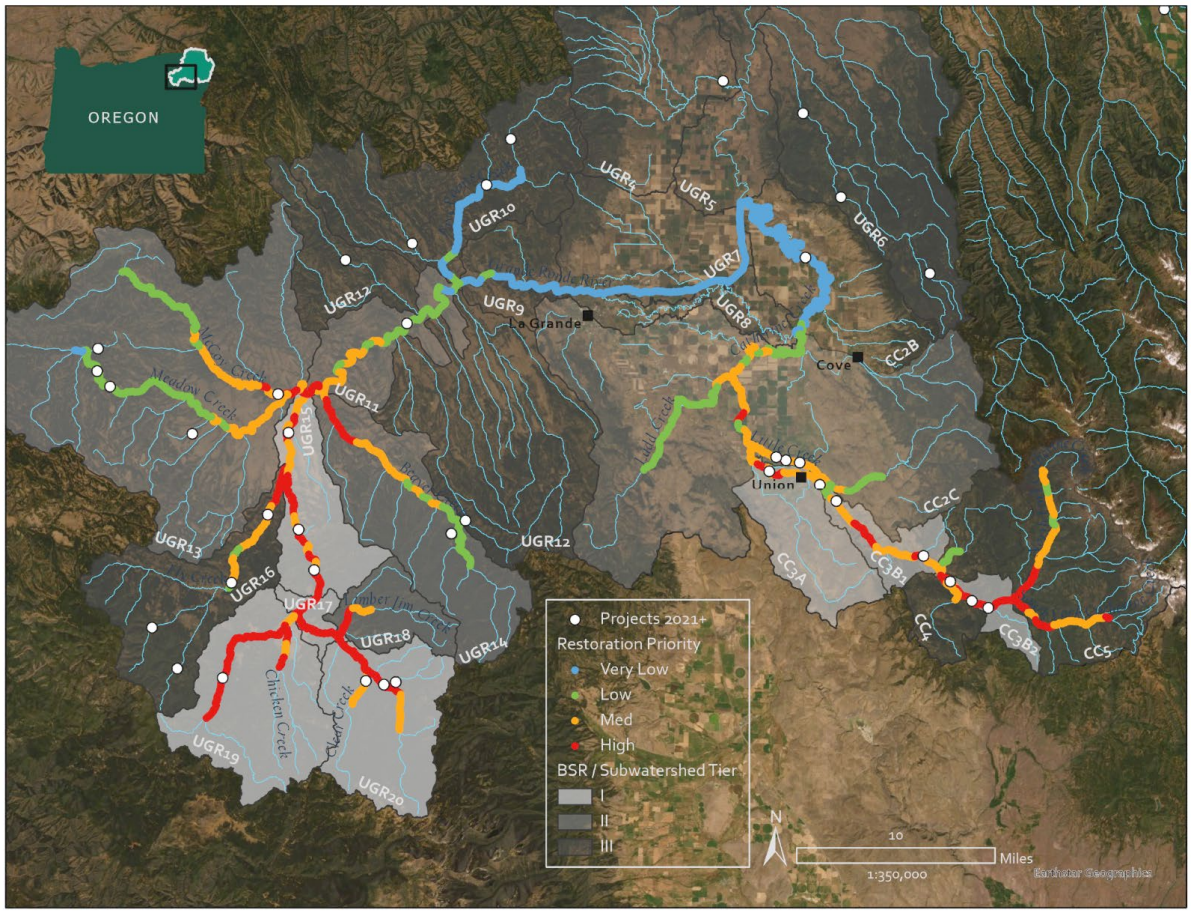

Figure 35. Restoration projects planned in the upper Grande Ronde River and Catherine Creek in 2021 and later, in relation to Atlas Tier I-III biological significant reaches (BSRs) and the restoration prioritization from Justice et al. 2017 developed in BPA project 2009-004-00. Most projects outside of the high and medium priority areas are either passage improvements or small, headwater stream meadow restoration projects by the USFS.

RM&E Methods and Designs

Snorkel Survey Protocol Updates

ODFW snorkel surveys conducted at Wallowa River restoration sites in 2022 indicated that the existing snorkel detection model developed by CRITFC and used by Grande Ronde partners to estimate abundance from snorkel counts (Staton et al. 2022) was poorly suited to estimate snorkel detection probability in very deep (e.g., pools > 0.5 m average depth) or complex channel units (e.g., > 0.2 pieces of large wood per m²) because these values exceed covariate ranges in the initial dataset used to develop the model. In response to this shortcoming, CRITFC and ODFW collected additional paired snorkel count and mark-recapture data in 2023, targeting deeper and more complex habitats that are within the known rearing area for Chinook Salmon. A description of this effort can be found under Objective D-1.

Freshwater Mussel Survey Methods

Xerces Society for Invertebrate Conservation in collaboration with CTUIR are developing a regional survey protocol for freshwater mussels. Freshwater mussels are an important component of tribal first foods and

are among the most threatened freshwater species globally. In order to assist with data collection needed to test and validate this protocol, we attended the freshwater mussel identification and sampling training held at the Oregon Chapter of the American Fisheries Society (AFS) meeting in Eugene, OR during spring, 2023. We tested the draft survey protocol during summer of 2023 in the Minam River watershed and submitted feedback and survey data to the Xerces Society.

IGF1 Sampling Methods

The increased use of large-scale process-based restoration techniques like those utilized in floodplain restoration projects produce complex habitat where traditional sampling techniques for juvenile salmonid growth estimation may lack efficacy. The addition of numerous channels and abundant cover habitat in the post-restoration environment can make it difficult to achieve the desired number of recaptures for accurate growth estimation in a repeat-sampling protocol. As such, monitoring efforts focused on assessing the effectiveness of these restoration projects would benefit from methodology to estimate growth responses using single-sampling approaches. Single-capture sampling methods can be applied to evaluate habitat-growth comparisons and may be particularly effective in contexts where recapture rates may be lowered due to low capture efficiency, dispersal patterns or other factors. One metric for assessing growth without the recapture of individuals is the concentration of insulin-like growth factor 1 (IGF1), which has been validated as an index of relative growth rate in juvenile salmonid fishes (Duguid et al. 2018; Beckman 2011; Bond et al. 2014). Plasma IGF1 concentration strongly correlates with growth rate and is highly responsive to shifts in habitat suitability as IGF1 concentration responds to changes in environmental conditions affecting growth within 4 days (Gabillard et al. 2006; Caldarone et al. 2016; Duguid et al. 2018). However, the use of IGF1 has largely been limited to either lethal sampling or to non-lethal sampling of larger individuals (i.e., smolts) than the size range of juvenile salmonids typically encountered in NE Oregon.

Prior to conducting a field pilot to evaluate the feasibility of using IGF1 to assess growth of smaller bodied juvenile salmonids, a hatchery study was conducted at the OHRC in 2023 using juvenile Steelhead/Rainbow trout to assess mortality across a range of body sizes (fork lengths ranging from 80 – 140 mm) and determine a minimum size threshold for non-lethal sampling. This study was followed up by an additional study in winter 2024 conducted at the Hagerman Fish Culture Experiment Station in Hagerman, Idaho to further refine the non-lethal blood draw methodology and provide additional mortality data (fork lengths ranging from 94-183 mm).

We plan to utilize the refined sample methodology determined by the hatchery studies to conduct a field pilot study in summer 2024 to evaluate the use of IGF1 as an index of recent growth in juvenile *O. mykiss* in the field. The objectives of the field pilot study are to (*i*) evaluate the validity of using plasma IGF1 values as an index of growth in juvenile *O. mykiss* in the field by assessing the relationship between individual growth rates and IGF1 concentrations and (ii) assess shifts in IGF1 values during the seasonal temperature shift from mid-summer to early fall.

References

Beckman, B.R., 2011. Perspectives on concordant and discordant relations between insulin-like growth factor 1 (IGF1) and growth in fishes. General and Comparative Endocrinology, Profiles in Comparative Endocrinology: Glen Van Der Kraak 170, 233–252. https://doi.org/10.1016/j.ygcen.2010.08.009.

Bond, M. H., B. R. Beckman, L. Rohrbach, and T. P. Quinn. 2014. Differential growth in estuarine and freshwater habitats indicated by plasma IGF1 concentrations and otolith chemistry in Dolly Varden salvelinus malma. Journal of Fish Biology 85(5):1429–1445.

Caldarone, E. M., S. A. MacLean, and B. R. Beckman. 2016. Evaluation of nucleic acids and plasma IGF1 for estimating short-term responses of postsmolt Atlantic Salmon (Salmo salar) to food availability. U.S. National Marine Fisheries Service Fishery Bulletin 114:288–301.

Duguid, W. D., T. W. Iwanicki, M. L. Journey, A. L. Noel, B. R. Beckman, and F. Juanes. 2018. Assessing indices of growth for field studies of Juvenile Salmon: An experiment and synthesis. Marine and Coastal Fisheries 10(2):204–223.

Gabillard, J.-C., B. B. Kamangar, and N. Montserrat. 2006. Coordinated regulation of the GH/IGF system genes during refeeding in Rainbow Trout (Oncorhynchus mykiss). Journal of Endocrinology 191:15–24.

Justice, C., S. M. White, D. A. McCullough, D. S. Graves, and M. R. Blanchard. 2017. Can stream and riparian restoration offset climate change impacts to salmon populations? Journal of Environmental Management 188:212–227.

Staton, B. A., C. Justice, S. White, E. R. Sedell, L. A. Burns, and M. J. Kaylor. 2022. Accounting for uncertainty when estimating drivers of imperfect detection: An integrated approach illustrated with snorkel surveys for riverine fishes. Fisheries Research 249:106209.

White, S. M., S. Brandy, C. Justice, K. A. Morinaga, L. Naylor, J. Ruzycki, E. R. Sedell, J. Steele, A. Towne, J. G. Webster, and I. Wilson. 2021. Progress Towards a Comprehensive Approach for Habitat Restoration in the Columbia Basin: Case Study in the Grande Ronde River. Fisheries:fsh.10562.

Wolf Water Resources. 2022. Upper Grande Ronde River, Union County, OR Sediment Budget Study. Page 35. Wolf Water Resources, Portland, OR.

Objective F-2: Represent tribal concerns in Columbia River basin tributary habitat RM&E policy discussions

Staff from CRITFC's River Ecology group participated in the Columbia Basin Collaborative (CBC) Estuary, Tributary & Mainstem Habitat meetings to develop regional recommendations to the Integration/Recommendations Group (IRG) regarding best management practices for habitat and salmon recovery in the Columbia River basin. This work with the CBC has provided a good opportunity to transfer lessons learned from extensive habitat-related RM&E in the Grande Ronde basin to a broader regional level and to ensure that tribal values and perspectives on habitat restoration and salmon recovery are considered in regional RM&E planning and funding.

Following a recent Motion for Stay in the long-running litigation over the operation of the dams on the mainstem Columbia River and lower Snake River (*NWF v. NMFS*), the four Columbia River Treaty Tribes and the states of Oregon and Washington (i.e., the "Six Sovereigns") drafted the Columbia Basin Restoration Initiative (CBRI) which includes a suite of recommendations needed to achieve recovery of healthy and abundant salmon populations. Our group has been actively participating in both internal and regional meetings focused on better aligning CRITFC's work with the goals of the CBRI.

Dissemination of Project Findings

Presentations and workshops

Justice, C., A. Ringelman, M. Kaylor, B. Staton, D. Graves, D. Kelsey, S. White, and L. Burns. Overview of aquatic habitat and biota monitoring using CRITFC's Tributary Habitat Assessment Protocol. Grande Ronde State of the Science Meeting. La Grande, OR. November 16, 2023

Kaylor, M. et al. Watershed-scale assessment of juvenile Chinook Salmon dispersal patterns. Oregon American Fisheries Society Annual Meeting. March 2nd, 2023.

Kaylor, M. and M. Bond., et al. Linking floodplain habitat availability with juvenile Chinook Salmon emergence timing and dispersal. NOAA Northwest Fisheries Science Center's Watershed Program Meeting. June 5th, 2023.

Kaylor, M et al. Patterns and drivers of juvenile salmon growth, emergence timing, and movement across NE Oregon watersheds. CRITFC Brown Bag Seminar Series. June 7th, 2023.

Staton, B., P. Gibson, C. Justice, M. Kaylor, M. Liermann, A. Ringelman, T. Sedell, R. Sharma, and S. White. Integrated Population Modeling of Grande Ronde Basin Spring Chinook Salmon: Using Monitoring Data to Link Habitat to Dynamics and Demography for Restoration Prioritization. Invited presentation for the monthly meeting of the Atlas Implementation Team. February 16, 2023.

Staton, B., P. Gibson, C. Justice, M. Kaylor, M. Liermann, A. Ringelman, T. Sedell, R. Sharma, and S. White. Integrated population modeling of Grande Ronde Spring Chinook Salmon: linking dynamics and habitation to monitoring data via SSMs. PNAMP Fish Monitoring Work Group Meeting (recording: https://www.youtube.com/watch?v=i0mF4y8B088; begins at timestamp 24:28). April 20, 2023.

Staton, B., and H. Hershey. Workshop instructed: Introductory Bayesian Inference with JAGS for Fish Biologists. National AFS Meeting, Grand Rapids, MI. August 19, 2023.

Staton, B., and H. Hershey. Workshop instructed: Intermediate Bayesian Inference with JAGS for Fish Biologists. National AFS Meeting, Grand Rapids, MI. August 20, 2023.

Publications (Published Papers, Draft Manuscripts and Technical Reports)

Justice, C., M. Kaylor, A. Ringelman, and B. Staton. May 2023. Evaluating salmonid and stream ecosystem response to conservations measures and environmental stressors in the Columbia River basin. Page 130. Columbia River Inter-Tribal Fish Commission, BPA Project # 2009-004-00, Portland, OR.

Kaylor, M., L. Ciepiela, M. Feden, J.T. Lemanski, C. Justice, J. Armstrong, B. Staton, S. Kelly, S. Narum, I. Tattam, and S. White. Juvenile wild spring Chinook Salmon exhibit variable dispersal patterns across a heterogeneous riverscape. Draft manuscript presented in Appendix D and will be submitted to *Ecosphere* in April 2024.

Quellet, V., A. Fullerton, D. Beauchamp, J.R. Bellmore, M. Kaylor, P. Kiffney, M. Liermann, S. Naman, S. Rhoades, J. Rosenfeld, G. Rossi, B. Sanderson, and S. White. Food for fish: Challenges and opportunities for quantifying foodscapes in river networks. In review at *WIREs Water*.

Rossi, G., J.R. Bellmore, J. Armstrong, C. Jeffres, S. Naman, S. Carlson, T. Grantham, M. Kaylor, S. White, J. Katz, and M. Power. Foodscapes for Salmon and Other Mobile Consumers in River Networks. Accepted at *BioScience.*

Staton, B., M. Liermann, P. Gibson, C. Justice, M. Kaylor, R. Sharma, and S. White. A state-space model to quantify density-dependence, demographic heterogeneity, and spatial synchrony in Grand Ronde River Chinook Salmon populations. Draft manuscript will be submitted in 2024. Presented in Appendix E.

References

Accords. 2008. 2008 Columbia Basin Fish Accords Memorandum of Agreement between the Three Treaty Tribes and FCRPS Action Agencies. Page 30. https://critfc.org/wp-content/uploads/2012/10/moa.pdf

CRITFC (Columbia River Inter-Tribal Fish Commission). 2021. Evaluating salmonid and stream ecosystem response to conservation measures and environmental stressors in the Columbia River basin. Page 72. Proposal to the Independent Scientific Review Panel, Portland, OR.

ISRP (Independent Scientific Review Panel). 2022. Final report: review of anadromous fish habitat and hatchery projects. Page 653. ISRP 2021-8, Portland, OR.

White, S., C. Justice, B. Staton, L. Burns, and M. Kaylor. 2022. Evaluating salmonid and stream ecosystem response to conservations measures and environmental stressors in the Columbia River basin. Page 74. Columbia River Inter-Tribal Fish Commission, BPA Project # 2009-004-00, Portland, OR.

Appendix A Data Storage and Access

Data collected under this project is currently managed in different ways depending on the data type. General spatial data such as monitoring sites, stream layers, land ownership, and various other datasets that are used for analyses but are not deliverable end products are stored in a geodatabase at CRITFC and managed for internal use by CRITFC GIS specialists and project managers. Physical habitat data collected by CRITFC using the CHaMP protocol from 2011 to 2017 is now managed by the StreamNet Program and is available to the public at https://www.streamnet.org/home/data-maps/champ/. Habitat data collected using CRITFC's Tributary Habitat Assessment protocol including drone imagery is stored on CRITFC servers and is available upon request. Once metric calculations are completed for 2022 habitat data, our plan is to migrate all habitat survey data to CRITFC's Centralized Database Management System (CDMS) with data available for download by the public upon request. Fish abundance data was recently uploaded to StreamNet's Data Store for use in expanding the Fish Density Analysis Tool (FDAT) developed by Dan Isaak and his team at the Rocky Mountain Research Station. These data are available for download at https://app.streamnet.org/datastore_search_classic.cfm?id=844. Water temperature data collected by CRITFC is stored on CRITFC's CDMS and is available for download upon request.

The code for the Grande Ronde spring Chinook state-space life cycle model and the data it fits to are stored in two separate GitHub repositories. We chose to organize it this way to enable tracking data-related changes separately from model-related changes, and this has proven to be quite useful. Further, all collaborators have access to the most current main and development versions and GitHub includes a useful issue tracker where needed changes can be discussed; these aspects have greatly facilitated collaboration. The data sets are not very large (relatively speaking; total of all files <5MB), which makes GitHub a workable solution for housing and updating the data sets for this endeavor. If the data were stored outside of basic text files (e.g., .csv format) or in very large files, we would need to find something different, as GitHub was not designed to track/host these sorts of files. Both repositories are private currently (only collaborators have access), however, we plan to make both completely public as supplements to the manuscript that presents this work.

Appendix B Foresight Drone Services UAS Survey Report

ForeSight Drone Services
UAS Field Operations and
Post-Processing Final Report

For the 2022 Upper Grande Ronde

Tributary Habitat Assessment Protocol

Prepared for:

Casey Justice, jusc@critfc.org

Columbia River Inter-Tribal Fish Commission

Prepared By:

Nick Wagner, nick@foresightdrones.com

ForeSight Drone Services, LLC

12/23/2022

FORESIGHT
DRONE SERVICES

Contents

Executive Summary

Why?

- ForeSight Drone Services LLC, Portland, OR, provided Unoccupied Aerial System (UAS) flight operations and image post-processing as part of the Tributary Habitat Assessment Protocol conducted on the Upper Grande Ronde watershed of northeast Oregon in 2022.
- The aerial imagery and maps are key to the documentation and assessment of spring chinook salmon habitat in the Grande Ronde River, and tributaries, by enabling measurement and analysis of metrics aimed at assessing stream structure, floodplain and riparian habitat, and substrate composition.

How?

- ForeSight operated a dual-payload DJI M300 RTK airframe with a DJI Zenmuse P1, 45-megapixel RGB camera, and the MicaSense Altum, a 6-band multispectral sensor.
- In 7 days of fieldwork, a 2-person crew from ForeSight covered 998 acres, nearly 16.5 river miles, of the upper Grande Ronde River and Meadow Creek -- 43% more acreage than proposed and planned.

What?

- ForeSight Drone Services delivered almost 3TB of data, including raw RGB and multi-spectral imagery, Agisoft Metashape project files, and derivative products like orthomosaics and digital elevation model (DEM) files, ready for import and analysis in GIS mapping software.
- RGB imagery was geolocated using a post-processed kinematic (PPK) workflow to correct image locations to within 5cm accuracies.
- RGB and multi-spectral imagery was post-processed using Agisoft Metashape Professional to generate final orthomosaics with resolutions of ~1.5cm/pixel RGB, and ~5.5cm/pixel multispectral.

Key Takeaways and Next Steps

- Compared to traditional methods, the PPK workflow saved considerable time in the field by eliminating most ground control points (GCPs) and reduced the impacts and access requirements on private lands.
- Studying a test-plot with survey-grade checkpoints could provide enhanced validation of the PPK workflow and could potentially eliminate the need for any GCP or checkpoints on future flights.
- Applying the field methods developed on this project to additional tributaries and evaluating archival data with updated post-processing methods, could accelerate the pace of science and restoration as part of the Tributary Habitat Assessment Protocol in the Grande Ronde basin.

Area of Interest

The Area of Interest (AOI) for this scope of work was defined by CRITFC and shown below in Image 1 as the white bounding polygons, encompassing 725 acres. For flight-planning purposes, the AOI was divided into sub-areas. Each sub-area boundary encompasses one or more complete stream segments, as defined by CRITFC. Sub-areas are identified with labels 1A through 21. The sub-area IDs are subsequently used in all file structure organization and file naming.

Much of the AOI is private land, and permission for UAS operations was obtained by CRITFC prior to flight operations. Other parts of the AOI are Oregon state park and/or state wayside lands and CRITFC maintained relations with these land managers and coordinated the necessary permits. Flights over US Forest Service (USFS) lands were coordinated with the Blue Mountains Interagency Dispatch Center out of La Grande.

The final mapped areas are shown in bright green in Image 1.

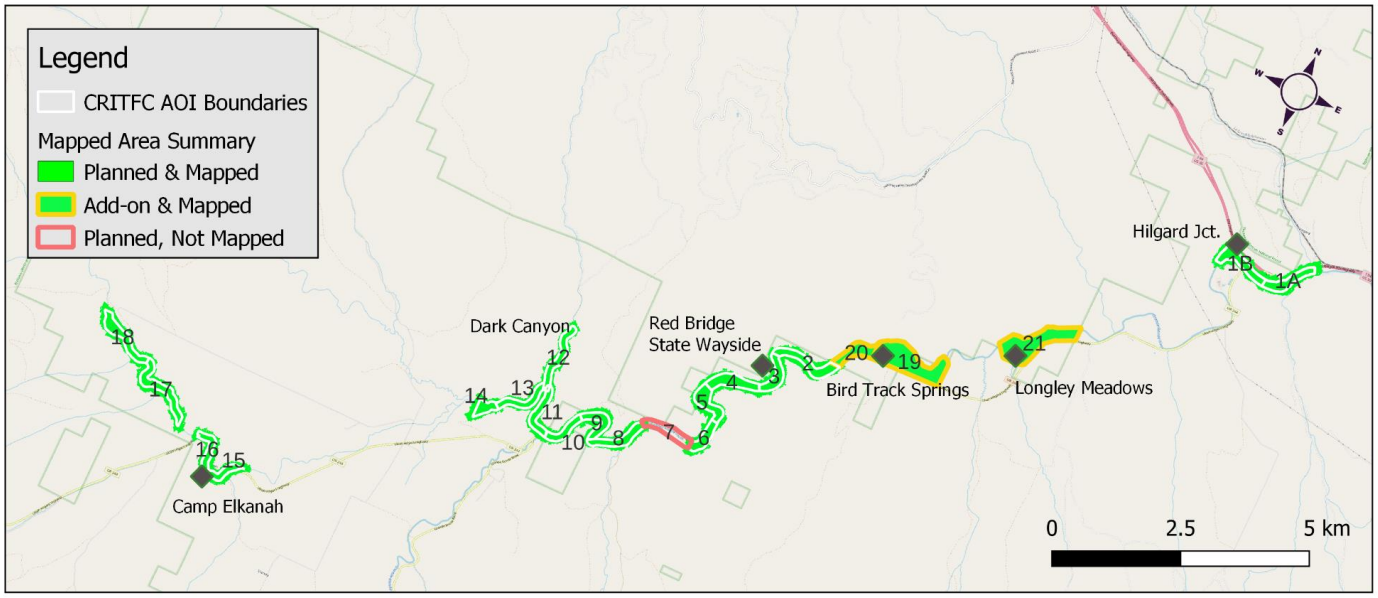

Image 1: Mapped Areas Overview

All of the planned AOI was flown and mapped except for one 41.4 acre sub-area (shown in red in Image 1) due to rescinded land-owner access.

USFS lands at sub-areas 19 and 20 (Bird Track Springs), and 21 (Longley Meadows) were added during the field work term to fill extra field-crew capacity. These areas are shown with a gold bounding polygon in Image 1. Raw imagery and associated data files from sub-areas 19, 20, and 21 were provided to the Grande Ronde Model Watershed for post-processing.

The total acres in all sub-area flight plans combined, with area 7 excluded, and areas 19-21 included, totals 998.8 acres.

Deliverables

Final data files were delivered to CRITFC's main office on Wednesday 12/21/22, contained on two hard drives including raw RGB and multi-spectral imagery, PPK corrected image locations, RGB orthomosaics and a digital elevation model. Seven-band multispectral orthomosaics are also included, along with normalized differential vegetation index (NDVI) raster files for each sub-area.

Final RGB orthomosaic resolution was ~1.5cm/pixel but varies slightly for each sub-area. See Image 2 for sample resolution.

Image 2 - RGB Sample detail showing large wood and substrate detail.

DEM resolution is half of the associated orthomosaic, or roughly 3cm/pixel. See Image 3 for sample DEM data beside RGB and NDVI. Final multispectral orthomosaic/NDVI resolution was ~5.5cm/pixel.

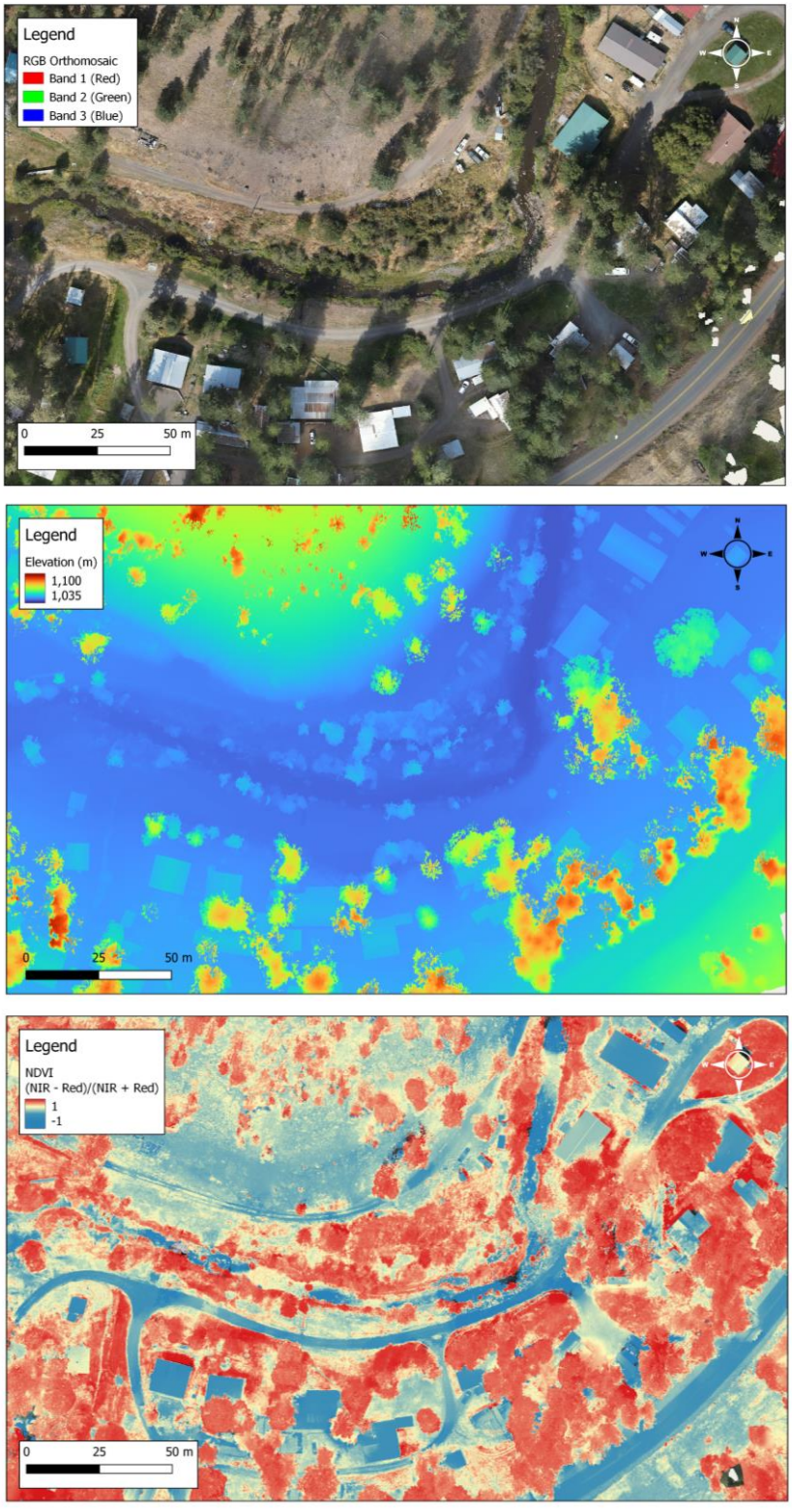

Image 3: Top - RGB orthomosaic (1.5cm/px). Middle - DEM (3cm/px). Bottom - NDVI (5.5cm/px).

Hard Drive Contents

The contents of the hard drives are summarized here to orient the receiver to the file structure and included files. At the top-level files are organized into folders for each of the 21 sub-areas.

Sub-areas 1A through 18 have the following structure:

- Top level sub-area folder (e.g. **fsd_area1A**)
  - **altum** - folder containing raw multispectral imagery
  - **p1** - folder containing raw RGB imagery, and associated data files
    - **DJI_<date><time>_<flight_number>_<sub_area>** - contains raw imagery and RINEX files for PPK processing.
      - Sub-areas with multiple flights will have multiple folders containing imagery and RINEX files.
    - **fsd_areaXX_ppk_itrf2014** - contains tab-delimited text files containing PPK corrected locations for each image of the flight.
      - Note, if there is more than one flight for a sub-area, there will be more than one folder with PPK corrections.
      - Use the *_Ellipsoidal file for use with Agisoft Metashape.
      - Some flights have a second PPK corrections folder with the same name as the sub-area. These PPK corrections were done in NAD83 coordinate reference system and are NOT recommended for use in Agisoft Metashape. Stick to the "itrf2014" corrections.
  - **fsd_area1a_v1.files**- this folder contains all the Agisoft Metashape project files. These files should not be accessed directly from a file explorer.
  - **area_1a_check_points** - a csv file containing only the checkpoints for the associated sub-area.
  - **area_1a_final_check_point_locations** - a csv file containing the recorded checkpoint locations from the field, along with the final locations from the orthomosaic/DEM in Metashape.
    - All checkpoint locations are marked with "ID" that corresponds to the CRITFC_UAS_Ground_Control_2022 layer in ArcGIS.
    - All final checkpoint locations from Metashape are denoted with a tick mark (')
    - Eg. Label "36" is the checkpoint location from the Arrow 100 in the field. Label "36'" is the final location of the checkpoint from the orthomosaic (with the elevation from the final DEM).
  - **area1a_multispectral_georeferencing_points.points** - a csv file exported from the QGIS georeferencer tool. These points were used to georeference the final multispectral orthomosaic and NDVI geoTiff files to the PPK-corrected RGB orthomosaic. This file records the original and final location of the reference points used. Most reference points used for georeferencing the multispectral layers were checkpoints (i.e. GCP tarps, or spray-painted targets), but sometimes other features (like unique downed trees, or paint markings on roadways) were used to get a more robust georeference over the entire map extent.
  - **fsd_area1a_v1.psx** - Agisoft Metashape project file.

    - **fsd_area1a_v1_multispec_NDVI** - single-band NDVI geoTiff. Not precisely georeferenced.
    - **fsd_area1a_v1_multispec_NDVI_GEOREFERENCED** - single-band NDVI geoTiff, precisely georeferenced to the RGB orthomosaic.
    - **fsd_area1a_v1_multispec_ORTHO** - reflectance calibrated* seven band (6 Altum bands, plus alpha channel for transparency) geoTiff. Not precisely georeferenced.
    - **fsd_area1a_v1_multispec_ORTHO_GEOREFERENCED** - reflectance calibrated* seven-band (6 Altum bands, plus alpha channel for transparency) geoTiff, precisely georeferenced to the RGB orthomosaic.
    - **fsd_area1a_v1_RGB_ORTHO** - four-band (R, G, B, plus alpha channel for transparency) geoTiff.
    - **fsd_area1a_v1_RGB_DEM** - single-band digital elevation model geoTiff. Elevation in meters.
- **ground_control** - folder containing CRITFC_UAS_Ground_Control_2022 exported data.
- **metashape_batch_files -** folder containing .xml batch files for use in Agisoft Metashape
- **micasense_reflectance_panel -** folder containing the reflectance calibration panel albedo values from MicaSense. Agisoft Metashape requires this file for reflectance calibration.

*Note, reflectance calibration was conducted in Agisoft Metashape according to MicaSense and Agisoft recommendations. Values in output bands are 16-bit integer values, with 100% reflectance for each band corresponding to the middle of the available range, i.e., 32768.

Sub-areas 19-21 contain only the raw p1 and Altum imagery. Raw imagery was provided to the Grande Ronde Model Watershed for post-processing.

Methods

UAS Overview

Given the large linear distance required for this project, efficiencies gained in flight operations based on proper platform selection helped to reduce overall costs of flight planning, operations, and post-production. For that reason, a commercial grade vertical take-off and landing (VTOL) platform with post-processed kinematic (PPK) capabilities was selected. The DJI M300 RTK satisfied these requirements and was outfitted with a dual payload solution that provided RGB and multisepctral imagery to produce high accuracy final map products.

Image 4: DJI M300 RTK with MicaSense Altum and DJI Zenmuse P1 payloads.

The RGB payload selected was the DJI Zenmuse P1, with a full-frame 45 MP sensor. and a global shutter mounted on a 3-axis gimbal and integrated with the airframe for shutter triggering and logging required for the PPK workflow.

The multispectral payload selected was the six-band MicaSense Altum with Quick Mount connection to the M300 airframe. The 6 bands are summarized in Table 1. Each of the 5 multispectral bands have a 3.2 MP sensor at 2064x1544 resolution, and a lower resolution thermal band at 160x120 pixels. The Altum system comes with a calibrated reflectance panel and a downwelling light sensor that are used to capture reflectance calibration data to be used in post-processing. More details can be found in the MicaSense Altum Integration Guide

Name	Center
Blue	475 nm
Green	560 nm
Red	668 nm
Red edge	717 nm
Near infrared	840 nm
Thermal	11 µm

Table 1: Altum bands summary.

PPK Overview

A PPK workflow was used to correct locations of RGB images to ensure high relative and absolute accuracy of final deliverables. The PPK process makes use of the GNSS hardware on-board an RTK

aircraft, along with publicly available corrections data from nearby reference station(s) to correct the location data for each image captured. A cloud-based correction service was used to apply corrections from the UNAVCO reference station (P022) near La Grande, OR resulting in individual image accuracies of 1.5 - 5.1cm horizontally, and 2.0 to 6.3cm vertically.

Due to limitations in the integration of multispectral sensors with RTK-capable platforms, PPK processing of multispectral imagery was deemed to be cost prohibitive, and prone to errors. Therefore, multispectral imagery was orthorectified and georeferenced without PPK, and only using the on-board GPS hardware. Absolute accuracy errors were minimized by aligning multispectral layers with the higher accuracy RGB layers using checkpoints and a polynomial algorithm.

Flight Planning

All flights were conducted under FAA Part 107. Visual line of sight was maintained to the aircraft, which required multiple take-off and landing locations to cover the linear AOI following the river. All flights were conducted within 2.5 hours of local solar noon to minimize shadows. Mission plans were programmed to ensure sufficient front and side overlap in both the RGB and the multispectral imagery. All flights were flown at 400’ AGL.

Flight Operations

A total of 27 flights were flown over 7 days, September 11th through September 17th, 2022. All available sub-areas of the AOI were completed after 5 field days. The two remaining field days were used to fly additional USFS areas that were planned to be flown by the Grande Ronde Model Watershed.

Access to most of the sub-areas was via Highway 244 and county roads facilitating easy transportation of equipment to the landing zone. However, several of the sub-areas were not accessible by vehicle, and equipment was backpacked in. The M300 case is not designed to be transported for long distances over rough terrain but strapping the case to a frame pack enabled remote access, with some difficulty. See Image 5.

Image 5: Packing UAS equipment into remote areas.

Sub-Area	Acreage	Date Flown	# Of Flights	Flight Duration (minutes)	P1 Images	P1 Data (GB)	Altum Images	Altum Data (GB)
1A	40	9/12/22	1	19	634	9.52	591	19
1B	47	9/12/22	1	21	692	10.79	673	21.6
2	51.6	9/11/22	2	38	748	12.83	777	25.01
3	34.5	9/12/22	1	21	592	11.81	549	17.6
4	49	9/11/22	1	23	643	12.12	578	18.56
5	42.5	9/11/22	1	22	703	11.94	674	21.64
6	29.9	9/11/22	1	14	436	7.36	412	13.23
8	41.6	9/13/22	1	23	661	12.77	627	20.12
9	33.7	9/12/22	1	17	560	8.81	551	17.69
10	27.7	9/12/22	1	16	449	7.12	448	14.38
11	36.5	9/13/22	1	23	619	10.3	591	19
12	43.3	9/13/22	1	23	704	13.15	743	23.85
13	33.6	9/14/22	1	22	589	11.63	544	17.49
14	21.3	9/14/22	1	12	378	8.58	373	11.98
15	22.7	9/14/22	1	14	434	8.47	418	13.41
16	27.4	9/14/22	1	19	570	11.21	539	17.3
17	53.8	9/15/22	2	31	941	18.9	930	29.89
18	48.7	9/15/22	2	26	764	14.26	750	24.09
19	150	9/16/22	3	58	1924	45.69	1911	54.94
20	47	9/16/22	1	20	640	14.69	608	19.67
21	117	9/17/22	2	51	1704	38.86	1503	48.23
TOTAL	**998.8**		**27**	**513**	**15385**	**300.81**	**14790**	**468.68**

Table 2: Flight and imagery summary.

In total, 15,385 RGB, and 14,790 six-band multispectral images were collected. Total flight time was 513 minutes over 27 flights, for an average of 19m per flight. Maximum flight time was 26m. On average, 3.85 flights per day were conducted, covering an average of 143 acres per day. See flight summary details in Table 2.

Image 6: Laying a vinyl tarp as a checkpoint.

Ground Control

The PPK workflow generates sub-meter accurate orthomosaics without the need for arrays of GCPs. Thus, the PPK workflow reduced the amount of time needed in the field to place, locate, and collect GCPs. Additionally, impact to and access to private lands was minimized.

Sparse checkpoints (CPs) were used to validate the final orthomosaics. Two to three targets were placed per sub-area. CPs were valuable for aligning the multispectral layers to the PPK RGB data layer.

CPs were a combination of vinyl tarps and spray-painted targets large enough to be identified in the final imagery. CPs were geolocated with a sub-meter accuracy GNSS receiver (Arrow 100/100+). The theoretical accuracy of the Arrow 100 is less than that of the PPK-corrected image locations, so using the Arrow 100 points to validate the final CP locations in the final orthomosaic leaves some uncertainty. This process could be improved by validating the PPK workflow with a set of survey-grade checkpoints, rather than the lower accuracy Arrow 100 points.

Post-Processing

Raw imagery was post-processed in a multi-step workflow to convert raw imagery into data products ready for advanced analysis.

PPK Corrections

PPK corrections were generated for RGB imagery using RINEX files from the M300 and a cloud-based correction service that leverages publicly available reference station data from the nearby UNAVCO (P022) station south of La Grande. Image corrections were downloaded in a tab-delimited file format with tags connecting positions to the original image files. These corrected locations were later used to reference images in Agisoft Metashape.

RGB

RGB imagery, along with the PPK corrections, were processed into orthomosaics and DEMs using Agisoft Metashape Professional. Additionally, a batch process file was developed and delivered to streamline post-processing and reduce the potential for errors.

Multispectral

Multispectral imagery was processed into orthomosaics, including an NDVI geoTiff for each sub-area, using Agisoft Metashape Professional. Agisoft Metashape handles the 6-band imagery, and provides tools for reflectance calibration, both with the calibrated reflectance panel images, as well as the downwelling light sensor data recorded in the image metadata. NDVI was calculated using the formula:

$$NDVI = (NIR - Red)/(NIR + RED)$$

After exporting from Metashape, multispectral layers were precisely geo-referenced to the PPK-corrected RGB orthomosaic using QGIS Georeferencer tool and a polynomial algorithm.

Checkpoint Analysis

After the final PPK-corrected RGB orthomosaic was created, checkpoint locations recorded in the field were compared to the final checkpoint locations in the orthomosaic, and altitude from the final DEM.

In total, 62 checkpoints were analyzed for horizontal (XY error) and vertical (Z) error. Results are summarized in Table 3. Full results can be seen in Attachment A.

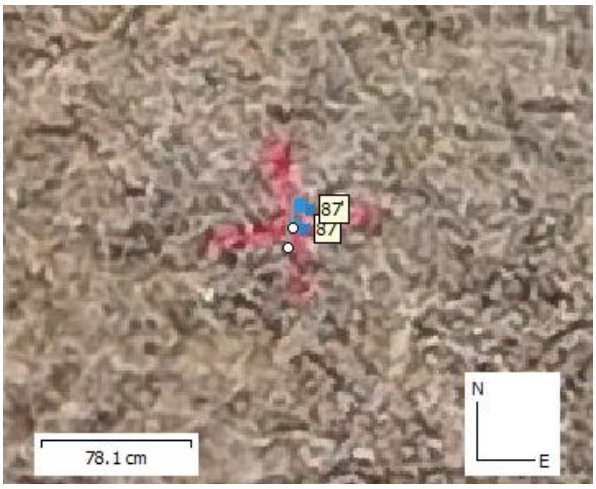

Image 7: Checkpoint residual error analysis in Agisoft Metashape. Field-based location for CP ID 87, with final location from the orthomosaic as marker 87'.

	XY - Horizontal (m)	Z - Vertical (m)
Median	0.63	0.79
Standard Deviation	0.49	1.16

Table 3: Residual Checkpoint Errors

Conclusion and Next Steps

- The selected UAS platform and payloads functioned effectively and reliably, when a detailed operations and airworthiness checklist was followed. This system is recommended for similar applications in the future.
- Compared to traditional methods with GCP arrays, the PPK workflow and sparse CPs saved considerable time, and minimized access requirements on private lands.
- Studying the PPK absolute accuracy on a test site with survey-grade CPs could further enhance confidence in the workflow and could potentially eliminate the need for any GCPs or CPs on future flights.
- The post-processing workflow is compute-intensive and benefits from a robust workstation configuration. Getting a workflow locked into a batch file .xml helps ensure copy-exact principles and minimizes the possibility of errors or omissions.
- Applying these field methods to more tributaries and river miles can accelerate the habitat assessment process. Additionally, these post-processing methods can be applied to archival imagery to push closer to actionable data and on-the-ground restoration.

List of Attachments

Attachment A - Residual Checkpoint Errors

Appendix C Geomorphic Unit Tool Analysis

NV5 GEOSPATIAL
powered by QUANTUM SPATIAL

May 3, 2022

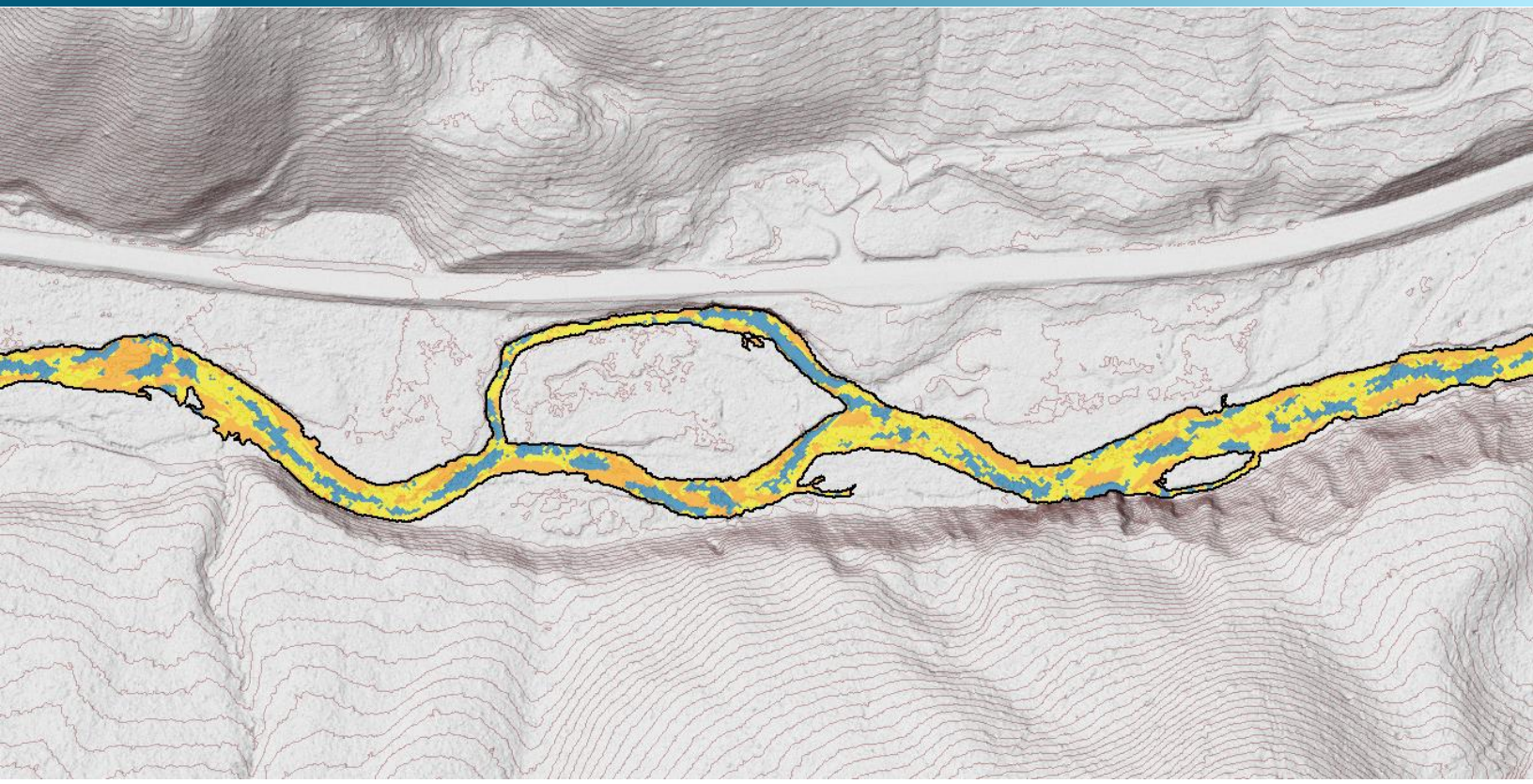

Grand Ronde Geomorphic Unit Tool Analysis

Prepared For:		*Prepared By:*
YAKAMA NEZ PERCE WARM SPRINGS UMATILLA	**Columbia River Inter-Tribal Fish Commission** 700 NE Multnomah St Portland, OR 97232	NV5 GEOSPATIAL powered by QUANTUM SPATIAL **QSI Corvallis** 1100 NE Circle Blvd, Ste. 126 Corvallis, OR 97330 PH: 541-752-1204

TABLE OF CONTENTS

INTRODUCTION

In September 2021, NV5 Geospatial (NV5) was contracted by the Columbia River Inter-Tribal Fish Commission (CRITFC) to delineate and classify the geomorphic character of 13 sites previously mapped through the Columbia Habitat Monitoring Program (CHaMP). This analysis is designed to support assessment and monitoring of instream and near-stream fish habitat conditions using the Geomorphic Unit Toolkit (GUT). This report accompanies the resulting spatial datasets and documents processing methods and approaches applied. Figure 1 shows the extent of the Upper Grand Ronde watershed and the specific sites of focus for this analysis.

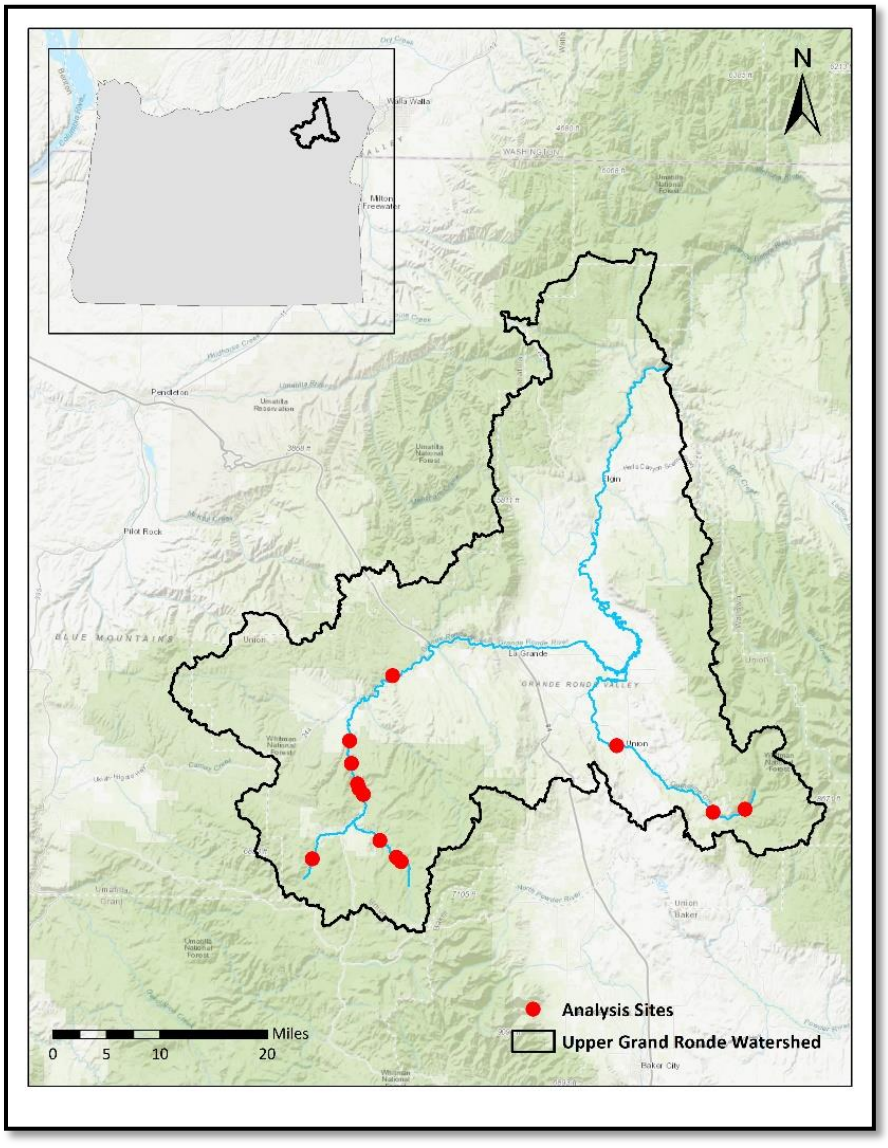

Figure 1: Upper Grande Ronde watershed with analysis site locations

Source Data

Topobathymetric Light Detection and Ranging (LiDAR) data was previously collected in the summer of 2020 for the Grande Ronde Basin site in Oregon. The topobathymetric lidar system uses two laser wavelengths to map both terrestrial (NIR wavelength) and bathymetric (Green wavelength) surfaces providing a seamless topobathymetric elevation model. Acquisition dates and acreage are shown in Table 1 and a geographic breakdown of acquisition dates and the GUT analysis sites are displayed in Figure 2.

Table 1: Upper Grand Ronde Lidar Acquisition

Project Site	Contracted Acres	Buffered Acres	Acquisition Dates	Data Type
Upper Grand Ronde, Oregon	76,189	93,681	08/17/2020 – 09/27/2020	Topobathymetric Lidar

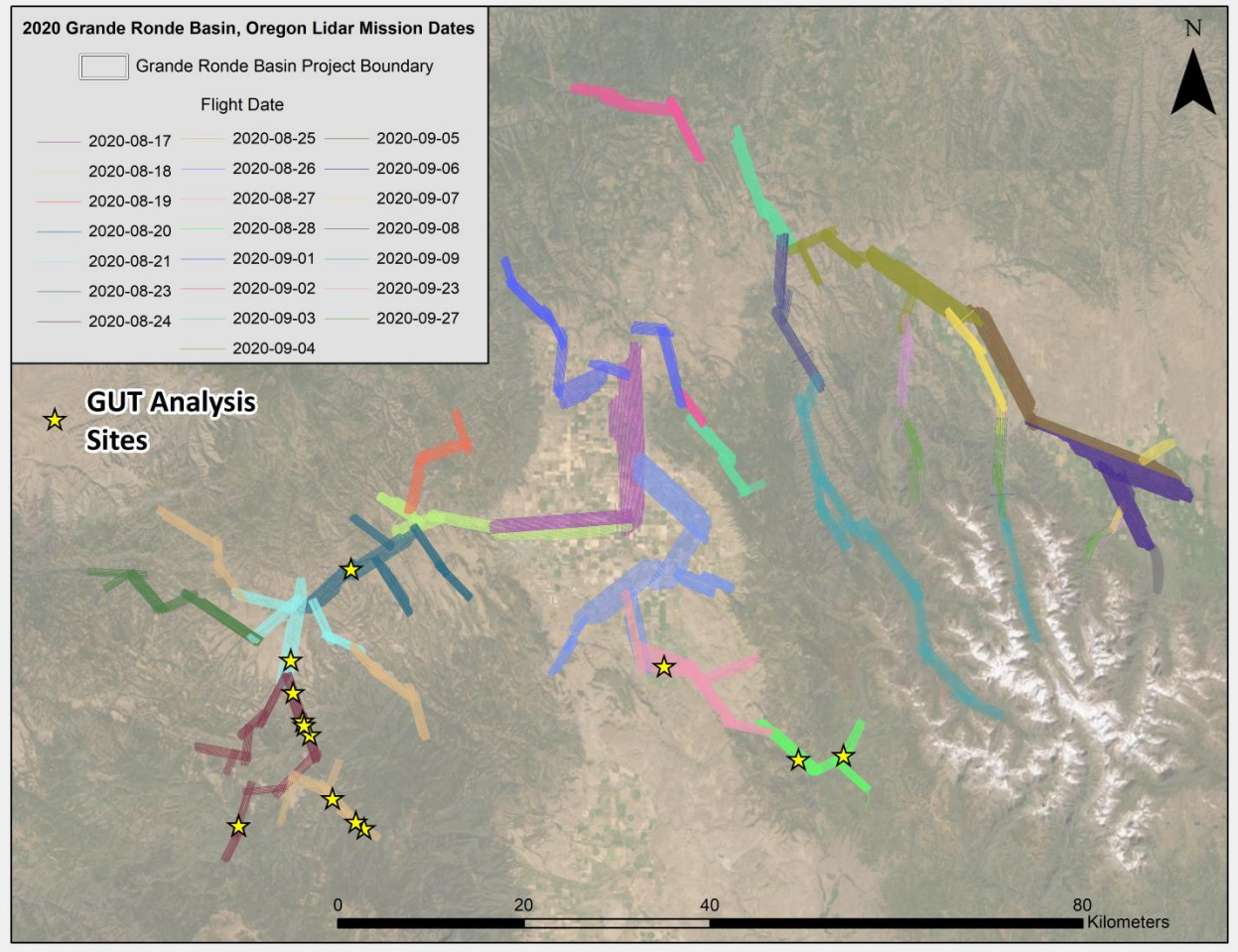

Figure 2: Bathymetric Lidar acquisition map along with the selected GUT analysis sites

Process overview

Successful application of the Geomorphic Unit Tool first requires derivation of a suite of intermediate datasets. These intermediates are inputs to the geomorphic classification and delineation process. One of the goals of this project was to test feasibility of automation to fully scale the process such that it could be run on complete river systems rather than isolated sites. For this reason, the specific methods used to generate each intermediate are discussed below as well as their potential influence on the final geomorphic unit outputs.

Bankfull Extent Polygon Generation

The bankfull extent polygon was generated based on an elevation model detrended by the river slope. Detrending was performed with Inverse Distance Weighted kriging of the water surface classified in the lidar. This detrended model is also known as a Relative Elevation Model (REM) where all elevation values have been normalized to the water surface elevation. Contour lines were then generated at 0.5ft intervals from the REM and the contour that best aligned with the top of the 1st major change in slope from the river's edge was selected as the bankfull. While this approach is very promising as far as an automated bankfull delineation, some areas still required manual edits. Specifically, areas where terrain mapping is not sufficiently detailed due to occluded LiDAR sampling or channels too narrow in width to obtain meaningful signal benefited from additional manual interpretation.

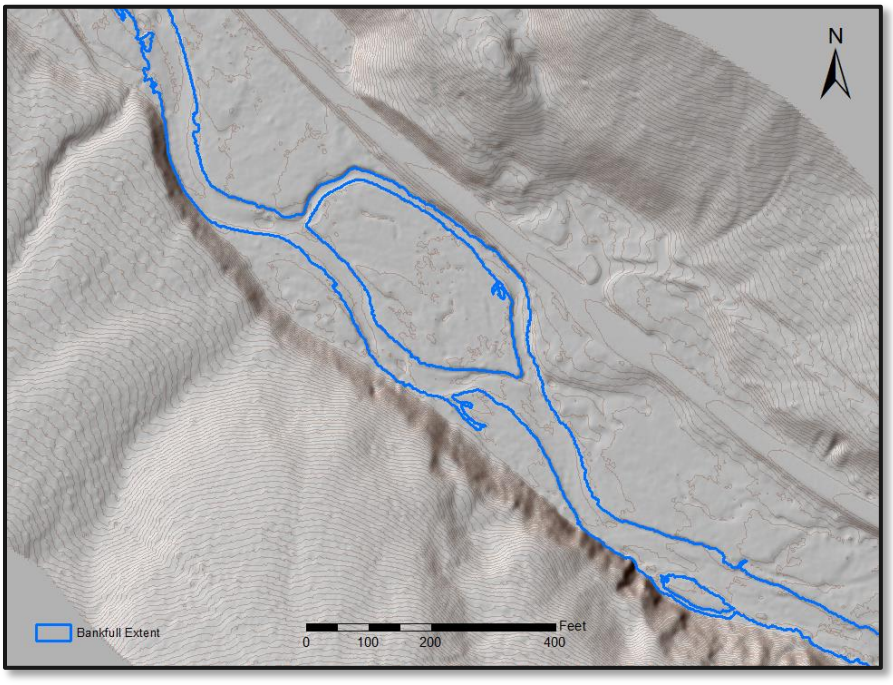

Figure 3: Bankfull Extent polygon example

Wetted Extent Polygon Generation

The wetted extent polygon was delineated directly from the lidar during the normal lidar processing workflow. To accurately map bathymetry, each lidar pulse penetrating the water surface needs to be refracted so wetted edge polygon is a normal deliverable for topobathymetric lidar projects. While refraction based wetted edge delineation is highly accurate, some additional manual editing may better represent connectivity of small channels during base flows.

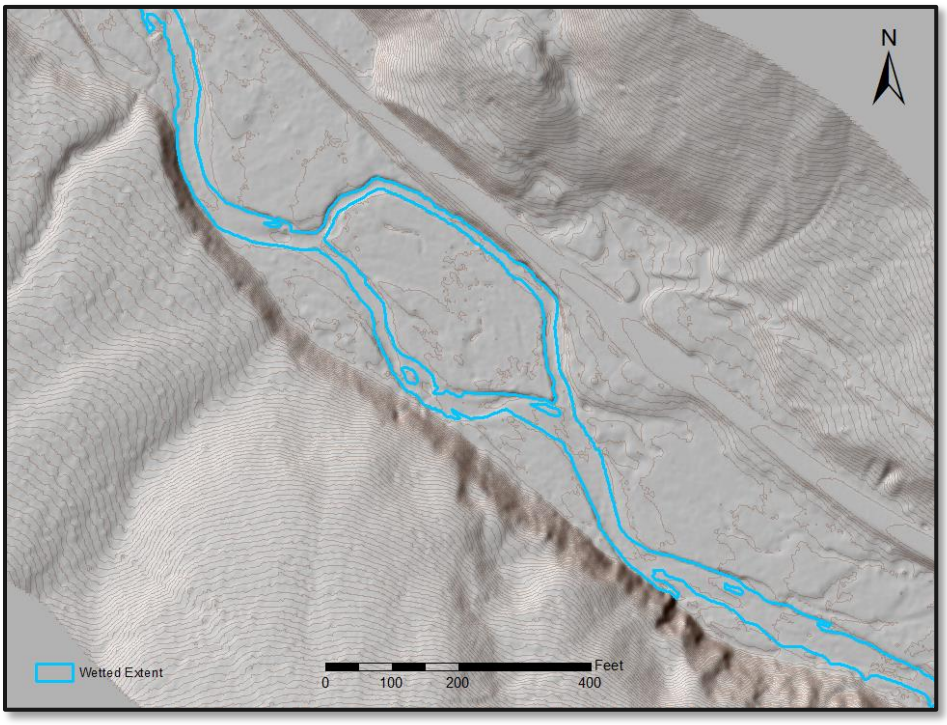

Figure 4: Wetted Extent polygon example

Stream Centerline Generation

Stream centerlines were generated for both the bankfull extent polygon and the wetted extent polygon using a customized Delaunay triangulation process. This process is a fully automatable method generating lines around all islands and connected side channels. Examples of the difference between the two centerlines are displayed below.

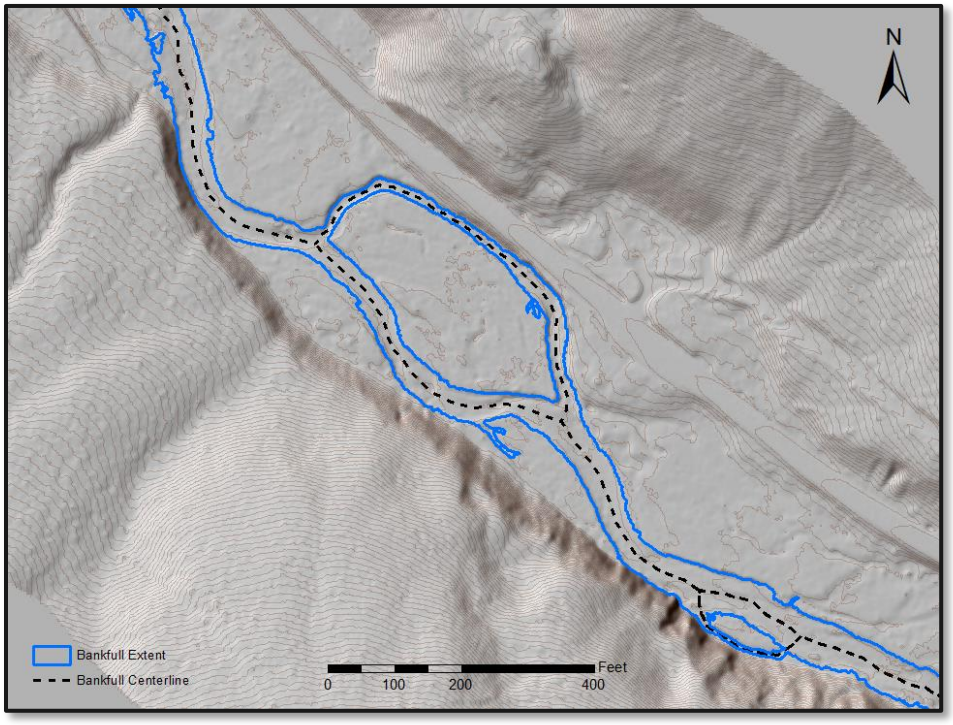

Figure 5: Bankfull Extent centerline example

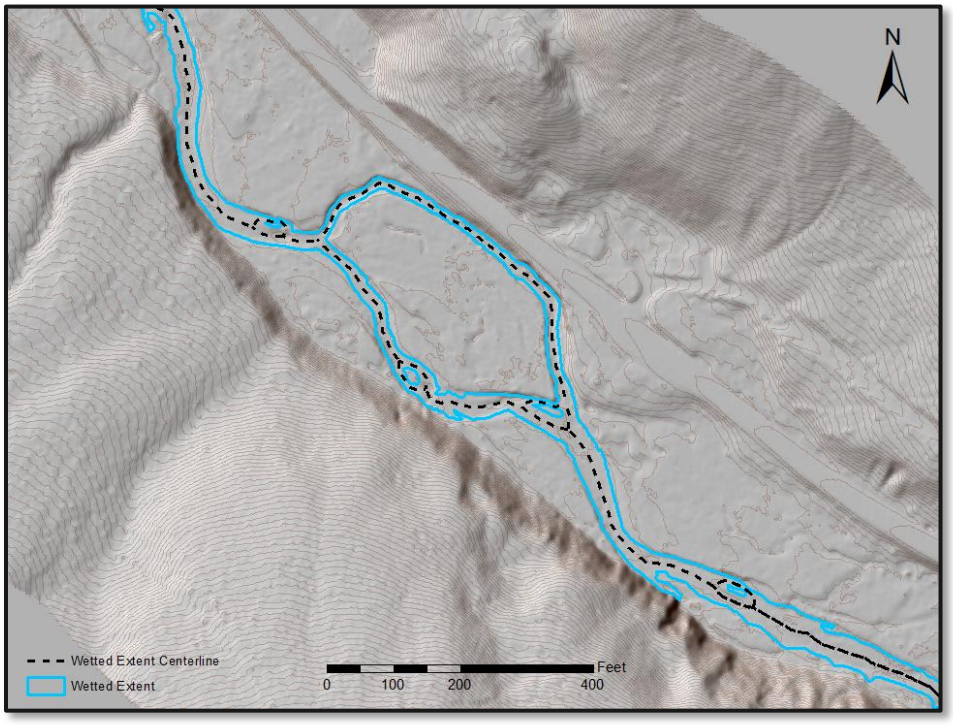

Figure 6: Wetted Extent centerline example

Thalweg Generation

Generation of the thalweg line was performed using least cost path analysis. Least cost path analysis uses cell by cell directional determination to generate a path line for lowest cost transition at each cell. This tool can require filtering of the elevation surface to remove fine-scale anomalies that can misdirect the path. Scalable automation of this process is promising but will require additional testing and evaluation. Additionally, thalwegs associated with secondary flow paths can also be input into the tool and affect the finest scale (Tier 3) classification. Secondary thalwegs were generated for one of the analysis sites and is covered in the results section below. Further investigation will still however be necessary to better understand the site-specific application of multiple thalwegs for main and side channels and their influence on geomorphic unit outputs.

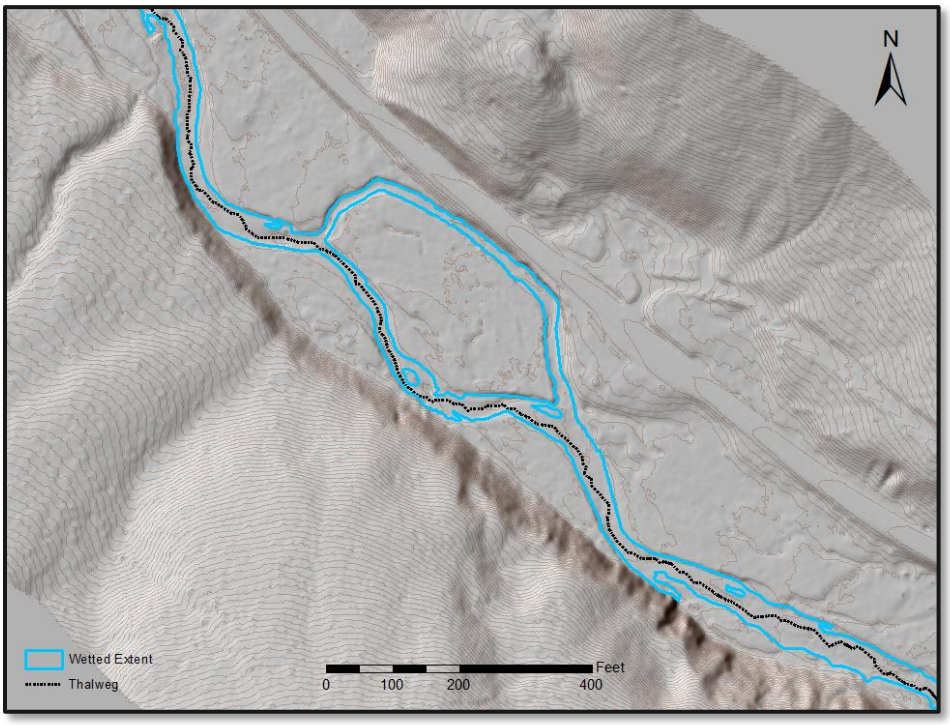

Figure 7: Thalweg with Wetted Extent example

Running PyGUT

The different tiers of stream morphology results were generated using PyGUT, which is the Python implementation of the Geomorphic Unit Toolkit (Wheaton et al 2015). PyGUT takes as inputs the bankfull extent polygon, wetted extent polygon, the stream centerline for both bankfull and wetted extents, the thalweg, and a DEM (digital elevation model) derived from bathymetric LiDAR. The workflow of the tool and its results are structured around a 3-tiered hierarchical classification system (Figure 8). The tool differentiates geomorphic units based on stage height (Tier 1), topographic shape (Tier 2), and geomorphic attributes such as position and orientation (Tier 3).

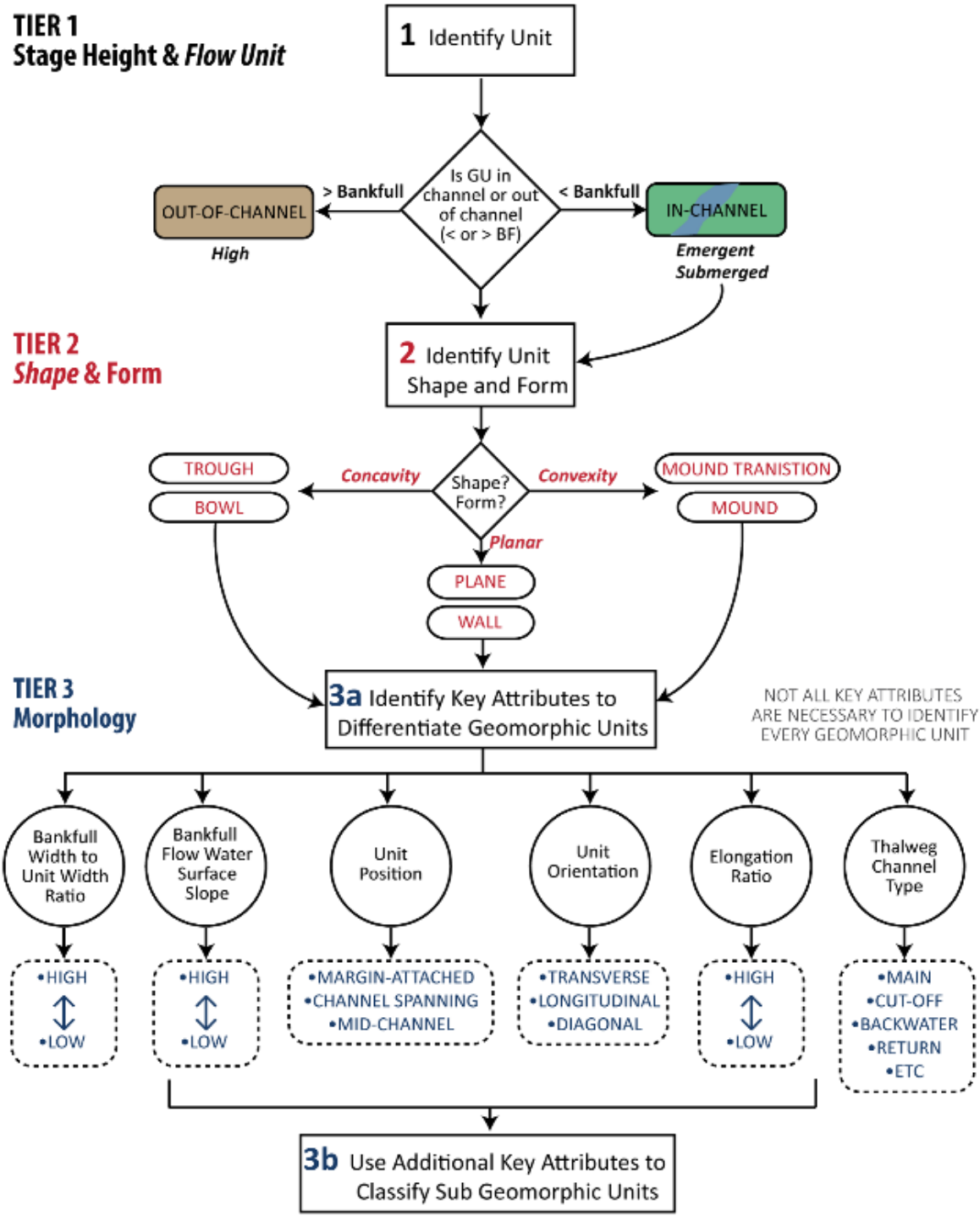

Figure 8: The 3-tiered hierarchical classification system of the Geomorphic Unit Toolkit.[1]

[1] http://gut.riverscapes.xyz/background.html

Upon running the PyGUT script, the output consists of polygon shapefiles in each of the three tiers. Figures 8 - 11 illustrates the distribution of tier 3 outputs. Through discussions with CRITFC it was determined that the Geomorphic Units output from the tool may be at higher classification resolution than is relevant to current monitoring protocols in the area. It may be advantageous in future projects to collapse some of the geomorphic unit classes to better represent features or interest in these systems.

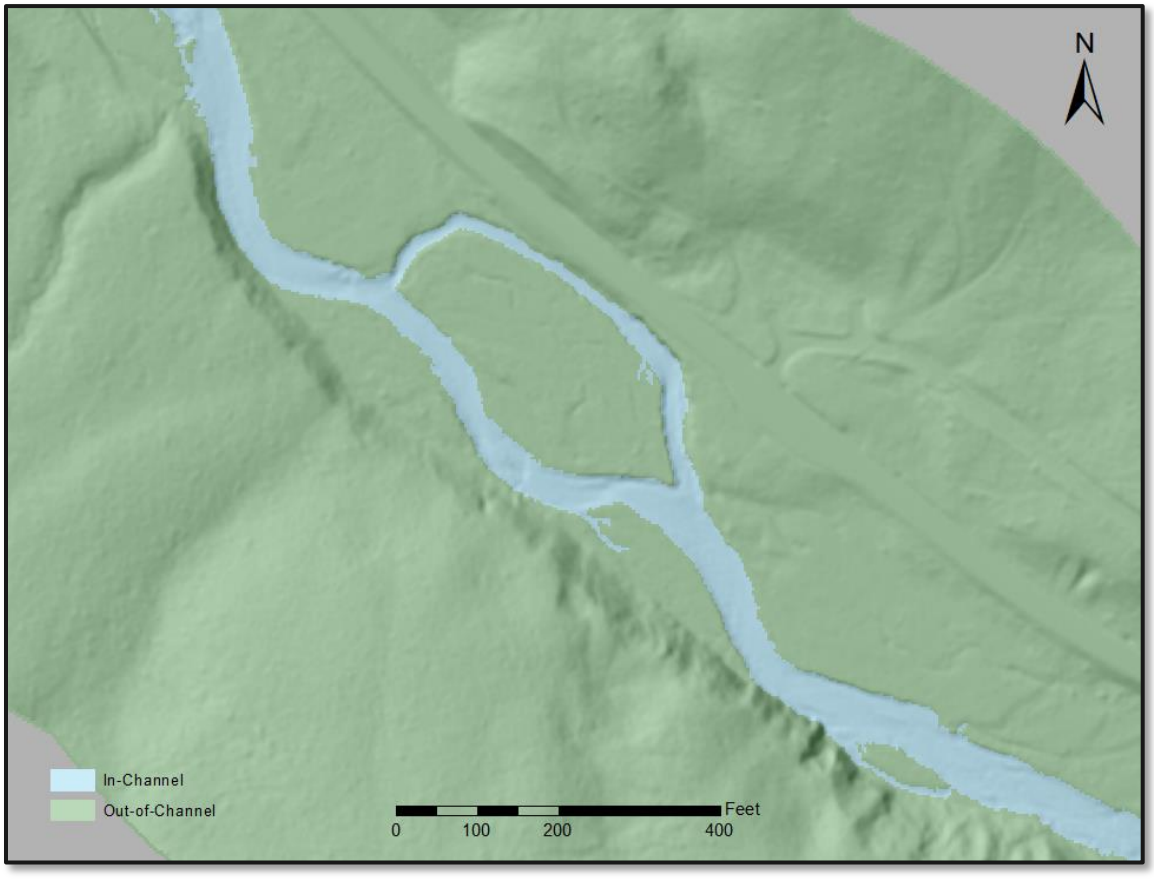

Figure 9: Tier 1 example

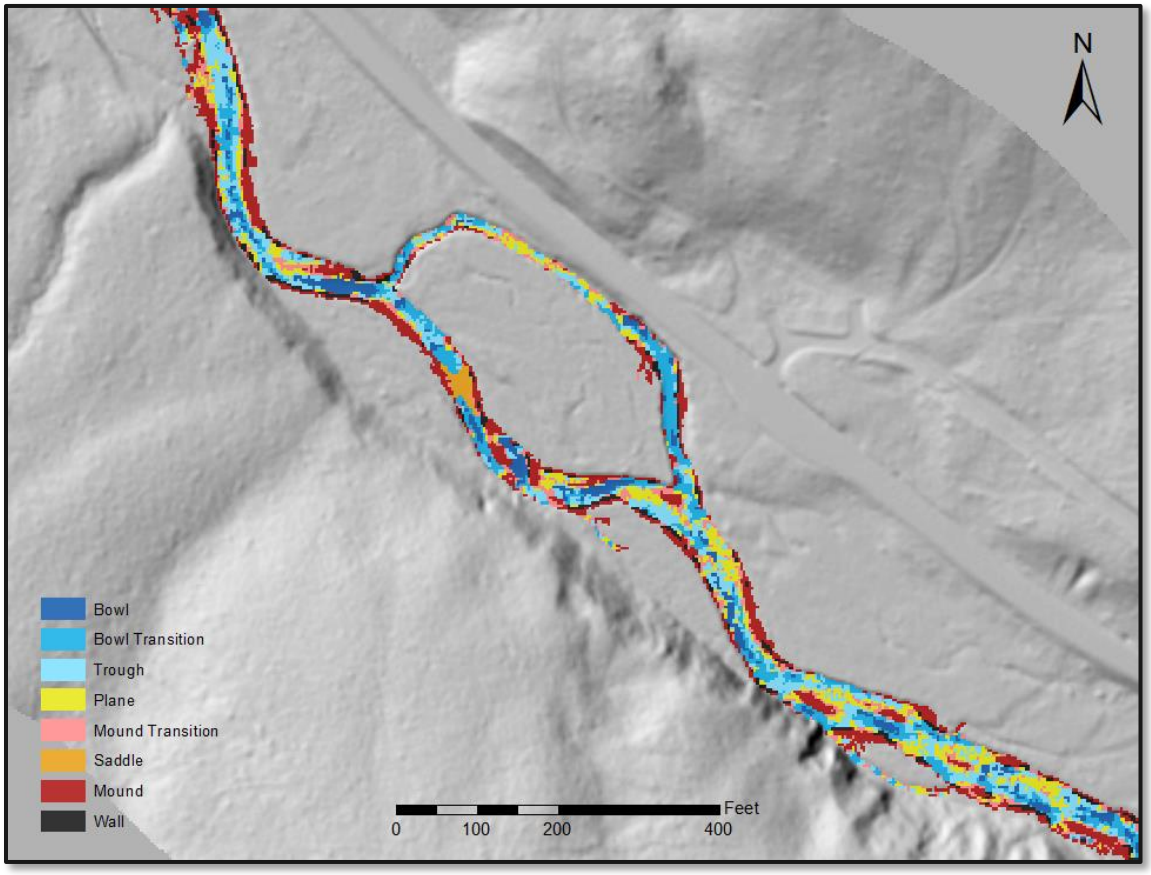

Figure 10: Tier 2 – Units example

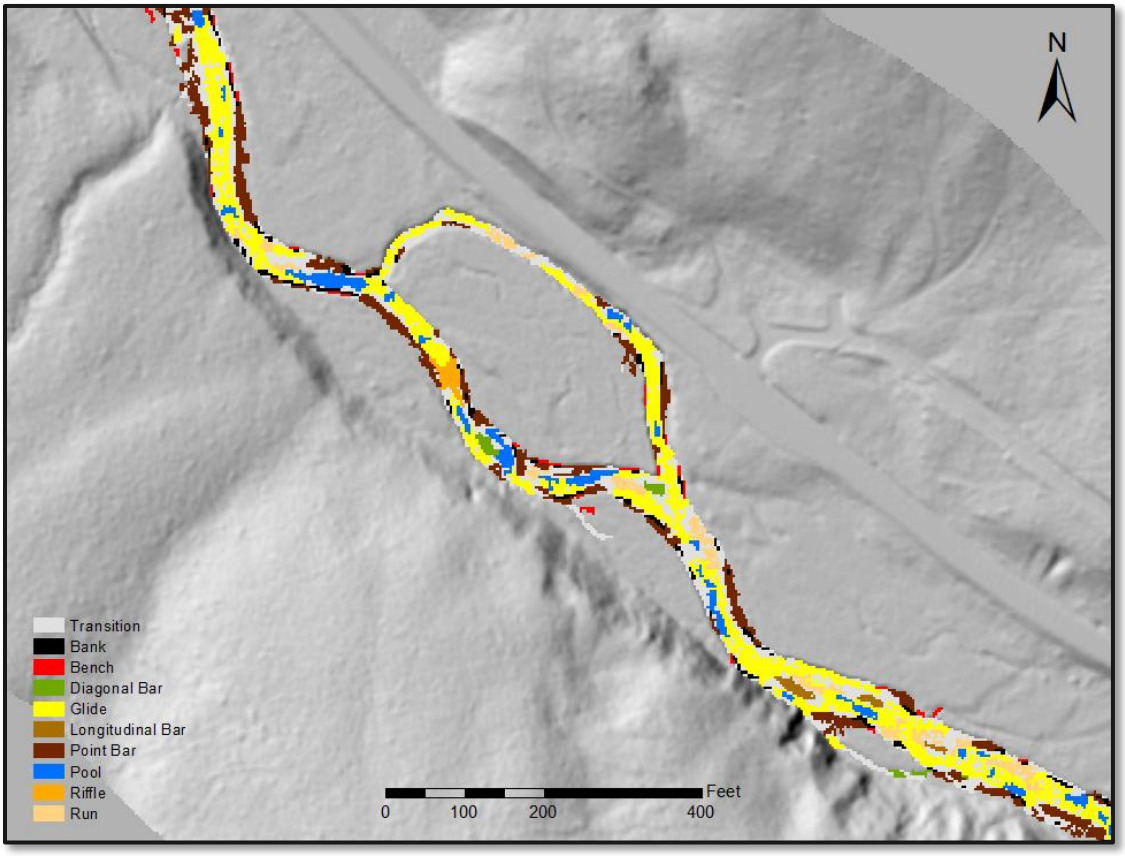

Figure 11: Tier 3 – SubUnits example

Secondary Thalwegs

Secondary thalwegs were generated for one of the analysis sites to compare the impact on the tier 3 geomorphic unit classifications. Addition of the secondary thalweg input changed less than 1% of the overall classification with the main change being the addition of more Riffle classification in lieu of Glide-Run, Margin Attached Bar, Mid Channel Bar, and Transition classifications.

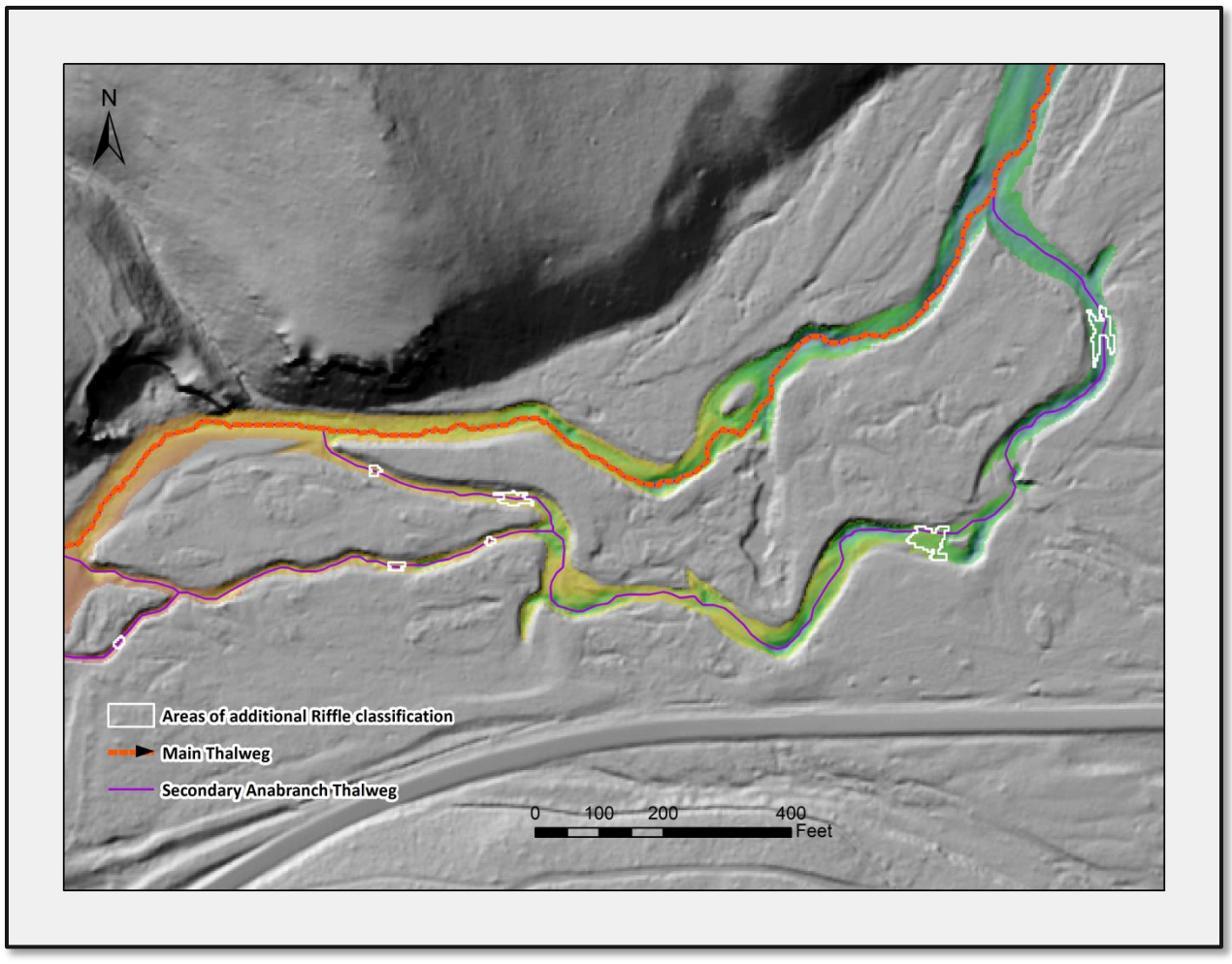

Figure 12: Area of classification changes at the Tier 3 level when Secondary Thalwegs are utilized

Appendix D Juvenile Salmon Dispersal using PBT

Juvenile wild spring Chinook Salmon exhibit variable dispersal patterns across a heterogeneous riverscape

Matthew J. Kaylor[1], Lindsy R. Ciepiela[2], Melody Feden[2], Joseph T. Lemanski[2], Casey Justice[1], Jonathan B. Armstrong[3], Benjamin A. Staton[1], Stefan Kelly[4], Shawn R. Narum[5], Ian A. Tattam[2], Seth M. White[4]

Affiliations

[1]Columbia River Inter-Tribal Fish Commission, Fishery Science Department, 700 NE Multnomah St., Suite. 1200, Portland, Oregon 97232.

[2]Oregon Department of Fish and Wildlife, East Region Fish Research, La Grande, OR.

[3]Oregon State University, Department of Fisheries, Wildlife, and Conservation Sciences. Corvallis, OR 97330

[4]Confederated Tribes of Warm Springs Reservation of Oregon, John Day, OR

[5]Columbia River Inter-Tribal Fish Commission, Hagerman Genetics Lab, Hagerman ID 83332

Abstract

For many aquatic taxa, juvenile dispersal from spawning locations to rearing habitats is a critical process influencing individual fitness and population dynamics. However, our understanding of dispersal patterns in naturally spawning populations remains largely unknown due to the logistical challenges of tracking movement at early life stages using traditional marking and tagging approaches. We evaluated dispersal patterns of a spring-run Chinook Salmon population in a NE Oregon riverscape using genetic parentage-based tagging to trace juveniles captured from summer rearing habitats to maternal parents sampled from spawning locations the prior year. We also estimated parr abundance across the watershed to adjust dispersal estimates for sampling bias, and to evaluate dispersal as the link between the distributions of spawners and their offspring. Overall dispersal of the 1,326 parr (*n* sampled = 3,388) paired to female adults (*n* = 64) was downstream-biased (median = -0.77 km; 68% dispersed downstream). Dispersal distances were high relative to those found in other studies, with 25% of parr dispersing more than 0.9 km upstream and 25% dispersing more than 3.7 km downstream (range = -28.6 -10.6 km). Dispersal patterns followed longitudinal trends with parr originating higher in the watershed showing downstream dispersal bias, higher variability in dispersal, and farther dispersal distances whereas juveniles originating downstream showed upstream bias, lower variability, and shorter distances. Nested within these trends, parr originating in the warmest sections of the mainstem typically dispersed to cooler portions of the mainstem or tributaries, suggesting that thermal conditions were a primary driver of observed dispersal. Lastly, dispersal distance was associated with larger length-at-capture for parr that dispersed downstream but not upstream, which may reflect the unique pattern of earlier emergence upstream, providing competitive advantages for downstream dispersers over later emerging conspecifics. Overall, these findings suggest that heterogeneity in biophysical conditions within and among watersheds may translate to variable patterns of dispersal. These findings additionally provide guidance for prioritizing restoration efforts to address limiting factors and maximize habitat use through better alignment with juvenile salmon ecology.

Introduction

Variation in physical habitat conditions, food resources, and biotic interactions (e.g., competition, predation) form dynamic landscapes of habitat quality (Stanford et al. 2005) that shape individual and population-level fitness (Griffen and Norelli 2015, Turlure et al. 2019). As this mosaic of landscape conditions shifts, movement allows animals to seek favorable habitats that enhance individual fitness; for example, by reducing competition (Einum et al. 2008, Yoshimoto 2009), avoiding sub-optimal or lethal environmental conditions (Elmore et al. 2017, Hahlbeck et al. 2022), and tracking food resources and thermal conditions to maximize growth opportunities (Armstrong et al. 2010, Baldock et al. 2016, Aikens et al. 2017). However, factors that constrain or prohibit movement are also dynamic across space and time, and vary among taxa, life stages, and individuals. Evaluating patterns of movement amongst this complexity provides insight into the critical factors that promote and restrict movement and the implications of movement patterns on fitness.

For riverine fishes, movement is mediated by both passive (i.e., downstream drift with water current during early life stages) and active (i.e., swimming independent of current) processes. As such, movement may be limited by individual characteristics and biophysical conditions including life stage- or size-specific swimming capacity, landscape constraints (e.g., physical or thermal barriers), perceptual extent (Lima and Zollner 1996), and risks associated with moving (e.g., predation). Via these factors, watershed heterogeneity in biophysical conditions should, in turn, generate variable patterns of individual movement. In salmonids, there is extreme variation in individual movement behavior (Quinn 2007), but the underlying mechanisms and how they are patterned across landscapes is often unknown.

The combined active and passive movement of juvenile salmon from spawning nests (redds) to rearing habitats, hereafter referred to as "dispersal", is a critical process affecting individual growth and survival (Einum and Nislow 2005), which collectively influence population dynamics through effects on juvenile distribution, habitat utilization, and production (Teichert et al. 2011, Einum et al. 2011). Anadromous salmon are highly fecund and their spawning locations are often clustered at both small (e.g., multiple redds within a pool tail-out) and large (i.e., core reaches within a basin) spatial scales (Beechie et al. 2008), resulting in high localized densities of recently emerged juveniles (Flitcroft et al. 2014). Juveniles that disperse to lower-density habitats typically exhibit greater growth and subsequent survival (Einum and Nislow 2005, Brunsdon et al. 2017, Aparicio et al. 2018), and collectively, these individual dispersal patterns can influence population-level density-dependent effects. Further, spatial patterns in juvenile rearing habitat quality may not align with spawning distributions, and dispersal facilitates juvenile habitat selection and rearing range expansion, including into tributaries and headwaters not used by spawning adults (Anderson et al. 2013, Scheu 2022). However, the spatial distribution of juvenile salmonids often mirrors adult spawning distributions (Foldvik et al. 2010, Atlas et al. 2015), suggesting limited overall dispersal, or alternatively, that spawning and rearing habitat are supplementary.

Empirical evaluations of juvenile salmon dispersal generally suggest that movement after emergence from redds to summer rearing habitat is limited (< 0.5 km of origin) and biased downstream (reviewed by Eisenhauer et al. 2021), conforming with the Restricted Movement Paradigm (RMP; Gerking 1959) which argues that most individuals in a population are sedentary during nonmigratory periods. However, unbiased and accurate dispersal estimates are limited and there is increasing evidence challenging the RMP in juvenile salmon as dispersal is evaluated across a wider range of environmental conditions (Eisenhauer et al. 2021). The majority of studies evaluating dispersal have done so by out-planting embryos or fry to

streams (reviewed by Eisenhauer et al. 2021), typically at small spatial scales and with low variability in biophysical conditions. Reducing variability is often necessary to test specific hypotheses and these studies have greatly informed our understanding of factors influencing dispersal (Einum and Nislow 2005; Einum et al. 2006; Brunsdon et al. 2017); however, few studies have evaluated dispersal in naturally spawning populations (but see Anderson et al. 2013).

Wild populations are exposed to greater variability in inter- and intra-specific competition, environmental conditions, habitat quality, and emergence timing (Kaylor et al. 2022), likely stimulating variable dispersal patterns across watersheds. Indeed, studies evaluating juvenile salmonid dispersal in naturally spawning populations have reported large-scale dispersal of tens or hundreds of kilometers associated with alternative life-history strategies (Bradford and Taylor 1997, Scheu 2022). We currently lack an understanding of dispersal at finer spatial scales (i.e., within natal rearing extents) and to our knowledge, no studies have evaluated population-level dispersal across the entirety of the adult spawning and juvenile rearing extents. This represents a fundamental knowledge gap, as dispersal largely dictates how landscape configuration (i.e., the spatial arrangement of habitat patches) affects early life stages of freshwater fish. Understanding these patterns and the mechanisms that drive them have important implications for prioritizing the types and locations of management efforts to maximize habitat use and benefit to juvenile salmonids.

In this study, we used a riverscape sampling approach and genetic parentage-based tagging (PBT) to quantify juvenile dispersal patterns of a wild population of spring-run Chinook Salmon in NE Oregon, USA. Additionally, we estimated parr abundance and distribution across the river network to relate spawning and dispersal patterns to parr distribution and to correct for sampling bias effects on our inference into population-level dispersal. Our objectives were to: 1) characterize overall dispersal patterns of a naturally spawning population; 2) evaluate variability in dispersal patterns across the spatial extent of spawning locations, including potential drivers of observed patterns; and 3) assess how dispersal distance and direction (upstream vs. downstream), and other biophysical factors (e.g., temperature, emergence timing, density) relate to parr length-at-capture.

Methods

Study area and species description

The study was conducted in the Middle Fork John Day River (MFJDR), a tributary of the John Day River in northeast Oregon. The MFJDR watershed encompasses 2,051 km^2 and flows northwest from its origins in the Blue Mountains to its confluence with the North Fork John Day River (Figure D-1). The study area is approximately 700 river kilometers (rkms) from the Columbia River estuary (subsequent rkm measurements are relative to the mouth of the MFJDR) and anadromous fish encounter three dams on the mainstem Columbia River *en route* to and from spawning grounds on the MFJDR. The region is characterized by hot summers with little precipitation and cold winters in which most of the precipitation is snow. Streamflow peaks during spring snowmelt – typically March to May – and is lowest during mid-to-late summer, a period coinciding with maximum water temperature. The timing of spring snowmelt and the onset of summer low flow conditions occurred early in 2021, and mainstem flows for the first week of July and August were 56% (28.5 cfs) and 75% (15.7 cfs), respectively, of 2012-2020 (period of record) average discharge (USGS gauge 14043840).

Spring-run Chinook Salmon in the MFJDR spawn throughout September with most spawning occurring between rkms 80-115 of the mainstem (Bare et al. 2021). Embryos incubate throughout the fall and winter, with emergence generally occurring between March and May; however, emergence occurs earlier in

upstream reaches where winter water temperatures are warmer (Kaylor et al. 2022). During summer rearing, parr are typically distributed throughout the mainstem spawning extent as well as in adjacent tributaries. As summer rearing transitions into winter-rearing, parr exhibit two main life history strategies: 1) fall-migrants leave summer rearing reaches to overwinter in larger mainstem habitats downstream and 2) spring-migrants overwinter in natal mainstem and tributary habitats overlapping the summer rearing extent. Both fall- and spring-migrants spend approximately one year in the stream following emergence before smoltification and downstream migration to the estuary in spring (Copeland and Venditti 2009, Bare et al. 2021). The John Day basin has no history of hatchery supplementation and hatchery adult strays into the basin are rare.

In addition to Chinook Salmon, the fish community in the MFJDR is comprised of steelhead/rainbow trout (*O. mykiss*), mountain whitefish (*Prosopium williamsoni*), northern pikeminnow (*Ptychocheilus oregonensis*), redside shiner (*Richardsonius balteatus*), bridgelip sucker (*Catostomus columbianus*), largescale sucker (*Catostomus macrocheilus*), speckled dace (*Rhinichthys osculus*) and sculpin (*Cottus spp.*)(Torgersen et al. 2006).

Adult sampling

We sampled adult Chinook Salmon in September 2020 during the peak of spawning activity (9/16/2020 – 9/23/2020). Surveyors (1-2 individuals per reach) walked the entire length of the spawning distribution on 9/16/2020 and 9/21/2020, collecting tissue samples from carcasses, recording redd locations, and noting locations of live adults using standard spawning ground survey techniques (Bare et al. 2021). We supplemented standard surveys with intensive daily surveys conducted by a smaller group of 2-4 surveyors, targeting locations of live adults. During both standard and intensive surveys, we examined carcass body cavities to determine sex and spawn completeness and we collected an operculum tissue sample (occasionally fin or heart tissue when operculum was degraded or not present). Tissue samples were pressed onto Whatman paper and inserted in paper coin envelopes to air dry.

Parr sampling

We selected parr sampling sites to achieve a spatially balanced distribution throughout the core rearing range of the mainstem (rkms 79-118) and associated tributaries (Figure D-1; Table D-1). Prior to parr sampling, we selected 30 mainstem sites: 10 sites were part of on-going research by Oregon Department of Fish and Wildlife (ODFW) and Confederated Tribes of the Warm Springs Reservation of Oregon (CTWSRO), and 20 sites were selected from an existing Columbia Basin-wide Generalized Random Tessellation Stratified sample (Stevens and Olsen 2004). However, parr were either not present or in too low abundance to sample at nine planned mainstem sites (rkms 80-90 and 111-113), resulting in 21 sampled mainstem sites. Given the potential importance of cool- and cold-water tributary use, we also sampled parr from nine tributaries. We incorporated samples from two reaches in Vinegar Creek and one reach in Camp Creek that were part of ongoing research by ODFW. We selected the remaining sampling reaches within tributaries to maximize spatial coverage of salmonid rearing habitat while accommodating time constraints dictated by stream temperatures and land ownership.

We sampled parr between 6/29/2021 and 8/19/2021, during summer rearing and prior to downstream movement associated with winter-rearing or outmigration. Based on predicted median emergence timing between 4/6/2021 and 5/10/2021 (Figure D-S2; Kaylor et al. 2022), parr sampling occurred approximately 3-4 months post-emergence. Tributaries were generally sampled earlier than mainstem sites (Table D-1), as warmer mainstem temperatures prohibited sampling for much of July. We captured parr using snorkel

seining methodology, except for in five shallow tributaries which we sampled with backpack electro-shockers. At each site, we navigated to a pre-determined GPS point and then progressed upstream. Parr from individual habitat units (e.g., a single pool) were kept in separate, labeled buckets and unit-specific GPS points were taken. We sampled a maximum of 25 parr from individual habitat units to ensure that we sampled from multiple units within each site. In smaller tributaries with low parr abundance, we combined parr from multiple units with total sampled length not exceeding 50 m. Captured parr were anesthetized, measured (fork length, nearest mm) and weighed (nearest 0.1 g). Small, non-lethal, caudal fin clips were pressed onto gridded Whatman paper, air-dried, and stored in paper folders for genetic processing. We allowed parr to recover in aerated buckets and then released them into the unit they were sampled from.

Genotyping

Tissue samples from adults and parr were genotyped to enable parentage analyses of parr to their parents. DNA was extracted from tissue samples using the Chelex 100 method, and then DNA libraries of barcoded individuals were prepared and sequenced following the genotyping-in-thousands method (GTseq; Campbell et al. 2015). The GTseq method entails one round of PCR to amplify targeted genetic loci and another to add barcodes to identify individuals. Then each sample was normalized and pooled into a sequencing library. The library was quantified and then sequenced using an Illumina NextSeq 2000 instrument. The GTseq panel included 354 single nucleotide polymorphisms (SNPs), with a subset of 254 putatively neutral markers intended for parentage analyses along with a genetic sex marker to verify males vs. females (see Hess et al. 2023 for details). All samples and genetic markers with 10% or more missing SNPs were considered failed genotypes and were not retained for analyses. Because some sampled carcasses were too degraded or scavenged to accurately determine sex, we relied on genetic sex assignments for all adults.

Parentage assignments (i.e., parr-adult pairings) were performed using CKMRsim software (Anderson 2020) and Close-Kin Mark-Recapture methods (Bravington et al. 2016) were used to estimate likelihoods between each adult and parr sample. We included pairwise relationships between parr and negative adult controls (adults originating outside the John Day River Basin), to assess the false positive and false negative rates expected for the adult-parr dataset and compared the log-likelihood ratio (LLR) distributions of MFJDR parentage assignments relative to negative control assignments to determine an LLR threshold. The LLR of negative control samples ranged from -29 to -1, whereas the distribution of MFJDR parent assignments exhibited a bimodal pattern, intersecting at an LLR value of approximately 12 (Figure D-S3). We applied a conservative LLR threshold of 20 and excluded parr-adult assignments with LLR lower than this value (false positive rate < 0.01). We only evaluated dispersal using parr-female pairs, as male carcass locations were not expected to provide reliable proxies of redds due to movement after spawning and spawning with multiple females (Murdoch et al. 2009).

Abundance estimates

We estimated parr abundance within sample reaches using snorkel and electrofishing surveys (Figure D-1), and then used these estimates to predict parr abundance across unsampled portions of the MFJDR watershed. We snorkeled 27 mainstem reaches (total length = 7.58 km) and continuous sections of the four largest tributaries (6.08 km). We conducted electrofishing surveys in five tributaries that were too shallow to snorkel (2.27 km; Table D-2).

Snorkel surveys were conducted at the habitat unit-level, in which snorkelers recorded counts of Chinook Salmon parr observed. For mainstem reaches, we progressed upstream until survey length exceeded 15x

bankfull width (range: 174-388 m). In tributaries, we progressed upstream until no parr were observed in three consecutive pools and we assumed that parr abundance upstream of this point was negligible. The exception was Big Boulder Creek, in which surveys were concluded at a private property boundary ~500 m upstream from the confluence. We visually delineated habitat units as pools, fast-non-turbulent (FNT; i.e., runs, glides), and fast-turbulent (FT; i.e., riffles). We sampled all pools and FNTs but sampled alternating FTs in mainstem sites and every fourth FT in tributaries due to time constraints and lower counts observed in these habitats (Kaylor et al. 2021).

To adjust for imperfect detection in snorkel surveys, we measured unit-specific habitat attributes that can affect detection and applied the model developed by Staton et al. (2022) to predict detection probability of each survey. These attributes included unit type, average depth, density of large wood pieces, and an observer-determined visibility index. For each unit (n = 432), we sampled 1000 detection probability values with replacement from the posterior predictive distributions given by Staton et al.'s model and used them to expand the partial snorkel counts to a distribution of abundance estimates. We imputed abundance for skipped units using mean density from sampled units of that site and unit type. We then summed across all units for each iteration to obtain 1000 abundance and density estimates per mainstem reach or tributary.

For smaller tributaries, we conducted equal-effort, single-pass electro-fishing surveys in one to three reaches and enumerated all captured parr. We expanded counts to abundance estimates using reach-scale capture efficiency estimates obtained from ODFW using paired single-pass and mark-recapture surveys conducted in MFJDR tributaries between 2019 and 2021. For each unit, we simulated 1000 abundance estimates by drawing from the distribution of capture efficiencies (mean = 0.26; SD = 0.083), and we generated reach-scale estimates by summing across all units within each reach.

We generated reach-, stream-, and basin-wide abundance estimates by predicting abundance at unsampled locations. We created prediction sites ~300 m in length between surveyed sites and predicted parr density for each unsampled site (# m^{-1}) using linear interpolation of sampled sites. We generated 1000 density predictions for each site, which we then multiplied by reach length to obtain a distribution of abundance predictions. We assumed that mainstem abundance was zero downstream of rkm 83 and upstream of rkm 117, as surveys conducted beyond these points indicated few or no parr. Lastly, we summed abundance estimates across reaches for each iteration to obtain a distribution of stream-specific and whole-basin abundance estimates.

Sampling bias adjustments

Population-level dispersal patterns may be influenced by sampling bias if sampled parr do not represent a random sample of the population (Wacker et al. 2021). Ideally, the number of parr sampled at each site would be proportional to parr abundance. This was logistically impractical as we did not have *a priori* abundance estimates and because abnormally warm temperatures in July prohibited mainstem sampling in some locations. To reduce sampling bias effects on dispersal inference, we calculated and assigned sampling weights to individual fish based on capture reach. Sampling weights were equal to the predicted proportion of the population located at each sampling reach (P_{pop}) divided by the respective reach sampling proportion (P_{samp}), where P_{pop} is equal to the mean predicted abundance at each reach divided by the predicted mean basin abundance (67,753) and P_{samp} is equal to the reach sample size divided by the total sample size (n = 3,388 parr). These weights therefore provide an estimate of the degree to which reaches were over- or under-sampled and were incorporated into models as weighting factors.

Temperature

To evaluate thermal conditions across the MFJDR in summer 2021, we used hourly water temperature data from loggers distributed across the watershed (Feden and Bliesner 2022). We downloaded data in fall 2021 from 38 mainstem locations (rkms 76-114) and all nine sampled tributaries, in which loggers were located within a kilometer upstream from the mainstem confluence. Temperature data were filtered through a standardized QA/QC process and visually inspected for errors. We summarized daily mean and max temperature and calculated mean daily maximum temperature (MDMT) across the months of June ($MDMT_{June)}$ and July ($MDMT_{July}$). All nine tributaries exhibited cooler temperatures compared to adjacent mainstem sections with the greatest differences occurring in Beaver Creek, Granite Boulder Creek, Dead Cow Gulch, and Clear Creek (Table D-1, Figure D-S1).

Dispersal analyses

We calculated dispersal as the stream distance between each parr-female pair such that negative values indicated downstream mainstem dispersal (i.e., parr captured downstream of female parent) and positive values indicated upstream mainstem dispersal. Tributary distance was negative if the tributary confluence was downstream of the female location, and positive if upstream of females. Thus, negative dispersal values indicate directionality of mainstem dispersal, and for tributary dispersers, reflects the total distance dispersed including downstream mainstem and upstream tributary dispersal. We also present total distance moved regardless of direction as a response variable.

We first evaluated the overall distribution of all dispersal estimates including the median, inter-quartile range (IQR), and 95% quantiles. We calculated metrics using weighted quantiles, in which weights were proportional to the estimated sampling bias of reaches and were applied to all parr captured within that reach (described above). We evaluated both dispersal and total distance for all parr and stratified by parr that were captured within the mainstem versus tributaries.

We evaluated spatial patterns of parr dispersal across the MFJDR using two approaches: 1) we used a general linear mixed-effects model (GLMM) to predict mean dispersal as a function of parr origin rkm (i.e., rkm of paired female), and 2) we evaluated dispersal at a finer-scale by grouping parr into sections based on their origin and plotting where they dispersed to using weighted density distributions. Dispersal distance was the response variable with model fit providing an estimate of upstream vs. downstream dispersal bias. We fitted the model with an interaction between origin rkm and an indicator variable for whether parr were captured within the mainstem or tributaries. The model also included the unique identifier of the female parent as a random effect with sampling bias weights applied to each individual parr. We fitted separate models with parr origin rkm as a linear, 2^{nd} order polynomial, and 3^{rd} order polynomial relationship and assessed model fit using AICc (Burnham and Anderson 2004) in which the 2^{nd} order polynomial relationship had the most support. The relationship between model residuals and river kilometer indicated heteroscedasticity and we therefore modeled the residual standard error as relationship as having a linear relationship with origin rkm and the response variable using the R package 'glmmTMB' (Brooks et al. 2017).

We used GLMMs to evaluate the factors (particularly dispersal distance) influencing parr size-at-capture after accounting for potential confounding effects of sampling date. We expected parr size to exhibit spatial patterns independent of dispersal as emergence timing is longitudinally structured in the MFJDR (Kaylor et al. 2022), which can translate to longitudinal patterns of parr summer size (Kaylor et al. 2021). Parr fork length was the response variable and we included distance moved, parr origin rkm (2^{nd} order polynomial),

mainstem vs tributary capture, dispersal direction (upstream vs. downstream), sampling day, max temperature ($MDMT_{July}$) of capture locations, and density at capture locations (parr m^{-1}) as fixed-effects, the unique identifier of the female parent as a random effect, and sample bias weights. To evaluate whether mainstem vs. tributary capture and dispersal direction were important factors describing size-dispersal relationships, we fitted each candidate model with different combinations of interactions and additive effects of these covariates. We assessed collinearity and removed models from the candidate set when the variance inflation factor exceeded 10 for one or more terms (Dormann et al. 2013). We used AICc to select a set of plausible models ($\Delta AICc < 2$) and then chose the model with the fewest parameters.

Results

Genotyping

We identified 161 redds across the mainstem MFJDR and a single redd in Clear Creek in September 2020 (Figure D-2; Figure D-S4), which is 60% of the 20-year mean of 272 redds. We sampled tissue from 141 individual spawners (41% of the estimated total spawners) and 113 of these samples were successfully genotyped (<10% of SNPs missing), of which 67 were females and used in analyses. The distribution of redds generally mirrored the distribution of successfully genotyped females across the study extent, except between rkms 90-100 (Figure D-S4) where genotyped females were relatively under-represented, and surveyors noted greater evidence of scavenging.

Of the 3,388 sampled parr, 1,326 (39.1%) were paired to a female adult, of which 595 (44.9%) were captured from mainstem sites and 731 (55.1%) from tributaries (Table D-1). At least one parr was assigned to 64 of the 67 females retained after genotyping, but apparent reproductive success was not uniform as just 16 females accounted for approximately 50% of the parr assigned to females (Figure D-S5).

Abundance estimates

Total parr abundance estimated across the MFJDR was 67,753 (95% CI = 63,365 – 73,750), with the mainstem accounting for nearly three-quarters of all parr (Table D-2). Among tributaries, total abundance estimates were greatest in Vinegar Creek, Granite Boulder Creek, and Clear Creek, accounting for 18.3% of total MFJDR basin abundance, whereas the other six tributaries individually accounted for less than 2% of total parr abundance.

The highest estimated densities within the mainstem occurred between rkms 91-96 and 100-106 (Figure D-2). These areas accounted for 28% of total redds observed in 2020 but 54% of total parr abundance (Figure 2), suggesting net immigration into this reach. In contrast, 35% of redds were observed downstream of rkm 90 and upstream of rkm 110, but we estimated that just 6.4% of all parr occupied these areas, which suggests net emigration or high rates of mortality. Consequently, the distribution of redds was not well associated with mainstem parr density ($p = 0.68$; Figure D-2B). Mainstem parr density was inversely related to July maximum temperature ($MDMT_{July}$; Figure D-2C,D).

Sampling-bias weights suggested that we under-sampled most mainstem sites and over-sampled most tributaries (Figure D-S6). The mean sampling-bias weight for parr sampled from the mainstem was 1.47, indicating approximately 50% more parr should have been sampled given our total sample size. In contrast, the mean sampling-bias weight for parr captured in tributaries was 0.51 (range: 0.21 – 1.89), indicating that we should have sampled around half as many parr.

Overall dispersal

Parr dispersal was downstream-biased (median = -0.77 km) and we estimated that 68% of parr dispersed downstream (Figure D-3A). Dispersal estimates varied widely (95% range: -14.9 – 6.2 km) and we estimated that 25% of parr dispersed farther than 3.7 km downstream and 25% dispersed at least 0.9 km upstream. Dispersal patterns differed for parr captured within the mainstem vs. tributaries (Figure D-3B,C): mainstem-captured parr exhibited downstream-bias (median = -1.43 km; 78% dispersed downstream) whereas dispersal was upstream biased for tributary-captured parr (median = 0.67 km; 57% dispersed upstream). The median estimated distance parr moved (regardless of direction) was 2.19 km and 25% of parr moved farther than 5.0 km (Figure D-3,D-F). Parr that dispersed downstream generally moved greater distances (inter-quartile range (IQR): 0.7 – 6.0 km; max = 28.6 km) than parr that moved upstream (IQR: 1.1 – 3.5 km; max = 10.6 km).

Spatial patterns of dispersal

Parr dispersal patterns varied as a function of where they originated (i.e., redd rkm) and dispersed to (i.e., mainstem vs. tributaries; Figure D-4). For parr that dispersed to mainstem locations (Figure D-4A), individuals originating low in the watershed (rkm < 90) exhibited upstream dispersal bias and low variability in dispersal estimates. Dispersal progressively transitioned towards downstream bias higher in the watershed, which was accompanied by increasing dispersal variance and range. In contrast, there was little apparent trend between parr origin and dispersal bias or distance for parr that dispersed to tributaries (Figure D-4B).

Dispersal patterns generally followed a trend of dispersal from warmer sections of the mainstem to slightly cooler sections or tributaries (Figure D-5; Figure D-6), which complements patterns between redds, parr distribution, and temperature (Figure D-2). For example, parr originating from rkms 84-89, where $MDMT_{July}$ exceeded 24.5 °C, either dispersed upstream to cooler mainstem habitats between rkms 91-97 ($MDMT_{July}$ < 23 °C) or to one of four tributaries between rkms 79.8 - 96.4 (Figure D-5) where $MDMT_{July}$ ranged from 17.5 to 23.1 °C near confluences with the mainstem and likely cooler farther upstream. This is further exemplified by the negative relationship between individual parr origin $MDMT_{July}$ and the difference between capture and origin $MDMT_{July}$ (Figure D-6B); there was little difference between capture and origin temperature for parr originating from areas where $MDMT_{July}$ was 23 °C or lower, but for parr originating from sections exceeding 23 °C, $MDMT_{July}$ averaged 2.5 °C lower at capture locations.

Insights on where juveniles originated for a given section can also be gleaned from Figure D-5. For example, the section between rkms 91-97 supported parr originating from nearly all parts of the watershed, whereas sections upstream only supported parr originating from nearby. Similarly, some tributaries such as Granite Boulder (rkm 95.1) supported parr originating across a wide spatial extent, whereas upstream tributaries supported parr from within several kilometers.

Post-dispersal size

The best model predicting parr length-at-capture across the MFJDR indicated that the effect of dispersal distance was dependent on dispersal direction (upstream vs. downstream) and location (mainstem vs. tributaries; Figure D-7A; Table D-S1). Dispersal distance was associated with longer length-at-capture for parr that dispersed downstream, and the effect was greater for parr that dispersed within the mainstem (0.30 mm km^{-1}; 95% CI: 0.22 - 0.39; $p < 0.001$) versus into tributaries (0.11 mm km^{-1}; 95% CI: 0.00 - 0.23; $p = 0.056$). In contrast, there was little trend between upstream dispersal distance and post-dispersal length for

parr that dispersed within the mainstem (-0.04 mm km^{-1}; 95% CI = -0.31 - 0.21; p = 0.727), but a negative relationship associated with dispersal to tributaries (-0.24 mm km^{-1}; 95% CI = -0.50 - 0.03; p = 0.077). Independent of dispersal, parr were predicted to average 6.2 mm longer when captured in the mainstem versus tributaries (95% CI = 4.97 - 7.75; $p < 0.001$), but that the additive effect of upstream versus downstream dispersal was minimal (95% CI = -0.59 – 1.20 mm). Parr length-at-capture was also spatially structured (Figure D-7B), exhibiting a parabolic pattern with nearly a 10 mm difference between parr originating farthest upstream (rkm 114) compared to middle sections (rkms 90-100) where predicted lengths were shortest. Later sampling dates (0.09 mm day^{-1}; 95% CI = 0.06 - 0.12; $p < 0.001$) and higher parr densities (0.22 mm parr m^{-1}; 95% CI = 0.06 - 0.38; $p = 0.007$) were associated with longer length-at-capture, whereas warmer maximum temperatures ($MDMT_{July}$) were associated with decreasing length (-1.09 mm °C; 95% CI = -1.38 - -0.80; $p < 0.001$; Figure D-S8). Collectively, the model fixed-effects explained 38% of the variation in length-at-capture and 65% with the random effect of unique female parent.

Discussion

Overall findings

We used genetic PBT to directly quantify wild juvenile Chinook Salmon dispersal from their origin to summer rearing habitats throughout the MFJD riverscape. Fish dispersed considerable distances (median = 2.19 km, max = 28.6 km), moving not only up or down the mainstem, but also into tributaries. We documented more extensive dispersal compared to prior studies conducted at smaller spatial scales or in experimental settings (see review by Eisenhauer et al. 2021). This suggests dispersal in wild populations may be higher in magnitude than currently recognized (Gerking 1959, Gowan et al. 1994, Rodriguez 2002), and (by extension) that the spatial configuration of spawning and rearing habitat is less constraining than previously thought. We found clear patterns in dispersal explained by initial landscape position and water temperature. Fish originating upstream tended to move downstream and vice versa. Nested within that broader pattern, fish responded to reach-level thermal heterogeneity, such that if they originated in reaches that became warmer during summer, they tended to disperse to cooler mainstem reaches or tributaries. This is a novel example of adaptive capacity (Beever et al. 2016) analogous to salmonids that spawn in ephemeral streams and disperse to perennial mainstems (Everest 1973). Lastly, our results suggest that broad patterns in biophysical processes across the riverscape – spatial structuring of emergence timing in this case – may shape the competitive advantages of dispersal strategies. In the MFJDR, emergence timing is progressively earlier upstream due to contributions of warmer groundwater in winter (Kaylor et al. 2022). Individuals that disperse downstream should have competitive advantages (i.e., size and dominance hierarchies) over later emerging conspecifics, whereas upstream dispersal should be competitively disadvantageous, which was supported by a positive effect of dispersal distance on parr length-at-capture for downstream dispersal but not for upstream dispersal. Collectively, this study provides an approach to effectively evaluate riverscape patterns and drivers of juvenile salmonid dispersal in naturally spawning populations that can be applied to other river systems, species, and life-stages.

Thermal conditions

Chinook parr dispersed from warmer sections of the river to cooler sections or into tributaries (e.g., Figure D-5, Figure D-6). Fish originating from areas in the MFJDR where $MDMT_{July}$ exceeded 23°C were captured as parr in areas that averaged 2.5 °C cooler, suggesting temperature is one of the mechanisms driving dispersal. The low thermal tolerance of the embryonic life stage (Dahlke et al. 2020) implies that spawning habitat should be cooler than rearing habitat, but spring Chinook salmon spawning, and thus the onset of

incubation, occurs after the warmest period of the year and lasts throughout winter. We found the highest densities of Chinook parr in the MFJDR downstream of tributary confluences or within the tributaries themselves. Previous studies have found that tributaries and their confluences are thermal refuges for salmonids (Sutton et al. 2007, Brewitt and Danner 2014, Wang et al. 2020) as tributaries often have greater groundwater inputs and shade (Dralle et al. 2018) compared to mainstem river channels. These thermal refuges allow salmonids to endure in river systems where many areas become thermally unsuitable during summer months (Wang et al. 2020). Our parr sampling in the summer of 2021 occurred as the Pacific Northwest experienced a record-breaking heat dome (White et al. 2023), possibly amplifying dispersal behavior from warmer to cooler habitats within the MFJDR and into tributaries. The climate conditions experienced in 2021 are predicted to increase in frequency and intensity (Fischer 2021, White et al. 2023), and dispersal may become increasingly necessary for warmer sections of this watershed and others to remain productive spawning and early rearing habitats. If thermal refuges are limited, density-dependent factors could limit growth and survival in these areas (Einum et al. 2006). Understanding patterns and drivers of dispersal and habitat use provides critical information to guide conservation and restoration efforts to ensure population viability and recovery.

Overall dispersal

Despite extensive research on fish spatial ecology, early life histories have been understudied because these individuals are too small to track using conventional tagging approaches (e.g., telemetry tags, PIT tags). By applying genetic parentage analysis to parr sampled across the spawning and rearing extent, our study provides a novel assessment of the full range of dispersal patterns expressed by a wild population of juvenile Chinook Salmon. Our results do not conform with the Restricted Movement Paradigm (Gowan et al. 1994) or the binary concept of "movers" and "stayers" (Rodriguez 2002), but instead suggest a continuum of overall mobility during this nonmigratory period of freshwater rearing. In a review of published estimates of juvenile Atlantic salmon dispersal, Eisenhauer et al. (2021) found that dispersal was generally downstream-biased and that nearly all individuals dispersed less than 500 m; however, the authors also presented original empirical results from 19 tributaries, in which a third of fish moved upstream and dispersal distances were more variable, with higher maximums (~3 km upstream and ~5 km downstream. Our results similarly suggest that approximately a third of individuals dispersed upstream, but that dispersal distance was even greater (~28 km downstream and ~11 km upstream). Further, there was no evidence of distinct groups of mobile and stationary individuals – characterized by a bimodal distribution (Rodriguez 2002). The expression of mobile and stationary groups may occur in other populations, species, and life-stages due to differences in genetic predisposition, environmental conditions, or biological factors such as variability in intra-specific competition. Alternatively, incomplete or biased sampling in previous studies could artificially generate bimodal distributions not characteristic of a random sample of the population.

Longitudinal dispersal patterns

Parr originating higher in the watershed exhibited greater variability in dispersal than parr originating lower in the basin. Prior studies suggest high variation in dispersal patterns are characteristic responses to variability in biophysical conditions and behavioral selection specific to localized watershed characteristics. For example, previous research has demonstrated extensive dispersal patterns of recently emerged salmon fry (10s or 100s of kilometers) associated with alternative early life-history strategies (Bradford and Taylor 1997, Daum and Flannery 2011, Schroeder et al. 2016, Scheu 2022). Within the MFJDR, variable dispersal may be attributed to several potential factors. First, progressively earlier emergence timing with distance upstream translated to fry being exposed to high flows for longer durations in this snowmelt-dominated

system (Figure D-S2), which by extension, could result in greater passive downstream dispersal. Alternatively, the longer duration since emergence and larger size of parr upstream suggests that differences in ontogeny could have been a contributing factor to greater dispersal variability. Larger individuals often disperse farther than smaller conspecifics (Anderson et al. 2013, Aparicio et al. 2018) and variability in dispersal may increase in later life stages (Yamamoto et al. 2021) as density-dependence exerts greater influence on dispersal (Einum et al. 2006). These patterns could also be attributed to the directional flow of river networks interacting with environmental conditions that contracted the juvenile rearing distribution. High summer temperatures were clearly a factor influencing dispersal and ultimately parr distribution. However, parr from upstream locations could move downstream with the flow to cooler habitats (e.g., tributary junctions), whereas parr originating downstream needed to move upstream against the current to find more thermally suitable habitat, thereby incurring higher energetic costs of movement. Lastly, dispersal was constrained by the extent of suitable rearing habitat, such that most available suitable habitat was downstream for upstream-originating fish, whereas downstream-originating fish experienced the opposite. This phenomenon of fish being "hemmed in" by thermal boundaries should theoretically occur when unfavorable offspring rearing conditions contract the extent of suitable rearing habitats from the initial spawning extent, whereas the opposite effect may manifest when adult spawners experience less favorable conditions than their offspring, causing expansion of the rearing extent. Across riverscapes, the conditions experienced across the parent-offspring life stages may be an important factor driving inter-annual variability in dispersal patterns.

Post-dispersal size distribution of parr

After accounting for parr origin (and by extension emergence timing) and other factors expected to influence parr body size, dispersal distance was associated with longer length-at-capture for parr that dispersed downstream, but not upstream. Mid-summer size integrates growth prior to, during, and after dispersal; consequently, the degree to which these findings reflect effects of size-at-dispersal vs. post-dispersal growth is uncertain, but our data provide insights to evaluate several potential mechanisms. Most studies report positive relationships between both downstream and upstream dispersal distance and size-at-dispersal (Close and Anderson 1992, Anderson et al. 2013, Aparicio et al. 2018, Eisenhauer et al. 2021), which could result from greater swimming capacity of larger individuals or if farther dispersal is associated with more favorable growth conditions (e.g., lower densities, higher prey availability) increasing post-dispersal growth (Brunsdon et al. 2017). It is unlikely that greater swimming capacity of larger individuals would result in farther dispersal distances downstream but not upstream. Model selection indicated a positive effect of parr density on post-dispersal size, which opposes the expected negative effect with density-dependence. We propose that there was a competitive advantage for individuals dispersing downstream but not upstream, stemming from the longitudinal structuring of emergence timing in the MFJDR (progressively earlier upstream). Early emergence provides competitive advantages over later-emerging conspecifics including larger size and the establishment of dominant feeding positions through prior residency (Einum and Fleming 2000). Downstream dispersal should afford competitive advantages over later emerging conspecifics, and the advantage should increase with distance downstream. In contrast, it would be challenging for individuals that disperse upstream to establish a competitive advantage since habitat occupancy and feeding positions are more likely to be established by conspecifics that are larger on average. In other river systems in which emergence timing occurs progressively later upstream (Kaylor et al. 2022), we hypothesize that competitive advantages would flip, favoring upstream dispersal.

Sampling bias corrections

Correcting for sampling bias had considerable effects on interpretation of dispersal patterns in the MFJDR (Figure D-S7). For example, dispersal was not biased upstream or downstream using uncorrected dispersal estimates (median = -0.03 km; 50% dispersed in each direction), but when sampling-bias corrections were applied, the overall dispersal distribution was clearly downstream-biased (median = -0.77 km; 68% dispersed downstream). This highlights the importance of obtaining a random sample of the population (Wacker et al. 2021) , or correcting for any sample biases, when quantifying dispersal. While it is ideal to minimize sampling bias through careful study design, if possible, we believe our approach effectively reduced sampling bias and improved characterization of population-level dispersal. If characterizing parr distribution is not a study objective, an alternative approach with fewer logistical challenges would be to conduct equal-effort sampling and genotyping of all (or a consistent proportion) juveniles captured at randomly selected habitats across the rearing extent.

Study considerations

We did not sample parr or conduct abundance surveys in the mainstem or tributaries downstream of Camp Creek, and consequently, our results may not reflect the full extent of dispersal and distribution present within this population. However, few age-0 juveniles from the MFJDR are captured in a downstream screw trap, and downstream rearing is not thought to be a common life history (Ian Tattam; unpublished data). Consequently, we hypothesize that parr dispersal outside of our study area likely had minimal effects on overall dispersal patterns at the population-level. Second, it is important to note that our dispersal estimates only represent individuals that survived to summer and that our approach defines dispersal based on two points in time. Sampling earlier in the year may have revealed different patterns, such as greater downstream bias associated with passive dispersal of recently emerged fry exposed to high flows (Saltveit et al. 1995). It is likely that some individuals passively dispersed downstream and later moved upstream (Yamamoto et al. 2021), but our sampling approach would not detect these patterns. Lastly, the early summer of 2021 was characterized by abnormally high air and water temperatures and low discharge. The dispersal patterns we observed, especially the effect of summer temperature on dispersal and parr distribution, likely differ considerably in cooler years with greater summer baseflow. On the other hand, the conditions were representative of those anticipated under climate change and our results provide insight into fish movement responses and the habitat attributes and locations that are likely to become increasingly important.

Conclusions

In a dendritic watershed, the majority of spring Chinook Salmon parr that survived to mid-summer (73%) occupied habitats within the mainstem river where nearly all spawning had occurred. Dispersal was widespread within the mainstem and into the tributaries, occurring in both downstream and upstream directions. Our results suggest that immigration into tributaries was driven primarily by behavioral thermoregulation. While tributaries to the MFJDR function as important summer thermal refuge, aggregation of parr in the tributaries could have density-dependent effects on growth and survival. Cooler sections of the mainstem – much of which have been the target of extensive restoration – supported the highest parr abundances, and downstream sections hosted parr originating from the broadest range of spawning locations whereas parr inhabiting upstream sections originated from a narrower spatial extent. This suggests that restoration of thermally tolerable habitat in these lower mainstem reaches will benefit parr from throughout the watershed and may be critical to maintain downstream sections as productive spawning habitats. Collectively, these observations suggest that improvement and downstream expansion

of suitable rearing habitat in the mainstem of the MFJDR and similar rivers in the interior Columbia River Basin will be required to reach biological and sociological recovery thresholds.

Acknowledgements

Implementing this study would not have been possible without the contributions of numerous agencies and individuals who aided in field efforts, planning, providing data, and interpreting results. Spawning surveys were conducted by ODFW, CTWSRO, the North Fork and South Fork John Day Watershed Councils, the U.S. Forest Service, and volunteers from numerous other agencies. We especially thank C. Bare for efforts to coordinate spawning surveys and modify protocols to accommodate this study. We thank the numerous individuals who assisted in juvenile fish sampling including, but not limited to J. Bailey, L. Blackburn, E. Booher, M. Cottingham, Z. Cunningham, H. Latzo, T. Sparrow, L. Osborne, C. Sheen, and A. Woolen. Additional logistical and planning support was provided by the MFIMW, particularly E. Booher and K. Bliesner. Genotyping was supported in the laboratory by E. Collins, L. Maxwell, and M. Moore and genotyping analyses were supported by E. Collins. J. Hetfield, L. Ulrich, K. Hammett, R. Trujillo, and J. Newsted provided instrumental motivation and creative inspiration during manuscript preparation. This research was supported by Bonneville Power Administration (BPA) funds as part of the Columbia Basin Fish Accords Agreement (project numbers 2009-004-00 & 2007-397-00), BPA funds administered to ODFW (project 1998-016-00), Pacific States Marine Fisheries Commission funds administered by the Oregon Watershed Enhancement Board, State of Oregon General funds, and the Bureau of Reclamation (adult salmon genotyping costs).

References

Aikens, E. O., M. J. Kauffman, J. A. Merkle, S. P. H. Dwinnell, G. L. Fralick, and K. L. Monteith. 2017. The greenscape shapes surfing of resource waves in a large migratory herbivore. Ecology Letters 20:741–750.

Anderson, E. C. 2020. CKMRsim: Inference of pairwise relationships using likelihood ratios. R package version 0.1.2.999.

Anderson, J. H., G. R. Pess, P. M. Kiffney, T. R. Bennett, P. L. Faulds, W. I. Atlas, and T. P. Quinn. 2013. Dispersal and tributary immigration by juvenile coho salmon contribute to spatial expansion during colonisation. Ecology of Freshwater Fish 22:30–42.

Aparicio, E., R. Rocaspana, A. De Sostoa, A. Palau-Ibars, and C. Alcaraz. 2018. Movements and dispersal of brown trout (*Salmo trutta* Linnaeus, 1758) in Mediterranean streams: influence of habitat and biotic factors. PeerJ 6:e5730.

Armstrong, J. B., D. E. Schindler, K. L. Omori, C. P. Ruff, and T. P. Quinn. 2010. Thermal heterogeneity mediates the effects of pulsed subsidies across a landscape. Ecology 91:1445–1454.

Atlas, W. I., T. W. Buehrens, D. J. F. McCubbing, R. Bison, and J. W. Moore. 2015. Implications of spatial contraction for density dependence and conservation in a depressed population of anadromous fish. Canadian Journal of Fisheries and Aquatic Sciences 72:1682–1693.

Baldock, J. R., J. B. Armstrong, D. E. Schindler, and J. L. Carter. 2016. Juvenile coho salmon track a seasonally shifting thermal mosaic across a river floodplain. Freshwater Biology 61:1454–1465.

Bare, C. M., I. A. Tattam, and J. R. Ruzycki. 2021. Chinook Salmon Productivity and Escapement Monitoring in the John Day River Basin. Oregon Department of Fish and Wildlife, John Day, OR.

Beechie, T., H. Moir, and G. Pess. 2008. Hierarchical Physical Controls on Salmonid Spawning Location and Timing. American Fisheries Society Symposium 65:83–101.

Beever, E. A., J. O'Leary, C. Mengelt, J. M. West, S. Julius, N. Green, D. Magness, L. Petes, B. Stein, A. B. Nicotra, J. J. Hellmann, A. L. Robertson, M. D. Staudinger, A. A. Rosenberg, E. Babij, J. Brennan, G. W. Schuurman, and G. E. Hofmann. 2016. Improving conservation outcomes with a new paradigm for understanding species' fundamental and realized adaptive capacity. Conservation Letters 9:131–137.

Bradford, M. J., and G. C. Taylor. 1997. Individual variation in dispersal behaviour of newly emerged chinook salmon (Oncorhynchus tshawytscha) from the Upper Fraser River, British Columbia. Canadian Journal of Fisheries and Aquatic Sciences 54:1585–1592.

Bravington, M. V., H. J. Skaug, and E. C. Anderson. 2016. Close-Kin Mark-Recapture. Statistical Science 31.

Brewitt, K. S., and E. M. Danner. 2014. Spatio-temporal temperature variation influences juvenile steelhead (*Oncorhynchus mykiss*) use of thermal refuges. Ecosphere 5:1–26.

Brooks, M., K. Kristensen, J. van Benthem, A. Magnusson, C. Berg, A. Nielsen, H. Skaug, M. Mächler, and B. Bolker. 2017. glmmTMB balances speed and flexibility among packages for zero-inflated generalized linear mixed modeling. The R Journal 9:378–400.

Brunsdon, E. B., D. J. Fraser, W. R. Ardren, and J. W. A. Grant. 2017. Dispersal and density-dependent growth of Atlantic salmon (*Salmo salar*) juveniles: clumped versus dispersed stocking. Canadian Journal of Fisheries and Aquatic Sciences 74:1337–1347.

Burnham, K. P., and D. R. Anderson. 2004. Multimodel Inference: Understanding AIC and BIC in Model Selection. Sociological Methods & Research 33:261–304.

Campbell, N. R., S. A. Harmon, and S. R. Narum. 2015. Genotyping-in-Thousands by sequencing (GT-seq): A cost effective SNP genotyping method based on custom amplicon sequencing. Molecular Ecology Resources 15:855–867.

Carmichael, R. W., and B. J. Taylor. 2010. Conservation and recovery plan for oregon steelhead populations in the middle columbia river steelhead distinct population segment. Oregon Department of Fish and Wildlife, Salem, OR.

CBPTF, (Columbia Basin Partnership Task Force). 2020. A vision for salmon and steelhead: goals to restore thriving salmon and steelhead to the columbia river basin.

Close, T. L., and C. S. Anderson. 1992. Dispersal, density-dependent growth, and survival of stocked steelhead fry in Lake Superior tributaries. North American Journal of Fisheries Management 12:728–735.

Copeland, T., and D. A. Venditti. 2009. Contribution of three life history types to smolt production in a Chinook salmon (Oncorhynchus tshawytscha) population. Canadian Journal of Fisheries and Aquatic Sciences 66:1658–1665.

Dahlke, F. T., S. Wohlrab, M. Butzin, and H.-O. Pörtner. 2020. Thermal bottlenecks in the life cycle define climate vulnerability of fish. Science 369:65–70.

Daum, D. W., and B. G. Flannery. 2011. Canadian-Origin Chinook Salmon Rearing in Nonnatal U.S. Tributary Streams of the Yukon River, Alaska. Transactions of the American Fisheries Society 140:207–220.

Dormann, C. F., J. Elith, S. Bacher, C. Buchmann, G. Carl, G. Carré, J. R. G. Marquéz, B. Gruber, B. Lafourcade, P. J. Leitão, T. Münkemüller, C. McClean, P. E. Osborne, B. Reineking, B. Schröder, A. K. Skidmore, D. Zurell, and S. Lautenbach. 2013. Collinearity: a review of methods to deal with it and a simulation study evaluating their performance. Ecography 36:27–46.

Dralle, D. N., W. J. Hahm, D. M. Rempe, N. J. Karst, S. E. Thompson, and W. E. Dietrich. 2018. Quantification of the seasonal hillslope water storage that does not drive streamflow. Hydrological Processes 32:1978–1992.

Ebersole, J. L., P. J. Wigington, J. P. Baker, M. A. Cairns, M. R. Church, B. P. Hansen, B. A. Miller, H. R. LaVigne, J. E. Compton, and S. G. Leibowitz. 2006. Juvenile Coho salmon growth and survival across stream network seasonal habitats. Transactions of the American Fisheries Society 135:1681–1697.

Einum, S., and I. A. Fleming. 2000. Selection against late emergence and small offspring in Atlantic salmon (*Salmo salar*). Evolution 54:628–639.

Einum, S., and K. H. Nislow. 2005. Local-scale density-dependent survival of mobile organisms in continuous habitats: an experimental test using Atlantic salmon. Oecologia 143:203–210.

Einum, S., K. H. Nislow, S. Mckelvey, and J. D. Armstrong. 2008. Nest distribution shaping within-stream variation in Atlantic salmon juvenile abundance and competition over small spatial scales. Journal of Animal Ecology 77:167–172.

Einum, S., G. Robertsen, K. H. Nislow, S. McKelvey, and J. D. Armstrong. 2011. The spatial scale of density-dependent growth and implications for dispersal from nests in juvenile Atlantic salmon. Oecologia 165:959–969.

Einum, S., L. Sundt-Hansen, and K. H. Nislow. 2006. The partitioning of density-dependent dispersal, growth and survival throughout ontogeny in a highly fecund organism. Oikos 113:489–496.

Eisenhauer, Z. J., P. M. Christman, J.-M. Matte, W. R. Ardren, D. J. Fraser, and J. W. A. Grant. 2021. Revisiting the restricted movement paradigm: the dispersal of Atlantic salmon fry from artificial redds. Canadian Journal of Fisheries and Aquatic Sciences 78:493–503.

Elmore, R. D., J. M. Carroll, E. P. Tanner, T. J. Hovick, B. A. Grisham, S. D. Fuhlendorf, and S. K. Windels. 2017. Implications of the thermal environment for terrestrial wildlife management. Wildlife Society Bulletin 41:183–193.

Everest, F. H. 1973. Ecology and management of summer steelhead in the Rogue River - Fishery Research Report Number 7. Page 45. Oregon State Game Commission, Corvallis, OR.

Feden, M. J., and K. L. Bliesner. 2022. Water Temperature Monitoring Strategy for the Middle Fork John Day Intensively Monitored Watershed 2022-2023. Middle Fork John Day Water Temperature Monitoring Subgroup, John Day, Oregon.

Fischer, E. M. 2021. Increasing probability of record-shattering climate extremes. Nature Climate Change 11.

Flitcroft, R., K. Burnett, J. Snyder, G. Reeves, and L. Ganio. 2014. Riverscape Patterns among Years of Juvenile Coho Salmon in Midcoastal Oregon: Implications for Conservation. Transactions of the American Fisheries Society 143:26–38.

Foldvik, A., A. G. Finstad, and S. Einum. 2010. Relating juvenile spatial distribution to breeding patterns in anadromous salmonid populations. Journal of Animal Ecology 79:501–509.

Fullerton, A. H., C. E. Torgersen, J. J. Lawler, R. N. Faux, E. A. Steel, T. J. Beechie, J. L. Ebersole, and S. G. Leibowitz. 2015. Rethinking the longitudinal stream temperature paradigm: region-wide comparison of thermal infrared imagery reveals unexpected complexity of river temperatures: complexity in longitudinal thermal profiles within and among rivers. Hydrological Processes 29:4719–4737.

Gerking, S. D. 1959. The restricted movement of fish populations. Biological Reviews 34:221–242.

Gowan, C., M. K. Young, K. D. Fausch, and S. C. Riley. 1994. Restricted movement in resident stream salmonids: A paradigm lost? Canadian Journal of Fisheries and Aquatic Sciences 51:2626–2637.

Griffen, B. D., and A. P. Norelli. 2015. Spatially variable habitat quality contributes to within-population variation in reproductive success. Ecology and Evolution 5:1474–1483.

Hahlbeck, N., W. R. Tinniswood, M. R. Sloat, J. D. Ortega, M. A. Wyatt, M. E. Hereford, B. S. Ramirez, D. A. Crook, K. J. Anlauf-Dunn, and J. B. Armstrong. 2022. Contribution of warm habitat to cold-water fisheries. Conservation Biology 36.

Hess, J. E., R. L. Horn, J. Stephenson, S. Willis, and S. R. Narum. 2023. Genetic assessment of Columbia River Stocks, 1/1/2022 - 12/31/2022 Annual Report, 2008-907-00. Page 405. Columbia River Inter-Tribal Fish Commission, Portland, OR.

Kaylor, M. J., J. B. Armstrong, J. T. Lemanski, C. Justice, and S. M. White. 2022. Riverscape heterogeneity in estimated Chinook Salmon emergence phenology and implications for size and growth. Ecosphere 13.

Kaylor, M. J., C. Justice, J. B. Armstrong, B. A. Staton, L. A. Burns, E. Sedell, and S. M. White. 2021. Temperature, emergence phenology and consumption drive seasonal shifts in fish growth and production across riverscapes. Journal of Animal Ecology 90:1727–1741.

Lima, S. L., and P. A. Zollner. 1996. Towards a behavioral ecology of ecological landscapes. Trends in Ecology & Evolution 11:131–135.

Murdoch, A. R., T. N. Pearsons, and T. W. Maitland. 2009. Use of Carcass Recovery Data in Evaluating the Spawning Distribution and Timing of Spring Chinook Salmon in the Chiwawa River, Washington. North American Journal of Fisheries Management 29:1206–1213.

Quinn, T. P. 2007. The Behavior and Ecology of Pacific Salmon and Trout. University of British Columbia Press.

Rodriguez, M. A. 2002. Restricted movement in stream fish: The paradigm is incomplete, not lost. Ecology 83:1–13.

Saltveit, S. J., T. Bremnes, and O. R. Linda. 1995. Effect of sudden increase in discharge in a large river on newly emerged Atlantic salmon (*Salmo salar*) and brown trout (*Salmo trutta*) fry. Ecology of Freshwater Fish 4:168–174.

Scheu, M. P. 2022. Downstream rearing Chinook Salmon (*Oncorhynchus tshawytscha*) in the Upper Mainstem of the John Day River. Masters, Oregon State University, Corvallis, Oregon.

Schroeder, R. K., L. D. Whitman, B. Cannon, and P. Olmsted. 2016. Juvenile life-history diversity and population stability of spring Chinook salmon in the Willamette River basin, Oregon. Canadian Journal of Fisheries and Aquatic Sciences 73:921–934.

Stanford, J. A., M. S. Lorang, and F. R. Hauer. 2005. The shifting habitat mosaic of river ecosystems. SIL Proceedings, 1922-2010 29:123–136.

Staton, B. A., C. Justice, S. White, E. R. Sedell, L. A. Burns, and M. J. Kaylor. 2022. Accounting for uncertainty when estimating drivers of imperfect detection: An integrated approach illustrated with snorkel surveys for riverine fishes. Fisheries Research 249:106209.

Stevens, D. L., and A. R. Olsen. 2004. Spatially Balanced Sampling of Natural Resources. Journal of the American Statistical Association 99:262–278.

Sutton, R. J., M. L. Deas, S. K. Tanaka, T. Soto, and R. A. Corum. 2007. Salmonid observations at a Klamath River thermal refuge under various hydrological and meteorological conditions. River Research and Applications 23:775–785.

Teichert, M. A. K., A. Foldvik, T. Forseth, O. Ugedal, S. Einum, A. G. Finstad, R. D. Hedger, and E. Bellier. 2011. Effects of spawning distribution on juvenile Atlantic salmon (*Salmo salar*) density and growth. Canadian Journal of Fisheries and Aquatic Sciences 68:43–50.

Torgersen, C. E., C. V. Baxter, H. W. Li, and B. A. McIntosh. 2006. Landscape influences on longitudinal patterns of river fishes: Spatially continuous analysis of fish-habitat relationships. American Fisheries Society Symposium 48:473–492.

Torgersen, C. E., D. M. Price, H. W. Li, and B. A. McIntosh. 1999. Multiscale thermal refugia and stream habitat associations of chinook salmon in northeastern oregon. Ecological Applications 9:301–319.

Turlure, C., N. Schtickzelle, Q. Dubois, M. Baguette, R. L. H. Dennis, and H. Van Dyck. 2019. Suitability and Transferability of the Resource-Based Habitat Concept: A Test With an Assemblage of Butterflies. Frontiers in Ecology and Evolution 7:127.

Wacker, S., H. J. Skaug, T. Forseth, Ø. Solem, E. M. Ulvan, P. Fiske, and S. Karlsson. 2021. Considering sampling bias in close-kin mark–recapture abundance estimates of Atlantic salmon. Ecology and Evolution 11:3917–3932.

Wang, T., S. J. Kelson, G. Greer, S. E. Thompson, and S. M. Carlson. 2020. Tributary confluences are dynamic thermal refuges for a juvenile salmonid in a warming river network. River Research and Applications 36:1076–1086.

White, R. H., S. Anderson, J. F. Booth, G. Braich, C. Draeger, C. Fei, C. D. G. Harley, S. B. Henderson, M. Jakob, C.-A. Lau, L. Mareshet Admasu, V. Narinesingh, C. Rodell, E. Roocroft, K. R. Weinberger, and G. West. 2023. The unprecedented Pacific Northwest heatwave of June 2021. Nature Communications 14:727.

Yamamoto, T., S. Kitanishi, and N. B. Metcalfe. 2021. Effect of parental phenotype on dispersal, growth and maturation of offspring in wild masu salmon (*Oncorhynchus masou*). Evolutionary Ecology 35:253–269.

Yoshimoto, J. 2009. Interspecific variation in competitor avoidance and foraging success in sap-attracted insects. European Journal of Entomology 106:529–533.

Zabel, R. W., and S. Achord. 2004. Relating size of juveniles to survival within and among populations of chinook salmon. Ecology 85:795–806.

Tables and figures

Table D-1: Parr sampling details for the mainstem Middle Fork John Day River and tributaries. MDMT = mean daily maximum temperature.

					Parr sampling			
Stream	**Rkm**	**July Q (L s^{-1})**	**June MDMT (°C)**	**July MDMT (°C)**	**Dates sampled**	**Parr sampled (*n*)**	**Parr paired to female (*n*)**	**Mean fork length (mm)**
Mainstem	-	596.0	15.7-23.0	21.8-26.2	7/13-8/9	1,592	595	67.3
Camp Cr.	79.8	12.2	20.2	21.3	7/9	28	13	60.0
Big Bldr Cr.	88.1	70.9	17.0	23.1	7/1-7/2	184	93	57.7
Beaver Cr.	92.8	21.3	16.8	19.6	7/14	63	12	62.2
Granite Bldr Cr.	95.1	124.3	12.7	17.5	6/30-7/22	292	80	68.3
Butte Cr.	96.4	4.1	15.8	18.8	7/14-7/20	248	70	61.1
Dead Cow Gulch	108.3	-	19.0	19.0	7/8-7/9	182	93	62.3
Vinegar Cr.	110.0	-	16.3	21.4	6/29-7/22	399	172	59.6
Davis Cr.	110.7	-	19.0	23.3	7/6-7/8	200	115	62.2
Clear Cr.	112.8	132.4	18.8	20.7	7/7-7/22	200	83	65.8
Total	-	-	-	-	6/29-8/9	3,388	1,326	64.7

Table D-2: Abundance estimates for the mainstem Middle Fork John Day River and tributaries.

Stream	**Rkm**	**Method**	**$\hat{N}$**	**$\hat{N}$ 95% CI**	**% of total (95% CI)**	**Mean density (# m^{-1})**	**Max density (# m^{-1})**
Mainstem	80-116	snorkel	49,096	45,149 - 54,937	72.6 (69.9 -75.3)	1.27	4.85
Camp Cr.	79.8	shock	1,054	727 - 2,373	1.6 (1.1 - 3.4)	0.27	0.31
Big Bldr Cr.	88.1	snorkel	1,151	1,064 - 1,258	1.7 (1.5 - 1.9)	2.38	3.34
Beaver Cr.	92.8	shock	256	181 - 479	0.4 (0.3 - 0.7)	1.03	1.03
Granite Bldr Cr.	95.1	snorkel	4,254	3,323 - 5,813	6.3 (4.9 - 8.5)	5.16	11.37
Butte Cr.	96.4	shock	1,064	848 - 1,566	1.6 (1.3 - 2.3)	0.88	2.13
Dead Cow Gulch	108.3	shock	1,110	859 - 1,694	1.6 (1.3 - 2.4)	1.69	2.17
Vinegar Cr.	110.0	snorkel	4,643	4,400 - 4,981	6.9 (6.2 - 7.5)	1.53	2.96
Davis Cr.	110.7	shock	1,246	957 - 1,954	1.8 (1.4 - 2.9)	1.63	2.81
Clear Cr.	112.8	snorkel	3,485	3,052 - 4,025	5.1 (4.4 - 6.0)	2.11	4.12
Total	-		67,753*	63,365* - 73,750*	-	-	

*Total abundance and confidence intervals differ from the sum of stream abundances, as total abundance was estimated from 1000 samples in which each sample was the sum of abundance estimates across all reaches.

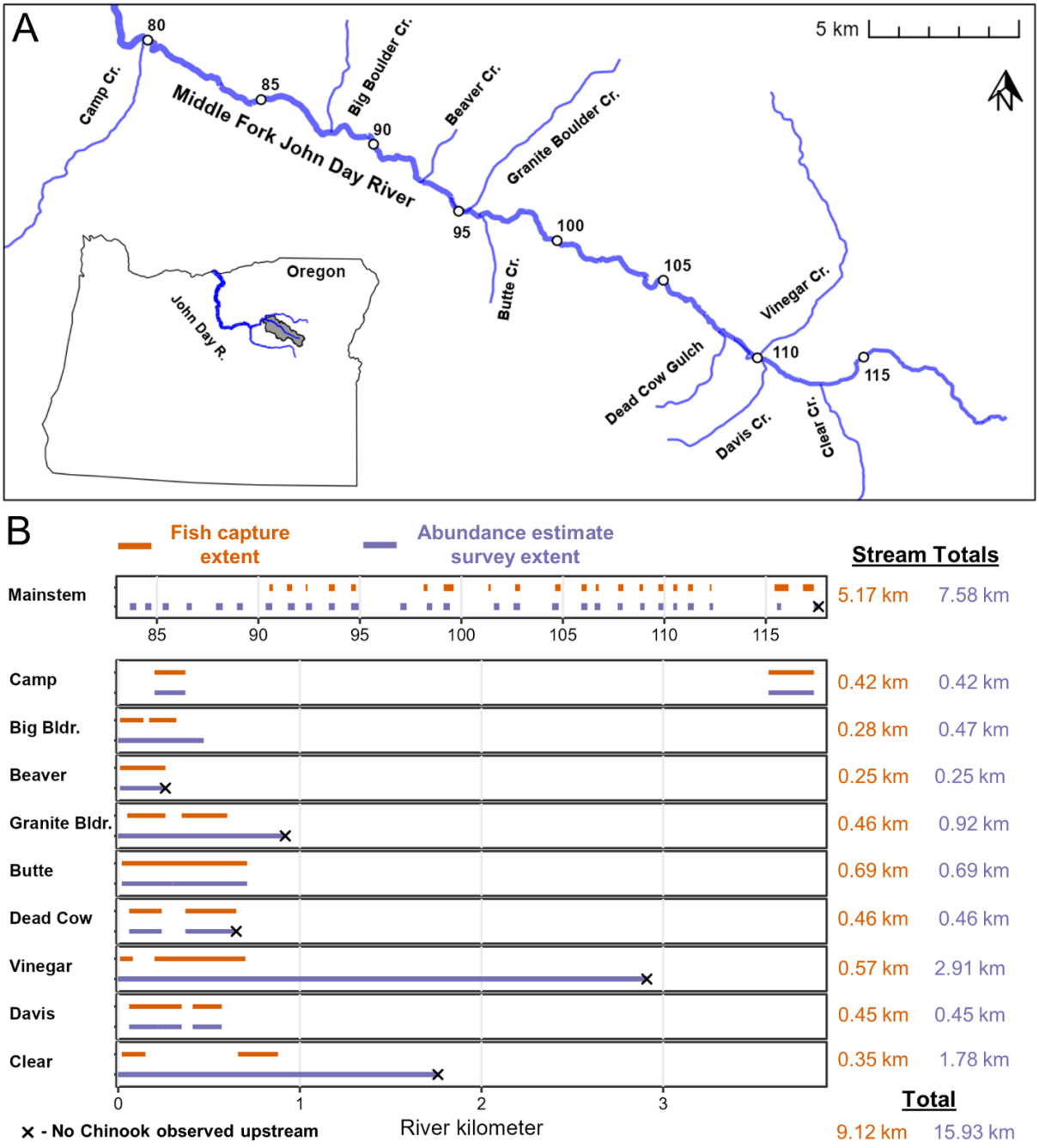

Figure D-1: (A) study extent across the mainstem MFJDR and nine sampled tributaries and (B) the extent of parr capture sampling (orange lines) and abundance estimate surveys (purple lines) within the mainstem and tributaries in summer 2021. Data from abundance surveys were used to estimate parr distribution across the MFJDR watershed and to assign sampling weights to captured parr. Open points in Panel A indicate river kilometers from the MFJDR mouth (5 km intervals) for reference in Panel B and subsequent figures. The total length of capture (orange) and abundance surveys (blue) within each stream is indicated in the right column of Panel B. Black x's indicate that no juvenile Chinook were observed upstream of this location for at least three successive pools, which we treated as the upstream extent of Chinook Salmon parr within each stream. The absence of a black x indicates that sampling did not occur upstream due to property access or other sampling constraints. Mainstem capture sampling was planned between rkm 80-90 but not conducted after snorkel surveys revealed that parr densities were too low to feasibly sample.

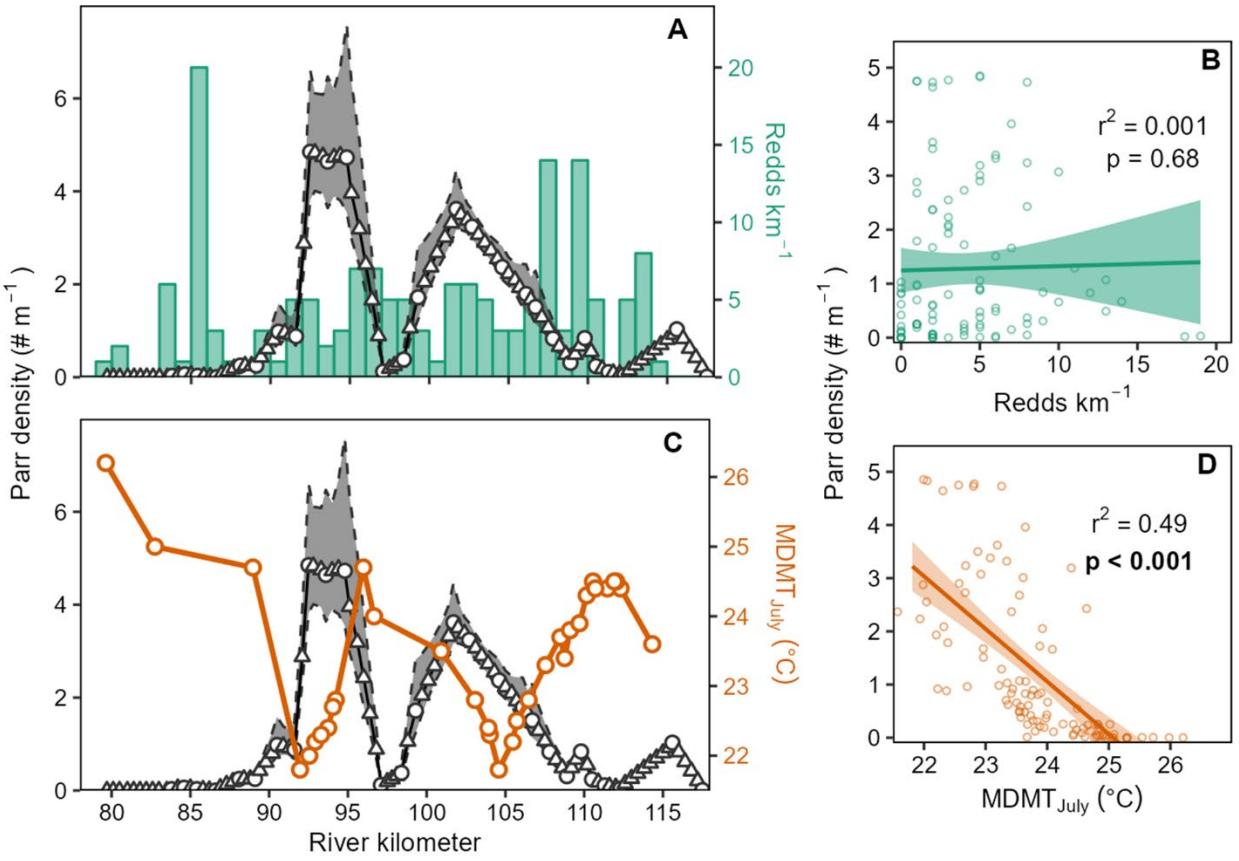

Figure D-2: (A) Spatial patterns of redds in 2020 (green bars) relative to the distribution of offspring (i.e., parr) in 2021 across the mainstem MFJDR, (B) the linear relationship between redd density and parr density, (C) the spatial patterns of July maximum temperature ($MDMT_{July}$; orange points and line) relative to parr density, and (D) the relationship between July maximum temperature and parr density. For density estimates, points represent snorkeled sites, triangles indicated prediction reaches, and grey shading between dashed lines show 95% confidence intervals.

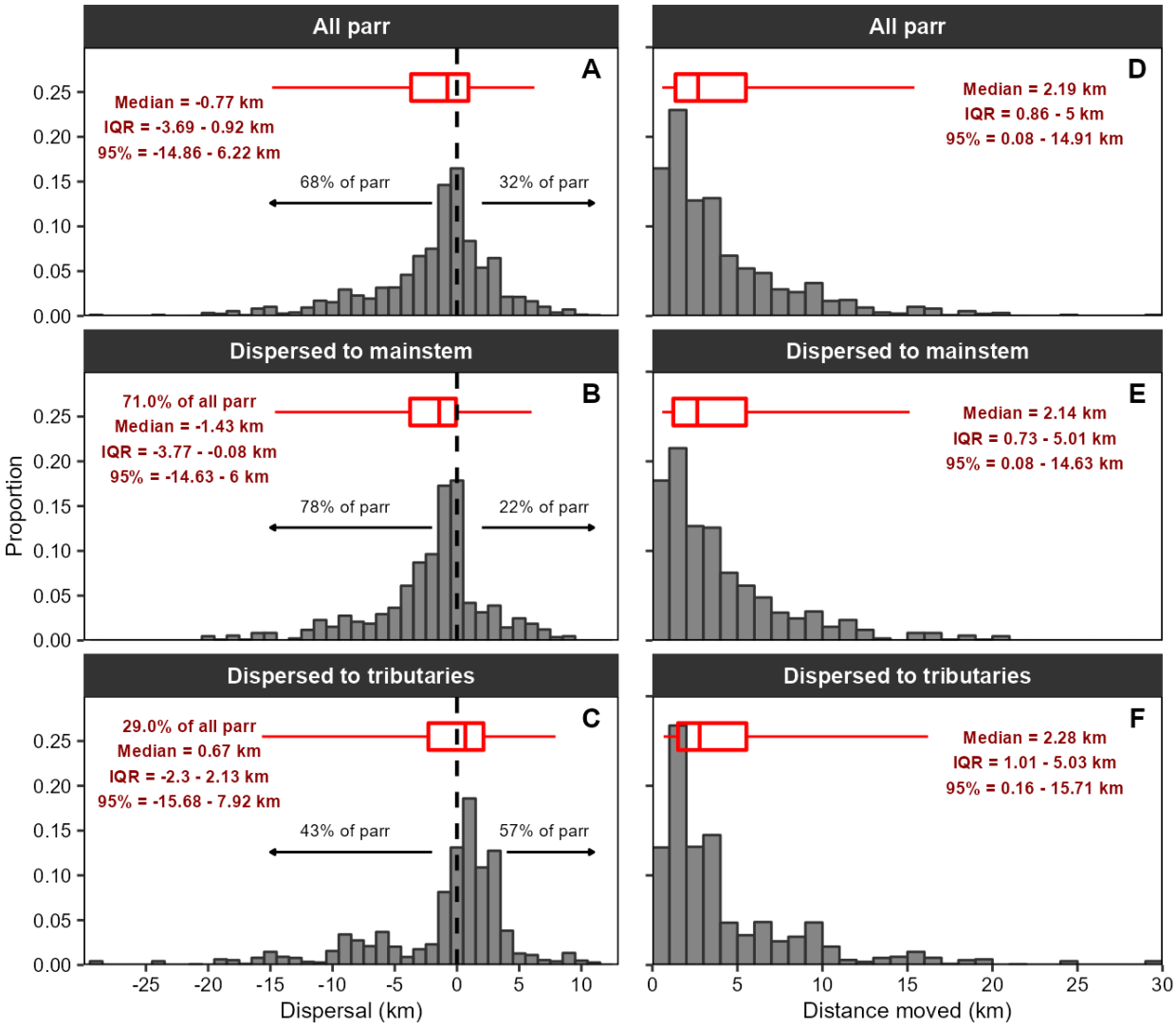

Figure D-3: (A-C) Overall distributions of sample-bias corrected dispersal and (D-F) total distance moved estimates. Box and whisker plots indicate median, inter-quartile range (IQR), and 95th percentiles.

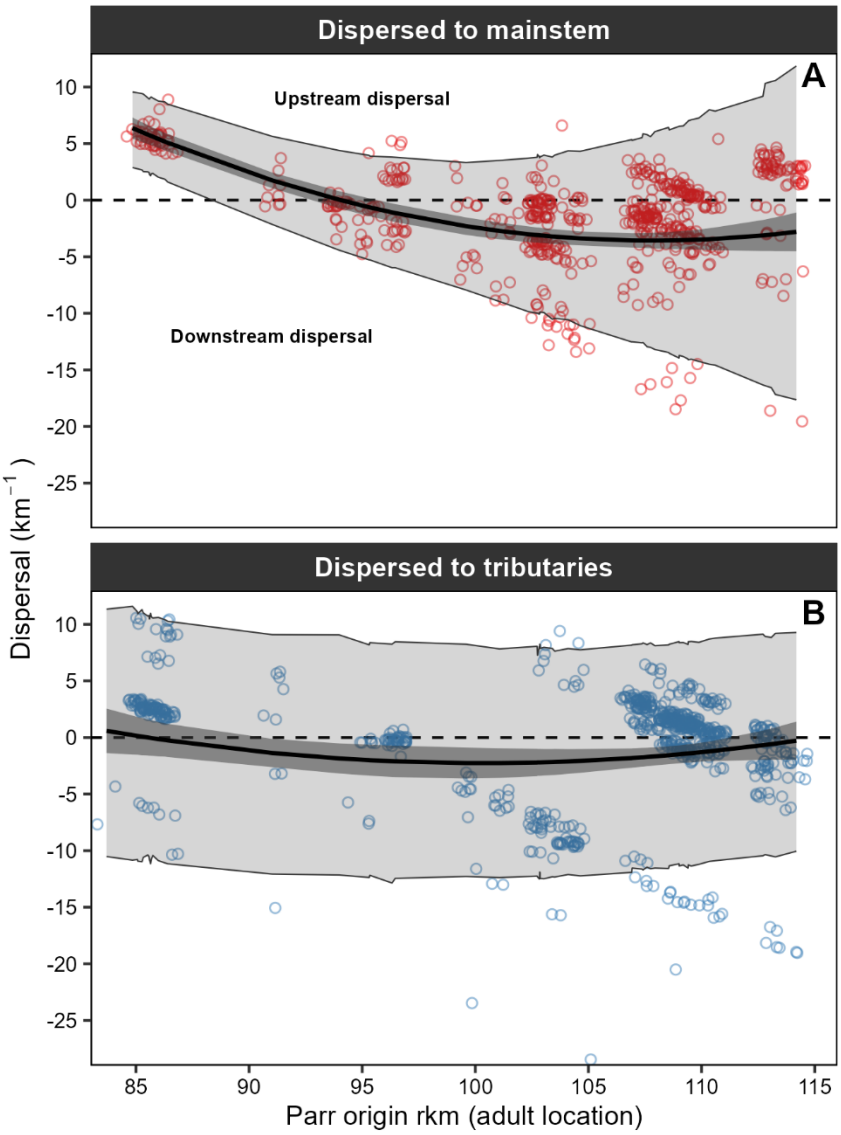

Figure D-4: (A) Parr origin (i.e., maternal parent location) versus dispersal for parr captured within the mainstem (red points) and (B) parr captured within tributaries (blue points). The apparent striation pattern in B is a result of captured parr distributing to, and then relatively small distances (0-1 km) within, spatially discrete and numerically fixed tributary confluences (n = 9). The solid line indicates the fitted relationship between parr origin and dispersal; dark shading indicates the 95% confidence interval of the fitted relationship; and the light shading indicates the 95% prediction interval.

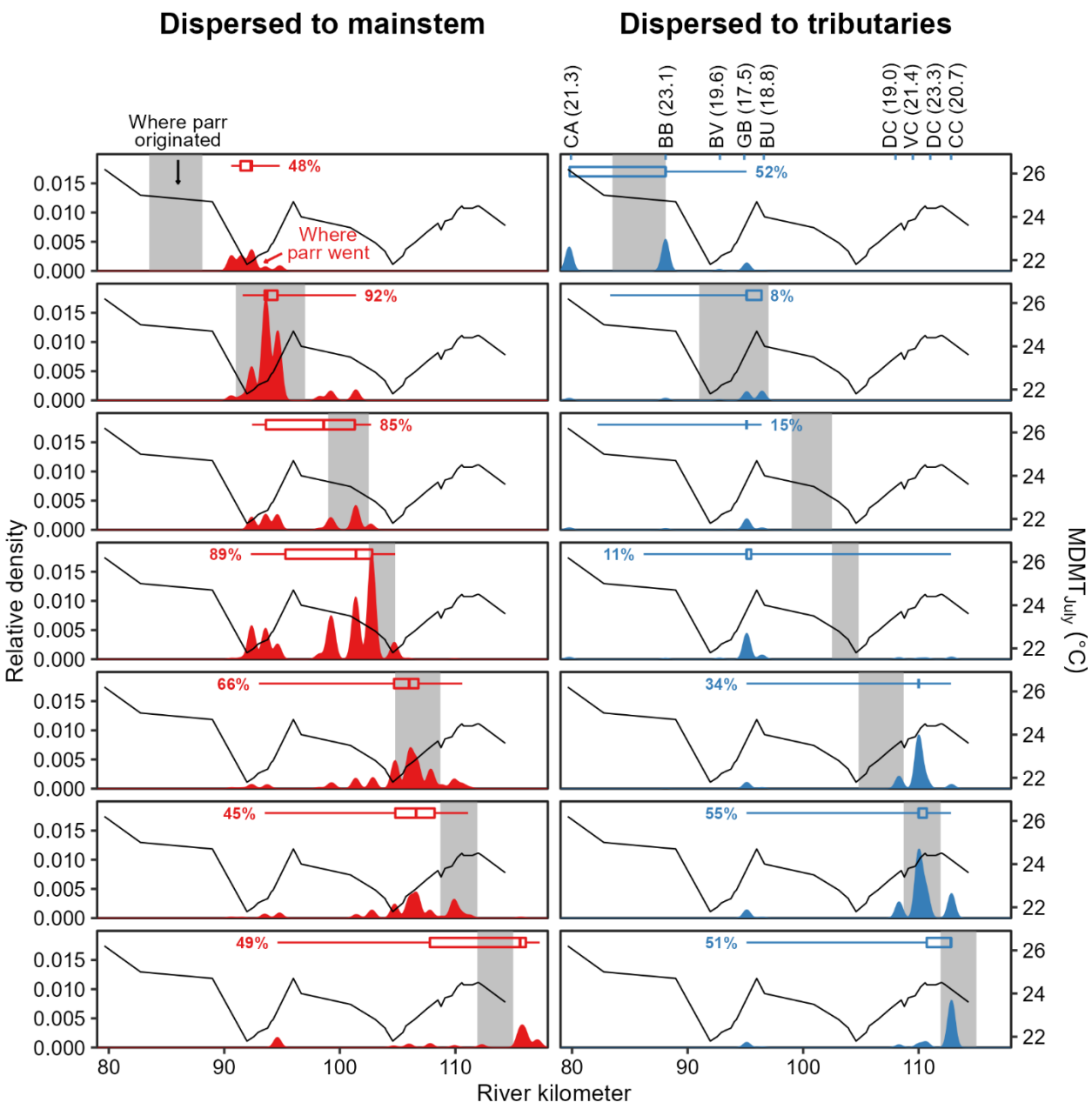

Figure D-5: Parr dispersal patterns from different sections of origin (rows). Grey boxes indicate the section parr originated from; density distributions portray where parr from each section dispersed to across the mainstem (red distributions) and to tributaries (blue distributions); box and whisker plots indicate median, inter-quartile range (IQR), and 95th percentiles of parr distributions for each section; percentages indicate the estimated percent of parr from that section that dispersed to mainstem locations (red) or into tributaries (blue); and the solid black line shows maximum temperature ($MDMT_{July}$) of the mainstem MFJD at that location. Tributary $MDMT_{July}$ are shown in the right panel in parentheses above tributary abbreviations: CA = Camp Creek, BB = Big Boulder Creek, BV = Beaver Creek, GB = Granite Boulder Creek, BU = Butte Creek, DC = Dead Cow Gulch, VC = Vinegar Creek, DC = Davis Creek, and CC = Clear Creek.

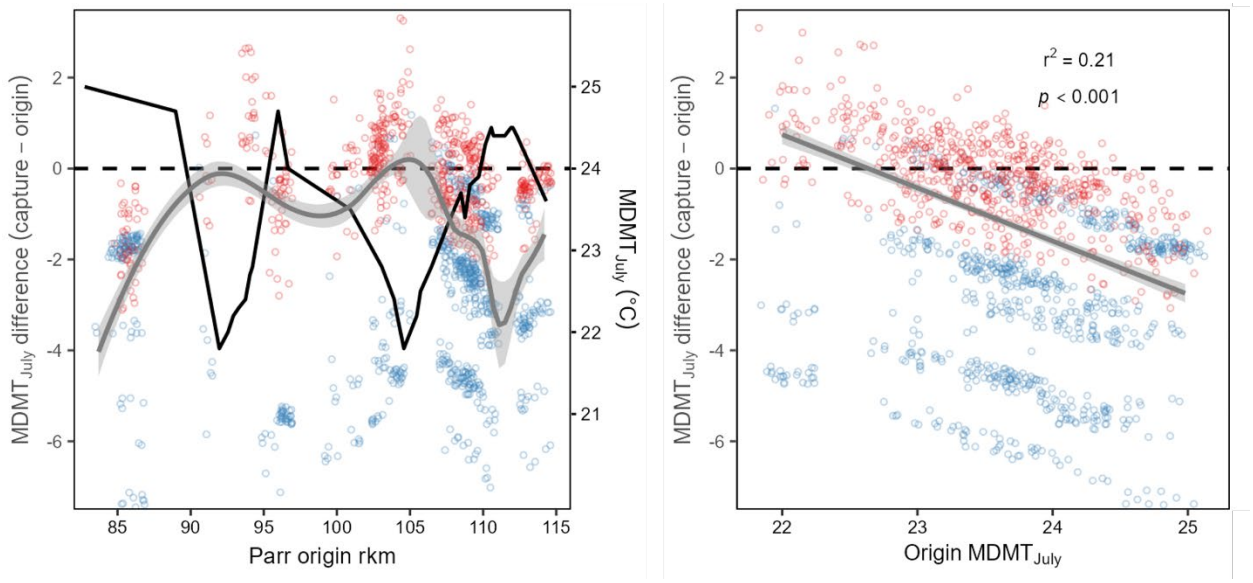

Figure D-6: (A) Stream temperature ($MDMT_{July}$; solid black line) and estimated differences in temperature between capture and origin locations for individual parr (points) across the MFJDR and (B) the relationship between parr origin temperature and the difference in temperature between capture and origin locations. The color of points indicates whether each individual parr was captured within the mainstem (red) or tributaries (blue). The solid grey line in panel A shows a LOESS fit. The figure highlights that parr originating in warmer areas tended to move to cooler areas.

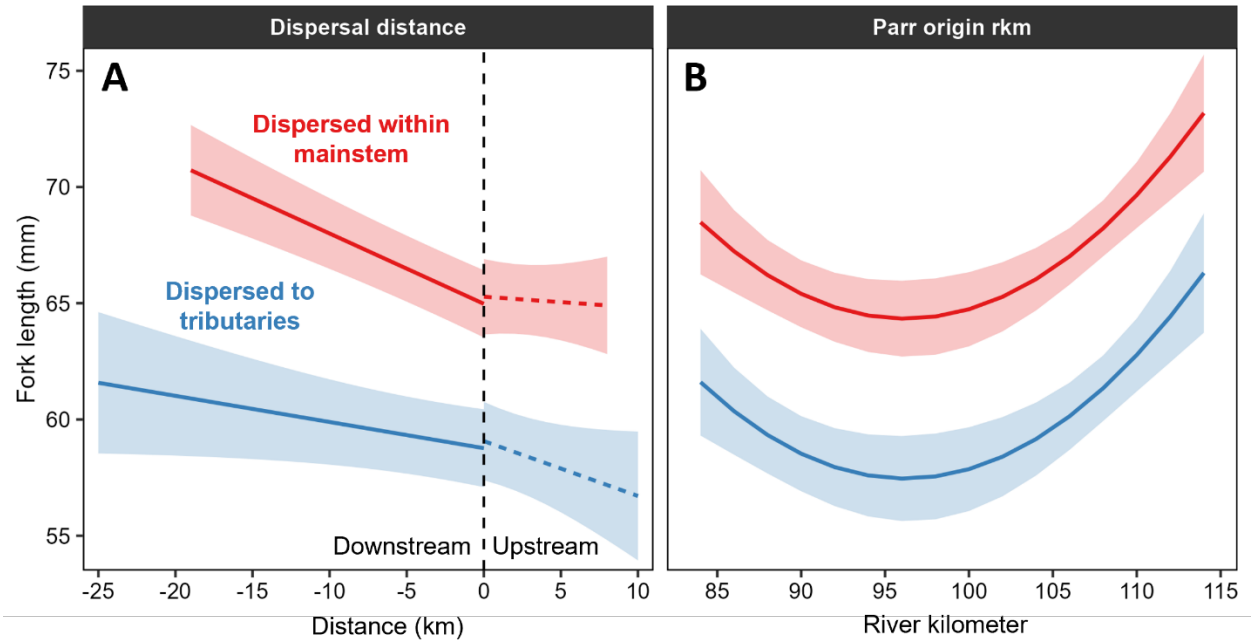

Figure D-7: Marginal effects of (A) dispersal distance and (B) parr origin river kilometer on post-dispersal parr fork length after accounting for effects of date of sampling, capture location temperature and capture location density (see Figure S8). Model selection indicated that the relationship between dispersal distance and fork length was dependent on whether parr dispersed within the mainstem (red) or to tributaries (blue) and whether parr dispersed downstream (solid line) or upstream (dashed line). Longitudinal patterns of parr size (B) are inversely related to estimated emergence timing, which was progressively earlier upstream of rkm 100 (Figure S2).

Supplemental Material

Table D-S1: General linear mixed-effects model results for the top supported model predicting parr length-at-capture. Origin rkm refers to the river kilometer parr originated from; Distance is the dispersal distance (km) regardless of upstream or downstream direction; Location refers to whether parr were captured within the mainstem or in tributaries (trib); Direction indicates whether parr dispersed upstream (up) or downstream; Max temp is the $MDMT_{July}$ (°C) of the reach parr were captured; Density is the estimated parr density (number m^{-1}) within the reach parr were captured; and Sampling date is the day of the calendar year parr were captured.

Term	Estimate	SE	z-value	p-value
Intercept	326.386	63.598	5.13	< 0.0001
Origin rkm	-5.367	1.306	-4.11	< 0.0001
Origin rkm^2	0.028	0.007	4.20	< 0.0001
Distance	0.302	0.044	6.87	< 0.0001
Location:trib	-6.210	0.631	-9.84	< 0.0001
Direction:up	0.304	0.457	0.67	0.506
Max temp	-1.091	0.146	-7.46	< 0.0001
Density	0.217	0.081	2.68	0.007
Sampling date	0.090	0.016	5.75	< 0.0001
Distance*Location:trib	-0.190	0.067	-2.85	0.004
Distance*Direction:up	-0.349	0.132	-2.65	0.008

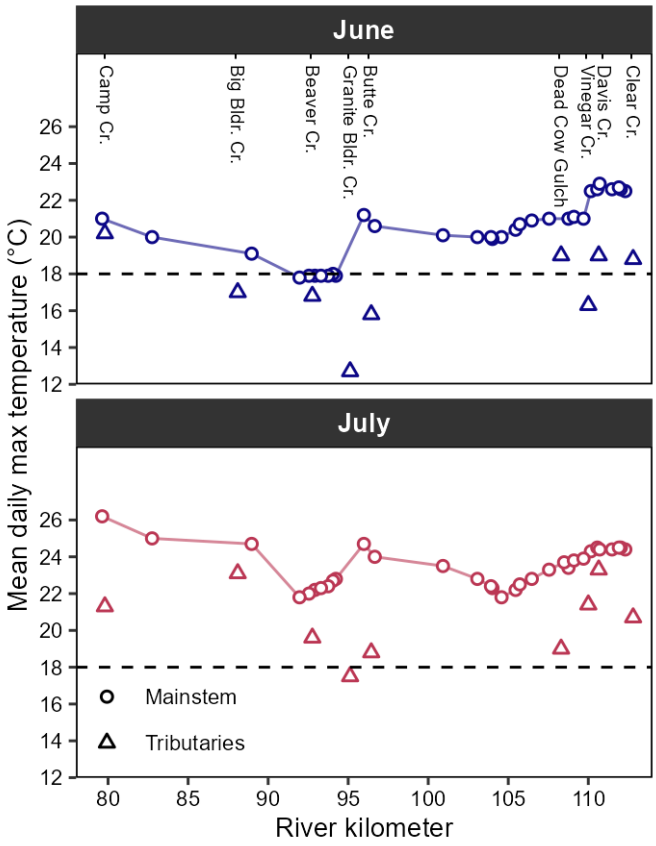

Figure D-S1: June (top) and July (bottom) MDMT across the sampling extent of the mainstem (open points and line) and the nine sampled tributaries (triangles). The river kilometer of tributaries represents the confluence with the mainstem.

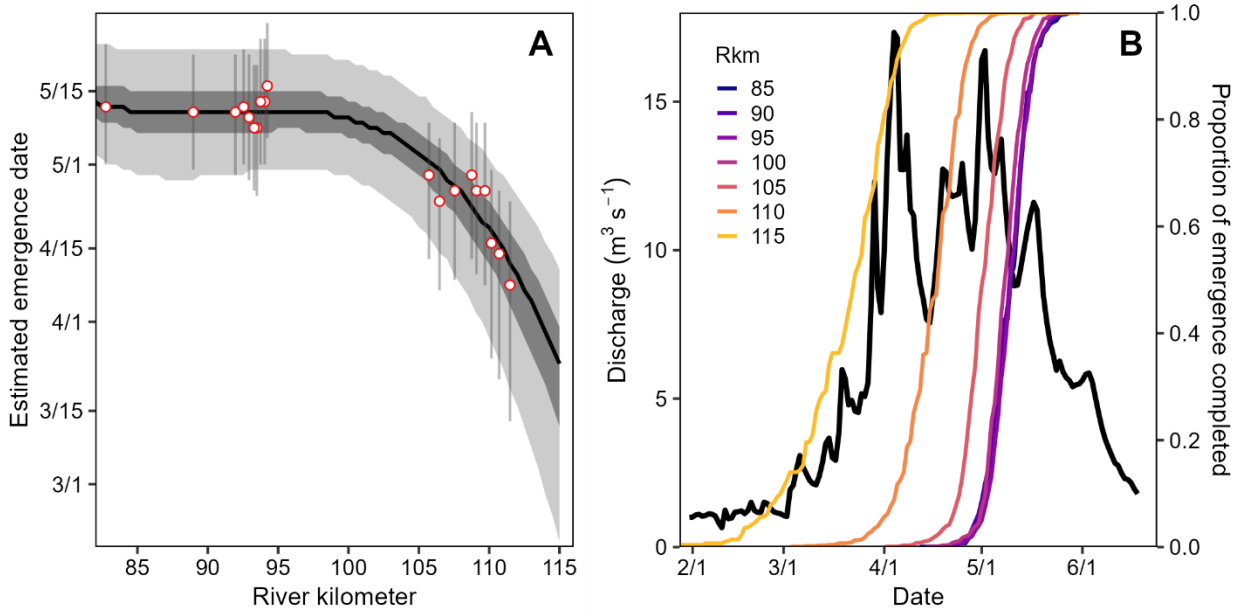

Figure D-S2: (A) Emergence timing estimates across the MFJDR for 2021 and (B) estimated discharge (m^3 s^{-1}) at the USGS Camp Creek gauge relative to cumulative distributions of emergence estimates at 5 km intervals. Emergence was first estimated at 19 locations with annual temperature data by simulating emergence given variation in spawn timing (see Kaylor et al. 2022). Points in panel A indicate median emergence timing and error indicates quantiles encompassing 95% of estimates. Emergence timing was then modeled as a function of river kilometer fit as a second-order polynomial.

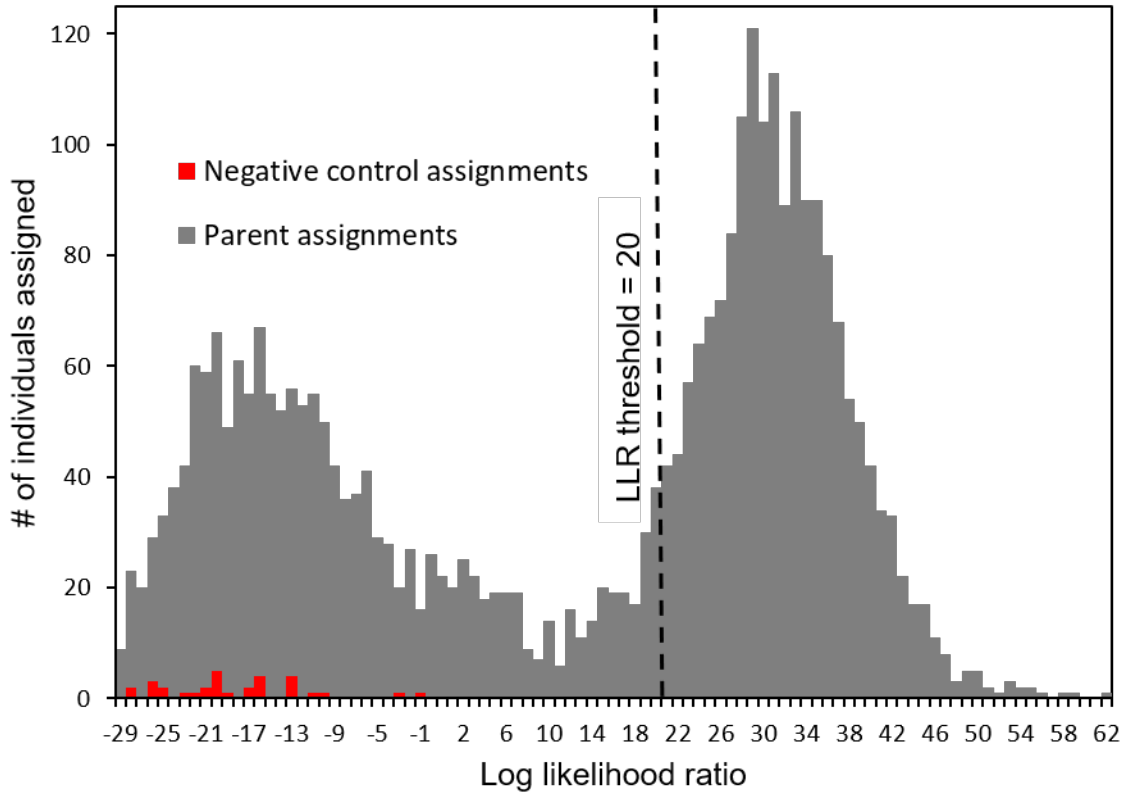

Figure D-S3: Distribution of log likelihood ratios for all MFJDR parr-adult assignments (grey bars) and for negative control samples (indicated by red bars). The bimodal distribution indicates two groups of parr-adult pairings, with those to the left of the dashed line considered unassigned to parents, and those to the right representing parr-adult assignments in which the adult was sampled and correctly assigned.

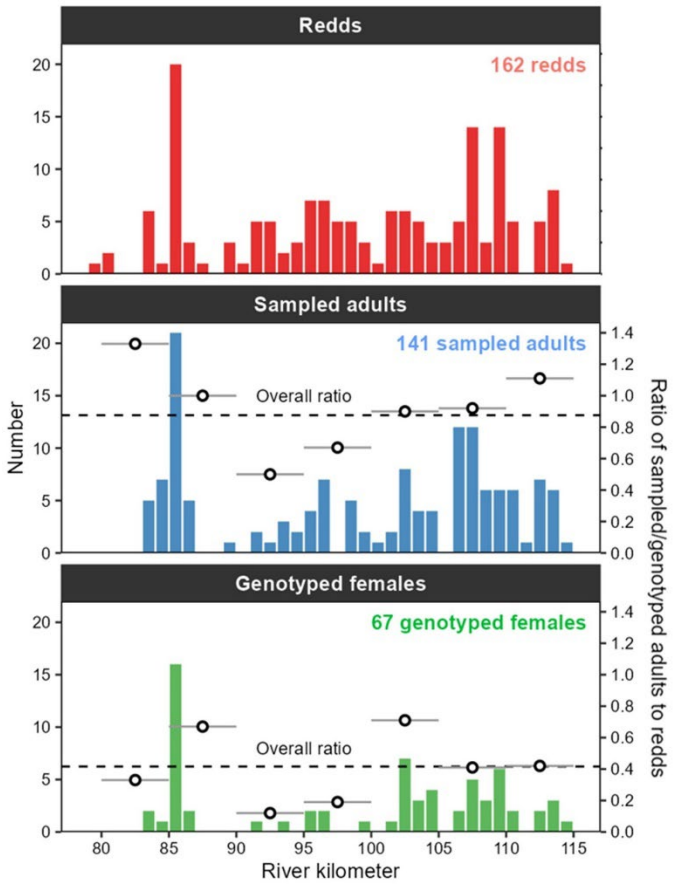

Figure D-S4: Number of redds (top; red bars), sampled adults (middle; blue bars), and successfully genotyped females (bottom; green bars) per kilometer in spawn year 2020. Points represent the ratio of sampled adults or genotyped females to redds for 5 km groupings (indicated by horizontal line associated with each point). Dashed lines indicate the overall ratio of sampled adults or genotyped females to redds. Ratios of genotyped females to redds (bottom panel) demonstrate sections where females were under-represented relative to redds (e.g., rkms 90-100).

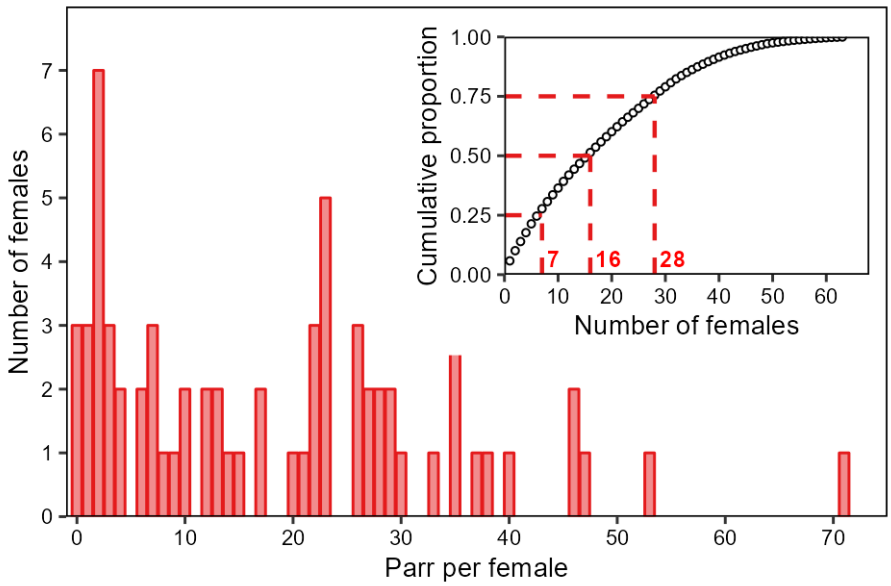

Figure D-S5: Distribution of number of parr paired to females after applying sampling bias correction. The inset shows the cumulative proportion of parr paired to females as the number of females – ranked by number of parr per female – increases. Out of the 67 females, 64 had ≥ 1 paired parr. The distribution shows non-uniform contributions of females to all sampled parr: the top 7, 16, and 28 females accounted for 25%, 50%, and 75% of all parr, respectively.

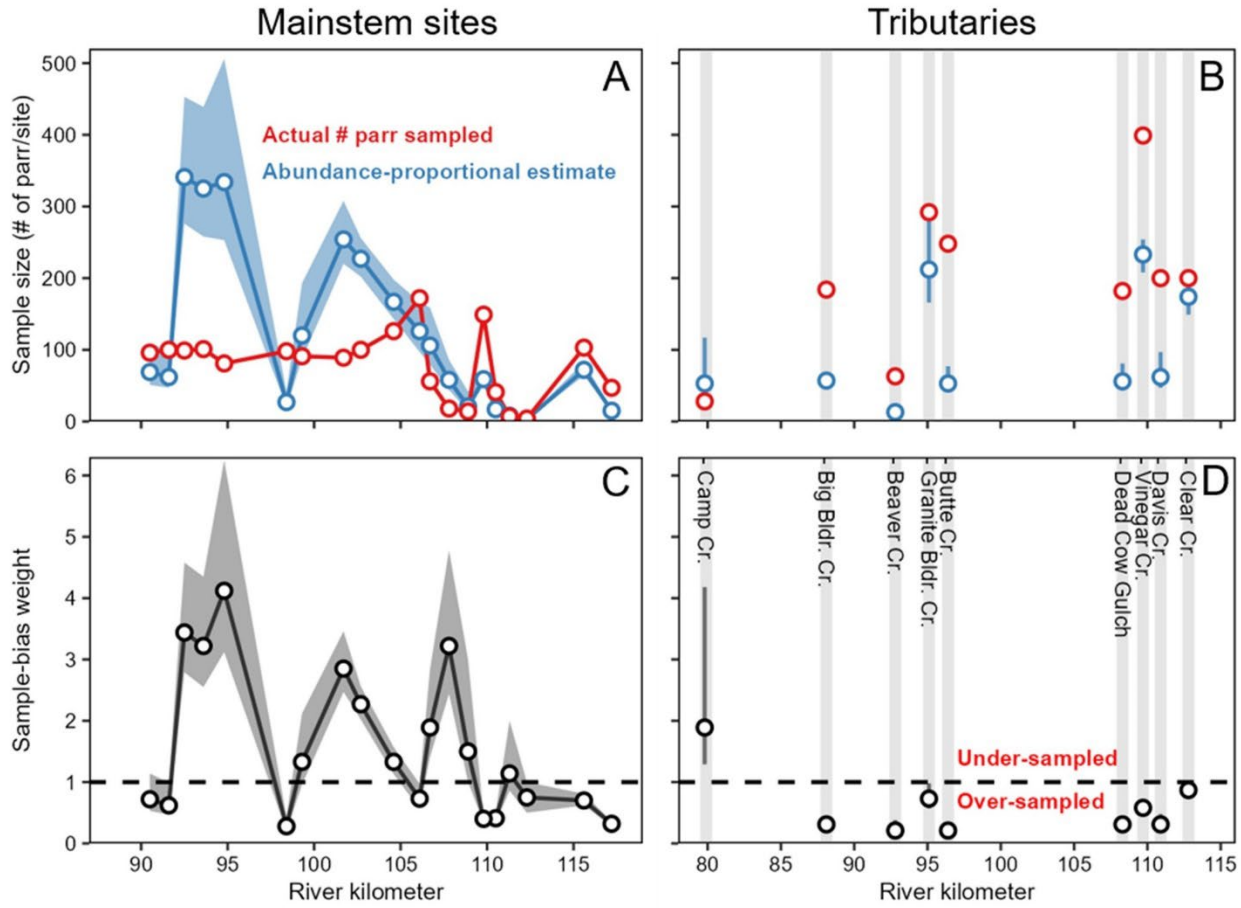

Figure D-S6: (A,B) Number of parr sampled at each mainstem site or tributary (red points and lines), estimated abundance-proportional median number of parr that should have been sampled at each site (blue points, lines, and shading), and (C,D) sample-bias weighting factors for each mainstem site or tributary (black lines, points, and shading). All shading and error bars represent 95% confidence intervals. Sample-bias weights greater than 1 indicate under-sampling (i.e., we should have sampled more parr), whereas values less than 1 indicate over-sampling. In general, most mainstem sites were under-sampled and most tributaries were over-sampled.

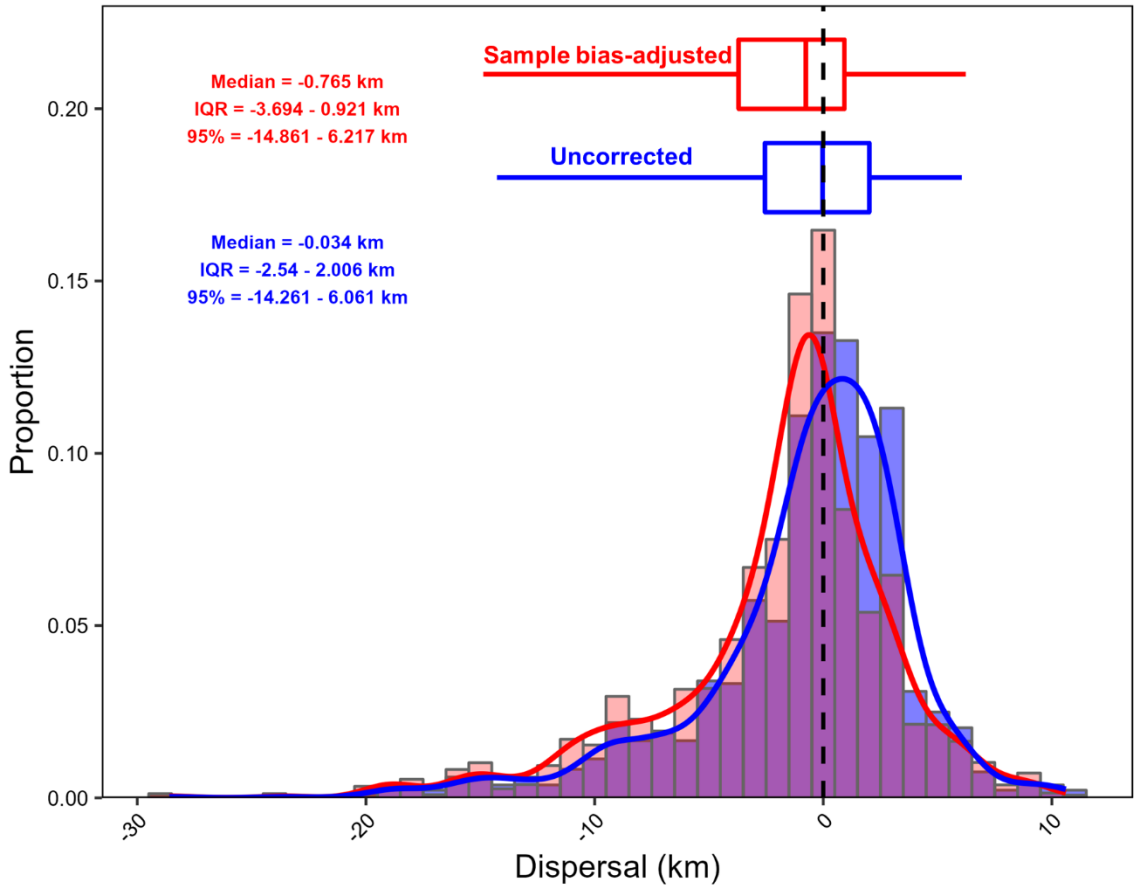

Figure D-S7: Distribution of dispersal estimates for all parr paired to females using raw values unadjusted for sampling-bias (blue) and simulated, sampling-bias-adjusted estimates (red). Box and whisker plots indicate median, inter-quartile range (IQR), and 95th percentiles.

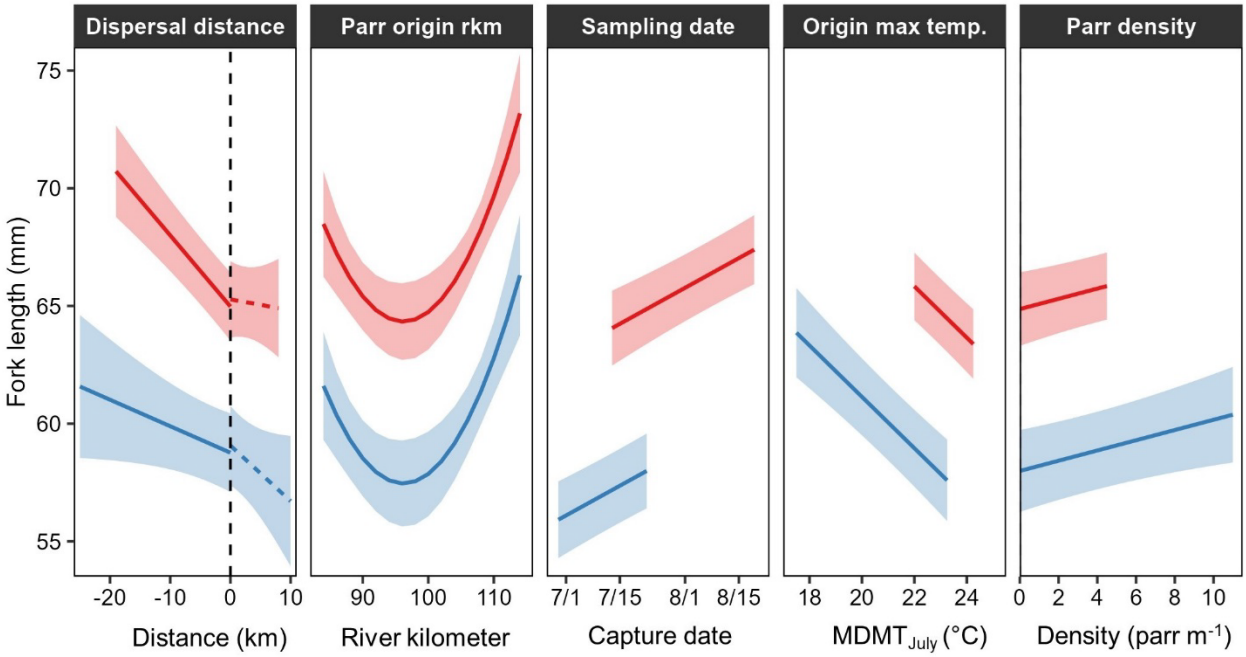

Figure D-S8: Marginal covariate effects for all covariates in the selected model predicting parr length-at-capture. Red indicates predictions for mainstem captured parr and blue indicates tributary captured parr.

Appendix E Grande Ronde Draft LCM Manuscript

Manuscript Title: A state-space model to quantify density-dependence, demographic heterogeneity, and spatial synchrony in Grande Ronde River Chinook Salmon populations

Manuscript Co-authors: Ben Staton, Martin Liermann, Polly Gibson, Casey Justice, Matt Kaylor, Rishi Sharma, Seth White

Keywords: State-space models, density-dependence, synchronous dynamics, Pacific salmon

NOTE:

- Some coauthors have not yet had a chance to contribute written content – in these cases we have included a Topical Outline.
- The "Supplement" referenced in this text is a large interactive webpage with many figures and tables showing detailed model output. It will be an online supplement to the submitted manuscript, and is not included in this text but is available upon request at time of writing.

Abstract

Pacific salmon populations face different mortality sources throughout life, requiring monitoring and modeling at various life stages to understand the relative influence of regulating processes. For example, density-dependence may be more important for freshwater juveniles, whereas environmentally forced ocean conditions may drive later-life outcomes independent of density – quantification of these kinds of phenomena requires spatiotemporal analyses with sufficient resolution. State-space models are a flexible and robust approach to analyzing time series population data. We constructed a state-space model for Grande Ronde Basin (NE Oregon, USA) spring Chinook Salmon that tracks the abundance of ~30 cohorts from 4 spawning populations as they transition through life, modeling variability in freshwater juvenile growth/survival using density-dependent relationships and stochastic process noise that acknowledges synchronous dynamics. Model substructures include rearing origin type, juvenile life history type, and adult age-of-return to account for heterogeneity at these scales. The model fits to empirical information collected by many monitoring projects and includes an index of habitat quality to scale density-dependent processes. Posterior predictive examinations revealed the model could reproduce data patterns and that noise terms largely conformed to model assumptions. We found evidence of early-life density-dependent survival and growth, with subsequent over-wintering and out-migration survival mediated by early-life growth rates. Parr rearing capacity and growth rates showed positive, though uncertain, relationships with weighted usable habitat availability. We found covariances to be overwhelmingly positive, indicating synchrony among populations within the basin. Simple post-hoc analyses illustrated that juvenile life history is important for increasing smolt production and inter-annual stability, and that increasing habitat availability would weaken density-dependence. Posteriors from this model reflect our current understanding of regulating processes throughout life for these populations that can be used to parameterize prospective simulations of alternative management actions on future population status.

Introduction

Population dynamics models are a widely used tool for synthesizing available knowledge and data to inform decision-making in fisheries resource management (Walters and Martell 2004) and they can be categorized in two primary varieties. Retrospective models seek to estimate unknown parameters from observed data and stated assumptions, and are by their nature statistical. They can be used to gain insights about ecological systems and test empirical support for alternative hypothesized processes regulating populations (Hilborn and Mangel 1997). Conversely, prospective models take parameter estimates and data summaries as inputs to predict population outcomes given a set of circumstances (e.g., management strategy evaluation; Punt et al. 2016, population viability analysis; Reed et al. 2002). The utility and reliability of prospective models are conditioned upon knowledge of population regulating processes. Thus, a key step in prospective modeling is rigorous retrospective analysis grounded in empirical observations.

Anadromous Pacific salmon (*Oncorhynchus* spp.) often have extensive biological monitoring data and there is broad interest in the development of prospective models for developing recovery plans. Given these species occupy a range of different habitat types as they progress through life stages, analyses are inherently spatiotemporal models that must quantify cohort-by-corhort abundance and mortality by life stage. Density-dependent factors have been widely observed to influence Pacific salmon populations, particularly growth and survival early in life (Walters et al. 2013; Grossman and Simon 2020), and it is essential that retrospective analyses disentangle these effects from extrinsic (e.g., environmental noise/forcing, harvest, density-independent) drivers (Zabel et al. 2006). Understanding the effects and strength of density-dependence across life states is critical for realistic prospective modeling of population dynamics (Rose et al. 2001; Reed et al. 2002). Although anadromous species tend to have reasonably predictable migrations that facilitate monitoring abundance and survival at various life stages, data collection is imperfect: sampling variability, missing years, and inconsistencies of scale are common. Therefore, analyses that account for these imperfections in the data while providing robust retrospective inference are important to parameterizing useful prospective models.

State-space models (SSMs; Newman et al. 2023) have grown in popularity in recent decades as a means to address challenges in retrospective population modeling. SSMs are time series models that partition noise into process (e.g., environmental) and observational components, making them useful for addressing measurement error bias (de Valpine and Hastings 2002; Lindén and Knape 2009; Newman et al. 2023), expressing relative weights for different data sources, and ensuring variability due to observation error is not carried forward to prospective analyses. SSMs are constructed by (*i*) specifying a set of process equations that represent expected population responses to intrinsic (e.g., density affects survival) and extrinsic (e.g., quantity and quality of available habitat) drivers, (*ii*) adding process noise to obtain the "latent" (i.e., true but hidden) state, and (*iii*) assuming that the data values have been observed with error, conditioned on the latent values via statistical likelihood functions (Auger-Méthé et al. 2021). Since SSMs are inherently time series models, they are useful for handling the time lags and linkages involved with modeling stage- and/or age-structured populations. Specific examples include: reducing time series bias (Walters 1985; Myers and Barrowman 1995), accounting for delayed effects (Beckerman et al. 2002), and preventing issues associated with overly simplistic treatments of age information (Zabel and Levin 2002). SSMs have been widely applied to salmon populations, however often only with adult time series (Su and Peterman 2012; Fleischman et al. 2013; Staton et al. 2017, 2020, 2021; Connors et al. 2022; Su 2023), due to the lack of data on intermediate life stages. SSMs that partition the salmon life cycle into with multiple life stages are less common, but when applied, they can provide robust and more detailed insights into population dynamics (Rivot et al. 2004; Perry et al. 2020; Jacobs et al. 2023).

Statistical models that include spatiotemporal variability often encounter spatial autocorrelation (González-Megías et al. 2005). Noisy extrinsic population drivers, such as inter-annual fluctuations in environmental

conditions, may vary at scales experienced by multiple populations (or population subcomponents) such that temporal variability may be shared (Ranta et al. 1997). Interest in quantifying spatial synchrony in population models has increased in recent years (Bjørnstad et al. 1999; Thorson et al. 2014; Riecke et al. 2019; Staton et al. 2020; Bouchard et al. 2022) because it can provide useful insights for conservation ecology, particularly when quantified at various life stages (Thorson et al. 2014). First, the strength of the portfolio effect (Schindler et al. 2015) is inversely related to synchrony, thus estimates of low correlation between populations can provide insights into which life stages greatest impact stability at aggregated scales. Second, and opposite to the stabilizing benefits of the portfolio effect, strongly synchronous population dynamics result in unstable aggregate-scale dynamics and increase the likelihood of simultaneous extirpation of multiple populations (Heino et al. 1997; Isaak et al. 2003). Third, knowledge of which life stages are most synchronous may be useful in predicting those that are likely to be co-affected by a changing climate (Hansen et al. 2020; Bouchard et al. 2022). Finally, a potential statistical advantage of accounting for synchrony may be to increase precision by facilitating information sharing in hierarchical time series models (i.e., reconstructing missing portions of partially overlapping or sparse time series; Staton et al. 2020).

In this article, we describe a state-space model for quantifying population dynamics parameters and synchrony that we developed for application to Grande Ronde basin spring Chinook Salmon (*O. tshawytscha*) populations. The model tracks the cohort-specific abundance through various life stages with linkages over time across cohorts via production relationships and within cohorts via transition probabilities. The model integrates many different data sources and fits to them simultaneously in a single joint likelihood as a means to maximize information use and enforce parameter consistency with all available data sets. Four spawning populations within the Grande Ronde basin are simultaneously analyzed, and where relevant, the model stratifies life stages by juvenile migratory strategy, rearing origin type, and adult return age. Our objectives are to (*i*) document the data the model was fitted to, (*ii*) present the model structure, (*iii*) highlight key inferences from the model, and (*iv*) demonstrate the utility of the model output with two simple post-hoc analyses. The ultimate purpose of the model is to enable parameterizing prospective simulations under future management intervention (e.g., habitat restoration, hatchery supplementation) and climate change scenarios.

Methods

Study Area and Populations

Topical Outline *– Will be written by Justice & Kaylor*

- Description of Grande Ronde basin: NE Oregon, tributary of Snake River, size
- Populations: Catherine Creek (CAT), Lostine River (LOS), Minam River (MIN), Upper Grande Ronde River (UGR); Figure E-1.
- Why these populations?
  - Rigorous and near-identical biological and habitat monitoring
  - Minam River is in wilderness area, no weir or hatchery
- Current depressed population status and historical/current causes
- Describe life history briefly:
  - Stream-type life history: out-migrate a full year after emergence in freshwater, return as either total age-3, -4, or -5.
  - Juvenile migratory strategy diversity: fall vs. spring migrants
  - Hatchery supplementation

Data Sources

The model relies upon a wealth of data sources, most of which have been gathered during routine biological monitoring (Figure E-2 – numbered circles denote specific data sources). We use six categories for presentation; categories *i-iv* include data sets assumed to have error and to which we assigned explicit likelihood functions, whereas we used those in categories *v-vi* in a deterministic sense: (*i*) juvenile and adult abundance, (*ii*) juvenile and adult survival rates, (*iii*) juvenile mean length, (*iv*) adult age/origin composition, (*v*) "auxiliary" information (e.g., hatchery smolt releases, weir removal numbers, fecundity-at-age), and (*vi*) weighted usable habitat. Although we refer these information sources colloquially as "data" in that the model fits to them or requires them to populate calculations, they are often externally derived estimates from raw monitoring data. For example, juvenile abundance estimates were obtained from rotary screw trap passage counts and expanded for imperfect detection, and many of the survival rate estimates were obtained from open capture-recapture models fitted to PIT-tag detection records. We allowed the model to acknowledge that these data sources (estimates) are not perfect representations by using the standard errors from the external estimation models as the standard deviations of observation error.

Abundance Data

Topical Outline *– Will be written by Gibson*

- *Juvenile*: fall screw trap passage (Gibson et al. 2023)
- *Juvenile*: spring screw trap passage (Gibson et al. 2023)
- *Adult*: total return-to-river
  - Assumed to be prior to any in-river mortality (harvest, weir removals, pre-spawn mortality; Bliesner et al. 2020; Brandt et al. 2021)

Survival Rate Data

Topical Outline *– Will be written by Gibson*

- *Juvenile*: PIT-tag survival estimates to LGR
  - Summer parr electrofishing → LGR (both fall and spring migrants; Gibson et al. 2023)
  - Fall parr at trap → LGR (fall migrants only; Gibson et al. 2023)
  - Winter parr electrofishing → LGR (spring migrants only; not in MIN; Gibson et al. 2023)
  - Spring smolt at trap → LGR (spring migrants only; Gibson et al. 2023)
  - HOR smolt release → LGR (Brandt et al. 2021)
- *Juvenile*: Comparative survival study estimates to inform LGR → BON survival by origin (McCann et al. 2022)
- *Adult*: PIT-tag counts observed with near 100% detection inform BON → LGR survival (DART 2023)

Mean Length Data

Topical Outline *– Will be written by Gibson*

- *Juvenile*: Fish measured when captured for PIT-tagging
  - Summer parr electrofishing (Gibson et al. 2023, corrected for inter-annual variability in sample timing; described in Staton et al. (2023))
  - Spring smolt at trap (Gibson et al. 2023, no correction needed, inter-annual sample timing direct result of migration timing)

Age/Origin Composition Data

Topical Outline *– Will be written by Gibson*

- *Adult*: Number of fish sampled by age and origin at weir
  - Briefly describe age method hierarchy
  - Only CAT, LOS, UGR have weir
  - Assume sampling occurred in proportion to relative abundance
- *Adult*: Number of carcasses sampled by age and origin
  - Available for all four populations
  - Assume sampling bias, model estimates correction factors

Auxiliary Information

There were several processes known to vary inter-annually and for which information was available, however we did not build process model components to describe variability. We did not fit the model to these information sources via an explicit likelihood (in part because they did not have estimates of observation uncertainty), rather we simply used their values in calculations, implicitly assuming they were known without error.

Topical Outline *– Will be written by Gibson*

- *Juvenile*: Number of hatchery smolt released (CAT, LOS, UGR only)
- *Adult*: Fishery harvest rates below BON
- *Adult*: Number of fish by age/origin harvested in each tributary
- *Adult*: Number of fish by age/origin removed at weir for broodstock or management of spawner origin composition
- *Adult*: Pre-spawn mortality
  - Estimated from carcass data
- *Adult*: Fecundity

Weighted Usable Habitat

Topical Outline *– Will be written by Justice*

- *Purpose*: To provide an index of available habitat quality/quantity that can be used to scale density-dependent quantities and provide a means for evaluating impacts of future changes to freshwater habitat resulting from restoration or climate change.
- *Derivation Workflow*:
  - Snorkel counts ►
  - Correct for imperfect detection probability (Staton et al. 2022) ►
  - Expand for unsnorkeled habitat to reach scale ►
  - Zero-inflated negative binomial generalized linear mixed models to identify habitat features (briefly describe variables) associated with high densities ►
  - Obtain reach-level weights by rescaling reach-specific predicted densities relative to the reach with maximum density ►
  - Obtain weighted usable habitat length (WUL) as the sum-product of reach-specific lengths and weights
- Calculations performed separately for each population

Model Description

The role of the state-space model is to estimate population dynamics parameters from empirical data in a statistically robust fashion. The model tracks the cohort-specific abundance of fish through various life stages and links these state variables over time across cohorts via production relationships (e.g., spawners produce eggs for the next generation) or within cohorts via transition probabilities (e.g., parr become smolt after surviving over winter). The model is structured to track fish separated by their demographic attributes, including (*i*) spawning population (CAT, LOS, MIN, UGR), (*ii*) juvenile migratory strategy (fall vs. spring migrants), (*iii*) rearing origin type (wild vs. hatchery spawned), and age of adult return (total age of 3, 4, or 5 years). Although process and observation model equations are mostly identical by population, migratory strategy, origin, and age, the parameters governing them vary according to this structure, where applicable, thus estimating and capturing demographic heterogeneity (e.g., differences in average survival by population or origin type). The structure of the model, including the life stages, transitions, and structures are shown in Figure E-2. All process and observation model equations (represented by arrows in Figure E-2) and assumed stochastic processes are described in complete detail in Appendix F; we have opted for a more narrative description of the model here and point the reader to the relevant equations in Appendix F for more details.

Although the model separately accounted for process and observation variability, it did not freely estimate the variance of both sources. Instead, we supplied estimates of the latter and it attributed the remaining noise unexplained by process equations to process noise – this has computational and statistical advantages relative to estimating both (Polansky et al. 2021). We assume process noise is the result of unmeasured and/or unmodeled environmental factors that vary annually; with the exception of two processes, we assume process noise is temporally independent. Conversely, we account for synchrony among populations by modeling process noise terms as arising from multivariate (log- or logit-) normal random processes (e.g., eq. F-1) and estimate the covariance matrix that stores the variances for each population and covariances among population pairs (eq. F-2, F-3; Riecke et al. 2019). Covariance matrices have certain constraints, which makes them difficult to estimate (Barnard et al. 2000) – our solution was to use the inverse-Wishart distribution (Gelman and Hill 2007; Gelman et al. 2014).

Freshwater Juvenile Processes

We initiated the life cycle at the egg stage, where the number of eggs for a given population was the product of female spawner abundance and fecundity from the previous year (eq. F-4). We assumed half of all age-4 and age-5 spawners were female and all age-3 spawners were male, and modeled fecundity as a function of time-varying mean length-at-age data to account for declines in size (Ohlberger et al. 2018) which may have implications for egg production at the population scale (Ohlberger et al. 2020). From the egg stage, we modeled egg-to-parr survival as a density-dependent process following Beverton-Holt dynamics (Moussalli and Hilborn 1986, eq. F-5) with process noise that was multivariate logit-normal and serially autocorrelated (via a lag-1 autoregressive process; eq. F-7). Maximum egg-to-parr survival was estimated as a free parameter for each population, however we modeled parr recruitment capacity as a linear function of WUL with log-normal error (eq. F-6); both maximum egg-to-parr survival and parr capacity were assumed time-constant. Total parr recruitment was then the product of total egg production and this density-dependent egg-to-parr survival (eq. F-8).

In addition to density-dependent processes affecting parr recruitment, freshwater juvenile survival rates have also been observed to be density-dependent for Snake River spring Chinook Salmon populations (Achord et al. 2003; Walters et al. 2013), including those in the Grande Ronde (Cooney et al. 2017; Staton et al. 2023). Growth rates of juvenile salmonids in freshwater have also been widely observed to be density-dependent (Grant and Imre 2005; Copeland and Venditti 2009; Walters et al. 2013; Myrvold and Kennedy 2015; Grossman and Simon 2020) and juvenile size has been found to be important for survival (Zabel and Achord 2004; Hostetter et al. 2015). We thus embedded process model equations to capture these intrinsic

population processes and linked them to available monitoring data in the form of mean length estimates. We modeled parr mean length as a power function of egg density (expressed as eggs per km WUL) as a representation of density-dependent growth (eq. F-9) and assumed process noise around the deterministic function was multivariate log-normal (eq. F-10). We then used mean parr size as a predictor variable in a logit-linear model to derive expected over-winter survival (eq. F-13) and in a log-linear model to derive expected growth from parr mean length to smolt mean length (eq. F-16); we then used smolt mean length to derive expected survival during the migration out of the basin to Lower Granite Dam (LGR; eq. F-19). This chain of linked process model equations enabled capturing delayed effects of density-dependent growth on survival later in life. Recognizing that extrinsic factors affect growth and survival rates as well as intrinsic processes, we included process noise for all three of these deterministic functions as well (eqs. F-14, F-17, and F-20, respectively).

Timing of migration out of the spawning and summer parr rearing habitats is an important feature of many Snake River spring Chinook Salmon populations (Copeland and Venditti 2009; Copeland et al. 2014), including those in the Grande Ronde basin, with one pulse of parr migrating downstream in the fall to rear over-winter lower in the basin (termed "fall migrants") and another that stays to rear over-winter in the more upstream summer habitats (termed "spring migrants") – both types migrate out of the basin the following spring as age-2 smolts. We ignored the potential presence of a third "fry migrant" type (Copeland and Venditti 2009), as this is not thought to be a specific life history in these populations. Modeling these two migratory strategies separately was important for the observation model as they are monitored for abundance and survival separately, and previous analyses suggest differential survival rates (Cooney et al. 2017; Staton et al. 2023). Following recruitment to the parr stage (eq. F-8), we estimated a time-constant expected apportionment rate (with inter-annual variation modeled with multivariate logit-normal process noise, eq. F-12) to obtain the number of parr that adopted each migratory strategy (eq. F-11). In the observation model, the abundance of parr fall migrants was linked to the fall screw trap passage estimate (eq. F-24) before over-winter rearing, and the abundance of smolt spring migrants was linked to the spring screw trap passage estimate following over-winter rearing (eq. F-25).

We tracked the abundance and fates of hatchery-origin (HOR) fish separately from natural-origin (NOR) fish for all applicable life stages. HOR smolts have been released in the spring prior to out-migration and we used the numbers of smolt released each year by population (except MIN, which has no hatchery supplementation) to initialize all process model calculations for HOR fish, unlike for NOR fish which have time linkages to previous generations through natural spawning. We did not model density-dependent or size-dependent survival processes for HOR fish.

Upon reaching LGR, information to separate juvenile migratory strategies was no longer available, so we combined all NOR smolt by population for tracking separately from HOR smolt. Further, external estimates of survival downstream through the mainstem Snake and Columbia Rivers were available based on origin only, not by population – making this survival rate (migration from LGR through Bonneville Dam [BON] to reach the estuary) the first process that we modeled without population heterogeneity. We assumed a time-constant expected value for each origin type and modeled inter-annual variability as being distributed multivariate logit-normal with non-zero covariance assumed among origin types (eq. F-22). We obtained the number of smolt reaching the estuary as the product of smolt abundance reaching LGR (eq. F-21) and this downstream migration survival rate through the mainstem/hydrosystem (eq. F-23).

Ocean Juvenile Processes

After reaching the estuary, ocean juveniles can mature and return as either total age-3, age-4, or age-5 after spending 1, 2, or 3 winters, respectively, at sea. Accordingly, we modeled ocean dynamics using two demographic rates: survival and maturation (Figure E-2). After surviving the first winter at sea, fish had the option to mature at age-3, those that did not must survive a second winter before the option to mature at

age-4, and those that did not must survive a third winter and at which point all survivors returned as age-5 (see eqs. F-37 and F-38). All parameters in a "full model" (i.e., time-varying survival for year-1, year-2, and year-3 and maturity after year-1 and year-2, by origin) were not estimable, so we made several simplifying assumptions. With respect to survival, we assumed only year-1 was time-varying (with lag-1 autocorrelation around a time-constant expected value, eq. F-34) and forced time-constant year-2 and year-3 survival. Further, we assumed that inter-annual process noise in NOR and HOR ocean survival was perfectly correlated but allowed a difference in magnitude via a freely estimated log-odds ratio that was time-constant but varied by population (eq. F-35). With respect to maturation rates, we estimated time-constant expected values for both year-1 and year-2 by population and origin, and introduced inter-annual process noise via multivariate logit-normal distributions (eq. F-36). We chose to simplify parameter structure in survival rather than for maturity because of the availability of commonly assumed values for ocean survival (CTC 1988), which we used as priors suggesting 0.6 and 0.7 for year-2 and year-3, respectively. The critical state representing output of the ocean juvenile process model was the number of mature fish (including age-3, which we term collectively "adults") returning to the Columbia River estuary by year, population, age, and origin.

Freshwater Adult Processes

Adults experience multiple sources of mortality upon return to the estuary and along their upstream migration to natal spawning tributaries, which we attempted to partition as finely yet accurately as possible. First, we subjected fish to an exploitation rate below BON which, according to the auxiliary information source, varied by year and origin, and we reduced the rate applied to age-3 fish to half that of age-4 and age-5 fish as a simple means to account for gill net selectivity (eq. F-40). Second, we subjected fish to an upstream survival rate that represented mortality (e.g., fishery, hydropower, predation) experienced on the migration between BON and LGR. We modeled upstream migration survival just as we did downstream survival through this corridor: time- and population-constant expected values by origin type, with inter-annual noise introduced via a multivariate logit-normal distribution allowing non-zero covariance among origin types (eq. F-39). Third, upon reaching the Grande Ronde River, we subtracted the number of fish known to be harvested by tributary fisheries, and fourth, we subtracted known removals upon reaching the weir (for broodstock and spawner composition management; Naylor et al. 2019; Kinzer et al. 2020) – both auxiliary information sources were available by year, age, origin, and population (eq. F-41). Fifth, upon reaching the spawning grounds, we applied a time- and population-varying pre-spawn survival rate that accounted for mortality experienced between prior sampling and spawning (eq. F-42). We obtained auxiliary estimates of pre-spawn survival by fitting binary GLMMs to carcass spawn success data (Supplement, Section 15.6). We assumed all surviving fish then contributed to spawning, such that 0% of age-3 spawners and 50% of age-4 and age-5 spawners were female and were assigned non-zero fecundity (Supplement, Section 15.5) based on their spawning year, age, and population to obtain total egg production (eq. F-4) to initiate calculations for the next cohort.

Observation Model

We linked observed outcomes to model-predicted latent states through the observation model – this is the likelihood that provides information to estimate unknown parameters. To formulate likelihoods, we used process model outcomes as the expected value and treated the observed point estimate as a random variable of a stochastic process with a pre-specified observation error magnitude (e.g., smolt trap passage: eqs. F-24 and F-25; PIT-tag-derived survival estimates: eqs. F-26 – F-30). We used log-normal distributions to represent the stochastic processes for observing abundance and mean length and logit-normal for survival rate data, where the standard deviation was the standard error of the observed value for that year (e.g., from Cormack-Jolly-Seber modeling; Gibson et al. 2023). We used binomial distributions to represent the stochastic process for observation of tags (i.e., as adults to inform survival from BON to LGR; eq. F-44) and multinomial distributions for frequencies of adults by age and origin observed at weirs (eq. F-46) and during carcass surveys (eq. F-51), such that the magnitude of assumed observation error was a function of

the sample size. In most cases, we linked observed values directly to latent states in this fashion (assuming unbiased sampling), however in the case of fitting to carcass data frequencies, we estimated correction factors that allowed biased carcass counts relative to weir counts with respect to age – preliminary analysis suggested larger carcasses were more likely to be sampled (eqs. F-47 – F-50). States and transitions with data sources informing them through the observation model are denoted in Figure E-2 by numbered circles.

Model Fitting

Bayesian Computation

We fitted the model to data using the Bayesian framework, as it is intuitive for the necessary integration over the many layers of uncertainty (i.e., process vs. observational variability; de Valpine and Hilborn 2005). Posterior distributions of estimated parameters provided a seamless method of propagation to estimate uncertainty in quantities derived from estimated parameters. We used JAGS (v4.3.1; Plummer 2003) to perform Markov Chain Monte Carlo (MCMC) calculations, invoked through Program R (R Core Team 2023) and the 'jagsUI' package (Kellner 2021). We used the 'postpack' package (Staton 2022) to perform all posterior summarization, with the exception of the 'posterior' package (Bürkner et al. 2023) for MCMC convergence and sampling diagnostics due to its implementation of modern and robust calculations (Vehtari et al. 2021). Our MCMC simulations involved four chains, each 150,000 iterations long with a burn-in period of 50,000 and a post-burn-in thinning rate of 25 – this resulted in 16,000 samples from the joint posterior retained for inference. MCMC diagnostics included the $\hat{R}$ statistic to diagnose convergence (values ≤ 1.01 ideal, we deemed <1.05 to be "no issue", <1.1 to be "acceptable", and >1.1 to be "concerning"), effective sample size to assess whether enough independent information exists to estimate posterior quantiles with precision (values >400 ideal), and MCMC coefficients of variation (expressed as MCMC standard error divided by mean) to assess the precision of posterior summaries (smaller values better); see Vehtari et al. (2021) for more details. We calculated MCMC diagnostics for every unobserved stochastic quantity and summarized them within model components (e.g., by life stage, population) as the percent of values failing to meet a specific threshold and visualized MCMC traceplots for quantities with high $\hat{R}$ (Supplement, Section 2). In reporting posterior summaries, we use the posterior mean and 95% equal-tailed credible limits (CRL). For all quantities calculated from parameters, we performed the calculation using each posterior sample prior to performing posterior summarization.

Priors

Our intent was to be as objective as possible and to allow primarily the data to shape the posterior; as such, we used nearly exclusively flat priors (Table F2). There were, however, several exceptions wherein we provided *a priori* information to (*a*) effectively exclude biologically implausible values or (*b*) estimate a parameter for which there was insufficient information in the data. As an example of use case (*a*), we used a Beta(2,8) prior for maximum egg-to-parr survival, which is relatively flat over 0.1-0.25 and renders values greater than 0.5 effectively impossible. Other parameters with non-flat priors included expected ocean survival (Beta[1,9] for year-1, Beta[60,40] for year-2, and Beta[70,30] for year-3; the latter two are examples of use case [*b*]) and expected maturation (Beta[1,9] for year-1 and Beta[8.5,1.5] for year-2). We constructed priors for covariance matrices using scaled inverse-Wishart distributions that suggested smaller values (e.g., <0.5 or 1) were more likely for standard deviation terms, recognizing that these reflect variability on the log- or logit-scale; the scaled inverse-Wishart also gave Uniform(-1,1) distributions on all correlation terms. Comparisons of non-flat priors to the posteriors (Supplement, Section 14) implied that posteriors were not majorly impacted by the priors.

Model Fit Diagnostics

We used two primary methods to assess conformance of the data with model assumptions – both relied on the posterior predictive distribution to quantify agreement between the model-expected outcomes and actual

outcomes. First, we performed a posterior predictive check as an overall index of fit (Supplement, Section 12; Gelman et al. 2014). We simulated data from the model using the assumptions for building the likelihood and evaluated the fit of both the simulated and observed data to the model; we expressed the results as a Bayesian p-value equal the proportion of MCMC iterations in which the observed data fitted more poorly (values near 0.5 are ideal; values >0.5 indicate a degree of over-dispersion). We calculated Bayesian p-values for each year within a given process and summarized them as the median and 2.5% and 97.5% percentiles, as well as the proportion of years with "extreme" p-values (i.e., <0.05 or >0.95).

However, posterior predictive checks only assessed the observed stochastic quantities and did not evaluate time trends or cycles in lack of fit. Thus, we used quantile-standardized residuals (Dunn and Smyth 1996) as a second means to investigate more detailed patterns in model-estimated noise terms (Supplement, Section 11). We used the posterior predictive distribution to calculate the cumulative probability of the realized (latent or observed) value such that values <0.5 corresponded to outcomes below model-expected values and those >0.5 above expectations. Across replicates of the same random process (i.e., years), we should expect these residuals to be distributed Uniform(0,1), meaning they should have a mean of 0.5, a standard deviation equal to $\sqrt{1/12}$, and lack any time series trends (assessed as the difference in averages of the first and last half of the time series) or cycles. Unlike Bayesian p-values, quantile-standardized residuals used the same fit statistic for all (observed and unobserved) stochastic values regardless of the assessed random process (e.g., logit-normal vs. binomial), providing a unified framework for assessing patterns in variability and conformance with model assumptions.

Analyses of Hypotheticals

We performed two post-hoc "hypothetical" analyses to further demonstrate the utility of the model and samples from its joint posterior. These are comparatively rudimentary examples of the types of prospective uses of model output – ultimate plans involve sampling from the posterior and performing stochastic simulation of population trajectories under climate change and habitat restoration scenarios.

Increased Habitat Availability

We constructed the model to assume availability of high-quality habitat affects parr capacity (eq. F-6) and density-dependent growth (eq. F-9), which we in turn use as a predictor of survival during over-winter rearing (eqs. F-13) and out-migration to LGR (eq. F-19). Thus, we can demonstrate the expected change in freshwater juvenile survival and production resulting from increases in WUL by some hypothetical amounts (50%, 100%, and 200%) from their current values. For each hypothetical increase level and posterior sample within each population, we used process model equations and estimates to calculate expected (i.e., without process noise) parr recruitment, growth/size, and size-dependent survival at a range of fixed egg production values (converted to spawner abundance for interpretability). We compared the shape of resulting density-dependent curves (*a*) survival from egg to smolt at LGR, (*b*) survival from parr to smolt at LGR, and (*c*) smolt arrivals at LGR across hypothetical habitat levels – we expected to find that with more available habitat, there would be higher survival and smolt arrivals to LGR for a fixed number of spawners.

Non-existent Fall Migrants

Life history diversity in the timing of migration out of spawning habitats to over-winter rearing habitats may be an important contributor to bolstering freshwater production (Copeland et al. 2014) and stabilizing inter-annual variability through portfolio effects (Thorson et al. 2014). We sought to perform a simple evaluation of how valuable the fall migrant strategy is to production and stability. Using posterior samples from the fitted model, we performed post-hoc calculations that assumed historical parr recruitment and post-recruitment survival (including process noise) was identical as previously observed, but hypothetically that all parr became spring migrants (i.e., setting $\pi_{y,i=\text{fall},j} = 0$ in eq. F-11). We compared the total mean and inter-annual CV of smolt abundance arriving at LGR (within and aggregated across populations) between this

hypothetical "no fall migrants" scenario and the actual posterior estimates. We expected to see a change in the magnitude of smolt production (resulting from different fall and spring migrants survival) and an increase in CV (due to reduction of asynchrony).

Results

MCMC Convergence and Model Fit

Considering the complexity of the estimation problem the model represented, we found we were able to achieve overall good convergence (Supplement, Section 2). 98% of unobserved stochastic quantities (i.e., parameters) fell into our "ideal/no issue" category ($\hat{R} < 1.05$), while 2% were deemed "acceptable" ($1.05 < \hat{R} < 1.1$) and none were deemed "concerning" ($\hat{R} > 1.1$). Parameters with $\hat{R} > 1.01$ were most often the latent states, though some variance and correlation parameters met this criterion in more rare cases, the coefficients of demographic relationships. Most parameters achieved >400 effective sample size for estimating 2.5^{th} and 97.5^{th} posterior percentiles – it was more common to have lower effective samples for estimating the mean.

Fit to the data was overall quite good as well, as evidenced by observed vs. predicted value scatterplots (Figure E-3), quantile-standardized residuals (Supplement, Section 11), and posterior predictive checks (Supplement, Section 12). Among all data sets, fits to the age/origin composition data (weir and carcass) were identified to be the poorest by both quantile-standardized residuals and posterior predictive checks, including some evidence for time trends in the of lack of fit (Supplement, Section 11.2.4).

General Life Cycle Survival Summary

Freshwater Juvenile Phase

Posterior mean egg-to-parr survival rates were very low but highly variable, averaging ~0.15 and ranging (~0.01-0.42) across years and populations (Figure E-4a). Theoretical maximum average survival (i.e., in the absence of density-dependence) ranged from 0.14 (UGR; 95% CRL: 0.07-0.23) to 0.21 (CAT; 95% CRL: 0.1-0.33) and parr rearing capacity ranged from 117,000 (95% CRL: 58,000-228,000) for CAT to 987,000 (95% CRL: 322,000-2,603,000) for MIN. Assuming the time series average for eggs-per-spawner (~1,750) and with 100 spawners per population (of all ages/sexes), this translates to expected parr recruits-per-spawner of 213 (95% CRL: 113-334) for UGR, 254 (95% CRL: 165-371) for LOS, 262 (95% CRL: 149-357) for CAT, and 294 (95% CRL: 191-426) for MIN. Process noise around the survival relationship implied by the Beverton-Holt function was moderately auto-correlated (Supplement, Sections 4.1 and 4.2), with AR(1) coefficients averaging 0.48 (95% CRL: 0.19-0.74) across populations.

Following recruitment, the majority of parr selected a spring migrant life history strategy, with a minimum average of 9% (95% CRL: 7-12%) of parr choosing to become fall migrants for UGR to a maximum average of 37% (95% CRL: 32-43%) for CAT (Figure E-5a). However, over-winter rearing survival was estimated to be higher for fall migrants (average: ~0.5-0.6) than for spring migrants (average: 0.2-0.3), ubiquitously and with relatively homogeneous averages across populations (Figure E-4b). Over-winter survival was also highly variable, such that the highest spring migrant survival values were similar to the lowest fall migrant survival values within each population (Figure E-4b). Survival of smolts to LGR was more variable across populations, with CAT and LGR each averaging ~0.4 and LOS and MIN each averaging ~0.6. During spring out-migration, HOR smolts released into each population in the spring experienced similar average survival to the NOR smolts from the same population (Figure E-4c). Upon reaching LGR, survival through the hydrosystem for NOR and HOR smolts was 0.51 (95% CRL: 0.46-0.57) and 0.57 (95% CRL: 0.48-0.66) in the average year, respectively (Figure E-4d). Although hydrosystem survival was highly variable across years (Figure E-4d), it lacked any major time trend (Supplement, Section 3.2.5). Time series of juvenile survival and abundance outcomes are shown in Supplement, Sections 3-6, and composite rates showing conversions across multiple life stages are shown in Supplement, Section 9.

Ocean Juvenile Phase

Survival during the first year at sea was low for NOR fish: across-year means ranged from 0.08 (95% CRL: 0.05-0.12) for UGR to 0.14 (0.1-0.18) for CAT, yet was highly variable with some rare years seeing survival <0.05 or >0.3 (Figure E-4e). Year-1 ocean survival was lower still for HOR fish – the odds of survival for HOR fish was 0.37 (95% CRL: 0.34-0.4) times that of NOR fish for CAT, though somewhat higher for LOS (0.54; 95% CRL: 0.5-0.59) and UGR (0.51; 0.46-0.56). Recall that we assumed survival in ocean year-2 and year-3 to be time-constant and used stronger priors – we found close consistency between the posterior and prior, though year-3 ocean survival for LOS and UGR were somewhat higher for the posterior than for the prior (Supplement, Section 14.1.2).

Few fish that survived year-1 chose to mature and return as age-3: <10% matured in the average year for NOR fish across all populations (Figure E-5b) with a consistent pattern for higher year-1 maturation rates in HOR fish. In contrast, many more of the fish that did not mature after year-1 and survived year-2 chose to mature as age-4: >75% in the average year and, again we found a pattern of higher maturation rates for HOR fish (Figure E-5c). Higher maturation rates indicate a tendency for HOR fish to return at younger ages than NOR fish. As in all other stochastic quantities presented thus far, maturation rates were quite variable, reaching as high as 30% for year-1 and as low as 30% for year-2.

Freshwater Adult Phase

The only stochastic process model component of the freshwater adult phase was the upstream migration from BON to LGR – ~80% of fish survived this migration in the average year, and compared with other quantites in the model, was not highly variable with values ranging 0.7-0.85. Most of the mortality sources experienced by mature adults were available as auxiliary data sources (i.e., no process or observation model to express them) and are displayed in Supplement, Section 15. These include (*i*) harvest rates below BON (<5% annually for NOR fish and 10-15% for HOR fish), (*ii*) harvest in tributaries (nearly exclusively LOS, <800 annually, primarily HOR and age-4), (*iii*) weir removals (all populations except MIN, <500 fish taken in 90% of year/population combinations since 2000, mostly HOR and age-3 and age-4), and (*iv*) pre-spawn mortality (lowest on average for MIN [0.02] and CAT [0.05], then LOS [0.14], and highest for UGR [0.22]). All mortality sources considered, composite average adult survival rates spanning return to the estuary to spawning ranged from 0.36-0.77, depending on origin and population Supplement, Section 9.5 – overall survival was higher for NOR fish than HOR fish, and was lowest for UGR and highest for MIN; considering all ages versus only age-4 and age-5 did not largely affect these estimates.

Demographic Relationships

Parr capacity was estimated to increase on average by 18,185 (95% CRL: 5,177-31,322) for every 1km increase in WUL (Figure E-6), but population-specific estimates ranged from 23,387 (95%CI: 7,619-61,651) for MIN to 49,635 (95%CI; 13,583-222,184) for UGR. Egg-to-parr survival was moderately or strongly density-dependent depending on the population, evidenced by declining survival with increasing egg production (Figure E-7a). Parr growth rates, indexed by parr mean length (Figure E-7c) too were estimated to be strongly density-dependent – years with the largest sizes (~75mm) corresponded to those with the lowest total egg production, and years of smaller sizes (~60-65mm) corresponded to those with higher densities. Over-winter survival was positively related to parr mean size to varying degrees in all populations except CAT (Figure E-7d): per 1SD increase in mean length (~5mm), the odds of survival changed by a factor of 1.16 (95% CRI 1.09-1.24) for LOS, 1.18 (95% CRI 0.87-1.59) for UGR, and 1.35 (95% CRI 1.2-1.51) for MIN – these rates were assumed to apply equally to fall and spring migrants. The change in mean length from parr to smolt was negatively related to parr size (i.e, greatest multiplicative change for smaller initial lengths; Supplement, Section 5.2.2), but when plotting the relationship between parr and smolt mean length years of larger parr still coincided with years of larger smolt (Figure E-7e). NOR smolt survival during out-migration

to LGR was positively related to smolt mean length, such that per 1SD increase in smolt mean length, the odds of survival for the average population changed by a factor of 1.23 (95% CRL: 1.13-1.33).

Synchronous Process Noise

Estimates of the correlation in process noise among populations were overwhelmingly positive (Figure E-8) – indicating years of higher-than-expected outcomes were shared to some degree among populations. The three processes with the highest correlations were year-1 ocean survival and year-1/year-2 maturation rates – the average correlation across population pairings for these processes had posterior means all >0.5, and no population pairing had posterior mean correlation estimated <0.25. The two processes modeling correlation among origins rather than populations, downstream and upstream mainstem migration survival, both estimated positive but uncertain correlation. Among survival processes, over-winter rearing survival from parr to smolt showed the lowest correlations. The only process that had predominately negative correlations was the probability that parr become fall migrants (Figure E-8).

Analyses of Hypotheticals

Increased Habitat Availability

Based on deterministic process model calculations only, we found that increasing WUL had the effect of weakening density-dependent survival during the freshwater juvenile phase – for a fixed spawner abundance, survival from egg-to-smolt at LGR was higher with increased WUL (Figure E-9a-d), as was parr-to-LGR smolt survival (Figure E-9e-h). The former shows density effects that are both direct (i.e., Beverton-Holt recruitment dynamics) and indirect (i.e., size affects survival, and size is density-dependent), whereas the latter shows only indirect effects. Converted to a relationship between LGR smolt and spawners (Figure E-9i-l), increasing WUL had the effect of increasing the number of smolt produced at a fixed number of spawners; notably, gains in this "recruitment function" were smaller at low spawner densities than at higher densities.

Non-existent Fall Migrants

We found that smolt arrivals to LGR would be lower and more variable if all parr had become spring migrants, rather than the mixture they exhibited in reality (Table E-1). The CAT, LOS, and MIN populations would have all produced 25-30% fewer smolt, and UGR would have produced 8% fewer smolt (26% reduction overall) – the difference is due to the smaller contribution of fall migrants to UGR than other populations (Figure E-5a). As predicted by the portfolio effect, the inter-annual CV of smolt arrivals increased, but not to a major degree – the CV of the aggregation of all populations was 44% with both migratory strategies and 46% with only spring migrants (Table E-1); the differences in variability were larger for populations with greater contribution of fall migrants.

Discussion

Topical Outline *– Will be written by Staton*

- Introductory paragraph: what we did/found; brief advantages and high points
  - Intent was not to identify causes of population status
  - Rather, now have parameterized models that represent hypotheses and their operation under past/current states of nature
    - ▷ With deterministic and stochastic elements decomposed
    - ▷ With stochastic elements decomposed into biological/environmental and observational
  - Able to sample from joint posterior to perform a wide array of useful calculations – 2 were demonstrated.

    - Had we used a simpler approach to analyze data, accounting for uncertainty, missing data, and parameter correlations would have been much more difficult.
- Section – Implications of Findings
    - Paragraph: Habitat Mediates Density-Dependent Relationships
        - Capacity and growth was positively related to quantity of high-quality habitat
        - Size-dependent survival relationships identified, strength varied by life-stage, migratory strategy, and population
        - Suggests density-dependence can be affected by changes in habitat
    - Paragraph: Life History Diversity Important
        - Both strategies are important
        - Most parr are spring migrants but they survive poorly over-winter
        - Opportunity for targeted restoration: small gains in survival would have larger production impact for spring than fall migrants
- Section – Caveats
    - Paragraph: Model Structure Choices
        - Thousands of possible model structures, why this one?
        - Mainstem survival process models very simplistic – not our area of expertise, mostly a bridge between ocean and freshwater model components. More complex models could be swapped in.
        - Tried many combinations of ocean process models, chose one that behaved well computationally and allowed maximal inference regarding Yr1 ocean survival, differences among origins, and maturation.
        - Alterations to retrospective analysis won't have large impacts, because model must recover the same SAR to be consistent with juvenile and adult abundance data.
    - Paragraph: Covariance Among Life Stages
        - Model treats process noise within a given life stage across populations as having non-zero covariance, but assumes processes within populations across life stages have zero covariance.
        - Lack of realism, examples:
            - Better-than-expected years of growth from egg $\rightarrow$ parr may coincide with better-than-expected growth from parr $\rightarrow$ smolt.
            - Better-than-expected years of ocean survival may coincide with years of higher or lower maturation rates.
        - Ultimate consequence: variance of simulated composite outcomes will be higher (likely) than it should be.
        - We chose to model among- rather than within-population covariance because we deemed it more important to evaluating aggregate returns to the Grande Ronde basin, a key output metric for prospective modeling.
- Section – Future Work
    - Prospective simulation modeling
    - Other hypotheses that can be tested
    - Among life stage covariance
    - Application to other populations

Acknowledgments

Topical Outline *– Will be written by Staton*

- Grande Ronde monitoring data collection organizations, countless biologists and technicians from ODFW (La Grande Research Station) and CTUIR
- S. Ellis and K. Self for harvest rate estimates below BON
- Work builds on initial work of T. Cooney
- B. Lessard and T. Garrison gave important input, especially around mainstem and ocean survival
- Internal agency reviewers and anonymous journal-appointed peer reviewers
- Funding sources

Competing Interests

The authors declare no competing interests.

Data Availability

Data used to fit the model are available in the GitHub repository at https://www.github.com/gibsonpp/GR-sslcm-data (archived at **DOI**). The code for model fitting, including the JAGS model definition, data formatting, and posterior summarization is available in the GitHub repository at https://www.github.com/bstaton1/GR-sslcm (archived at **DOI**).[1].

[1]These repositories will be archived and made public upon manuscript submission.

References

Achord, S., Levin, P. S., and Zabel, R. W. 2003. Density-dependent mortality in Pacific salmon: The ghost of impacts past? *Ecology Letters*, 6(4):335–342. doi:10.1046/j.1461-0248.2003.00438.x.

Auger-Méthé, M., Newman, K., Cole, D., Empacher, F., Gryba, R., King, A. A., Leo-Barajas, V., Flemming, J. M., Nielsen, A., Petris, G., and Thomas, L. 2021. A guide to state–space modeling of ecological time series. *Ecological Monographs*, 91(4):e01470. doi:10.1002/ecm.1470.

Barnard, J., McCulloch, R., and Meng, X.-L. 2000. Modeling covariance matrices in terms of standard deviations and correlations, with application to shrinkage. *Statistica Sinica*, 10(4):1281–1311. URL: https://www.jstor.org/stable/24306780.

Beckerman, A., Benton, T. G., Ranta, E., Kaitala, V., and Lundberg, P. 2002. Population dynamic consequences of delayed life-history effects. *Trends in Ecology & Evolution*, 17(6):263–269. doi:10.1016/S0169-5347(02)02469-2.

Bjørnstad, O. N., Ims, R. A., Lambin, X., Bjørnstad, O. N., Ims, R. A., Lambin, X., Bjørnstad, O. N., Ims, R. A., Lambin, X., Bjørnstad, O. N., Ims, R. A., Lambin, X., Bjørnstad, O. N., Ims, R. A., and Lambin, X. 1999. Spatial population dynamics: Analyzing patterns and processes of population synchrony. *Trends in Ecology & Evolution*, 14(11):427–432. doi:10.1016/S0169-5347(99)01677-8.

Bliesner, K. L., Craft, N. M., Feldhaus, J. W., and Ruzycki, J. R. 2020. A compendium of viable salmonid population abundance and productivity field and analysis methods for natural origin adult Chinook salmon populations in the Snake River spring/summer-run ESU of northeast Oregon from 1949-2019. Technical report, Oregon Department of Fish and Wildlife, East Region Fish Research. URL: https://nrimp.dfw.state.or.us/DataClearinghouse/default.aspx?p=202&XMLname=1151.xml.

Bouchard, C., Buoro, M., Lebot, C., and Carlson, S. M. 2022. Synchrony in population dynamics of juvenile Atlantic salmon: Analyzing spatiotemporal variation and the influence of river flow and demography. *Canadian Journal of Fisheries and Aquatic Sciences*, 79(5):782–794. doi:10.1139/cjfas-2021-0017.

Brandt, E. J., Smith, J. D., Feldhaus, J. W., and Ruzycki, J. R. 2021. Lower Snake River Compensation Plan: Oregon spring Chinook salmon evaluation studies, 2019. Annual Progress Report, Oregon Department of Fish and Wildlife, Northeast-Central Oregon Research and Monitoring, Salem, OR. URL: https://www.fws.gov/sites/default/files/documents/2019%20ODFW%20CHS%20Annual%20Report.pdf.

Bürkner, P.-C., Gabry, J., Kay, M., and Vehtari, A. 2023. posterior: Tools for working with posterior distributions. R package version 1.4.1. URL: https://mc-stan.org/posterior/.

Connors, B. M., Siegle, M. R., Harding, J., Rossi, S., Staton, B. A., Jones, M. L., Bradford, M. J., Brown, R., Bechtol, B., Doherty, B., Cox, S., and Sutherland, B. J. G. 2022. Chinook salmon diversity contributes to fishery stability and trade-offs with mixed-stock harvest. *Ecological Applications*, 32(8):e2709. doi:10.1002/eap.2709.

Cooney, T. D., Jonasson, B. C., Sedell, E. R., Hoffnagle, T. L., and Carmichael, R. W. 2017. Grande Ronde spring Chinook populations: Juvenile based models. In *NOAA Fisheries' Interior Columbia Basin Life-Cycle Modeling*, pages 1–30.

Copeland, T. and Venditti, D. A. 2009. Contribution of three life history types to smolt production in a Chinook salmon (*Oncorhynchus tshawytscha*) population. *Canadian Journal of Fisheries and Aquatic Sciences*, 66(10):1658–1665. doi:10.1139/F09-110.

Copeland, T., Venditti, D. A., and Barnett, B. R. 2014. The importance of juvenile migration tactics to adult recruitment in stream-type Chinook salmon populations. *Transactions of the American Fisheries Society*, 143(6):1460–1475. doi:10.1080/00028487.2014.949011.

CTC 1988. Exploitation rate analysis - Appendix 2 to Chinook technical committee 1987 annual report. Technical Report TCCHINOOK (88)-2, CTC Analytical Work Group. URL: https://www.psc.org/download/35/chinook-technical-committee/2150/tcchinook88-2app2.pdf.

DART 2023. PIT tag adult returns conversion rate. URL: https://www.cbr.washington.edu/dart/query/pitadult_conrate.

de Valpine, P. and Hastings, A. 2002. Fitting population models incorporating process noise and observation error. *Ecological Monographs*, 72(1):57–76. doi:10.1890/0012-9615(2002)072[0057:FPMIPN]2.0.CO;2.

de Valpine, P. and Hilborn, R. 2005. State-space likelihoods for nonlinear fisheries time-series. *Canadian Journal of Fisheries and Aquatic Sciences*, 62(9):1937–1952. doi:10.1139/f05-116.

Dunn, P. K. and Smyth, G. K. 1996. Randomized quantile residuals. *Journal of Computational and Graphical Statistics*, 5(3):236–244. doi:10.1080/10618600.1996.10474708.

Fleischman, S. J., Catalano, M. J., Clark, R. A., and Bernard, D. R. 2013. An age-structured state-space stock–recruit model for Pacific salmon (Oncorhynchus spp.). *Canadian Journal of Fisheries and Aquatic Sciences*, 70(3):401–414. doi:10.1139/cjfas-2012-0112.

Gelman, A., Carlin, J. B., Stern, H. S., Dunson, D. B., Vehtari, A., and Rubin, D. B. 2014. *Bayesian Data Analysis*. Texts in Statistical Science. Chapman & Hall/CRC, Boca Raton, FL, 3 edition.

Gelman, A. and Hill, J. 2007. *Data Analysis Using Regression and Multilevel and Hierarchical Models*. Cambridge University Press, New York.

Gibson, P. P., Drascic, F. J., Haynes, D. R., McMichael, G. A., Ofiara, J. A., Raines, M. A., and Warnock, C. R. 2023. Investigations into the life history of naturally produced spring Chinook salmon and summer steelhead in the Grande Ronde River subbasin, 2022. BPA Annual Report for Project 1992-026-04, Oregon Department of Fish and Wildlife, La Grande, OR. URL: https://nrimp.dfw.state.or.us/DataClearinghouse/default.aspx?p=202&XMLname=42707.xml.

González-Megías, A., Gómez, J. M., and Sánchez-Piñero, F. 2005. Consequences of spatial autocorrelation for the analysis of

metapopulation dynamics. *Ecology*, 86(12):3264–3271. doi:10.1890/05-0387.

Grant, J. W. A. and Imre, I. 2005. Patterns of density-dependent growth in juvenile stream-dwelling salmonids. *Journal of Fish Biology*, 67(sB):100–110. doi:10.1111/j.0022-1112.2005.00916.x.

Grossman, G. D. and Simon, T. N. 2020. Density-dependent effects on salmonid populations: A review. *Ecology of Freshwater Fish*, 29(3):400–418. doi:10.1111/eff.12523.

Hansen, B. B., Grøtan, V., Herfindal, I., and Lee, A. M. 2020. The Moran effect revisited: Spatial population synchrony under global warming. *Ecography*, 43(11):1591–1602. doi:10.1111/ecog.04962.

Heino, M., Kaitala, V., Ranta, E., and Lindström, J. 1997. Synchronous dynamics and rates of extinction in spatially structured populations. *Proceedings of the Royal Society of London. Series B: Biological Sciences*, 264(1381):481–486. doi:10.1098/rspb.1997.0069.

Hilborn, R. and Mangel, M. 1997. *The Ecological Detective: Confronting Models with Data*. Number 28 in Monographs in Population Biology. Princeton University Press, Princeton, New Jersey.

Hostetter, N. J., Evans, A. F., Loge, F. J., O'Connor, R. R., Cramer, B. M., Fryer, D., and Collis, K. 2015. The influence of individual fish characteristics on survival and detection: Similarities across two salmonid species. *North American Journal of Fisheries Management*, 35(5):1034–1045. doi:10.1080/02755947.2015.1077176.

Isaak, D. J., Thurow, R. F., Rieman, B. E., and Dunham, J. B. 2003. Temporal variation in synchrony among chinook salmon (*Oncorhynchus tshawytscha*) redd counts from a wilderness area in central Idaho. *Canadian Journal of Fisheries and Aquatic Sciences*, 60(7):840–848. doi:10.1139/f03-073.

Jacobs, G. R., Thurow, R. F., Petrosky, C. E., Osenberg, C. W., and Wenger, S. J. 2023. Life-cycle modeling reveals high recovery potential of at-risk wild Chinook salmon via improved migrant survival. *Canadian Journal of Fisheries and Aquatic Sciences*. doi:10.1139/cjfas-2023-0167.

Kellner, K. 2021. *jagsUI: A Wrapper Around 'rjags' to Streamline 'JAGS' Analyses*. R package version 1.5.2. URL: https://CRAN.R-project.org/package=jagsUI.

Kinzer, R., Arnsberg, B., Harbeck, J., Maxwell, A., Orme, R., Rabe, C., and Vatland, S. 2020. Snake River Basin adult Chinook salmon and steelhead monitoring, 2019. Annual Report, Nez Perce Tribe, Department of Fisheries Resources Management, Research Division, Lapwai, ID. URL: https://www.fws.gov/sites/default/files/documents/2019%20NPT%20Snake%20River%20Basin%20Adult%20Chinook%20Salmon%20and%20Steelhead%20Monitoring.pdf.

Lindén, A. and Knape, J. 2009. Estimating environmental effects on population dynamics: Consequences of observation error. *Oikos*, 118(5):675–680. doi:10.1111/j.1600-0706.2008.17250.x.

McCann, J., Chockley, B., Cooper, E., Scheer, G., Haeseker, S., Lessard, B., Copeland, T., Ebel, J., Storch, A., and Rawding, D. 2022. Comparative survival study of PIT-tagged spring/summer/fall Chinook, summer steelhead, and sockeye, 2022. Annual Report BPA Contract #19960200, CSS Oversight Committee and Fish Passage Center, Portland, OR. URL: https://www.fpc.org/documents/CSS/CSS%20Final%20Revised%202022.pdf.

Moussalli, E. and Hilborn, R. 1986. Optimal stock size and harvest rate in multistage life history models. *Canadian Journal of Fisheries and Aquatic Sciences*, 43(1):135–141. doi:10.1139/f86-014.

Myers, R. A. and Barrowman, N. J. 1995. Time series bias in the estimation of density-dependent mortality in stock-recruitment models. *Canadian Journal of Fisheries and Aquatic Sciences*, 52(1):223–232. doi:10.1139/f95-022.

Myrvold, K. M. and Kennedy, B. P. 2015. Density dependence and its impact on individual growth rates in an age-structured stream salmonid population. *Ecosphere*, 6(12):1–16. doi:10.1890/ES15-00390.1.

Naylor, L., Crump, C., Van Sickle, A., and Startzel-Holt, B. 2019. Monitoring and evaluation of supplemented spring Chinook salmon and life histories of wild summer steelhead in the Grande Ronde Basin. Annual Report for BPA Project #2007-083-00, Confederated Tribes of the Umatilla Indian Reservation, Pendleton, OR. URL: https://www.cbfish.org/Document.mvc/Viewer/P164991.

Newman, K., King, R., Elvira, V., de Valpine, P., McCrea, R. S., and Morgan, B. J. T. 2023. State-space models for ecological time-series data: Practical model-fitting. *Methods in Ecology and Evolution*, 14(1):26–42. doi:10.1111/2041-210X.13833.

Ohlberger, J., Schindler, D. E., Brown, R. J., Harding, J. M. S., Adkison, M. D., Munro, A. R., Horstmann, L., and Spaeder, J. 2020. The reproductive value of large females: Consequences of shifts in demographic structure for population reproductive potential in Chinook salmon. *Canadian Journal of Fisheries and Aquatic Sciences*, 77(8):1292–1301. doi:10.1139/cjfas-2020-0012.

Ohlberger, J., Ward, E. J., Schindler, D. E., and Lewis, B. 2018. Demographic changes in Chinook salmon across the Northeast Pacific Ocean. *Fish and Fisheries*, 19(3):533–546. doi:10.1111/faf.12272.

Perry, R. W., Plumb, J. M., Hance, D. J., and Tiffan, K. F. 2020. Using a state-space life-cycle model to simulate population trajectories of natural-origin Snake River Basin fall Chinook slamon under the 2020 biological opinion proposed action. In Tiffan, K. F. and Perry, R. W., editors, *Research, Monitoring, and Evaluation of Emerging Issues and Measures to Recover the Snake River Fall Chinook Salmon ESU*, BPA Annual Report for Project #199102900, pages 82–120. United States Geological Survey, Cook, WA. URL: https://doi.org/10.13140/RG.2.2.23170.30406.

Plummer, M. 2003. JAGS: A program for analysis of Bayesian graphical models using Gibbs sampling. *3rd International Workshop on Distributed Statistical Computing (DSC 2003); Vienna, Austria*, 124. URL: https://www.r-project.org/conferences/DSC-2003/Drafts/Plummer.pdf.

Polansky, L., Newman, K. B., and Mitchell, L. 2021. Improving inference for nonlinear state-space models of animal population

dynamics given biased sequential life stage data. *Biometrics*, 77(1):352–361. doi:10.1111/biom.13267.

Punt, A. E., Butterworth, D. S., de Moor, C. L., Oliveira, J. A. A. D., and Haddon, M. 2016. Management strategy evaluation: Best practices. *Fish and Fisheries*, 17(2):303–334. doi:10.1111/faf.12104.

R Core Team 2023. *R: A Language and Environment for Statistical Computing*. R Foundation for Statistical Computing, Vienna, Austria. R Version 4.3.0. URL: https://www.R-project.org/.

Ranta, E., Kaitala, V., Lindström, J., and Helle, E. 1997. The Moran effect and synchrony in population dynamics. *Oikos*, 78(1):136–142. doi:10.2307/3545809.

Reed, J. M., Mills, L. S., Dunning Jr., J. B., Menges, E. S., McKelvey, K. S., Frye, R., Beissinger, S. R., Anstett, M.-C., and Miller, P. 2002. Emerging issues in population viability analysis. *Conservation Biology*, 16(1):7–19. doi:10.1046/j.1523-1739.2002.99419.x.

Riecke, T. V., Sedinger, B. S., Williams, P. J., Leach, A. G., and Sedinger, J. S. 2019. Estimating correlations among demographic parameters in population models. *Ecology and Evolution*, 9(23):13521–13531. doi:10.1002/ece3.5809.

Rivot, E., Prévost, E., Parent, E., and Baglinière, J. L. 2004. A Bayesian state-space modelling framework for fitting a salmon stage-structured population dynamic model to multiple time series of field data. *Ecological Modelling*, 179(4):463–485. doi:10.1016/j.ecolmodel.2004.05.011.

Rose, K. A., Cowan, J. H., Winemiller, K. O., Myers, R. A., and Hilborn, R. 2001. Compensatory density dependence in fish populations: Importance, controversy, understanding and prognosis. *Fish and Fisheries*, 2(4):293–327. doi:10.1046/j.1467-2960.2001.00056.x.

Schindler, D. E., Armstrong, J. B., and Reed, T. E. 2015. The portfolio concept in ecology and evolution. *Frontiers in Ecology and the Environment*, 13(5):257–263. doi:10.1890/140275.

Staton, B. 2022. *postpack: Utilities for Processing Posterior Samples Stored in 'mcmc.lists'*. R package version 0.5.4. URL: https://CRAN.R-project.org/package=postpack.

Staton, B., Justice, C., Kaylor, M., and Ringelman, A. 2023. Objective E-1: Grande Ronde phase 12 - development of a spring Chinook statistical estimation life cycle model. In *Evaluating Salmonid and Stream Ecosystem Response to Conservation Measures and Environmental Stressors in the Columbia River Basin*, Annual Report for BPA Project #2009-004-00, pages 69–83. Columbia River Inter-Tribal Fish Commission, Portland, OR. URL: https://critfc.org/wp-content/uploads/2023/07/23_03.pdf.

Staton, B. A., Catalano, M. J., Connors, B. M., Jr, L. G. C., Jones, M. L., Walters, C. J., Fleischman, S. J., and Gwinn, D. C. 2020. Evaluation of methods for spawner–recruit analysis in mixed-stock Pacific salmon fisheries. *Canadian Journal of Fisheries and Aquatic Sciences*, 77(7):1149–1162. doi:10.1139/cjfas-2019-0281.

Staton, B. A., Catalano, M. J., and Fleischman, S. J. 2017. From sequential to integrated Bayesian analyses: Exploring the continuum with a Pacific salmon spawner-recruit model. *Fisheries Research*, 186:237–247. doi:10.1016/j.fishres.2016.09.001.

Staton, B. A., Catalano, M. J., Fleischman, S. J., and Ohlberger, J. 2021. Incorporating demographic information into spawner–recruit analyses alters biological reference point estimates for a western Alaska salmon population. *Canadian Journal of Fisheries and Aquatic Sciences*, 78(12):1755–1769. doi:10.1139/cjfas-2020-0478.

Staton, B. A., Justice, C., White, S., Sedell, E. R., Burns, L. A., and Kaylor, M. J. 2022. Accounting for uncertainty when estimating drivers of imperfect detection: An integrated approach illustrated with snorkel surveys for riverine fishes. *Fisheries Research*, 249:106209. doi:10.1016/j.fishres.2021.106209.

Su, Z. 2023. Evaluation of management performance of a new state-space model for pink salmon (*Oncorhynchus gorbuscha*) stock–recruitment analysis. *Canadian Journal of Fisheries and Aquatic Sciences*, 80(8):1268–1288. doi:10.1139/cjfas-2022-0262.

Su, Z. and Peterman, R. M. 2012. Performance of a Bayesian state-space model of semelparous species for stock-recruitment data subject to measurement error. *Ecological Modelling*, 224(1):76–89. doi:10.1016/j.ecolmodel.2011.11.001.

Thorson, J. T., Scheuerell, M. D., Buhle, E. R., and Copeland, T. 2014. Spatial variation buffers temporal fluctuations in early juvenile survival for an endangered Pacific salmon. *Journal of Animal Ecology*, 83(1):157–167. doi:10.1111/1365-2656.12117.

Vehtari, A., Gelman, A., Simpson, D., Carpenter, B., and Bürkner, P.-C. 2021. Rank-Normalization, Folding, and Localization: An Improved Rhat for Assessing Convergence of MCMC (with Discussion). *Bayesian Analysis*, 16(2):667–718. doi:10.1214/20-BA1221.

Walters, A. W., Copeland, T., and Venditti, D. A. 2013. The density dilemma: Limitations on juvenile production in threatened salmon populations. *Ecology of Freshwater Fish*, 22(4):508–519. doi:10.1111/eff.12046.

Walters, C. J. 1985. Bias in the estimation of functional relationships from time series data. *Canadian Journal of Fisheries and Aquatic Sciences*, 42(1):147–149. doi:10.1139/f85-018.

Walters, C. J. and Martell, S. J. D. 2004. *Fisheries Ecology and Management*. Princeton University Press, Princeton, New Jersey.

Zabel, R. W. and Achord, S. 2004. Relating size of juveniles to survival within and among populations of Chinook salmon. *Ecology*, 85(3):795–806. doi:10.1890/02-0719.

Zabel, R. W. and Levin, P. S. 2002. Simple assumptions on age composition lead to erroneous conclusions on the nature of density dependence in age-structured populations. *Oecologia*, 133(3):349–355. doi:10.1007/s00442-002-1051-0.

Zabel, R. W., Scheuerell, M. D., McClure, M. M., and Williams, J. G. 2006. The interplay between climate variability and density dependence in the population viability of Chinook salmon. *Conservation Biology*, 20(1):190–200. doi:10.1111/j.1523-1739.2005.00300.x.

TABLE E-1. Inter-annual mean and coefficient of variation (%CV) of NOR smolt reaching LGR in the presence (real) and hypothetical absence of the fall migrant life history type. Findings indicate that smolt abundance would have been lower on average and more variable across years if all parr had been spring migrants.

	Inter-Annual Mean			Inter-Annual %CV	
	Real[1,3]	**All Spring[2,3]**	**%Δ**	**Real[1]**	**All Spring[2]**
CAT	5.5 (0.3)	3.9 (0.2)	-30% (3%)	51% (8%)	59% (9%)
LOS	16.3 (0.8)	11.1 (0.6)	-32% (2%)	58% (8%)	59% (7%)
MIN	23.1 (1.2)	17.2 (1.1)	-25% (2%)	51% (5%)	57% (6%)
UGR	6.5 (0.5)	5.9 (0.5)	-8% (1%)	80% (9%)	79% (10%)
Total	51.3 (1.8)	38.1 (1.5)	-26% (1%)	44% (4%)	46% (4%)

Posterior summaries represented as mean (standard deviation).

[1] Based on the observed time series, in which both spring and fall migrants were present.

[2] Based on the hypothetical case where no parr recruits were fall migrants – calculated after model fitting by assuming all parr recruits experience the higher mortality rates of the spring migrant life history type.

[3] Abundance expressed as thousands of natural-origin smolt reaching Lower Granite Dam.

FIGURE E-1. Map of the Grande Ronde River basin, showing the watersheds for the four populations we model, the location of fish monitioring projects, and the extent of Chinook Salmon spawning in each tributary.

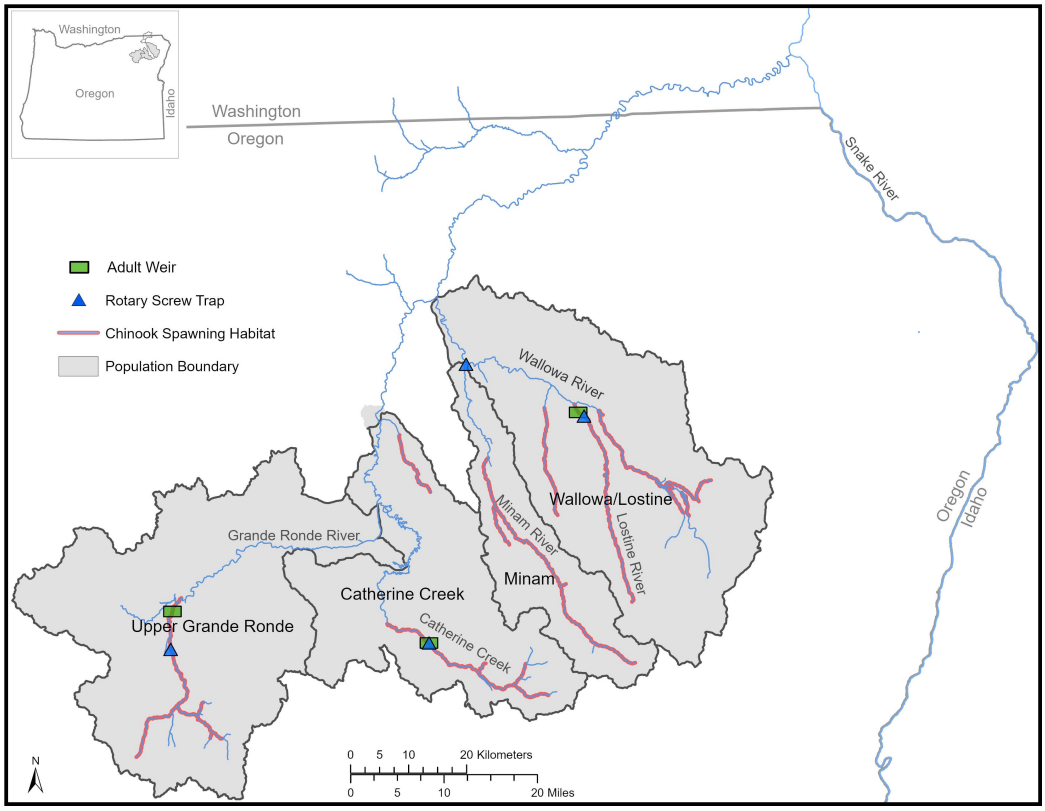

FIGURE E-2. Schematic of the life stages and transitions captured in the state-space life cycle model for Grande Ronde spring Chinook Salmon. Diagram shows one generation for one population. Boxes represent abundances of fish (states), arrows represent changes (rates) among stages, and circled numbers represent quantities with data sources informing them. Blue states have associated mean length, and blue arrows are expressed as functions of mean length.

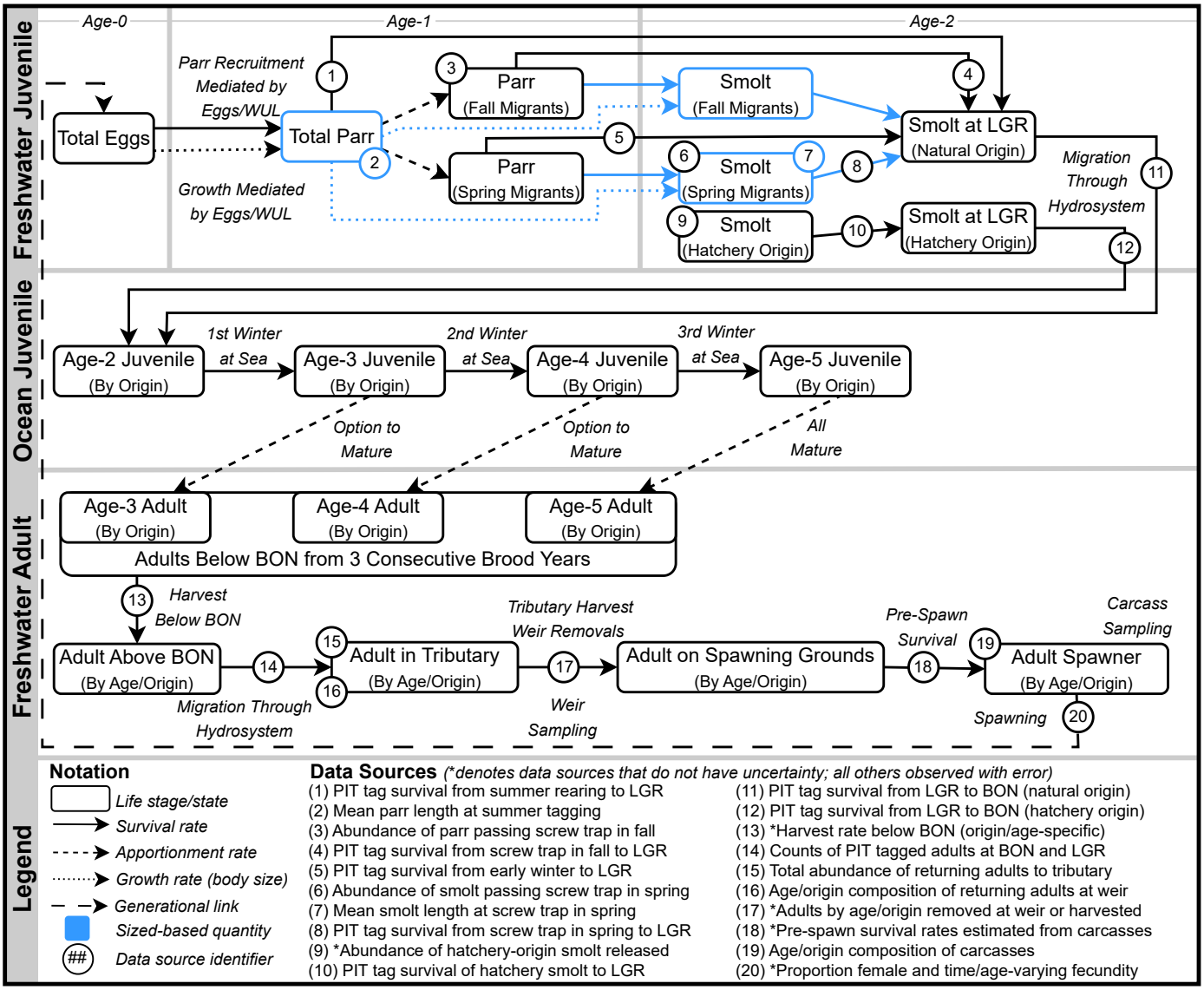

FIGURE E-3. Consistency between fitted values (posterior means) and point estimates for nearly all data sources with an explicit likelihood function; only parr and smolt mean length data have been omitted here for space. Each data point is one year for one population, with the exceptions of panels *g*, *h*, and *i*, which display values for both NOR and HOR survival rates, and in the cases of *h* and *i*, these rates apply equally to all populations. More detailed visualizations of model fit are shown in the Supplement (Section 3: model fits as time series with magnitude of observation uncertainty shown; Section 11: diagnostics based on quantile-standardized residuals; Section 12: posterior predictive checks).

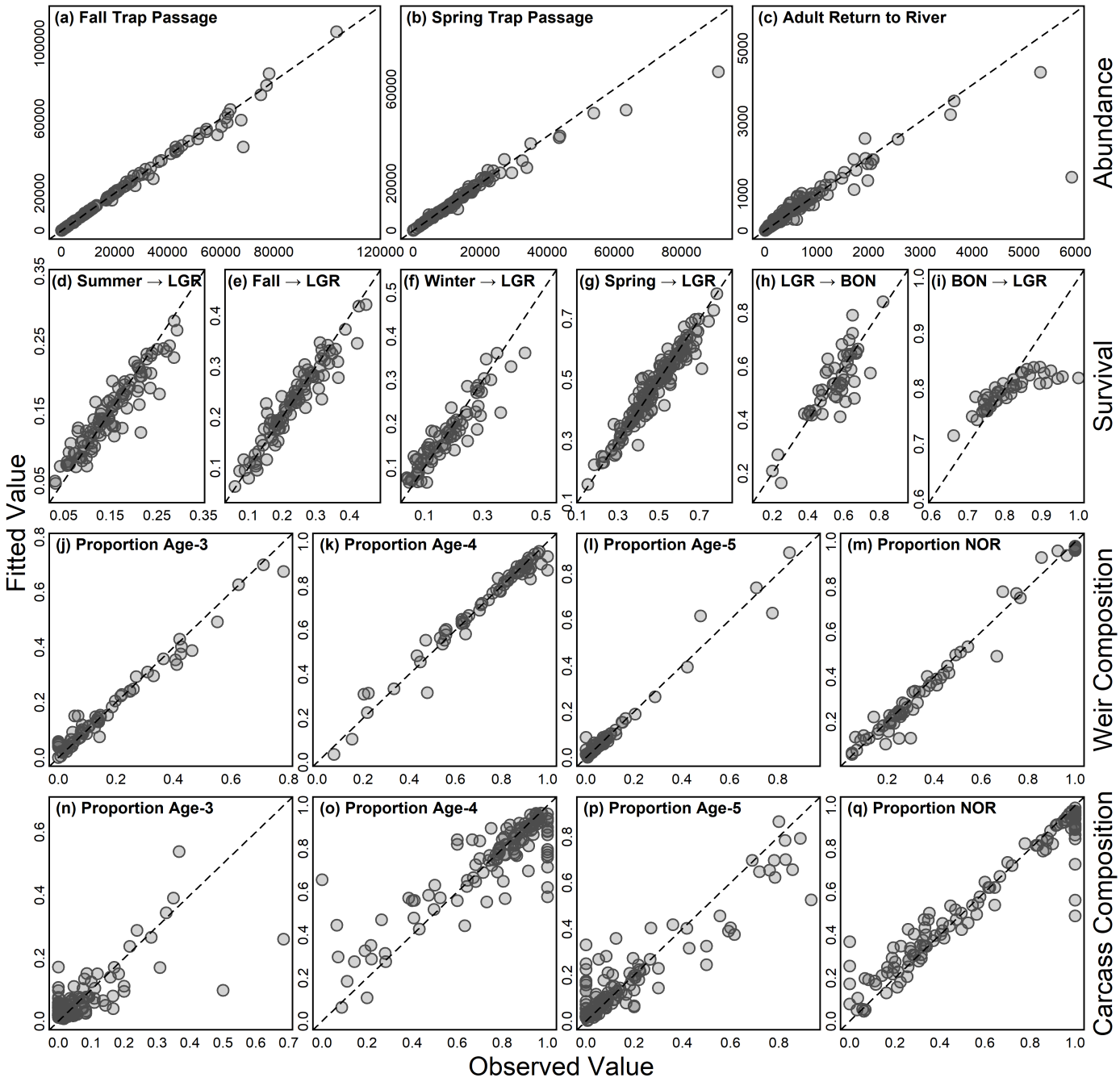

FIGURE E-4. Survival probability parameters estimated by the state-space model, separated by stage transition and other demographic features (migratory type, origin, population) where applicable. Small points show posterior means of year-specific latent values (jitter for visual effect only) and large points show the average across years. Information about mortality due to sources/stages not displayed here was either assumed known without error (e.g., prespawn mortality) or expressed as strong prior information with no inter-annual variability (i.e., mortality experienced in ocean-1 → ocean-2 and ocean-2 → ocean-3).

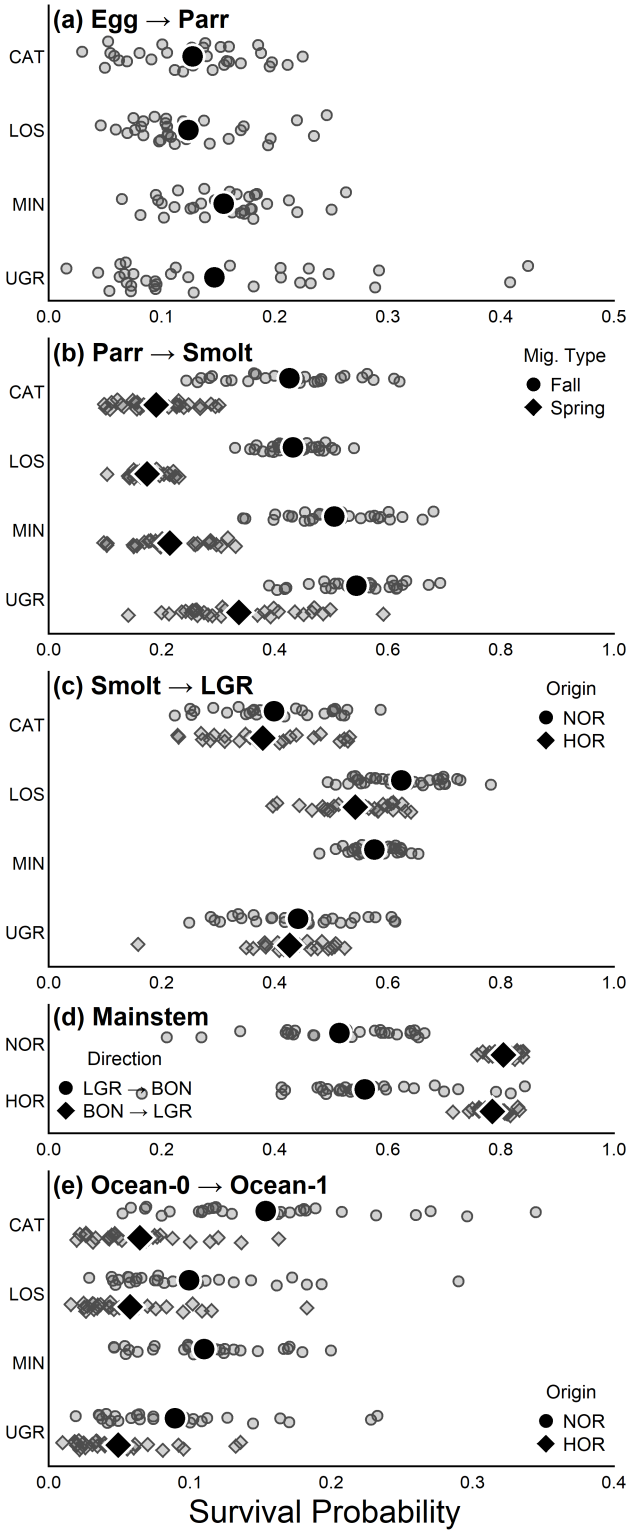

FIGURE E-5. Transition probability parameters (unrelated to survival) estimated by the state-space model, separated by life stage, popoulation, and origin (where applicable). Small points show posterior means of year-specific latent values (jitter for visual effect only) and large points show the average across years.

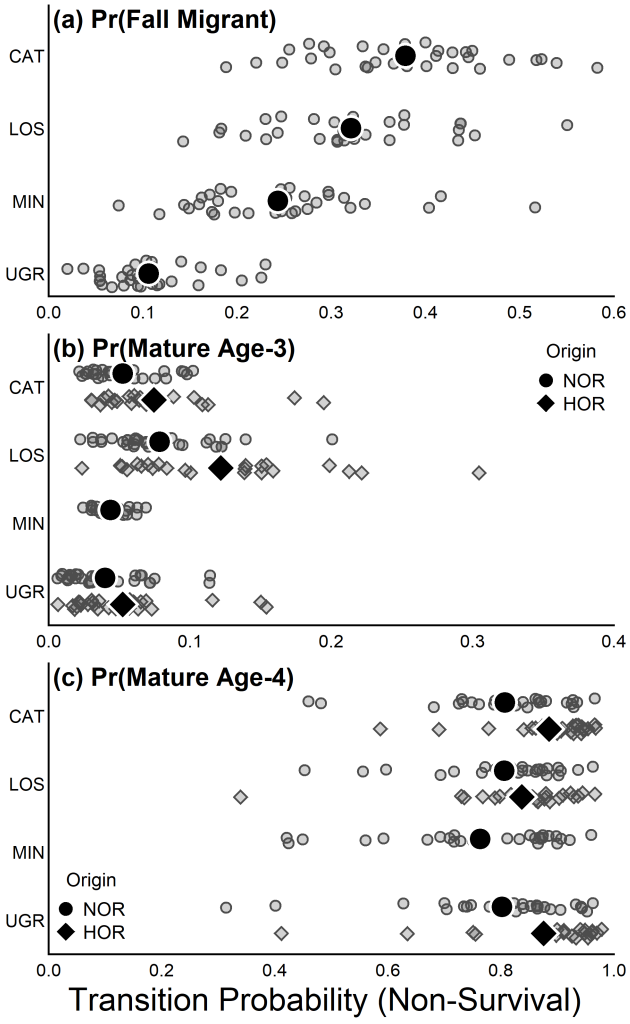

FIGURE E-6. Estimated relationship between parr capacity and weighted usable habitat length (WUL). Darker gray/thicker error bars represent 80% credible regions and lighter gray/thinner error bars represent 95% credible regions.

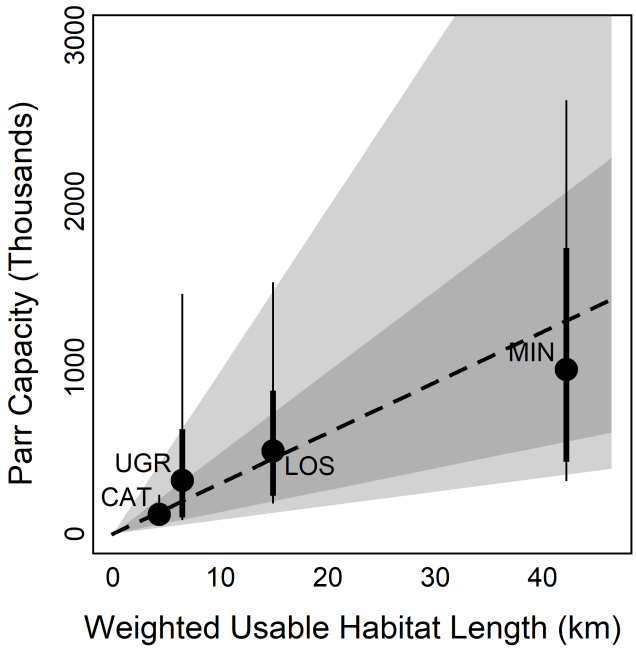

FIGURE E-7. Estimated relationships showing density effects on recruitment (panels *a* and *b*) and mean length (panel *c*), and length effects on future length (panel *e*) and survival (panels *d* and *f*). Process model deterministic relationships are shown as the posterior mean (thick line) and 95% credible region (shaded region); points show latent values. Panels within the same row show the process model relationship for each of the four populations; *x*- and *y*-axis limits are identical for all panels within a row.

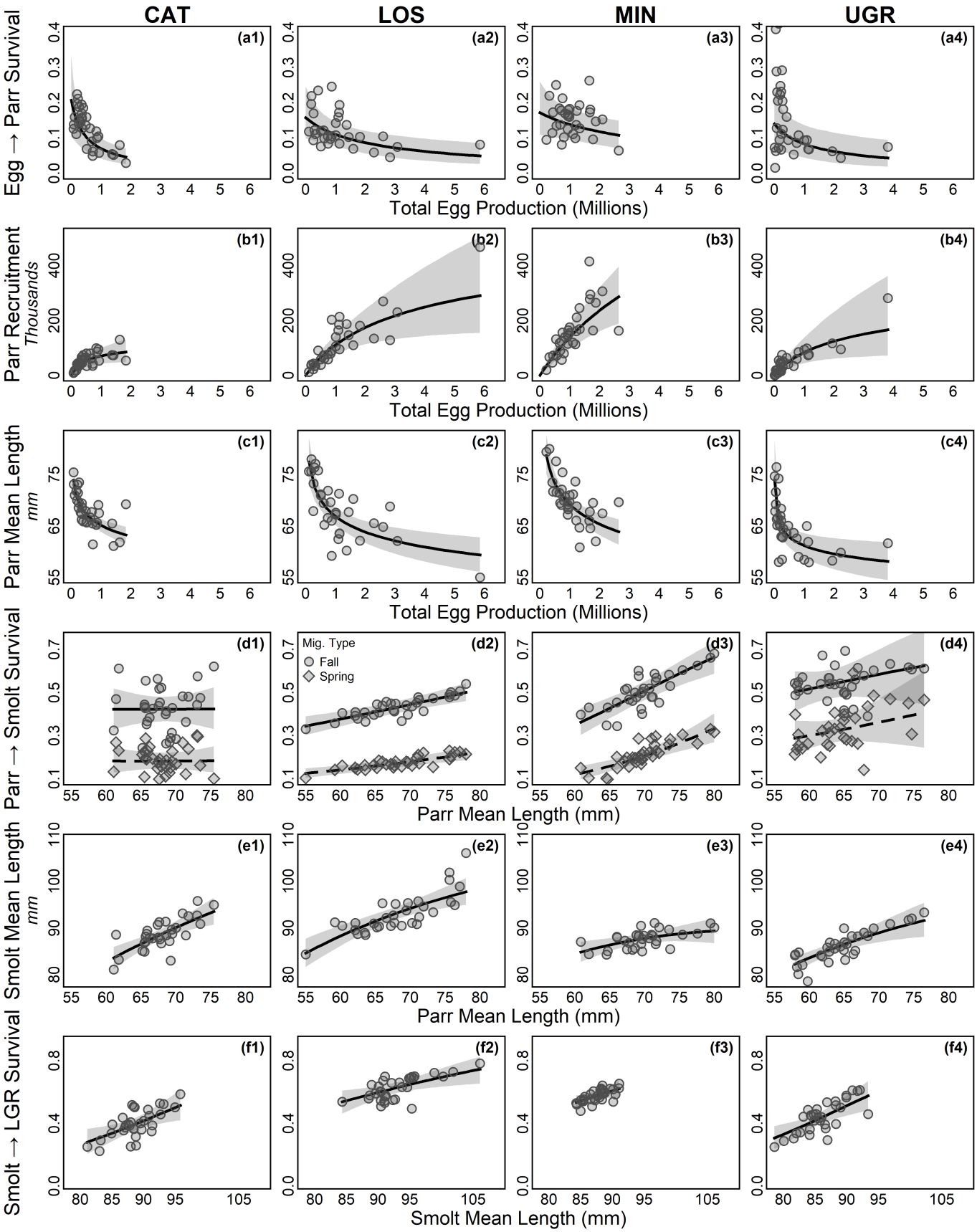

FIGURE E-8. Correlation terms of the covariance matrices controlling process variability. Posterior means of population pair-specific correlations are displayed as points, and the posterior of the average of the 6 pairs is summarized in black (thin lines are 95% CRIs, thick lines 50% CRIs, and cross marks are means). Survival processes are denoted by $x \rightarrow y$, whereas non-survival transition processes are denoted by $\Pr(x)$. The correlation in survival processes representing the migration downstream and upstream through the mainstem (LGR $\rightarrow$ BON and BON $\rightarrow$ LGR, respectively) represent among-origin correlation, hence the lack of points.

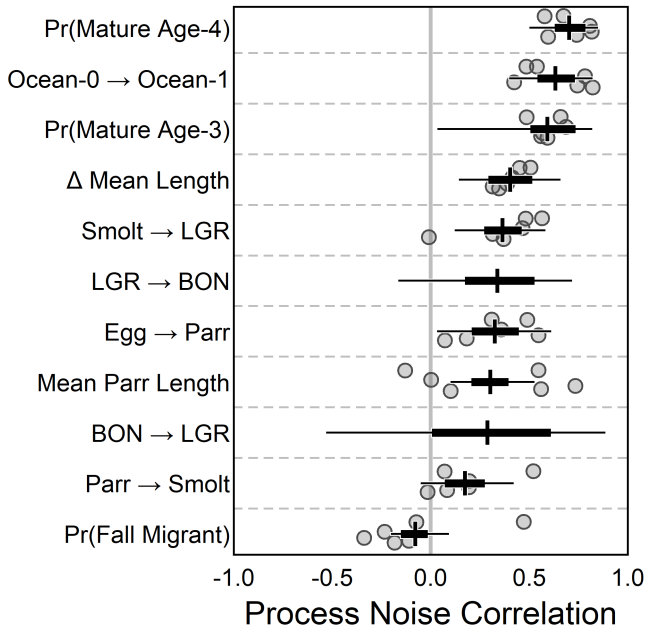

FIGURE E-9. Freshwater juvenile density-dependent relationships under current (solid lines) and increased (broken lines) weighted usable habitat (WUL). Panels (*a-d*): composite survival from egg-to-smolt at LGR including both direct (i.e., egg density affects egg survival via Beverton-Holt dynamics) and indirect (i.e., egg density affects growth rates, size affects parr and smolt survival) density effects; panels (*e-h*): composite survival from parr-to-smolt at LGR which includes only indirect effects; panels (*i-l*): smolt reaching LGR. Calculations operate based on density of eggs – *x*-axis converted to approximate spawner abundance (all ages, origins, and sexes) for ease of interpretation. Gray bands show the 95% credible region for the current relationship only; lines show posterior means.

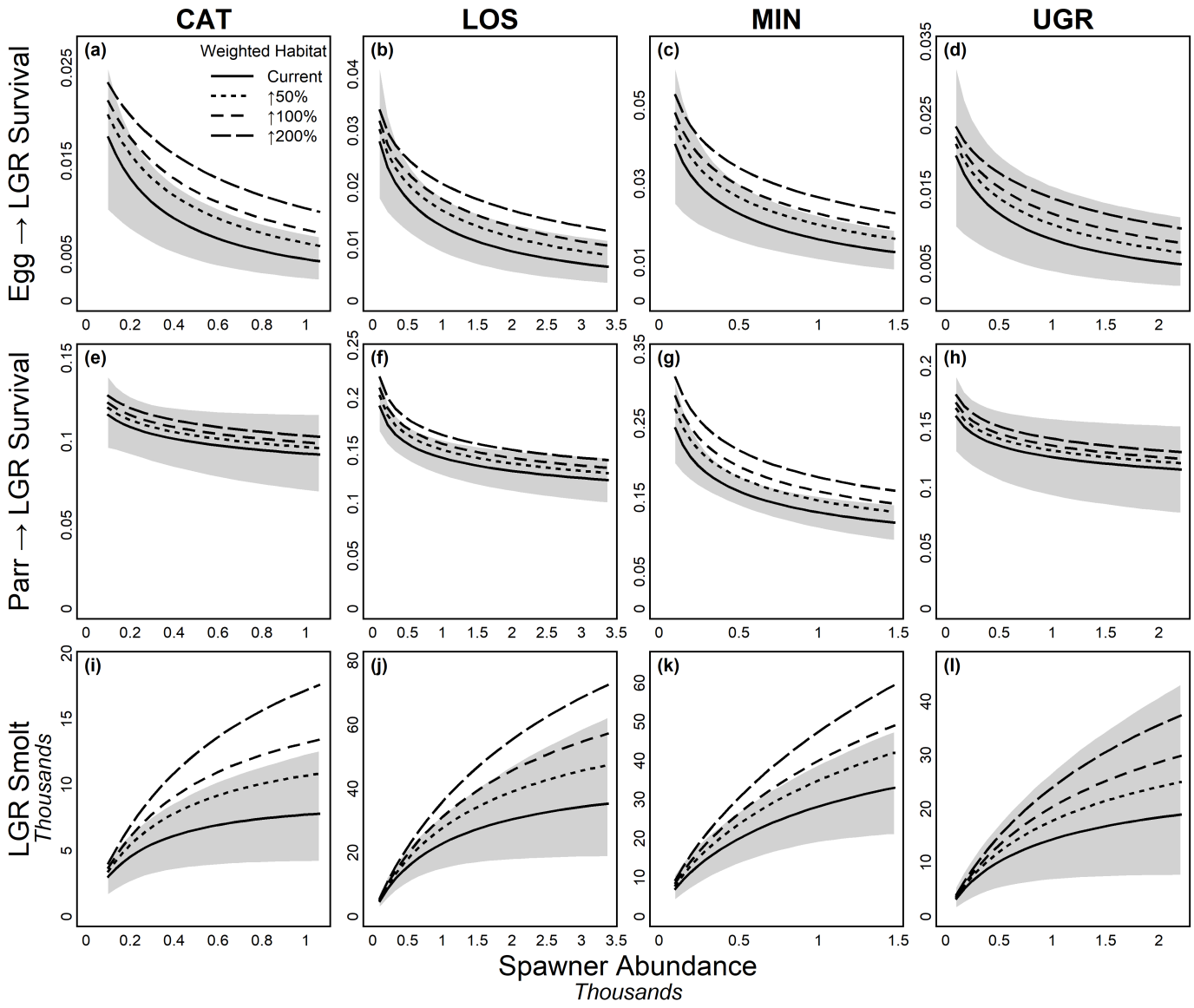

Appendix F Grande Ronde LCM Math Description

Syntactical and Statistical Conventions

The state-space life cycle model symbology aims for consistency in mathematical representation of quantities but this has created some conventions that require devoted explanation. All quantities are defined in Tables F-1, F-2, F-3, and F-4 and a catalog of all equations is provided in Table F-5.

(1) For simplicity, the term "adult" is used to refer to any mature individual returning to spawn, including age-3 "jacks".

(2) Life stage-specific states are defined by capital letters, these include: eggs (E), parr (P), smolt (M), ocean juveniles (O), adults returning to river (R), or adults with potential to spawn (S).

(3) Parameters (e.g., survival terms, non-survival transition probabilities, coefficients in relationships, etc.) are predominately denoted by Greek symbols and are used consistently where possible, e.g., ϕ for survival rates or ψ for maturation rates.

(4) Subscripts denote placement of a quantity in a larger array (i.e., the index), e.g., y denotes a specific year and j a specific population (see Table F-1).

(5) Superscripts are most often used syntactically to further describe the quantity, not in a mathematical sense. E.g., M^b represents smolt abundance *before* out-of-basin migration and M^a represents smolt abundance *after* out-of-basin migration. As such, M^b is not "M raised to the power b"; if the quantity M^b must be raised to the power c, it will be written $(M^b)^c$.

(6) Survival terms to transition from state A to state B in year y for population j are denoted by $\phi_{y,j}^{A\rightarrow B}$.

(7) The expected value of a stochastic process is expressed by a dot, e.g., $\dot{\phi}_j^{A\rightarrow B}$ – this is the value expected in the absence of process (biological/environmental) variability.

(8) In some cases, calculations are performed on vectors rather than scalars. Vectors are denoted via boldface, and the dimension of the vector is denoted using $1{:}n$ syntax. E.g., $\boldsymbol{\phi}_{y,1:n_j}^{A\rightarrow B}$ represents a vector of parameters representing the transition (survival) probability from state A to state B in year y, where each element stores the value for each population.

(9) Mathematical operations performed on two vectors $\boldsymbol{C}$ and $\boldsymbol{D}$ are performed in an element-wise fashion, and the resulting vector will have identical dimensions to both $\boldsymbol{C}$ and $\boldsymbol{D}$.

(10) In some cases, a calculation is performed differently for a subset of the possible index values. For example, to denote that k should take on only the values of 1 and 3 (not 2), we would write, $k \in [1, 3]$.

(11) $\log(x)$ represents the natural logarithm of x and it is implied that the constraint $x > 0$ is satisfied.

(12) $\text{logit}(p)$ represents the log odds of p (i.e., $\log[p/(1-p)]$)) and it is implied that the constraint $0 < p < 1$ is satisfied.

(13) All quantities are used in a likelihood component are denoted by a "hat", e.g., a survival term ($\hat{\phi}_{y,j}^{A\rightarrow B}$) and its logit-normal standard error ($\hat{\sigma}_{\phi_{y,j}^{A\rightarrow B}}$, which is used as a direct estimate of observation error variability).

(14) Stochastic processes are represented by $x_y \sim \text{F}(\theta_1, \theta_2)$, where x_y is a random variable, F() is some probability density (mass) function (N() for univariate normal, MVN() for multivariate normal, B() for binomial, b() for beta, M() for multinomial, D() for Dirichlet, SIW() for scaled inverse-Wishart, and U() for uniform), and θ_1 and θ_2 are parameters of the probability distribution.

Process noise was modeled by assuming year-specific values are multivariate logit-normal random variables around the deterministic value. This enabled modeling covariability in demographic rates (Riecke et al. 2019; Bouchard et al. 2022) among populations or origins, which is advantageous for estimation involving incompletely overlapping time series and provides useful ecological insights by quantifying synchrony in demographic rates (Thorson et al. 2014; Connors et al. 2022). The covariance matrices of these random variables are denoted by Σ, and have a common structure for all model components. Take the hypothetical survival term $\phi_{y,j}^{A\to B}$ as an example. The random process introducing inter-annual variability and inter-population covariability is expressed as:

$$\operatorname{logit}\left(\boldsymbol{\phi}_{y,1:n_j}^{A\to B}\right) \sim \operatorname{MVN}\left[\operatorname{logit}\left(\dot{\boldsymbol{\phi}}_{y,1:n_j}^{A\to B}\right), \Sigma_{\phi^{A\to B}}\right] \tag{F-1}$$

where $\Sigma_{\phi^{A\to B}}$ is an $n_j \times n_j$ matrix constructed of population-specific variance terms $\left(\sigma_{\phi_j^{A\to B}}\right)^2$ and correlation terms specific to each pair of populations j and j' $\rho_{\phi_{j,j'}^{A\to B}}$:

$$\begin{bmatrix} \left(\sigma_{\phi_{j=1}^{A\to B}}\right)^2 & \sigma_{\phi_{j=1}^{A\to B}} \cdot \sigma_{\phi_{j=2}^{A\to B}} \cdot \rho_{\phi_{j=1,j'=2}^{A\to B}} & \dots & \sigma_{\phi_{j=1}^{A\to B}} \cdot \sigma_{\phi_{j=n_j}^{A\to B}} \cdot \rho_{\phi_{j=1,j'=n_j}^{A\to B}} \\ \sigma_{\phi_{j=2}^{A\to B}} \cdot \sigma_{\phi_{j=1}^{A\to B}} \cdot \rho_{\phi_{j=2,j'=1}^{A\to B}} & \left(\sigma_{\phi_{j=2}^{A\to B}}\right)^2 & \dots & \sigma_{\phi_{j=2}^{A\to B}} \cdot \sigma_{\phi_{j=n_j}^{A\to B}} \cdot \rho_{\phi_{j=2,j'=n_j}^{A\to B}} \\ \vdots & \vdots & \ddots & \vdots \\ \sigma_{\phi_{j=n_j}^{A\to B}} \cdot \sigma_{\phi_{j=1}^{A\to B}} \cdot \rho_{\phi_{j=n_j,j'=1}^{A\to B}} & \sigma_{\phi_{j=n_j}^{A\to B}} \cdot \sigma_{\phi_{j=2}^{A\to B}} \cdot \rho_{\phi_{j=n_j,j'=2}^{A\to B}} & \dots & \left(\sigma_{\phi_{j=n_j}^{A\to B}}\right)^2 \end{bmatrix} \tag{F-2}$$

In cases where a quantity varies annually and covaries by origin but is identical across populations, $\Sigma_{\phi^{A\to B}}$ would have dimensions $n_o \times n_o$:

$$\begin{bmatrix} \left(\sigma_{\phi_{o=1}^{A\to B}}\right)^2 & \sigma_{\phi_{o=1}^{A\to B}} \cdot \sigma_{\phi_{o=2}^{A\to B}} \cdot \rho_{\phi^{A\to B}} \\ \sigma_{\phi_{o=2}^{A\to B}} \cdot \sigma_{\phi_{o=1}^{A\to B}} \cdot \rho_{\phi^{A\to B}} & \left(\sigma_{\phi_{o=2}^{A\to B}}\right)^2 \end{bmatrix} \tag{F-3}$$

Covariance matrices have certain constraints, which makes them difficult to estimate (Barnard et al. 2000). One solution is to use an inverse-Wishart distribution – random variables from which meet the positive definite constraint – as a prior for modeling covariance matrices (Gelman and Hill 2007; Gelman et al. 2014). Although Riecke et al. (2019) recommend against the use of this prior distribution, they provided an alternative "separation strategy" only for the case of 2×2 covariance matrices; Barnard et al. (2000) proposed a strategy for the general $n \times n$ case. As most of our matrices were 4×4, we attempted the Barnard et al. (2000) approach, however the MCMC sampler we used did not permit it, and it would have been very computationally inefficient even if possible. Thus, we used the more convenient scaled inverse-Wishart distribution as the prior, which solves some of the issues of the unscaled version (Gelman and Hill 2007; Gelman et al. 2014; Plummer 2017, Table F-3). Although the stochastic process requires the Σ term, the component σ and ρ terms were the parameters of interest for inference regarding magnitude of inter-annual

variability and synchrony.

Freshwater Juvenile Phase

Process Model

Egg Production, Parr Recruitment, and Parr Mean Length

The life cycle begins at the egg stage immediately after spawning. Total egg production was the sum product of age-specific spawner abundance ($S^{a}_{y,k,o,j}$, from eq. F-42, below), proportion female-at-age (Ω_k), and fecundity-at-age ($f_{y,k,j}$):

$$E_{y,j} = \sum_{o}^{n_o} \sum_{k}^{n_k} S^{a}_{y,k,o,j} \cdot \Omega_k \cdot f_{y,k,j} \tag{F-4}$$

Spawners of age-4 or age-5 were assumed to be 50% female and age-3 spawners were assumed 100% male (i.e., $\Omega_{k=1} = 0$; $\Omega_{k\in[2,3]} = 0.5$; approximately equal to values estimated from carcass data). Fecundity was predicted from length-fecundity relationships based on Grande Ronde-origin hatchery broodstock and time-varying mean length-at-age data (ODFW, unpublished). Both Ω_k and $f_{y,k,j}$ were assumed known without error.

Expected egg-to-parr survival was assumed to be a density-dependent process following Beverton-Holt dynamics with "productivity" parameter α_j (i.e., theoretical maximum egg-to-parr survival probability, in the absence of density effects) and capacity parameter β_j (i.e., theoretical maximum parr recruitment abundance):

$$\dot{\phi}^{E\rightarrow P^b}_{y,j} = \frac{1}{\frac{1}{\alpha_j} + \frac{E_{y,j}}{\beta_j}} \tag{F-5}$$

To facilitate later analyses (not documented here) investigating the effects of habitat restoration and climate change on population dynamics, parr capacity was modeled as a function of weighted usable habitat length specific to each population (WUL_j)[1]:

$$\log(\beta_j) \sim \mathrm{N}\left[\log(\lambda \cdot \mathrm{WUL}_j), \sigma_\beta\right] \tag{F-6}$$

where λ is the expected change in parr capacity per 1 km change in weighted usable habitat length, and σ_β is the log-normal standard deviation of variability in this relationship not captured by WUL values.

Realized (i.e., with process noise) egg-to-parr survival was a multivariate logit-normal random variable around the expected value ($\dot{\phi}^{E\rightarrow P^b}_{y,j}$) from eq. F-5. Rather than assume egg-to-parr survival anomalies (i.e.,

[1] Derivation of WUL_j is too detailed to describe fully here. Briefly, the relative ability of stream segments with different habitat characteristics to hold rearing parr was expressed in terms of the density of fish predicted to reside there by a complex generalized linear mixed model. The model was fitted to density estimates based on detectability-adjusted (Staton et al. 2022) summer snorkel counts with local habitat characteristics (e.g., pool frequency, water temperature, large wood density, etc.) as predictor variables. The weight of each stream segment was assigned based on the predicted density relative value to the segment with the highest value; WUL_j was then equal to the sum of segment-specific weight and length within the known spawning and rearing extent for each population.

inter-annual variability in egg-to-parr survival beyond that explained by density-dependence) are completely random across years, a lag-1 autoregressive process [AR(1); coefficient denoted $\kappa_j^{E\rightarrow P^b}$] was used to account for serial autocorrelation:

$$\text{logit}\left(\boldsymbol{\phi}_{y,1:n_j}^{E\rightarrow P^b}\right) \sim \text{MVN}\left\{\text{logit}\left(\dot{\boldsymbol{\phi}}_{y,1:n_j}^{E\rightarrow P^b}\right) + \boldsymbol{\kappa}_{1:n_j}^{E\rightarrow P^b} \cdot \left[\text{logit}\left(\boldsymbol{\phi}_{y-1,1:n_j}^{E\rightarrow P^b}\right) - \text{logit}\left(\dot{\boldsymbol{\phi}}_{y-1,1:n_j}^{E\rightarrow P^b}\right)\right], \Sigma_{\phi^{E\rightarrow P^b}}\right\} \quad \text{(F-7)}$$

Thus, the covariance matrix $\Sigma_{\phi^{E\rightarrow P^b}}$ captures variability in the white noise (i.e., non-correlated) portion of the survival anomaly. Total parr recruitment ($P_{y,j}^b$) was then the product of total egg production and egg-to-parr survival:

$$P_{y,j}^b = \phi_{y,j}^{E\rightarrow P^b} \cdot E_{y,j} \quad \text{(F-8)}$$

In addition to density-dependent egg-to-parr survival (eq. F-5), there was reason to expect that parr growth/size is density-dependent, both from the literature on salmonid early life history (Grant and Imre 2005; Copeland and Venditti 2009; Walters et al. 2013; Myrvold and Kennedy 2015; Grossman and Simon 2020) and previous analyses on Grande Ronde Spring Chinook Salmon populations (Cooney et al. 2017; Staton et al. 2023). Given the established relationships between size and survival (Zabel and Achord 2004; Hostetter et al. 2015), growth and density (e.g., Grant and Imre 2005), and survival and density (Achord et al. 2003; Walters et al. 2013), it is possible that growth could be a useful mechanism to model density effects on post-recruitment juvenile survival. Expected parr mean length ($\dot{L}_{y,j}^{P^b}$, mm fork length) was modeled as a power function of egg density, which expressed on the logarithmic scale was:

$$\log\left(\dot{L}_{y,j}^{P^b}\right) = \omega_{0,j} + \omega_{1,j} \cdot \log\left(\frac{E_{y,j}}{\text{WUL}_j}\right) \quad \text{(F-9)}$$

and the realized parr mean length as being multivariate log-normally distributed around $\dot{L}_{y,j}^{P^b}$ with covariance matrix $\Sigma_{L^{P^b}}$:

$$\log\left(\boldsymbol{L}_{y,1:n_j}^{P^b}\right) \sim \text{MVN}\left[\log\left(\dot{\boldsymbol{L}}_{y,1:n_j}^{P^b}\right), \Sigma_{L^{P^b}}\right] \quad \text{(F-10)}$$

Migratory Strategy Apportionment

Like many populations of stream-type spring Chinook Salmon in the Columbia River basin, those in the Grande Ronde display life history diversity with respect to juvenile migratory phenology and over-winter rearing habitat use (Copeland et al. 2014). Some portion of parr recruits ($P_{y,j}^b$) migrate from the headwaters rearing areas in the fall and rear over-winter farther downstream (termed "fall migrants" and indexed by i = fall) and the remaining portion migrate the following spring during the out-of-basin migration (termed "spring migrants" and indexed by i = spring). Due to this difference in migratory phenology, these two groups

of fish are monitored separately (Gibson et al. 2023) depending on when they pass the rotary screw trap located in each tributary. Separate abundance and survival data in the observation model required that the process model track fish using these strategies separately, thus they were apportioned:

$$P^{a}_{y,i,j} = P^{b}_{y,j} \cdot \pi_{y,i,j} \tag{F-11}$$

where $P^{a}_{y,i,j}$ is migratory strategy-specific parr abundance and $\pi_{y,i,j}$ is the proportion that take on each migratory strategy. The expected value of the proportion of fall migrants ($\dot{\pi}_{i=\text{fall},j}$) was assumed to be time-constant and the realized values were modeled as having a multivariate logit-normal distribution with covariance matrix $\Sigma_{\pi_{i=\text{fall}}}$:

$$\text{logit}\left(\boldsymbol{\pi}_{y,i=\text{fall},1:n_j}\right) \sim \text{MVN}\left[\text{logit}\left(\dot{\boldsymbol{\pi}}_{i=\text{fall},1:n_j}\right), \Sigma_{\pi_{i=\text{fall}}}\right] \tag{F-12}$$

With only two migratory strategies, the proportion that were spring migrants was obtained as the complement: $\pi_{y,i=\text{spring},j} = 1 - \pi_{y,i=\text{fall},j}$.

Survival to Smolt Stage and Smolt Mean Length

The model assumed that some inter-annual variability in over-winter survival (i.e., the transition from age-1 parr to age-2 smolt prior to out-migration) can be explained by parr mean length[2]. This was achieved by modeling expected over-winter survival (denoted by $\dot{\phi}^{P^a \rightarrow M^b}_{y,i,j}$) as a logit-linear function of parr mean length:

$$\text{logit}\left(\dot{\phi}^{P^a \rightarrow M^b}_{y,i,j}\right) = \gamma_{0,i,j} + \gamma_{1,j} \cdot L^{*P^b}_{y,j} \tag{F-13}$$

where $L^{*P^b}_{y,j}$ is parr mean length centered and scaled based on the mean and standard deviation of observed mean lengths (denoted $\hat{L}^{P^b}_{y,j}$) across years for population j, respectively. Thus, $\gamma_{0,i,j}$ represents the expected log-odds of survival for type i in population j in a year with average parr mean length, and $\gamma_{1,j}$ represents the expected change in the log-odds for every additional standard deviation increase in parr mean length. Then, for each migratory strategy separately, realized over-winter survival was a multivariate logit-normal random variable around the expected value with covariance matrix $\Sigma_{\phi^{P^a \rightarrow M^b}}$ (assumed common among migratory strategies):

$$\text{logit}\left(\boldsymbol{\phi}^{P^a \rightarrow M^b}_{y,i,1:n_j}\right) \sim \text{MVN}\left[\text{logit}\left(\dot{\boldsymbol{\phi}}^{P^a \rightarrow M^b}_{y,i,1:n_j}\right), \Sigma_{\phi^{P^a \rightarrow M^b}}\right] \tag{F-14}$$

The abundance of natural origin smolt (indexed by o = NOR, hatchery-origin smolt releases described in Section) before out-migration was then:

$$M^{b}_{y,i,o=\text{NOR},j} = P^{a}_{y,i,j} \cdot \phi^{P^a \rightarrow M^b}_{y,i,j} \tag{F-15}$$

[2]The assumption that parr length is related to over-winter survival can be relaxed by forcing $\gamma_{1,j}$ in eq. F-13 to zero rather than assigning it an uninformative prior distribution; in this case over-winter survival would be assumed to fluctuate around a time-constant expected value.

Similar to the use of parr mean length to explain inter-annual variability in over-winter survival, smolt mean length ($L_{y,j}^{M^b}$) may be useful for explaining inter-annual variability in out-migration survival. Only spring migrant smolt have been measured for mean length (as they pass the screw trap), thus the i subscript is omitted from quantities related to smolt mean length. Preliminary analyses revealed that smolt mean length was positively related to parr mean length, but that the relationship was non-linear.

Preliminary analyses on the observed mean length data revealed that smolt mean length was positively related with parr mean length, but that the relationship was non-linear (Staton et al. 2023). This non-linearity was captured by modeling the expected multiplicative change in mean length from the parr to smolt stages as a log-linear function of (scaled and centered) parr mean length:

$$\log\left(\dot{\Delta}_{y,j}^{L^{P^b}\rightarrow L^{M^b}}\right) = \theta_{0,j} + \theta_{1,j} \cdot L_{y,j}^{*P^b} \tag{F-16}$$

The realized multiplicative change in mean length was multivariate log-normally distributed around $\dot{\Delta}_{y,j}^{L^{P^b}\rightarrow L^{M^b}}$ with covariance matrix $\Sigma_{\Delta^{L^{P^b}\rightarrow L^{M^b}}}$:

$$\log\left(\boldsymbol{\Delta}_{y,1:n_j}^{L^{P^b}\rightarrow L^{M^b}}\right) \sim \text{MVN}\left[\log\left(\dot{\boldsymbol{\Delta}}_{y,1:n_j}^{L^{P^b}\rightarrow L^{M^b}}\right), \Sigma_{\Delta^{L^{P^b}\rightarrow L^{M^b}}}\right] \tag{F-17}$$

Smolt mean length was then the product:

$$L_{y,j}^{M^b} = L_{y,j}^{P^b} \cdot \Delta_{y,j}^{L^{P^b}\rightarrow L^{M^b}} \tag{F-18}$$

Hatchery Inputs

For populations with hatchery supplementation (CAT, LOS, and UGR), hatchery-origin smolt releases (Brandt et al. 2021, assumed known without error) were stored in the variable $M_{y,i=\text{spring},o=\text{HOR},j}^{b}$; the very rare occasions in which hatchery-origin parr were released the prior year were ignored, thus $M_{y,i=\text{fall},o=\text{HOR},j}^{b} = 0$ for all y and j. Abundance (and often survival) of hatchery-origin fish was tracked separately from natural-origin fish for all subsequent life stages.

Seaward Migration

The model separates mortality sources experienced during seaward migration into two stages: (*i*) from the natal tributary to Lower Granite Dam (LGR), the first in a series of eight hydroelectric dams encountered during the downstream migration through the Snake and Columbia rivers, and (*ii*) from LGR to the ocean. Mortality source (*i*) was not identifiable when separated by migratory strategy, thus it was assumed identical between natural-origin fall and spring migrants (i.e., $\phi_{y,i=\text{fall},o=\text{NOR},j}^{M^b\rightarrow M^a} = \phi_{y,i=\text{spring},o=\text{NOR},j}^{M^b\rightarrow M^a}$ for all j and y); the i dimension is thus omitted when defining these quantities below. Both mortality sources were separable by origin type (see Section)

Expected out-of-basin migration survival for natural-origin smolt was a logit-linear function of smolt mean length:

$$\text{logit}\left(\dot{\phi}^{M^b \to M^a}_{y,o=\text{NOR},j}\right) = \tau_{0,j} + \tau_{1,j} \cdot L^{*M^b}_{y,j} \tag{F-19}$$

where $L^{*M^b}_{y,j}$ has been centered and scaled on the measured smolt mean length values ($\hat{L}^{M^b}_{y,j}$), just as for $L^{*P^b}_{y,j}$ in eqs. F-13 and F-16. For hatchery-origin smolt, expected out-of-basin survival was assumed to be time-constant (i.e., all $\dot{\phi}^{M^b \to M^a}_{y,o=\text{HOR},j}$ were equal within a population). For each origin separately, realized out-of-basin migration survival was a multivariate logit-normal random variable around the expected value with covariance matrix $\Sigma_{\phi^{M^b \to M^a}}$ (assumed common across origin types):

$$\text{logit}\left(\boldsymbol{\phi}^{M^b \to M^a}_{y,o,1:n_j}\right) \sim \text{MVN}\left[\text{logit}\left(\dot{\boldsymbol{\phi}}^{M^b \to M^a}_{y,o,1:n_j}\right), \Sigma_{\phi^{M^b \to M^a}}\right] \tag{F-20}$$

and the abundance of smolt reaching LGR after surviving the migration out-of-basin was:

$$M^a_{y,i,o,j} = M^b_{y,i,o,j} \cdot \phi^{M^b \to M^a}_{y,o,j} \tag{F-21}$$

Survival during the downstream migration through the hydrosystem on the Snake and Columbia rivers was modeled as a single survival rate, specific to each year and origin but shared among populations ($\phi^{M^a \to O^0}_{y,o}$). Realized survival rates were multivariate logit-normal random variables around a time-constant expected value ($\dot{\phi}^{M^a \to O^0}_{o}$) with covariance matrix $\Sigma_{\phi^{M^a \to O^0}}$:

$$\text{logit}\left(\boldsymbol{\phi}^{M^a \to O^0}_{y,1:n_o}\right) \sim \text{MVN}\left[\text{logit}\left(\dot{\boldsymbol{\phi}}^{M^a \to O^0}_{1:n_o}\right), \Sigma_{\phi^{M^a \to O^0}}\right] \tag{F-22}$$

and the abundance of fish reaching the ocean by origin and population was:

$$O^0_{y,o,j} = \phi^{M^a \to O^0}_{y,o} \sum_{i}^{n_i} M^a_{y,i,o,j} \tag{F-23}$$

The summation across migration strategies (i) in eq. F-23 indicates that the fates of fish with differing migratory strategies were not tracked separately after the $M^a_{y,i,o,j}$ stage.

Observation Model

The observation model components for the freshwater juvenile life stage were fitted to three primary data types: (*i*) abundance of juveniles passing rotary smolt traps (located in each tributary; Gibson et al. 2023) in either the fall or spring, (*ii*) survival of juveniles from several PIT-tagging events to LGR (Brandt et al. 2021; Gibson et al. 2023), and (*iii*) the mean length of sampled individuals during two of the PIT-tagging events (Gibson et al. 2023). For all types, the information supplied to the model were externally compiled estimates (e.g., survival from Cormack-Jolly-Seber models) and the estimated standard error was supplied to the model as a measure of observation error variability.

An even more fully integrated model would involve constructing the join likelihood based on the frequency of PIT-tag detection histories. This was deemed unnecessary given (*a*) external estimates have been pre-compiled as well as their estimates of uncertainty (thus the model is consistent with published/established estimates), (*b*) much additional observational model complexity would be needed (e.g., detection probabilities), and (*c*) it would be unlikely to lead to greater parameter identifiability in the process model (e.g., allowing $\phi^{M^b \rightarrow M^a}_{y,i=\text{fall},o=\text{NOR},j} \neq \phi^{M^b \rightarrow M^a}_{y,i=\text{spring},o=\text{NOR},j}$). The practice of performing estimation based on raw data versus pre-compiled estimates that are treated as data is recommended to be avoided, especially if the uncertainty in pre-compiled estimates cannot be acknowledged (Brooks and Deroba 2015). However, Staton et al. (2017) investigated this topic in the context of state-space (adult-to-adult age-structured spawner-recruit) models and found little difference in inferences between models that were integrated to varying degrees with respect to the extent of data pre-compilation, so long as uncertainty from the compilation step is accounted for.

Abundance Data Sources

Fish with the fall migratory strategy pass the screw trap in the fall as parr and fish with the spring migratory strategy pass the screw trap the following spring as smolt. The estimated passage abundances during these time periods were used in log-normal likelihoods by assuming:

$$\log\left(\hat{P}^a_{y,i=\text{fall},j}\right) \sim \text{N}\left[\log\left(P^a_{y,i=\text{fall},j}\right), \hat{\sigma}_{P^a_{y,i=\text{fall},j}}\right] \tag{F-24}$$

for the fall screw trap estimate and

$$\log\left(\hat{M}^b_{y,i=\text{spring},o=\text{NOR},j}\right) \sim \text{N}\left[\log\left(M^b_{y,i=\text{spring},o=\text{NOR},j}\right), \hat{\sigma}_{M^b_{y,i=\text{spring},o=\text{NOR},j}}\right] \tag{F-25}$$

for the spring screw trap estimate.

Survival Data Sources

Natural-origin juveniles have been PIT-tagged during four separate events in most years and populations: (*i*) in summer prior to migratory strategy divergence, (*ii*) as fall migrant parr that pass the screw trap in the fall, (*iii*) in winter in the headwaters (after fall migrants leave, thus applies only to spring migrants; also not available for Minam River), and (*iv*) as spring migrant smolt pass the screw trap. Hatchery-origin smolt released in the spring were also PIT-tagged prior to release. All five of these tag groups have their survival estimated from the time of tagging to their arrival at LGR. These estimates (and their associated standard errors) were used in logit-normal likelihoods by assuming the following for each tag group.

Summer tag group:

$$\text{logit}\left(\hat{\phi}^{P^b \rightarrow M^a}_{y,j}\right) \sim \text{N}\left[\text{logit}\left(\frac{\sum_i^{n_i} M^a_{y,i,o=\text{NOR},j}}{P^b_{y,j}}\right), \hat{\sigma}_{\phi^{P^b \rightarrow M^a}_{y,j}}\right] \tag{F-26}$$

Fall tag group:

$$\text{logit}\left(\hat{\phi}^{P^a \rightarrow M^a}_{y,i=\text{fall},j}\right) \sim \text{N}\left[\text{logit}\left(\frac{M^a_{y,i=\text{fall},o=\text{NOR},j}}{P^a_{y,i=\text{fall},j}}\right), \hat{\sigma}_{\phi^{P^a \rightarrow M^a}_{y,i=\text{fall},j}}\right] \tag{F-27}$$

Winter tag group:

$$\text{logit}\left(\hat{\phi}^{P^a \rightarrow M^a}_{y,i=\text{spring},j}\right) \sim \text{N}\left[\text{logit}\left(\frac{M^a_{y,i=\text{spring},o=\text{NOR},j}}{P^a_{y,i=\text{spring},j} \cdot \phi^{P^b \rightarrow P^a}_{j}}\right), \hat{\sigma}_{\phi^{P^a \rightarrow M^a}_{y,i=\text{spring},j}}\right] \tag{F-28}$$

(where $\phi^{P^b \rightarrow P^a}_{j}$ is a time-constant model-estimated survival from summer tagging to winter tagging for parr that ultimately become spring migrants and $j \in [\text{CAT}, \text{LOS}, \text{UGR}]$).

Spring tag group:

$$\text{logit}\left(\hat{\phi}^{M^b \rightarrow M^a}_{y,i=\text{spring},o=\text{NOR},j}\right) \sim \text{N}\left[\text{logit}\left(\phi^{M^b \rightarrow M^a}_{y,i=\text{spring},o=\text{NOR},j}\right), \hat{\sigma}_{\phi^{M^b \rightarrow M^a}_{y,i=\text{spring},o=\text{NOR},j}}\right] \tag{F-29}$$

Hatchery smolt tag group:

$$\text{logit}\left(\hat{\phi}^{M^b \rightarrow M^a}_{y,i=\text{spring},o=\text{HOR},j}\right) \sim \text{N}\left[\text{logit}\left(\phi^{M^b \rightarrow M^a}_{y,i=\text{spring},o=\text{HOR},j}\right), \hat{\sigma}_{\phi^{M^b \rightarrow M^a}_{y,i=\text{spring},o=\text{HOR},j}}\right] \tag{F-30}$$

for hatchery-origin smolt releases ($j \in [\text{CAT}, \text{LOS}, \text{UGR}]$).

Much research has been devoted to studying the survival of Chinook Salmon smolt migrating through the hydrosystem on the Snake and Columbia rivers. In particular, the Comparative Survival Study has tracked the survival of a variety of tagging groups going back to the early 2000s; estimates from a recent report (McCann et al. 2022, Table A.1) were used to serve as empirical observations (with estimates of uncertainty) with which to inform this component of our model. Provided by McCann et al. (2022) are annual estimates of in-stream survival along the migration from LGR through Bonneville Dam (BON); separate time series are available for natural-origin (we used the "Aggregate Wild Chinook" estimates as none were available for Grande Ronde populations only, denoted $\hat{\phi}^{M^a \rightarrow O^0}_{y,o=\text{NOR}}$ here) and for hatchery-origin (we used the "Catherine Creek AP" estimates, denoted $\hat{\phi}^{M^a \rightarrow O^0}_{y,o=\text{HOR}}$ here). These estimates were treated as representative of the survival for each population, which implies an assumption that the different populations experienced similar conditions during this migration and attributes all variability to either random process or observation noise (i.e., no factors known to influence hydrosystem survival such as size, flood pulses, barging intensity were included). Similar to the other survival data sets, these estimates were assumed to have been made with logit-normal random error around the process model values to build the likelihood:

$$\text{logit}\left(\hat{\phi}^{M^a \rightarrow O^0}_{y,o}\right) \sim \text{N}\left[\text{logit}\left(\phi^{M^a \rightarrow O^0}_{y,o}\right), \hat{\sigma}_{\phi^{M^a \rightarrow O^0}_{y,o}}\right] \tag{F-31}$$

Mean Length Data Sources

Individual fish lengths have been measured upon capture for PIT-tagging (Gibson et al. 2023). The mean length (and the associated standard errors) of all captured fish (tagged and untagged; only fish ≥ 55mm can receive a PIT-tag) was used in log-normal likelihoods by assuming:

$$\log\left(\hat{L}_{y,j}^{P^b}\right) \sim \mathrm{N}\left[\log\left(L_{y,j}^{P^b}\right), \hat{\sigma}_{L_{y,j}^{P^b}}\right] \tag{F-32}$$

for mean length data for the summer parr tagging group and

$$\log\left(\hat{L}_{y,j}^{M^b}\right) \sim \mathrm{N}\left[\log\left(L_{y,j}^{M^b}\right), \hat{\sigma}_{L_{y,j}^{M^b}}\right] \tag{F-33}$$

for mean length data for the smolt tagging group. Because the each population had approximately 1,000 fish tagged and measured during each tagging event, the standard errors on the mean length estimates were quite small.

Preliminary analyses revealed that parr mean length estimates had inter-annual variability attributable to the median sample date (capture method is active), so a standardization was devised and applied prior to model fitting (Staton et al. 2023, Figure 26 therein). All uses of $\hat{L}_{y,j}^{P^b}$ in this document refer to the standardized version. Although timing has varied for smolt mean length estimates ($\hat{L}_{y,j}^{M^b}$), it was caused by migratory timing not sample timing, thus should treated as process noise.

Ocean Juvenile Phase

Process Model

Spring Chinook Salmon in the Grande Ronde basin migrate to sea as age-2 smolt and can return as either age-3, age-4, or age-5 adults. That is, ocean juveniles spend between 1 and 3 winters at sea and some fraction make the return migration after each winter. Thus, ocean dynamics were divided into two types of demographic rates: survival and maturation. Attempting to freely estimate all desired parameters (i.e., time varying year-1, year-2, and year-3 survival rates and maturation rates after year-1 and year-2) revealed that these parameters were confounded given the available data, requiring more simplifying assumptions and stronger prior information than in other parts of the model.

Survival Rates

Year-1 natural-origin[3] ocean survival was modeled as a multivariate logit-normal random variable around a time-constant expected value ($\dot{\phi}_{o=\mathrm{NOR},j}^{O^0 \to O^1}$) with covariance matrix $\Sigma_{\phi^{O^0 \to O^1}}$, but included a lag-1 autoregressive process as a means to account for ocean conditions that may affect survival in a temporally non-independent fashion (e.g., Mantua et al. 1997):

[3]All o = NOR in eq. F-34, omitted for brevity.

$$\text{logit}\left(\boldsymbol{\phi}_{y,o,1:n_j}^{O^0\to O^1}\right) \sim \text{MVN}\left\{\text{logit}\left(\dot{\boldsymbol{\phi}}_{o,1:n_j}^{O^0\to O^1}\right) + \boldsymbol{\kappa}_{1:n_j}^{O^0\to O^1} \cdot \left[\text{logit}\left(\boldsymbol{\phi}_{y-1,o,1:n_j}^{O^0\to O^1}\right) - \text{logit}\left(\dot{\boldsymbol{\phi}}_{o,1:n_j}^{O^0\to O^1}\right)\right], \Sigma_{\phi^{O^0\to O^1}}\right\} \tag{F-34}$$

The first simplifying assumption surrounding ocean survival rates was that process variation was negligible in year-2 and year-3, thus we forced the brood year-specific values of $\phi_{y,o=\text{NOR},j}^{O^1\to O^2}$ and $\phi_{y,o=\text{NOR},j}^{O^2\to O^3}$ to take on the same value for all years (i.e., $\dot{\phi}_{o=\text{NOR},j}^{O^1\to O^2}$ and $\dot{\phi}_{o=\text{NOR},j}^{O^2\to O^3}$, respectively). Further, it was discovered that reasonably strong priors would be needed to inform $\dot{\phi}_{o=\text{NOR},j}^{O^1\to O^2}$ and $\dot{\phi}_{o=\text{NOR},j}^{O^2\to O^3}$ to allow identifiability of the maturity parameters (Table F-3); priors were used for ocean survival rather than maturity parameters because commonly assumed values were available for the former (CTC 1988). The second simplifying assumption was that natural- and hatchery-origin ocean survival rates were perfectly correlated across years within populations, but offset by a time-constant log-odds ratio (δ_j):

$$\begin{aligned}
\text{logit}\left(\phi_{y,o=\text{HOR},j}^{O^0\to O^1}\right) &= \text{logit}\left(\phi_{y,o=\text{NOR},j}^{O^0\to O^1}\right) + \delta_j \\
\text{logit}\left(\phi_{y,o=\text{HOR},j}^{O^1\to O^2}\right) &= \text{logit}\left(\phi_{y,o=\text{NOR},j}^{O^1\to O^2}\right) + \delta_j \\
\text{logit}\left(\phi_{y,o=\text{HOR},j}^{O^2\to O^3}\right) &= \text{logit}\left(\phi_{y,o=\text{NOR},j}^{O^2\to O^3}\right) + \delta_j
\end{aligned} \tag{F-35}$$

Maturation Rates

Realized maturation rates (i.e., the proportion of fish from a given brood year alive and in the ocean at the beginning of a year that make the return migration that year) were modeled as multivariate logit-normal random variables around time-constant expected values ($\dot{\psi}_{o,j}^{O^w}$; w is the number of winters spent in the ocean) with covariance matrix $\Sigma_{\psi^{O^w}}$ (assumed common across origins):

$$\begin{aligned}
\text{logit}\left(\boldsymbol{\psi}_{y,o,1:n_j}^{O^1}\right) &\sim \text{MVN}\left[\text{logit}\left(\dot{\boldsymbol{\psi}}_{o,1:n_j}^{O^1}\right), \Sigma_{\psi^{O^1}}\right] \\
\text{logit}\left(\boldsymbol{\psi}_{y,o,1:n_j}^{O^2}\right) &\sim \text{MVN}\left[\text{logit}\left(\dot{\boldsymbol{\psi}}_{o,1:n_j}^{O^2}\right), \Sigma_{\psi^{O^2}}\right]
\end{aligned} \tag{F-36}$$

Since age-5 was the last modeled age of maturity, all fish alive and in the ocean after the third year at sea mature and return that year (i.e., all $\psi_{y,o,j}^{O^3} = 1$).

Return to Columbia River

Based on the sources of process variation modeled in eqs. F-34, F-35, and F-36 and the initial abundance of ocean juveniles ($O_{y,o,j}^0$, eq. F-23), the abundance of ocean juveniles after a given number of winters (w, superscripts in all O^w symbols) was modeled as a sequence of survival, maturation of surviving fish, and survival of non-maturing fish:

$$
\begin{aligned}
O^1_{y,o,j} &= O^0_{y,o,j} \cdot \phi^{O^0 \to O^1}_{y,o,j} \\
O^2_{y,o,j} &= O^1_{y,o,j} \cdot (1 - \psi^{O^1}_{y,o,j}) \cdot \phi^{O^1 \to O^2}_{y,o,j} \\
O^3_{y,o,j} &= O^2_{y,o,j} \cdot (1 - \psi^{O^2}_{y,o,j}) \cdot \phi^{O^2 \to O^3}_{y,o,j}
\end{aligned}
\tag{F-37}
$$

That is, fish reaching the ocean as age-2 juveniles ($O^0_{y,o,j}$) must survive one winter to become age-3 ocean juveniles ($O^1_{y,o,j}$); if they do not mature at age-3 (with probability $1 - \psi^{O^1}_{y,o,j}$), then they must survive another winter to become age-4 ocean juveniles ($O^2_{y,o,j}$), and if they do not mature at that point (with probability $1 - \psi^{O^2}_{y,o,j}$), they must survive a third winter to become age-5 ocean juveniles ($O^3_{y,o,j}$).

The abundances of ocean juveniles ($O^1_{y,o,j}$, $O^2_{y,o,j}$, and $O^3_{y,o,j}$) from a given cohort were organized by brood year, however they returned in different years and ages to spawn. Returning mature fish were placed into the correct year and age of return to the mouth of the Columbia River before the upstream migration ($R^b_{y,k,o,j}$) based on the following rule: members of the cohort spawned in brood year y returned at the k^{th} possible age of maturity to produce the cohort for brood year $y + A_{\min} + k - 1$. As an example, fish spawned in brood year $y = 2000$ returned in 2003 as age-3 ($k = 1$), in 2004 as age-4 ($k = 2$), or in 2005 as age-5 ($k = 3$) – see Table F-6 for a visual of this example. Thus, the abundance of fish spawned in brood year y returning as age-3, age-4, and age-5, respectively, was:

$$
\begin{aligned}
R^b_{y+A_{\min}+1-1,1,o,j} &= O^1_{y,o,j} \cdot \psi^{O^1}_{y,o,j} \\
R^b_{y+A_{\min}+2-1,2,o,j} &= O^2_{y,o,j} \cdot \psi^{O^2}_{y,o,j} \\
R^b_{y+A_{\min}+3-1,3,o,j} &= O^3_{y,o,j} \cdot \psi^{O^3}_{y,o,j}
\end{aligned}
\tag{F-38}
$$

This, however, leaves 12 ($\sum_k^{n_k} A_{\min} + k - 1$) age/year combinations per origin unpopulated with returning adults (the first 3 missing years for age-3 returns, first 4 missing years for age-4 returns, and first 5 missing years for age-5 returns; see Table F-6). This occurs because no juvenile process model outcomes existed that would ultimately become these $R^b_{y,k,o,j}$ values in these early years. Thus, to initialize the adult returns for natural-origin fish, these 12 year/age return abundances were estimated as unknown parameters with fairly restrictive priors (Table F-3) with boundaries loosely informed by the ranges of adult returns-at-age observed in the early years of the data time series. Initial abundances of age-specific hatchery-origin returns were handled by the "straying model" (see Section , below).

Observation Model

No data sources were used to inform ocean juvenile population dynamics – estimation of these quantities was enabled by (*i*) reasonably precise information about the abundance and composition of fish entering the ocean and returning to natal tributaries, (*ii*) the simplifying assumptions described above (i.e., time-constant second and third year ocean survival and perfectly correlated but offset origin-specific survival), and (*iii*) through the use of reasonably strong priors for second and third year ocean survival (Table F-3).

Freshwater Adult Phase

Process Model

There are a variety of mortality sources that occur along the upstream migration from the mouth of the Columbia River to the point of spawning in natal tributaries in Grande Ronde basin. For ease of presentation, we separate these processes into three categories depending on where they occur spatiotemporally: (*i*) downstream of Bonneville Dam (BON) at the beginning of the upstream migration, (*ii*) along the upstream migration in the mainstem Columbia and Snake rivers between BON and LGR, and (*iii*) after arrival to the natal tributaries and up until the point of spawning.

Processes Downstream of BON

Prior to reaching BON, returning adults are subjected to harvest mortality from fisheries (harvest rate denoted by $U_{y,k,o}$). These estimates were supplied to the model as known without error (i.e., non-stochastic; used in eq. F-40, below).

Processes Between BON and LGR

Upon arrival to BON, survival to LGR has been monitored (since 2000; $y = 10$) via PIT-tags with high (>0.95) detection probabilities, enabling estimation of survival along this portion of the migration. The survival rate between BON and LGR was assumed to vary by origin (but not by population) as multivariate logit-normal random variables around expected values ($\dot{\phi}_o^{R^b \to R^a}$) with covariance matrix $\Sigma_{\phi^{R^b \to R^a}}$. In years without these PIT-tag counts, however, the survival from BON to LGR was found to be confounded with ocean survival; this was resolved by using the expected value rather than estimating the value for these years:

$$\text{logit}\left(\boldsymbol{\phi}_{y,1:n_o}^{R^b \to R^a}\right) \begin{cases} = \text{logit}\left(\dot{\boldsymbol{\phi}}_{1:n_o}^{R^b \to R^a}\right) & \text{if } y < 10 \\ \sim \text{MVN}\left[\text{logit}\left(\dot{\boldsymbol{\phi}}_{1:n_o}^{R^b \to R^a}\right), \Sigma_{\phi^{R^b \to R^a}}\right] & \text{if } y \geq 10 \end{cases} \tag{F-39}$$

Examination of the adult composition data indicated that hatchery-origin adults returned to Grande Ronde populations in early years that could not be attributed to hatchery-origin smolt releases to these populations. Further, the Minam River population (which has no hatchery supplementation program) has had hatchery adults found in carcass surveys in many of the years since monitoring began. Without a process model adjustment, the observation model would treat these unexpected non-zero hatchery-origin counts as impossible. This model component is referred to as the "straying model" (total abundance of entering strays denoted $G_{y,o,j}$), and it applied only in years/populations in which the presence of non-zero hatchery-origin returning adults could not otherwise be explained due to zero-valued hatchery-origin smolt releases. Thus, all $G_{y,o=\text{NOR},j} = 0$ and all $G_{y,o=\text{HOR},j} = 0$ in years where non-zero hatchery-origin smolt releases to population j could have explained non-zero hatchery-origin adult returns in year y at age k. The age composition of these strays was assumed to be time-constant ($p_{k,j}^G$; where $\sum_k^{n_k} p_{k,j}^G = 1$) and was used to apportion $G_{y,o,j}$.

The abundance of adults arriving to natal spawning tributaries by age and origin ($R_{y,k,o,j}^a$) was:

$$R^{a}_{y,k,o,j} = R^{b}_{y,k,o,j} \cdot (1 - U_{y,k,o}) \cdot \phi^{R^b \rightarrow R^a}_{y,o} + \left(G_{y,o,j} \cdot p^{G}_{k,j} \right) \tag{F-40}$$

Processes in Natal Tributary

Upon arrival to the natal tributary, populations with a weir and hatchery program (all populations except the Minam River, indexed by j = MIN) have some number of adults removed each year for broodstock and as a means to minimize natural spawning of hatchery-origin fish. These weir removals (denoted by $B_{y,k,o,j}$; all $B_{y,k,o,j=\text{MIN}} = 0$) were supplied to the model as known without error, as were the number of fish estimated to have been in the natal tributaries prior to spawning (Bratcher et al. 2017). Thus, the abundance of potential spawners was:

$$S^{b}_{y,k,o,j} = \max\left(R^{a}_{y,k,o,j} - B_{y,k,o,j} - H_{y,k,o,j}, 1 \right) \tag{F-41}$$

The maximum constraint was used to ensure all $S^{b}_{y,k,o,j} > 0$.

It is well-known that some potential spawners die prior to spawning (e.g., Bowerman et al. 2021); these "pre-spawn survival" outcomes are denoted by $\phi^{S^b \rightarrow S^a}_{y,j}$. The initial desire was to allow for the model to internally estimate time-varying pre-spawn survival probabilities, but it was discovered that the observational data (counts of spawned vs. gravid female carcasses) were not informative enough for all populations to prevent parameter confounding with egg-to-parr survival. As alternative, binary logistic regression models were fitted that included year-specific random effects around a time-constant expected value (one per population; success represented by year-specific counts of spawned female carcasses, trials represented by total female carcasses examined) and the resulting time- and population-varying estimates were supplied to the model as known without error. The abundance of adults spawning successfully was then:

$$S^{a}_{y,k,o,j} = S^{b}_{y,k,o,j} \cdot \phi^{S^b \rightarrow S^a}_{y,j} \tag{F-42}$$

This $S^{a}_{y,k,o,j}$ value was used to calculate total egg production ($E_{y,j}$) in eq. F-4 to link the the spawner abundance to the parr recruitment abundance in the next generation.

Observation Model

The adult observation model relied on three primary data types: (*i*) total abundance of adult returns to the natal tributaries, (*ii*) information about survival on the upstream migration between LGR and BON, and (*iii*) composition data to inform the relative abundance of adults of different ages and origins returning each year.

Abundance Data Source

Total tributary return abundance has been estimated annually external to the model using a combination of weir counts, mark-recapture methods, and spawning ground surveys (Bliesner et al. 2020; Brandt et al. 2021). For each population and year, these have been compiled into a point estimate ($\hat{R}^{a}_{y,j}$; the lack of o or k indices indicates the estimate is aggregated across these dimensions) and an estimate of observation

uncertainty ($\hat{\sigma}_{R^a_{y,j}}$, expressed as a log-normal standard error). The model assumed the point estimate is made with log-normal observation error around the model-predicted total returns to the tributary to build the likelihood for this component:

$$\log\left(\hat{R}^a_{y,j}\right) \sim \mathrm{N}\left[\log\left(\sum_{o}^{n_o}\sum_{k}^{n_k} R^a_{y,k,o,j}\right), \hat{\sigma}_{R^a_{y,j}}\right] \tag{F-43}$$

Survival Data Sources

The model fitted to counts of PIT-tag detections of known Grande Ronde-origin fish passing BON ($\hat{x}^{\mathrm{BON}}_{y,o}$) and LGR ($\hat{x}^{\mathrm{LGR}}_{y,o}$) to inform the migratory survival rate between these two locations (DART 2023)[4]. The latter was assumed to be a binomial random variable to build the likelihood component for this data set:

$$\hat{x}^{\mathrm{LGR}}_{y,o} \sim \mathrm{B}\left(\phi^{R^b \to R^a}_{y,o}, \hat{x}^{\mathrm{BON}}_{y,o}\right) \tag{F-44}$$

Composition Data Sources

Since the model is both age- and origin-structured, it required data to inform the relative abundance of adults returning according to these different classes. These data took the form of two sources: (*i*) those collected at weirs located within three of the four populations ($\hat{x}^{R^a}_{y,ko,j}$) and (*ii*) those collected during carcass surveys ($\hat{x}^{S^{a'}}_{y,ko,j}$), given the Minam River population does not have a weir (Naylor et al. 2019; Kinzer et al. 2020; Brandt et al. 2021). The weir was assumed to have fish representatively with respect to age and origin composition and both data sources were fitted to by assuming multinomial sampling in which there were $n_{ko} = 6$ possible outcomes: $n_k = 3$ ages of return by $n_o = 2$ origins. Further,the observed sample size ($\sum_{ko}^{n_{ko}} \hat{x}^{R^a}_{y,ko,j}$) as the multinomial sample size rather than attempting to adjust it for non-independent sampling (Maunder 2011); alternative sample size selections would likely be arbitrary, and past analyses have suggested that inferences are robust to rational alternatives (see Supplement A of Staton et al. 2021). The model-expected composition by age and origin ($p^{R^a}_{y,ko,j}$) was calculated from the return abundance by age and origin, reorganized such that age and origin fell along the same array dimension ($R^a_{y,ko,j}$) rather than along two dimensions as shown in the process model ($R^a_{y,k,o,j}$):

$$p^{R^a}_{y,ko,j} = \frac{R^a_{y,ko,j}}{\sum_{ko}^{n_{ko}} R^a_{y,ko,j}} \tag{F-45}$$

which was used as the multinomial expected frequency to build the likelihood:

[4]https://www.cbr.washington.edu/dart/query/pitadult_conrate; exact query settings described at https://github.com/bstaton1/GR-sslcm/issues/93.

$$\hat{\boldsymbol{x}}^{R^a}_{y,1:n_{ko},j} \sim \mathrm{M}\left(\boldsymbol{p}^{R^a}_{y,1:n_{ko},j}, \sum_{ko}^{n_{ko}} \hat{x}^{R^a}_{y,ko,j}\right) \tag{F-46}$$

Preliminary analyses revealed an age sampling bias of carcass surveys relative to weir sampling, which required a correction to ensure reliable fits to all data sets while recovering unbiased true age composition data for the Minam River population, which had only carcass composition data. For the three populations with paired composition data (i.e., $j \in [\mathrm{CAT}, \mathrm{LOS}, \mathrm{UGR}]$), correction factors were estimated in a hierarchical fashion:

$$z_{k,j} \sim \mathrm{N}\left(\dot{z}_k, \sigma_{z_k}\right) \tag{F-47}$$

where $k = 1$ or $k = 3$ ($k = 2$ was treated as the baseline category), $z_{k,j}$ are age- and population-specific coefficients, $\dot{z}_k$ are their expectations across populations, and σ_{z_k} are their standard deviations across populations. These coefficients were used in the following log-linear model to derive the correction factors ($\zeta_{k,j}$):

$$\log\left(\zeta_{k,j}\right) = z_{k=1,j} \cdot \mathrm{age3}_k + z_{k=3,j} \cdot \mathrm{age5}_k \tag{F-48}$$

where $k \in [1, 2, 3]$, $\mathbf{age3}_{1:n_k} = [1\ 0\ 0]$ is a dummy variable indicating whether each value of k corresponds to age-3, and $\mathbf{age5}_{1:n_k} = [0\ 0\ 1]$ is a dummy variable indicating whether each value of k corresponds to age-5. These correction factors were averaged across populations to obtain the correction factors for the Minam River population:

$$\zeta_{k,j=\mathrm{MIN}} = \mathrm{mean}\left(\zeta_{k,j\in[\mathrm{CAT,LOS,UGR}]}\right) \tag{F-49}$$

These correction factors were used to calculate the expected proportions by age and origin for carcass surveys ($p^{S^{a'}}_{y,ko,j}$):

$$p^{S^{a'}}_{y,ko,j} = \frac{S^a_{y,ko,j} \cdot \zeta_{k,j}}{\sum_{ko}^{n_{ko}} S^a_{y,ko,j} \cdot \zeta_{k,j}} \tag{F-50}$$

which was used as the multinomial expected frequency to build the likelihood by assuming:

$$\hat{\boldsymbol{x}}^{S^{a'}}_{y,1:n_{ko},j} \sim \mathrm{M}\left(\boldsymbol{p}^{S^{a'}}_{y,1:n_{ko},j}, \sum_{ko}^{n_{ko}} \hat{x}^{S^{a'}}_{y,ko,j}\right) \tag{F-51}$$

References

Achord, S., Levin, P. S., and Zabel, R. W. 2003. Density-dependent mortality in Pacific salmon: The ghost of impacts past? *Ecology Letters*, 6(4):335–342. doi:10.1046/j.1461-0248.2003.00438.x.

Barnard, J., McCulloch, R., and Meng, X.-L. 2000. Modeling covariance matrices in terms of standard deviations and correlations, with application to shrinkage. *Statistica Sinica*, 10(4):1281–1311. URL: https://www.jstor.org/stable/24306780.

Bliesner, K. L., Craft, N. M., Feldhaus, J. W., and Ruzycki, J. R. 2020. A compendium of viable salmonid population abundance and productivity field and analysis methods for natural origin adult Chinook salmon populations in the Snake River spring/summer-run ESU of northeast Oregon from 1949-2019. Technical report, Oregon Department of Fish and Wildlife, East Region Fish Research. URL: https://nrimp.dfw.state.or.us/DataClearinghouse/default.aspx?p=202&XMLname=1151.xml.

Bouchard, C., Buoro, M., Lebot, C., and Carlson, S. M. 2022. Synchrony in population dynamics of juvenile Atlantic salmon: Analyzing spatiotemporal variation and the influence of river flow and demography. *Canadian Journal of Fisheries and Aquatic Sciences*, 79(5):782–794. doi:10.1139/cjfas-2021-0017.

Bowerman, T. E., Keefer, M. L., and Caudill, C. C. 2021. Elevated stream temperature, origin, and individual size influence Chinook salmon prespawn mortality across the Columbia River Basin. *Fisheries Research*, 237:105874. doi:10.1016/j.fishres.2021.105874.

Brandt, E. J., Smith, J. D., Feldhaus, J. W., and Ruzycki, J. R. 2021. Lower Snake River Compensation Plan: Oregon spring Chinook salmon evaluation studies, 2019. Annual Progress Report, Oregon Department of Fish and Wildlife, Northeast-Central Oregon Research and Monitoring, Salem, OR. URL: https://www.fws.gov/sites/default/files/documents/2019%20ODFW%20CHS%20Annual%20Report.pdf.

Bratcher, K. W., Yanke, J. A., and Bailey, T. D. 2017. Lower Snake River Compensation Plan: Oregon spring Chinook salmon harvest monitoring, 2016. Annual Progress Report, Oregon Department of Fish and Wildlife, East Region Fish Research, Salem, OR. URL: https://www.fws.gov/sites/default/files/documents/2016%20ODFW%20Spring%20Chinook%20Harvest.pdf.

Brooks, E. N. and Deroba, J. J. 2015. When "data" are not data: The pitfalls of post hoc analyses that use stock assessment model output. *Canadian Journal of Fisheries and Aquatic Sciences*, 72(4):634–641. doi:10.1139/cjfas-2014-0231.

Connors, B. M., Siegle, M. R., Harding, J., Rossi, S., Staton, B. A., Jones, M. L., Bradford, M. J., Brown, R., Bechtol, B., Doherty, B., Cox, S., and Sutherland, B. J. G. 2022. Chinook salmon diversity contributes to fishery stability and trade-offs with mixed-stock harvest. *Ecological Applications*, 32(8):e2709. doi:10.1002/eap.2709.

Cooney, T. D., Jonasson, B. C., Sedell, E. R., Hoffnagle, T. L., and Carmichael, R. W. 2017. Grande Ronde spring Chinook populations: Juvenile based models. In *NOAA Fisheries' Interior Columbia Basin Life-Cycle Modeling*, pages 1–30.

Copeland, T. and Venditti, D. A. 2009. Contribution of three life history types to smolt production in a Chinook salmon (*Oncorhynchus tshawytscha*) population. *Canadian Journal of Fisheries and Aquatic Sciences*, 66(10):1658–1665. doi:10.1139/F09-110.

Copeland, T., Venditti, D. A., and Barnett, B. R. 2014. The importance of juvenile migration tactics to adult recruitment in stream-type Chinook salmon populations. *Transactions of the American Fisheries Society*, 143(6):1460–1475. doi:10.1080/00028487.2014.949011.

CTC 1988. Exploitation rate analysis - Appendix 2 to Chinook technical committee 1987 annual report. Technical Report TCCHINOOK (88)-2, CTC Analytical Work Group. URL: https://www.psc.org/download/35/chinook-technical-committee/2150/tcchinook88-2app2.pdf.

DART 2023. PIT tag adult returns conversion rate. URL: https://www.cbr.washington.edu/dart/query/pitadult_conrate.

Dorazio, R. M., Gotelli, N. J., and Ellison, A. M. 2011. Modern methods of estimating biodiversity loss from presence-absence surveys. In Grillo, O., editor, *Biodiversity Loss in a Changing Planet*, pages 277–302. InTech. URL: https://www.intechopen.com/books/biodiversity-loss-in-a-changing-planet/modern-methods-of-estimating-biodiversity-from-presence-absence-surveys.

Gelman, A., Carlin, J. B., Stern, H. S., Dunson, D. B., Vehtari, A., and Rubin, D. B. 2014. *Bayesian Data Analysis*. Texts in Statistical Science. Chapman & Hall/CRC, Boca Raton, FL, 3 edition.

Gelman, A. and Hill, J. 2007. *Data Analysis Using Regression and Multilevel and Hierarchical Models*. Cambridge University Press, New York.

Gibson, P. P., Drascic, F. J., Haynes, D. R., McMichael, G. A., Ofiara, J. A., Raines, M. A., and Warnock, C. R. 2023. Investigations into the life history of naturally produced spring Chinook salmon and summer steelhead in the Grande Ronde River subbasin, 2022. BPA Annual Report for Project 1992-026-04, Oregon Department of Fish and Wildlife, La Grande, OR. URL: https://nrimp.dfw.state.or.us/DataClearinghouse/default.aspx?p=202&XMLname=42707.xml.

Grant, J. W. A. and Imre, I. 2005. Patterns of density-dependent growth in juvenile stream-dwelling salmonids. *Journal of Fish Biology*, 67(sB):100–110. doi:10.1111/j.0022-1112.2005.00916.x.

Grossman, G. D. and Simon, T. N. 2020. Density-dependent effects on salmonid populations: A review. *Ecology of Freshwater Fish*, 29(3):400–418. doi:10.1111/eff.12523.

Hostetter, N. J., Evans, A. F., Loge, F. J., O'Connor, R. R., Cramer, B. M., Fryer, D., and Collis, K. 2015. The influence of individual fish characteristics on survival and detection: Similarities across two salmonid species. *North American Journal of Fisheries Management*, 35(5):1034–1045. doi:10.1080/02755947.2015.1077176.

Kinzer, R., Arnsberg, B., Harbeck, J., Maxwell, A., Orme, R., Rabe, C., and Vatland, S. 2020. Snake River Basin adult Chinook

salmon and steelhead monitoring, 2019. Annual Report, Nez Perce Tribe, Department of Fisheries Resources Management, Research Division, Lapwai, ID. URL: https://www.fws.gov/sites/default/files/documents/2019%20NPT%20Snake%20River%20Basin%20Adult%20Chinook%20Salmon%20and%20Steelhead%20Monitoring.pdf.

Mantua, N. J., Hare, S. R., Zhang, Y., Wallace, J. M., and Francis, R. C. 1997. A Pacific Interdecadal climate oscillation with impacts on salmon production. *Bulletin of the American Meteorological Society*, 78(6):1069–1080. doi:10.1175/1520-0477(1997)078<1069:APICOW>2.0.CO;2.

Maunder, M. N. 2011. Review and evaluation of likelihood functions for composition data in stock-assessment models: Estimating the effective sample size. *Fisheries Research*, 109(2):311–319. doi:10.1016/j.fishres.2011.02.018.

McCann, J., Chockley, B., Cooper, E., Scheer, G., Haeseker, S., Lessard, B., Copeland, T., Ebel, J., Storch, A., and Rawding, D. 2022. Comparative survival study of PIT-tagged spring/summer/fall Chinook, summer steelhead, and sockeye, 2022. Annual Report BPA Contract #19960200, CSS Oversight Committee and Fish Passage Center, Portland, OR. URL: https://www.fpc.org/documents/CSS/CSS%20Final%20Revised%202022.pdf.

Myrvold, K. M. and Kennedy, B. P. 2015. Density dependence and its impact on individual growth rates in an age-structured stream salmonid population. *Ecosphere*, 6(12):1–16. doi:10.1890/ES15-00390.1.

Naylor, L., Crump, C., Van Sickle, A., and Startzel-Holt, B. 2019. Monitoring and evaluation of supplemented spring Chinook salmon and life histories of wild summer steelhead in the Grande Ronde Basin. Annual Report for BPA Project #2007-083-00, Confederated Tribes of the Umatilla Indian Reservation, Pendleton, OR. URL: https://www.cbfish.org/Document.mvc/Viewer/P164991.

Plummer, M. 2017. JAGS Version 3.4.0 User Manual. URL: https://sourceforge.net/projects/mcmc-jags/.

Riecke, T. V., Sedinger, B. S., Williams, P. J., Leach, A. G., and Sedinger, J. S. 2019. Estimating correlations among demographic parameters in population models. *Ecology and Evolution*, 9(23):13521–13531. doi:10.1002/ece3.5809.

Staton, B., Justice, C., Kaylor, M., and Ringelman, A. 2023. Objective E-1: Grande Ronde phase 12 - development of a spring Chinook statistical estimation life cycle model. In *Evaluating Salmonid and Stream Ecosystem Response to Conservation Measures and Environmental Stressors in the Columbia River Basin*, Annual Report for BPA Project #2009-004-00, pages 69–83. Columbia River Inter-Tribal Fish Commission, Portland, OR. URL: https://critfc.org/wp-content/uploads/2023/07/23_03.pdf.

Staton, B. A., Catalano, M. J., and Fleischman, S. J. 2017. From sequential to integrated Bayesian analyses: Exploring the continuum with a Pacific salmon spawner-recruit model. *Fisheries Research*, 186:237–247. doi:10.1016/j.fishres.2016.09.001.

Staton, B. A., Catalano, M. J., Fleischman, S. J., and Ohlberger, J. 2021. Incorporating demographic information into spawner–recruit analyses alters biological reference point estimates for a western Alaska salmon population. *Canadian Journal of Fisheries and Aquatic Sciences*, 78(12):1755–1769. doi:10.1139/cjfas-2020-0478.

Staton, B. A., Justice, C., White, S., Sedell, E. R., Burns, L. A., and Kaylor, M. J. 2022. Accounting for uncertainty when estimating drivers of imperfect detection: An integrated approach illustrated with snorkel surveys for riverine fishes. *Fisheries Research*, 249:106209. doi:10.1016/j.fishres.2021.106209.

Thorson, J. T., Scheuerell, M. D., Buhle, E. R., and Copeland, T. 2014. Spatial variation buffers temporal fluctuations in early juvenile survival for an endangered Pacific salmon. *Journal of Animal Ecology*, 83(1):157–167. doi:10.1111/1365-2656.12117.

Walters, A. W., Copeland, T., and Venditti, D. A. 2013. The density dilemma: Limitations on juvenile production in threatened salmon populations. *Ecology of Freshwater Fish*, 22(4):508–519. doi:10.1111/eff.12046.

Zabel, R. W. and Achord, S. 2004. Relating size of juveniles to survival within and among populations of Chinook salmon. *Ecology*, 85(3):795–806. doi:10.1890/02-0719.

Table F-1. Various indices and dimensional constants used in defining the structure and scope for the state-space life cycle model for Grande Ronde spring Chinook Salmon.

Type	Symbol	Description
Indices	j	[1]Population; $j \in [\text{CAT}, \text{LOS}, \text{MIN}, \text{UGR}]$
	y	[2]Year; $y \in [1, \ldots, n_y]$
	k	[3]Age of maturation; $k \in [1, \ldots, n_k]$
	i	[4]Juvenile migratory strategy; $i \in [\text{fall}, \text{spring}]$
	o	[5]Origin type; either natural- or hatchery-origin; $o \in [\text{NOR}, \text{HOR}]$
	ko	[6]Unique age/origin combinations; $ko \in [1, \ldots, n_{ko}]$
	w	Number of winters spent at sea prior to maturation; $w \in [1, 2, 3]$
Scoping Constants	$y_{\min}$	[2]First year modeled; equal to 1991 here; first brood year with juvenile data
	$y_{\max}$	[2]Last year modeled; equal to 2022 here; last return year with adult data
	$A_{\min}$	[3]Minimum total age of maturation; equal to 3 here
	$A_{\max}$	[3]Maximum total age of maturation; equal to 5 here
Dimensional Constants	n_j	[1]Number of populations modeled; equal to 4 here
	n_y	[2]Number of years modeled; equal to 32 here
	n_k	[3]Number of ages at maturation modeled; equal to 3 here
	n_i	[4]Number of migratory strategies modeled; equal to 2 here
	n_o	[5]Number of origins modeled; equal to 2 here
	n_{ko}	[6]Number of unique age/origin combinations

[1] "Population" is used to distinguish among the tributaries within the Grande Ronde basin with sufficient data to model complete life cycle population dynamics. Abbreviations are: Catherine Creek (CAT), Lostine River (LOS), Minam River (MIN), and Upper Grande Ronde River (UGR).

[2] "Year" refers to the year of spawning; for juvenile phases this is the year fish were spawned (i.e., brood year) and for adult phases this is the year of return (i.e., calendar year).

[3] "Age" refers to the total age, i.e., the number of winters experienced (including the winter spent as an egg). For example, eggs fertilized in brood year 2000 were age-0 until they hatched in spring of 2001 (age-1), migrated to sea in spring/summer of 2002 (age-2), and returned to spawn in one of 2003 (age-3), 2004 (age-4), or 2005 (age-5). $k = 1$ is the first age of maturation (age-3) and $k = 3$ is the last age of maturation (age-5).

[4] "Migratory strategy" refers to the timing of migration from headwaters rearing areas – either as fall (as age-1) or spring (age-2) migrants. Regardless, all fish make the out-of-basin migration at age-2.

[5] "Origin" refers to the rearing type: natural-origin (NOR) vs. hatchery-origin (HOR).

[6] Most quantities treat age (k) and origin (o) as two separate dimensions of a larger array. However, for fitting to compositional data by age and origin, we collapse these two dimensions into one. $ko \in [1, 2, 3]$ represents age-3, age-4, and age-5 for natural-origin fish, respectively, and $ko \in [4, 5, 6]$ represents these same ages for hatchery-origin fish, respectively.

Table F-2. Symbology used to represent the key states (i.e., abundance at life stage/group) and rates (i.e., transition probabilities among states) in the presentation of the state-space life cycle model for Grande Ronde spring Chinook Salmon. The majority of rates presented in this table are hierarchically structured/estimated, where the population- and/or origin-specific expected value and standard deviation are free parameters (or a function of free parameters) presented in Table F-3. Equation numbers reference any equation that uses that quantity.

Type	Symbol	Eq(s).	Description
Freshwater Juvenile			
States	$E_{y,j}$	F-4, F-5, F-8	Total egg production
	$P^{b}_{y,j}$	F-8, F-11, F-26	Parr abundance at end of summer (*before* migratory strategy apportionment)
	$P^{a}_{y,i,j}$	F-11, F-13, F-15, F-27, F-28	Parr abundance *after* migratory strategy apportionment
	$M^{b}_{y,i,o,j}$	F-15, F-21, F-25	In-basin smolt abundance, immediately following over-winter mortality and *before* migration out of basin; hatchery-origin smolt releases introduced here
	$M^{a}_{y,i,o,j}$	F-21, F-23, F-26, F-27, F-28, F-29, F-30	Smolt abundance at Lower Granite Dam *after* migration out of basin
	$L^{P^b}_{y,j}$	F-10, F-13, F-16, F-18, F-32	Parr mean length at end of summer ($L^{*P^b}_{y,j}$ is scaled and centered on the observed time series $\hat{L}^{P^b}_{y,j}$)
	$L^{M^b}_{y,j}$	F-18, F-19, F-33	Smolt mean length before migration out of basin ($L^{*M^b}_{y,j}$ is scaled and centered on the observed time series $\hat{L}^{M^b}_{y,j}$)
Rates	$\phi^{E\rightarrow P^b}_{y,j}$	F-7, F-8	Survival rate from egg to end of summer parr
	$\pi_{y,i,j}$	F-11, F-12	Proportion of parr at end of summer that have migratory strategy i
	$\phi^{P^a\rightarrow M^b}_{y,i,j}$	F-14, F-15	Over-winter survival from parr year to smolt year; i.e., to move from total age-1 to total age-2
	$\phi^{M^b\rightarrow M^a}_{y,i,o,j}$	F-20, F-21, F-29, F-30	Migration survival from within basin to Lower Granite Dam
	$\phi^{M^a\rightarrow O^0}_{y,o}$	F-22, F-23, F-31	Migration survival downstream through hydrosystem to reach ocean
Ocean Juvenile			
States	$O^{w}_{y,o,j}$	F-23, F-37, F-38	Abundance of ocean juveniles after experiencing w winter(s) at sea, where $w \in [0, 1, 2, 3]$

Table F-2. Symbology used to represent the key states (i.e., abundance at life stage/group) and rates (i.e., transition probabilities among states) in the presentation of the state-space life cycle model for Grande Ronde spring Chinook Salmon. The majority of rates presented in this table are hierarchically structured/estimated, where the population- and/or origin-specific expected value and standard deviation are free parameters (or a function of free parameters) presented in Table F-3. Equation numbers reference any equation that uses that quantity. *(continued)*

Type	Symbol	Eq(s).	Description
	$\phi_{y,o,j}^{O^w \to O^{w+1}}$	F-34, F-35, F-37	Survival of ocean juveniles from the end of winter w to the end of winter $w+1$ at sea, where $w \in [0, 1, 2]$
Rates	$\psi_{y,o,j}^{O^w}$	F-36, F-37, F-38	Proportion of ocean juveniles alive at the end of winter w at sea that make spawning migration before winter $w+1$, where $w \in [1, 2, 3]$
Freshwater Adult			
	$R_{y,k,o,j}^{b}$	F-38, F-40	Abundance of adults (i.e., mature) arriving at the estuary (*before* upstream main-stem migration)
	$R_{y,k,o,j}^{a}$	F-40, F-41, F-43, F-45	Abundance of adults arriving at their natal tributary (*after* upstream main-stem migration)
	$G_{y,k,o,j}$	F-40	Abundance of adult strays
	$B_{y,k,o,j}$	F-41	Abundance of adults removed at weir, primarily for broodstock
	$H_{y,k,o,j}$	F-41	Abundance of adults removed at weir, primarily for broodstock
	$S_{y,k,o,j}^{b}$	F-41, F-42	Abundance of adults following weir removals (e.g., for hatchery broodstock but *before* pre-spawn mortality)
States	$S_{y,k,o,j}^{a}$	F-4, F-42, F-50	Abundance of spawning adults *after* pre-spawn mortality
	$U_{y,k,o}$	F-40	Fishery harvest rate downstream of Bonneville Dam
	$\phi_{y,o}^{R^b \to R^a}$	F-40, F-44	Survival from all mortality sources during the migration between Bonneville Dam and arrival to natal tributaries
	$\phi_{y,j}^{S^b \to S^a}$	F-42	Pre-spawn survival rate
	Ω_k	F-4	Proportion of spawners that are female by age
Rates	$f_{y,k,j}$	F-4	Eggs per female spawner

Table F-3. Free parameters (i.e., that have a prior that is not function of other free parameters) estimated by the state-space life cycle model for Grande Ronde spring Chinook Salmon. Distributions and their parameterizations are defined in the footnotes.

Symbol	Prior[1,2,3,4,5,6]	Eq.	Description
Freshwater Juvenile			
α_j	$\mathrm{b}(2, 8)$	F-5	Maximum expected egg-to-parr survival rate; Beverton-Holt productivity
σ_β	$\mathrm{U}(0, 5)$	F-6	Among-population SD of parr capacity not explained by WUL_j
λ	$\mathrm{N}\left(0, 1 \times 10^{-8}\right)$	F-6	Expected change in parr capacity per 1 km change in WUL_j; prior bounded by $(0, \infty)$
$\Sigma_{\phi_j^{E \to P^b}}$	$\mathrm{SIW}(0.30, 2)$	F-7	Covariance matrix for egg-to-parr survival rate (white noise portion only); constructed of $\sigma_{\phi_j^{E \to P^b}}$ and $\rho_{\phi_{j,j'}^{E \to P^b}}$ following eq. F-2
$\kappa_j^{E \to P^b}$	$\mathrm{U}(-1, 1)$	F-7	Lag-1 autoregressive coefficient for egg-to-parr survival rate
$\omega_{0,j}$	$\mathrm{N}\left(0, 1 \times 10^{-3}\right)$	F-9	Intercept of density-dependent parr size relationship
$\omega_{1,j}$	$\mathrm{N}\left(0, 1 \times 10^{-3}\right)$	F-9	Slope of density-dependent parr size relationship
$\Sigma_{L^{P^b}}$	$\mathrm{SIW}(0.10, 2)$	F-10	Covariance matrix for variability in parr mean length not explained by egg density; constructed of $\sigma_{L_j^{P^b}}$ and $\rho_{L_{j,j'}^{P^b}}$ following eq. F-2
$\dot{\pi}_{i=\mathrm{fall},j}$	$\mathrm{b}(1, 1)$	F-12	Expected proportion of summer parr that are fall migrants
$\Sigma_{\pi_{i=\mathrm{fall}}}$	$\mathrm{SIW}(0.30, 2)$	F-12	Covariance matrix for variability in the proportion of summer parr that are fall migrants; constructed of $\sigma_{\pi_{i=\mathrm{fall},j}}$ and $\rho_{\pi_{i=\mathrm{fall},j,j'}}$ following eq. F-2
$\phi_j^{P^b \to P^a}$	$\mathrm{b}(1, 1)$	F-28	Survival from summer tagging to winter tagging for summer parr that are spring migrants
$\gamma_{0,i,j}$	$\mathrm{t}\left(0, 1.57^{-2}, 7.76\right)$	F-13	Intercept of over-winter survival vs. parr size relationship
$\gamma_{1,j}$	$\mathrm{t}\left(0, 1.57^{-2}, 7.76\right)$	F-13	Slope of over-winter survival vs. parr size relationship
$\Sigma_{\phi^{P^a \to M^b}}$	$\mathrm{SIW}(0.30, 2)$	F-14	Covariance matrix for variability in over-winter survival not explained by parr mean length; constructed of $\sigma_{\phi_j^{P^a \to M^b}}$ and $\rho_{\phi_{j,j'}^{P^a \to M^b}}$ following eq. F-2
$\theta_{0,j}$	$\mathrm{N}\left(0, 1 \times 10^{-3}\right)$	F-16	Intercept of change in parr to smolt mean length vs. parr mean length relationship
$\theta_{1,j}$	$\mathrm{N}\left(0, 1 \times 10^{-3}\right)$	F-16	Slope of change in parr to smolt mean length vs. parr mean length relationship

Table F-3. Free parameters (i.e., that have a prior that is not function of other free parameters) estimated by the state-space life cycle model for Grande Ronde spring Chinook Salmon. Distributions and their parameterizations are defined in the footnotes. *(continued)*

Symbol	Prior[1,2,3,4,5,6]	Eq.	Description
$\Sigma_{\Delta^{LP^b}\to L^{M^b}}$	SIW(0.15, 2)	F-17	Covariance matrix for variability in the change in mean length from parr to smolt not explained by parr mean length; constructed of $\sigma_{\Delta^{LP^b}_{j}\to L^{M^b}}$ and $\rho_{\Delta^{LP^b}_{j,j'}\to L^{M^b}}$ following eq. F-2
$\tau_{0,j}$	$\mathrm{t}(0, 1.57^{-2}, 7.76)$	F-19	Intercept of smolt migration survival to LGR vs. smolt mean length relationship
$\tau_{1,j}$	$\mathrm{t}(0, 1.57^{-2}, 7.76)$	F-19	Slope of smolt migration survival to LGR vs. smolt mean length relationship
$\Sigma_{\phi^{M^b}\to M^a}$	SIW(0.30, 2)	F-20	Covariance matrix for variability in smolt migration survival to LGR not explained by smolt mean length; constructed of $\sigma_{\phi^{M^b}_{j}\to M^a}$ and $\rho_{\phi^{M^b}_{j,j'}\to M^a}$ following eq. F-2
$\dot{\phi}^{M^a\to O^0}_{o}$	b(1, 1)	F-22	Expected migration survival from LGR to ocean
$\Sigma_{\phi^{M^a}\to O^0}$	SIW(0.30, 2)	F-22	Covariance matrix for variability in smolt migration survival from LGR to ocean; constructed of $\sigma_{\phi^{M^a}_{o}\to O^0}$ and $\rho_{\phi^{M^a}\to O^0}$ following eq. F-3
Ocean Juvenile			
$\dot{\phi}^{O^0\to O^1}_{o=\mathrm{NOR},j}$	b(1, 9)	F-34	Expected first year ocean survival for natural origin fish
$\Sigma_{\phi^{O^0}\to O^1}$	SIW(0.30, 2)	F-34	Covariance matrix for variability in first year ocean survival (white noise portion only); constructed of $\sigma_{\phi^{O^0}_{j}\to O^1}$ and $\rho_{\phi^{O^0}_{j,j'}\to O^1}$ following eq. F-2
$\kappa^{O^0\to O^1}_{j}$	U(−1, 1)	F-34	Lag-1 autoregressive coefficient for first year ocean survival
$\dot{\phi}^{O^1\to O^2}_{o=\mathrm{NOR},j}$	b(60, 40)		Expected second year ocean survival for natural origin fish
$\dot{\phi}^{O^2\to O^3}_{o=\mathrm{NOR},j}$	b(70, 30)		Expected third year ocean survival for natural origin fish
δ_j	$\mathrm{t}(0, 1.57^{-2}, 7.76)$	F-35	Log-odds ratio to convert natural origin to hatchery origin ocean survival
$\dot{\psi}^{O^1}_{o,j}$	b(1, 9)	F-36	Expected maturation rate after $w = 1$ winter at sea
$\dot{\psi}^{O^2}_{o,j}$	b(8.5, 1.5)	F-36	Expected maturation rate after $w = 2$ winters at sea

Table F-3. Free parameters (i.e., that have a prior that is not function of other free parameters) estimated by the state-space life cycle model for Grande Ronde spring Chinook Salmon. Distributions and their parameterizations are defined in the footnotes. *(continued)*

Symbol	Prior[1,2,3,4,5,6]	Eq.	Description
$\Sigma_{\psi^{O^1}}$	SIW(0.15, 2)	F-36	Covariance matrix for variability in maturation rate after $w = 1$ winter at sea; constructed of $\sigma_{\psi_j^{O^1}}$ and $\rho_{\psi_{j,j'}^{O^1}}$ following eq. F-2
$\Sigma_{\psi^{O^2}}$	SIW(0.30, 2)	F-36	Covariance matrix for variability in maturation rate after $w = 2$ winters at sea; constructed of $\sigma_{\psi_j^{O^2}}$ and $\rho_{\psi_{j,j'}^{O^2}}$ following eq. F-2
Freshwater Adult			
$R^b_{y,k=1,y,o,j}$	U(0, 50)		Return abundance of natural-origin age-3 fish in years without process model link; only for $y \in [1, 2, 3]$ and o = NOR
$R^b_{y,k=2,y,o,j}$	U(0, 200)		Return abundance of natural-origin age-4 fish in years without process model link; only for $y \in [1, 2, 3, 4]$ and o = NOR
$R^b_{y,k=3,y,o,j}$	U(0, 200)		Return abundance of natural-origin age-5 fish in years without process model link; only for $y \in [1, 2, 3, 4, 5]$ and o = NOR
$\dot{\phi}_o^{R^b \rightarrow R^a}$	b(1, 1)	F-39	Expected adult migration survival from BON to LGR
$\Sigma_{\phi^{R^b \rightarrow R^a}}$	SIW(0.30, 2)	F-40	Covariance matrix for variability in migration survival from BON to LGR; constructed of $\sigma_{\phi_o^{R^b \rightarrow R^a}}$ and $\rho_{\phi^{R^b \rightarrow R^a}}$ following eq. F-3
$G_{y,o,j}$	U(0, 500)	F-40	Total hatchery-origin "strays"; only for o = HOR and y where presence of HOR adults could not be explained by non-zero smolt releases
$p^G_{k,j}$	D(1, 1, 1)	F-40	Age composition of hatchery-origin "strays"
$\dot{z}_k$	U(−10, 10)	F-47	Across-population expected coefficient of log-linear carcass composition correction model; only for $k \in [1, 3]$
σ_{z_k}	U(0, 5)	F-47	Across-population SD for coefficients of log-linear carcass composition correction model; only for $k \in [1, 3]$

Prior Distributions in Table F-3

[1] Beta Distribution: $\mathrm{b}(\mathrm{shape}_1, \mathrm{shape}_2)$

[2] Normal Distribution: N(mean, precision)

[3] Uniform Distribution: U(lower, upper)

[4] *t*-Distribution: t(mean, precision, degrees of freedom); this specific $\mathrm{t}(0, 1.57^{-2}, 7.76)$ prior results in approximately a U(0, 1) prior after inverse-logit transformation (Dorazio et al. 2011).

[5] Dirichlet Distribution: $\mathrm{D}(\mathrm{shape}_1, \mathrm{shape}_2, \mathrm{shape}_3)$

[6] Scaled Inverse-Wishart Distribution: SIW($\mathbf{S}$, degrees of freedom); $\mathbf{S}$ is a vector of scale parameters for scaled-Wishart; see Plummer (2017) page 62 for details on this prior. Briefly, the scale parameters of 0.10 - 0.30 places higher prior weight on small values of the component σ parameters, which was intentional because these represent variability on the log- or logit-scale. Setting the degrees of freedom to 2 results in a U$(-1, 1)$ prior on the ρ components.

Table F-4. Symbology used to represent the data sources in the presentation of observation model components of the state-space life cycle model for Grande Ronde spring Chinook Salmon. All data sources listed here have an explicit likelihood component and were thus assumed to be observed with error.

Type	Symbol	Eq.	Description
Freshwater Juvenile			
Abundance	$\hat{P}^{a}_{y,i=\text{fall},j}$	F-24	Estimated smolt trap passage of parr in the fall
	$\hat{\sigma}_{P^{a}_{y,i=\text{fall},j}}$	F-24	Log-normal SE of estimated smolt trap passage of parr in the fall
	$\hat{M}^{b}_{y,i=\text{spring},o=\text{NOR},j}$	F-25	Estimated smolt trap passage of smolt in the spring
	$\hat{\sigma}_{M^{b}_{y,i=\text{spring},o=\text{NOR},j}}$	F-25	Log-normal SE of estimated smolt trap passage of smolt in the spring
Survival	$\hat{\phi}^{P^{b}\rightarrow M^{a}}_{y,j}$	F-26	Estimated survival from summer tagging to LGR
	$\hat{\sigma}_{\phi^{P^{b}\rightarrow M^{a}}_{y,j}}$	F-26	Logit-normal SE of estimated survival from summer tagging to LGR
	$\hat{\phi}^{P^{a}\rightarrow M^{a}}_{y,i=\text{fall},j}$	F-27	Estimated survival from fall tagging to LGR
	$\hat{\sigma}_{\phi^{P^{a}\rightarrow M^{a}}_{y,i=\text{fall},j}}$	F-27	Logit-normal SE of estimated survival from fall tagging to LGR
	$\hat{\phi}^{P^{a}\rightarrow M^{a}}_{y,i=\text{spring},j}$	F-28	Estimated survival from winter tagging to LGR
	$\hat{\sigma}_{\phi^{P^{a}\rightarrow M^{a}}_{y,i=\text{spring},j}}$	F-28	Logit-normal SE of estimated survival from winter tagging to LGR
	$\hat{\phi}^{M^{b}\rightarrow M^{a}}_{y,i=\text{spring},o=\text{NOR},j}$	F-29	Estimated survival from spring tagging to LGR
	$\hat{\sigma}_{\phi^{M^{b}\rightarrow M^{a}}_{y,i=\text{spring},o=\text{NOR},j}}$	F-29	Logit-normal SE of estimated survival from spring tagging to LGR
	$\hat{\phi}^{M^{b}\rightarrow M^{a}}_{y,i=\text{spring},o=\text{HOR},j}$	F-30	Estimated survival of hatchery-origin smolt releases to LGR
	$\hat{\sigma}_{\phi^{M^{b}\rightarrow M^{a}}_{y,i=\text{spring},o=\text{HOR},j}}$	F-30	Logit-normal SE of estimated survival of hatchery-origin smolt releases to LGR
	$\hat{\phi}^{M^{a}\rightarrow O^{0}}_{y,o}$	F-31	Estimated aggregate survival of smolt through hydrosystem
	$\hat{\sigma}_{\phi^{M^{a}\rightarrow O^{0}}_{y,o}}$	F-31	Logit-normal SE of estimated aggregate survival of smolt through hydrosystem
	$\hat{L}^{P^{b}}_{y,j}$	F-32	Estimated parr mean length (mm fork length) at summer tagging

Table F-4. Symbology used to represent the data sources in the presentation of observation model components of the state-space life cycle model for Grande Ronde spring Chinook Salmon. All data sources listed here have an explicit likelihood component and were thus assumed to be observed with error. *(continued)*

Type	Symbol	Eq.	Description
Length	$\hat{\sigma}_{L^{P^b}_{y,j}}$	F-32	Log-normal SE of estimated parr mean length at summer tagging
	$\hat{L}^{M^b}_{y,j}$	F-33	Estimated smolt mean length (mm fork length) at spring tagging
	$\hat{\sigma}_{L^{M^b}_{y,j}}$	F-33	Log-normal SE of estimated smolt mean length at spring tagging
Freshwater Adult			
Abundance	$\hat{R}^{a}_{y,j}$	F-43	Estimated total adult return to tributary (all ages/origins)
	$\hat{\sigma}_{R^{a}_{y,j}}$	F-43	Log-normal SE of estimated total adult return to tributary
Survival	$\hat{x}^{\text{BON}}_{y,o}$	F-44	Count of Grande Ronde-origin PIT-tagged adults detected at BON
	$\hat{x}^{\text{LGR}}_{y,o}$	F-44	Count of Grande Ronde-origin PIT-tagged adults detected at LGR
Composition	$\hat{x}^{R^a}_{y,ko,j}$	F-46	Count of sampled adults returning to tributary by age/origin; only for $j \in [\text{CAT}, \text{LOS}, \text{UGR}]$
	$\hat{x}^{S^{a'}}_{y,ko,j}$	F-51	Count of sampled carcasses by age/origin

TABLE F-5. Catalog of all equations presented, separated by life phase (freshwater juvenile, ocean juvenile, or freshwater adult) and model component (process model or observation model).

Model	Eq.	Description
Generic		
	F-1	Syntax for quantities assumed to follow a multivariate logit-normal distribution
	F-2	Covariance structure for quantities that vary across populations
Syntax	F-3	Covariance structure for quantities that vary across origins, not populations
Freshwater Juvenile		

Table F-5. Catalog of all equations presented, separated by life phase (freshwater juvenile, ocean juvenile, or freshwater adult) and model component (process model or observation model). *(continued)*

Model	Eq.	Description
	F-4	Obtain total egg production
	F-5	Obtain expected egg-to-parr survival as a function of egg density
	F-6	Obtain parr capacity as a function of weighted usable habitat length
	F-7	Add stochasticity to egg-to-parr survival
	F-8	Obtain total parr recruitment
	F-9	Obtain expected parr mean length as a function of egg density
	F-10	Add stochasticity to parr mean length
	F-11	Obtain migratory strategy-specific parr abundance
	F-12	Add stochasticity to migratory strategy apportionment rates
	F-13	Obtain expected over-winter survival; related to parr mean length
	F-14	Add stochasticity to over-winter survival
	F-15	Obtain natural-origin smolt abundance prior to out-of-basin migration
	F-16	Obtain expected multiplicative change in mean length from parr to smolt
	F-17	Add stochasticity to multiplicative change in mean length from parr to smolt
	F-18	Obtain smolt mean length
	F-19	Obtain expected migration survival from in-basin to LGR
	F-20	Add stochasticity to migration survival from in-basin to LGR
	F-21	Obtain smolt abundance at LGR
	F-22	Add stochasticity to migration survival from LGR to ocean
Process	F-23	Obtain initial abundance of ocean juveniles

Table F-5. Catalog of all equations presented, separated by life phase (freshwater juvenile, ocean juvenile, or freshwater adult) and model component (process model or observation model). *(continued)*

Model	Eq.	Description
	F-24	Assumption for fall screw trap count data likelihood
	F-25	Assumption for spring screw trap count data likelihood
	F-26	Assumption for summer tagging event survival data likelihood
	F-27	Assumption for fall tagging event survival data likelihood
	F-28	Assumption for winter tagging event survival data likelihood
	F-29	Assumption for spring tagging event survival data likelihood (NOR)
	F-30	Assumption for spring tagging event survival data likelihood (HOR)
	F-31	Assumption for migration through hydrosystem survival data likelihood
	F-32	Assumption for parr mean length data likelihood
Observation	F-33	Assumption for smolt mean length data likelihood
Ocean Juvenile		
	F-34	Add stochasticity to first year ocean survival
	F-35	Obtain HOR ocean survival
	F-36	Add stochasticity to maturation rates
	F-37	Obtain abundance of ocean juveniles by ocean age
	F-38	Obtain return abundance of adults by total age
Freshwater Adult		
	F-39	Add stochasticity to migration survival from BON to LGR
	F-40	Obtain return abundance to natal tributary
	F-41	Obtain abundance of potential spawners reaching spawning grounds
Process	F-42	Obtain abundance of successful spawners

Table F-5. Catalog of all equations presented, separated by life phase (freshwater juvenile, ocean juvenile, or freshwater adult) and model component (process model or observation model). *(continued)*

Model	Eq.	Description
	F-43	Assumption for natal tributary return abundance data likelihood
	F-44	Assumption for migration from BON to LGR survival data likelihood
	F-45	Obtain expected composition by age and origin of adults counted at weirs
	F-46	Assumption for age and origin composition at weir data likelihood
	F-47	Add stochasticity to carcass composition correction factor coefficients
	F-48	Obtain correction factors for populations with weir and carcass data
	F-49	Obtain correction factors for population with carcass composition data only
	F-50	Obtain expected composition by age and origin of carcasses
Observation	F-51	Assumption for age and origin carcass composition data likelihood

Table F-6. Year of return based on age of return and brood year. For example, adults that were progeny of spawners in 2000 (their brood year) returned to spawn in 2003 as age-3, 2004 as age-4, and 2005 as age-5 (shown in blue). The return years with red brood years show the age-specific return abundances that were estimated because no previous states (e.g., parr, smolt) were available for these early brood years (see Section for more details).

	Brood Year of Returning Adults by Age		
Return Year	**Age-3**	**Age-4**	**Age-5**
1991	1988	1987	1986
1992	1989	1988	1987
1993	1990	1989	1988
1994	1991	1990	1989
1995	1992	1991	1990
1996	1993	1992	1991
⋮	⋮	⋮	⋮
2003	2000	1999	1998
2004	2001	2000	1999
2005	2002	2001	2000
⋮	⋮	⋮	⋮
2022	2019	2018	2017